RAB-A2a dependent membrane traffic in *Arabidopsis thaliana*

Astrid Alexandra Diana Woollard

St. Catherine's College
Department of Plant Sciences
University of Oxford

A thesis submitted for the degree
Doctor of Philosophy

Trinity Term 2013

Contents

Acknowledgements **x**

Abstract **xii**

Abbreviations and Acronyms **xiii**

1 Introduction **1**

1.1 The endomembrane system 1

1.2 Evolution and diversification of eukaryotic endomembrane systems 2

1.3 The endomembrane system 3

1.3.1 Crucial membrane trafficking steps and trafficking pathways 3

1.3.2 Traffic between Endoplasmic Reticulum and Golgi 5

1.3.3 Post-Golgi traffic 6

1.3.4 Endosomal traffic 6

1.3.5 Endocytosis 7

1.3.6 Traffic during cytokinesis 7

1.3.7 Polar auxin transport 8

1.4 Rab GTPases as membrane traffic regulators and tools to study membrane traffic 10

1.4.1 Structure of Rab GTPases 11

1.4.2 Regulation of Rab GTPases 11

1.4.3 Classification of Rab GTPases 13

1.4.4 The Rab-A clade 14

1.4.5 The Rab-B clade 17

1.4.6 The Rab-C clade 18

1.4.7 The Rab-D clade 18

1.4.8 The Rab-E clade 18

1.4.9 The Rab-F clade . . . 19
1.4.10 The Rab-G clade . . . 21
1.4.11 The Rab-H clade . . . 22
1.5 The discovery of GFP as a tool in cell biology . . . 22
1.6 Thesis objective . . . 25

2 Materials and Methods **26**

2.1 Materials . . . 26
2.1.1 Plant material and growth medium . . . 26
2.1.2 Bacterial strains and growth media . . . 26
2.1.3 Antibiotics . . . 27
2.1.4 Chemicals . . . 27
2.1.5 Plasmids . . . 27
2.1.6 Oligonucleotide primers . . . 28
2.1.7 Enzymes . . . 29
2.1.8 Antibodies . . . 29
2.1.9 Other lab equipment . . . 29
2.2 Methods . . . 30
2.2.1 Plant growth conditions and transformation . . . 30
2.3 Cloning . . . 31
2.3.1 Polymerase Chain Reaction . . . 31
2.3.2 Restriction enzyme digestion of DNA . . . 31
2.3.3 Agarose Gel Electrophoresis . . . 31
2.3.4 DNA gel purification . . . 32
2.3.5 Gateway cloning . . . 32
2.3.6 DNA ligation . . . 32
2.3.7 Bacterial transformation . . . 32
2.3.8 Competent cells for transformation . . . 33
2.3.9 Purification of plasmid DNA from bacteria . . . 34
2.3.10 Sequencing . . . 35
2.4 Histochemical GUS staining . . . 36
2.5 Protein analysis . . . 36
2.5.1 Protein extraction . . . 36

2.5.2 Western Blot . . . 36
2.6 Confocal Laser Scanning Microscopy . . . 38
2.6.1 Imaging . . . 38
2.6.2 Drug treatments . . . 38
2.6.3 Stainings . . . 39
2.6.4 FRAP analysis . . . 39

3 Generation and characterisation of dominant negative marker lines 41
3.1 Introduction . . . 41
3.1.1 The dominant negative approach . . . 42
3.1.2 The dexamethasone inducible system . . . 42
3.1.3 The fluorescent marker line set . . . 44
3.2 Results . . . 45
3.2.1 The dexamethasone inducible system: pOpON2.1 . . . 45
3.2.2 Dominant negative RAB-A2a pOpON2.1 transgenic *Arabidopsis* plants show stronger root growth inhibition than pH-TOP lines . . . 46
3.2.3 pOpON2.1 transgenic plant lines are more rapidly induced than pH-TOP lines. . . . 48
3.2.4 pOpON2.1 transgenic plants accumulate more dominant negative RAB-A2a than pH-TOP lines . . . 50
3.2.5 Selection of marker lines and transformants . . . 51
3.2.6 Specificity of dominant negative RAB-A2a . . . 55
3.3 Conclusions . . . 58

4 Investigating the effect of the dominant negative RAB-A2a mutant on membrane traffic in *Arabidopsis thaliana.* 61
4.1 Introduction . . . 61
4.1.1 RAB-A2a and the TGN as a central trafficking hub . . . 62
4.1.2 Selected fluorescent markers help to elucidate trafficking pathways dependent on RAB-A2a . . . 63
4.2 Results . . . 67
4.2.1 Dominant negative RAB-A2a affects PIN2:GFP trafficking . . . 67
4.2.2 Default traffic to the PM is not affected by dominant negative RabA2a 75
4.2.3 Traffic to the vacuole is not affected by dominant negative RAB-A2a . . 81

4.2.4 Endocytosis of FM4-64 and transport to the tonoplast is not affected by dominant negative RAB-A2a . . . 87
4.3 Conclusions . . . 88

5 Investigation of the PIN2:GFP trafficking defect 90
5.1 Introduction . . . 90
5.1.1 Vacuolar targeting and degradation of PIN2 . . . 91
5.1.2 PIN2 trafficking and the actin cytoskeleton . . . 92
5.1.3 PIN2 polarity and endocytosis . . . 92
5.2 Results . . . 94
5.2.1 Expression of dominant negative RAB-A2a enhances vacuolar traffic of PIN2:GFP . . . 94
5.2.2 PIN2:GFP labelled PVCs are insensitive to Wortmannin in presence of dominant negative RAB-A2a . . . 94
5.2.3 RAB-A2a dependent traffic of PIN2:GFP is independent of the actin cytoskeleton . . . 96
5.2.4 PIN2:GFP recycling is affected by expression of dominant negative RAB-A2a . . . 97
5.2.5 PIN2:GFP endocytosis is not affected by dominant negative RAB-A2a . 101
5.2.6 Delivery of *de novo* synthesised PIN2:GFP to the PM is not affected by dominant negative RAB-A2a . . . 103
5.3 Conclusions . . . 105

6 General Discussion 108
6.1 A review of PIN2:GFP trafficking . . . 109
6.2 Examination of PIN2:GFP trafficking in the presence of dominant negative RAB-A2a . . . 113
6.2.1 The default route of PIN2:GFP to the PM is not inhibited by dominant negative RAB-A2a . . . 113
6.2.2 PIN2:GFP recycling is inhibited in the presence of dominant negative RAB-A2a . . . 115
6.2.3 Trafficking of PIN2:GFP to the vacuole is enhanced in the presence of dominant negative RAB-A2a . . . 116

6.2.4 A model for RAB-A2a dependent PIN2:GFP trafficking in *Arabidopsis thaliana* 118
6.3 Future directions 121

A Additional images **123**

Bibliography **127**

List of Figures

1.1 Graphical representation of vesicle formation. 3
1.2 Graphical representation of vesicle targeting. 4
1.3 Graphical representation of vesicle fusion. 5
1.4 Rab activity cycle 10
1.5 Graphical representation of typical Rab sequence. 11
1.6 The Rab-A clade 17
1.7 Overview of fluorescent protein techniques with genetic tags 24

2.1 Graphical representation of the pOpON2.1 vector generated with pDRAW software 28
2.2 Screenshots demonstrating analysis of FRAP experiments using Zeiss LSM Browser. 40

3.1 The dexamethasone inducible system 43
3.2 Graphical representation of the pOpON2.1 dexamethasone inducible construct 45
3.3 Root growth of selected pOpON2.1 dominant negative RAB-A2a lines 47
3.4 Root growth of the pH-TOP dominant negative RAB-A2a line 2NI 1.5A 47
3.5 Root growth of the pH-TOP dominant negative RAB-A2a line 2NI 1.6C 48
3.6 GUS stainings of pOpON2.1 inducible dominant negative lines (Col-0 2NI) . . 49
3.7 GUS stainings of pH-TOP inducible dominant negative lines (Col-0 2NI) 49
3.8 Western blot of a pOpON2.1 line with inducible dominant negative RAB-A2a . 50
3.9 Western blot of a pH-TOP line with inducible dominant negative RAB-A2a . . 51
3.10 Quantification of western blot results. 52
3.11 Possible wound inducibility of pH-TOP lines. 53
3.12 Dominant negative RAB-A2a causes localisation of mCherry:RAB-A2a and YFP:RAB-A1e to Golgi-like bodies. 56
3.13 Localisation of mCherry:RAB-A5c. 57

4.1 Steady state localisation of fluorescent markers used in this work. 64
4.2 Root growth assay of selected PIN2:GFP A2aNI lines 68
4.3 Trafficking of PIN2:GFP is affected by the dominant negative RAB-A2a. 68
4.4 Root growth assay of selected PIN2:GFP A2aWT lines 69
4.5 Western blot of PIN2:GFP A2aWT and A2aNI 70
4.6 Localisation of PIN2:GFP is not altered in the presence of excess wild type RAB-A2a 70
4.7 BFA treatment reveals a possible role for RAB-A2a in PIN2:GFP cycling . . . 71
4.8 Root growth assay of selected PIN2:GFP A5cNI lines 72
4.9 Trafficking of PIN2:GFP in meristematic, epidermal root cells is not affected by dominant negative A5c 72
4.10 Root growth assay of selected BRI1:GFP A2aNI lines 73
4.11 Localisation of BRI1:GFP is not affected in the presence of dominant negative RAB-A2a. 74
4.12 BRI1:GFP cycling is not affected by the dominant negative RAB-A2a. 75
4.13 Root growth assay of selected nlsRm-2A-secGFP A2aNI lines 76
4.14 Dominant negative RAB-A2a does not affect default secretion. 77
4.15 Root growth assay of selected YFP:NPSN12 A2aNI lines 78
4.16 Root growth assay of selected YFP:PIP1;4 A2aNI lines 79
4.17 Trafficking of the PM markers YFP:NPSN12 and YFP:PIP1;4 is not affected by dominant negative RAB-A2a. 80
4.18 Root growth assay of selected YFP:VAMP711 A2aNI lines 81
4.19 Root growth assay of selected YFP:RAB-G3f A2aNI lines 82
4.20 Trafficking of YFP:VAMP711 and YFP:RAB-G3f is not affected by dominant negative RAB-A2a. 83
4.21 Root growth assay of selected BP80:GFP A2aNI lines 84
4.22 Root growth assay of selected RAB-F2b:GFP A2aNI lines 85
4.23 Trafficking of BP80:GFP and RAB-F2b:GFP is not affected by dominant negative RAB-A2a 86
4.24 FM4-64 endocytosis and transport to the tonoplast are not affected by dominant negative RAB-A2a 87

5.1 Dominant negative RAB-A2a causes enhanced PIN2:GFP signal in lytic vacuoles after dark treatment. 95
5.2 PIN2:GFP labelled PVCs are insensitive to Wortmannin in the presence of dominant negative RAB-A2a. 96
5.3 The actin cytoskeleton is not involved in RAB-A2a dependent PIN2:GFP trafficking. 97
5.4 RAB-A2a function is involved in PIN2:GFP recycling 99
5.5 RAB-A5c function is not involved in PIN2:GFP recycling 100
5.6 PIN2:GFP endocytosis is not affected by dominant negative RAB-A2a 102
5.7 PIN2:GFP delivery to the PM is not affected by dominant negative RAB-A2a . 103

6.1 Overview of PIN2 trafficking 109
6.2 Different scenarios for the default route of PIN2:GFP to the PM 114
6.3 Possible trafficking scenarios of PIN2:GFP to the vacuole 115
6.4 Different scenarios for PIN2:GFP recycling pathways. 117
6.5 A model for RAB-A2a dependent PIN2:GFP trafficking in *Arabidopsis thaliana* 119

A.1 Dominant negative RAB-A2a causes localisation of YFP:RAB-A1e to Golgi-like bodies. 124
A.2 Dominant negative RAB-A2a causes localisation of mCherry:RAB-A2a to Golgi-like bodies. 125
A.3 Dominant negative RAB-A2a causes prominent intracellular localisation of PIN2:GFP. 126

List of Tables

1.1 BFA effects are plant and tissue specific. 9

2.1 Antibiotics and their concentrations used in this project 27

2.2 Drugs and their concentrations used in this project 38

3.1 Further screening of pOpON2.1 lines. 54

4.1 Fluorescent proteins are used as markers to study different trafficking pathways. 64

5.1 FRAP measurements 104

Acknowledgements

First and foremost, I would like to thank my supervisors Dr Ian Moore and Dr Gail Preston for giving me the opportunity to work in their labs and to explore this exciting topic. Their enduring support were invaluable for the success of this project. I am very grateful for their continued advice and guidance during my time at Oxford. It has been a great pleasure to work with two so passionate scientists and to learn from them. Thank you for believing in me.

Thanks to everyone in the Moore and Preston labs for providing a great work atmosphere and useful discussions. Especially, I would like to thank Anja Hörger, Francisco Javier López Baena, Helen Fones, Irene Jiménez Guerrero, Kenneth Au and Monika Kalde. I will miss the baking rota and the fun we had. I would also like to thank the other members of the Department of Plant Sciences for their generous support, most importantly Prof. Liam Dolan, Dr Mark Fricker and Prof. Hugh Dickinson. Further, I want to acknowledge St. Catherine's College for efficient administration and providing a friendly and motivating atmosphere outside of the lab.

My family and friends made me feel as if Vienna was just around the corner, especially in tough times. I do not have the words to say how grateful I am. You are all wonderful people and I am proud to know you. Many thanks for your love and all your support, especially to my mother Teresa Woollard, to my aunt Eva Richter-Mahrer and my very best friends Andreea Borza, Andrea Rosenberger, Barbara Killian, Evelyn Grünwerth and Jo-Marie Chan, and to the two best housemates I ever had, Michael Müller and Nick Rounthwaite.

Special thanks go to the best partner I could wish for, Phillip Tait. Thank you for your loving support, your patience and the strength you gave me during the final months of this project. I am not sure how I would have managed this very stressful time without you. Thank you for

everything. Together, we can climb any mountain. I love you.

I would like to thank Niko Geldner for making the WAVE lines available before they were published. Further thanks go to Department of Plant Sciences and the BBSRC for funding the first three years of this project, and to my mother Teresa Woollard for funding my final year at Oxford.

Finally, I would like to thank my examiners Dr Lee Sweetlove and Dr Silke Robatzek for their constructive comments on my thesis.

Abstract

Rab GTPases are major regulatory proteins of vesicle traffic and thus responsible for membrane identity, vesicle targeting and vesicle fusion. The angiosperm Rab GTPase family is grouped into eight clades (Rab-A to Rab-H) that are broadly conserved in animals and yeasts. It has been proposed that the Rab-A clade has diversified in land plants giving rise to six plant-specific structural subclasses, Rab-A1 to Rab-A6. Previous work suggests that the *Arabidopsis* Rab-A2 and Rab-A3 proteins define a novel endosomal compartment that lies on a pathway between the Golgi and the plasma membrane. In dividing cells, the Rab-A2/A3 compartment is implicated in biosynthetic traffic to the cell plate but it is unclear what traffics through this compartment in non-dividing cells.

In this project, I investigated a range of membrane trafficking pathways in *Arabidopsis thaliana.* These were probed for dependency on RAB-A2a function, using the dominant negative approach combined with fluorescent marker technology. The data presented in this thesis suggests that RAB-A2a acts on a protein recycling pathway that is used by PIN2:GFP.

Abbreviations and Acronyms

ABA Aminobutyric acid

ADP Adenosine-di-phosphate

ARF ADP-ribosylation factor

ARF-GEF ARF Guanine nucleotide exchange factor

Ath *Arabidopsis thaliana*

ATP Adenosine-tri-phosphate

AUX1 Auxin-resistant 1

BABA β-Aminobutyric acid

BAK1 BRI1 associated receptor kinase 1

BEX BFA-visualized exocytic trafficking defective

BFA Brefeldin A

BLAST Basic Local Alignment Search Tool

BOR1 Boron 1

bp Base pair

BP80 Binding Protein of 80kD

BRI1 Brassinosteroid-insensitive 1

BY-2 Bright yellow 2

CaMV Cauliflower mosaic virus

CFP Cyan fluorescent protein

CLSM Confocal Laser Scanning Microscopy

Col-0 Columbia ecotype of *Arabidopsis thaliana*

COP Coat protein

Cyt D Cytochalasin D

DEX Dexamethasone

dH_2O Distilled water

DMF Dimethylformamide

DMSO Dimethylsulfoxide

DNA Deoxyribonucleic acid

dNTP Deoxyribonucleotide triphosphate

E. coli *Escherichia coli*

EDTA Ethylene-diamino-tetra-acetic acid

EGFP Enhanced GFP

ER Endoplasmic reticulum

ES1 Endosidin 1

ESCRT Endosomal sorting complex required for transport

Ffh fifty-four homologue

FLIP Fluorescence loss in photobleaching

FLS2 Flagellin Sensitive 2, also: Flagellin Sensing 2

FM1-43 N-(3-Triethylammoniumpropyl)-4-(4-(Dibutylamino) Styryl) Pyridinium Dibromide

FM4-64 N-(3-Triethylammoniumpropyl)-4-(6-(4-(Diethylamino) Phenyl) Hexatrienyl) Pyridinium Dibromide

FRAP Fluorescence recovery after photobleaching

FRET Fluorescence resonance energy transfer

GAP GTPase activating protein

GARP Golgi-associated retrograde protein

GDF GDI displacement factor

GDI GDP dissociation inhibitor

GDP Guanine nucleotide di-phosphate

GEF Guanine nucleotide exchange factor

GFP Green fluorescent protein

GGTase Geranylgeranly transferase

GR rat glucocorticoid receptor

GRE Glucocorticoid receptor element

GST Glutathione S-transferase

GTP Guanine nucleotide tri-phosphate

GUS *E.coli* β-glucuronidase

HEPES N-[2-hydroxylethyl] piperazine-N'-[2-ethanesulfonic acid]

IAA Indole-3-acetic acid

IPTG Iso-Propyl-β-D-thiogalactopyranoside

KOR Korrigan

LB Luria-Bertani (bacterial growth medium)

LRR Leucine rich repeat

LRR-RLK LRR-Receptor like kinase

MORN membrane occupancy and recognition nexus

MS Murashige and Skoog plant growth medium

NPSN Novel plant SNARE protein

Nta *Nicotiana tabaccum*

OD_{600} Optical density at 600nm

PCR Polymerase chain reaction

PEN penetration

PGE Post-Golgi Endosome

PIN PIN FORMED

PIP1;4 Plasma membrane integral protein

PIPES Piperazine-N,N-bis(2-ethanesulfonic acid)

PM Plasma membrane

PRA Prenylated Rab acceptor

PVC Pre-vacuolar compartment

PVE Pre-vacuolar endosome

PVDF Polyvinylidene difluoride

RAB-A2aNI Dominant negative mutant of RAB-A2a

Rab Ras-related protein in rat brain

Rab GGTase Rab geranylgeranyl transferase

REP Rab escort protein

RER Retrieval of early ER

RFP Red fluorescent protein

RHD Root hair defective

RNA Ribonucleic acid

ROR Roscovitine resistant

SAR Secretion-associated and Ras-related

SDS Sodium Dodecyl Sulphate

SEC Secretory agent

secGFP secreted GFP

siRNA small interfering RNA

SNAP Souble NSF Association Protein

SNARE SNAP (Soluble NSF Attachment Protein) REceptor

SNX Sorting nexin

SOB Super optimal broth

ST Sialyl-transferase

SYP Syntaxins of plants

T4SS Type 4 secretion system

TBE Tris/borate/EDTA

TBS Tris-buffered saline

TCR1 Tissue Culture Room 1

T-DNA Transfer DNA of *Agrobacterium tumefaciens*

TEMED Tetra-methyl-ethylene-diamine

TGN Trans-Golgi network

TRAPP Transport protein particle

Tris Trisaminomethane

Tyr Tyrphostin

VAMP Vesicle associated membrane protein

VFT Vps Fifty Three

VHA-a1 vacuolar H(+)-ATPase subunit a1

VPS vacuolar protein sorting

VSR Vesicle sorting receptor

v/v volume per volume

Wm Wortmannin

WT wild type

w/v weight per volume

X-Gluc 5-Bromo-4-chloro-3-indolyl β-D-glucuronide

YFP Yellow fluorescent protein

YPT Yeast protein transport

Chapter 1

Introduction

1.1 The endomembrane system

Cells are the basic structural and functional units of living organisms. Cells are enclosed by the plasma membrane (PM), which serves as a protective barrier and interacts with the environment *via* proteins inserted into the PM. The cell's shape is maintained by the cytoskeleton, a scaffold that helps with endocytosis, a process of material uptake from the environment; it also helps with movement of cells and holds organelles in place. The fluid-filled space within a cell is called the cytosol, where organelles and vesicles reside and interact through membrane trafficking [1].

Membrane trafficking is achieved by the endomembrane system, a set of membraneous organelles, compartments and vesicles, and is essential to eukaryotic life. Proteins, lipids and carbohydrates are transported from synthesis to action sites where they play crucial roles for cell growth and differentiation as well as for more specialised functions, such as defence responses against pathogens. Material exchange between the cell and its extracellular environment, which is necessary for nutrient uptake, development and environmental responses, are also excerted via membrane traffic[1].

Plant membrane traffic shares basic mechanisms and core components with yeast and animal systems. However, it also exhibits several unique features, such as its distinct organisation and more specialised functions like cell plate formation during cytokinesis and polar auxin transport, which are still poorly understood [1].

1.2 Evolution and diversification of eukaryotic endomembrane systems

The capability to form internal, membrane-bound compartments and to create an endomembrane system has been crucial to progress from prokaryotic to eukaryotic life. This machinery was necessary to facilitate internalisation and digestion of extracellular material, ensure accurately targeted intracellular transport and enable surface remodelling and secretion. Proposed hypotheses of endomembrane system evolution range from endosymbiotic to autogenous paradigms [2, 3, 4, 5, 6].

Previous studies identified common core components of the trafficking machinery: small GTPases, adaptor and coat proteins. Rab GTPases are well known regulators of membrane traffic and ensure membrane specificity as well as vesicle fusion with the correct target membrane. Other crucial protein factors include SNAREs (SNAP (Soluble NSF Attachment Protein) REceptor), tethering complexes and syntaxin binding proteins [7]. Many components of the eukaryotic trafficking machinery have undergone gene duplication which gave rise to additional functions and different subcellular localisation. Interestingly, there is no strong correlation between multicellularity and the complexity of the endomembrane system. The degree of expansion of essential trafficking components varies amongst current species [7].

The origin of the endomembrane compartments is still poorly understood, perhaps because the complexity of eukaryotic systems varies considerably. For example, some lineages lack apparent Golgi stacks [8]. However, there are a few examples from the prokaryotic kingdom where analogous structures to the eukaryotic system exist. In *E. coli* internal stacks of PM are generated by the function of Ffh (fifty-four homologue, a signal recognition particle) and SecE (a translocon). These stacks closley resemble the structure of a eukaryotic endoplasmic reticulum (ER) and even contains FtsY ribosome complexes [9]. Another example comes from the phylum *Planctomycetes.* Membrane bound nucleoids have been described, which could be early progenitors of the nuclear envelope [10].

However, the reconstruction of evolutionary events remains challenging and it will be interesting to see how current models will be shaped by including information coming from comparative genomic and molecular evolutionary studies.

1.3 The endomembrane system

1.3.1 Crucial membrane trafficking steps and trafficking pathways

In this section, the basic trafficking steps of the endomembrane system will be described, owing to data from animal, plant and yeast research.

Vesicle formation

The formation of vesicles requires the activation of small GTPases by their guanine exchange factors (GEF), which catalyse exchange of GDP to GTP, and thus leads to recruitment of coat proteins. The respective cargo is sorted into the forming vesicle by interaction with these coat proteins in the case of membrane bound cargo. Soluble cargo, however, is sorted into the respective vesicles by interaction with cargo receptors that will in turn interact with coat proteins.

There are coat proteins I (COPI) and coat proteins II (COPII) coat proteins. COPI vesicles consist of a seven subunit coat (coatamer, four inner: β, γ, δ and ζ, and three outer proteins: α, β' and ε) and mediate Golgi to ER traffic [11]. COPII coated vesicles are necessary for ER to Golgi transport and consist of four proteins: the SAR1 GTPase activating protein (GAP) SEC23 that directly interacts with the SAR1 GTPase, SEC24 is the cargo-binding subunit, SEC13 and SEC31 function as GAP activity augmentors [12, 13].

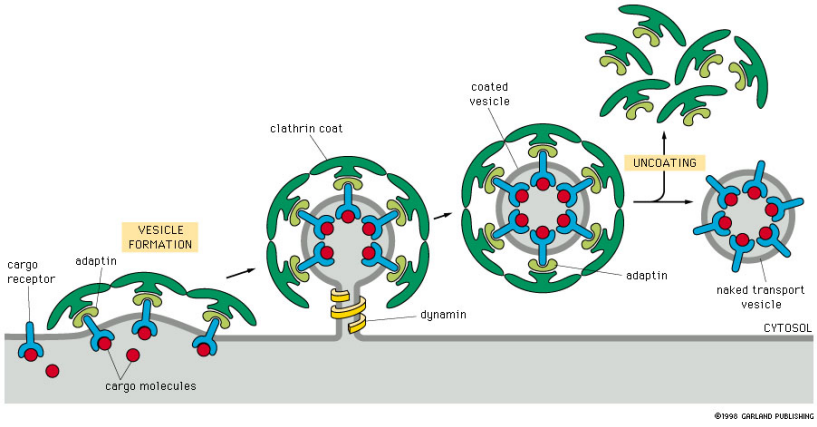

Figure 1.1: Graphical representation of vesicle formation. Small GTPases are activated, which recruit coat proteins. Cargo is sorted into the forming vesicle. Dynamin (a GTPase) is required for scission of newly formed vesicles from the membrane. Sorting of vesicles happen once they shed their coat. Image taken from [1].

Post-Golgi traffic is mediated by vesicles containing hetero-tetrameric adaptor protein (AP) complexes that are surrounded by clathrin triskella (figure 1.1). AP complexes consist of two large adaptins (interaction with clathrin), a medium and a small adaptin, which bind cargo *via* their tail domain [11, 14] .

Sorting of membrane proteins requires sorting signals and cargo receptors. Well studied sorting signals are, for example, the ER retention signal K/HDEL or the vacuolar sorting signals NTPP/CTPP [15, 16]. The ERD2 K/HDEL receptors recycle cargo back to the ER [15] and several vacuolar sorting receptors have been identified of which vesicle sorting receptor 1 (VSR1) is best studied [17, 18]. *Arabidopsis* encodes three retrieval of early ER (RER1) cargo receptors that function in ER localisation [19]. Vacuolar sorting is achieved by μ-adaptins on vacuolar sorting receptors that recognise tyrosine motifs [20].

Vesicle fusion

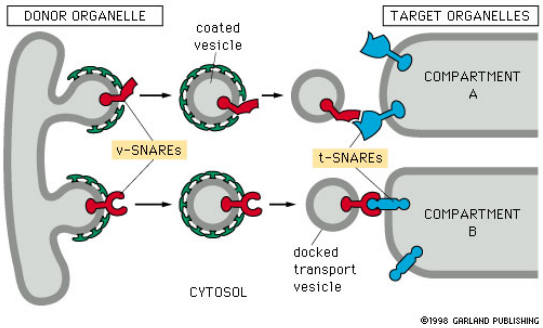

Figure 1.2: Graphical representation of vesicle targeting. Vesicles are formed at the donor organelle and contain vesicle SNARES (v-SNAREs). Once the vesicle shed its coat, v-SNARES are recognised by target SNARES (t-SNARES) at the target organelle. Image taken from [1].

Fusion with the target membrane occurs with the help of Rab GTPases and SNARE (soluble NSF attachment protein receptor) complexes after the vesicle has shed its coat (figures 1.1 and 1.2). Rab GTPases, which are described in detail later in this introduction, interact with protein tethering complexes on the target membrane [21], such as transport protein particle (TRAPP) at the *cis*-Golgi, VFT/GARP at the trans-Golgi, and C-VPS at the vacuolar membrane; multiple components of the Vps34/COG complex are involved in Golgi retrograde transport [22, 23]. SNARE proteins residing on the opposite membranes form a trans-complex that result in vesicle fusion (figure 1.3).

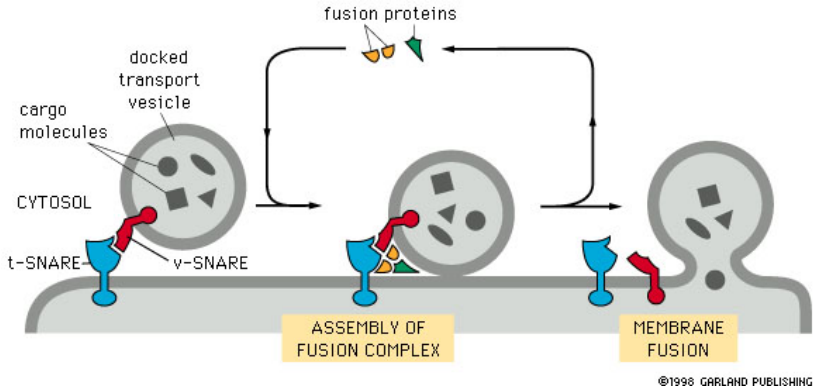

Figure 1.3: Graphical representation of vesicle fusion. Once vesicles are recruited to the membrane by recognition of the respective v- and t-SNARE pairs, fusion proteins are recruited, which lead to fusion of the vesicle with the target membrane and release of vesicle cargo. Image taken from [1].

1.3.2 Traffic between Endoplasmic Reticulum and Golgi

ER and Golgi stacks are a close and dynamic molecule exchange system. One can distinguish between anterograde (ER to Golgi) and retrograde (Golgi to ER) traffic in plants. As mentioned earlier, COPII coated vesicles play a crucial role in anterograde transport. The important key players to mention are the GTPase SAR1 and its exchange factor SEC12 [24]. An *Arabidopsis* SAR1 mutant that preferentially binds GTP caused accumulation of Golgi markers in the ER as well as the vacuolar marker sporamin and the storage protein phaseolin [25, 26, 27]. Further, RAB-D2a has been implicated in ER to Golgi transport as its dominant negative mutant significantly slowed down the recovery of Golgi-localised sialyl-transferase (ST-GFP) after Brefeldin-A (BFA) treatment [28].

COPI coated vesicles, on the other hand, have been implicated in Golgi to ER traffic as COPI vesicles, ADP-Ribosylation Factor 1 (ARF1) GTPase and COPI proteins have been found at the cis-Golgi [29, 30]. In Tobacco plants, ER-resident calreticulin and secretory α-amylase fused to HDEL were found in COPI vesicles [29]. The dominant negative mutant of ARF1 was shown to affect the ER to Golgi traffic, reminiscent of BFA action. Therefore, it is suggested that ARF1 is involved in COPI vesicle formation as carriers of Golgi to ER retrograde transport [25, 31].

1.3.3 Post-Golgi traffic

The Golgi apparatus is the major sorting organelle in plants. Several trafficking pathways diverge from the Golgi to the PM and a variety of vacuoles.

The default secretory pathway of soluble cargo to the PM is channelled through the *trans*-Golgi [32]. The exact mechanism or signalling components involved in PM targeting are not known. However, syntaxins and SNAP25 homologues, including PEN1 (SYP121) and its Barley orthologue ROR2, have been localised to the PM as well as SYP122, which is involved in pathogen response [33, 34, 35]. Other *Arabidopsis* PM proteins, such as the auxin efflux carriers PIN FORMED 1 (PIN1) and PIN2 and the auxin influx carrier AUXIN RESISTANT 1 (AUX1) have been assigned to specific sub-domains of the PM [36, 37, 38].

Vacuolar pathways can be divided into three routes: traffic to the protein storage vacuole, traffic to the lytic vacuole and retrograde transport from pre-vacuolar compartments (PVC). In order to target a protein for vacuolar transport, it must have one out of three sorting signals: a cleavable signal at the amino- or carboxy-terminal end or a region within the mature protein [39]. Amino-terminal signals are recognised by the vesicle sorting receptor (VSR) binding protein of 80kD (BP80) which mediates packaging of cargo into clathrin-coated vesicles for transport to the PVC and vacuolar compartments [40]. Vacuolar storage proteins, however, typically have a carboxy-terminal sorting signal or a signal within the mature protein and are transported via Golgi-derived vesicles as opposed to clathrin-coated vesicles [41]. Retrograde traffic from the PVC is necessary to recycle vacuolar sorting receptors to the *trans*-Golgi after they release their cargo into the PVC [42].

1.3.4 Endosomal traffic

Endosomal traffic encompasses both endocytic and biosynthetic pathways and controls protein composition of the PM and how the plant reacts to extracellular stimuli by sorting of signalling receptors, transporters and other PM proteins. PM proteins are either continuously endocytosed and recycled (sorting back to the PM *via* retromer) or directed to the vacuole for degradation (with the help of endosomal sorting complex required for transport (ESCRT) complexes). Endosomes coordinate recognition, concentration and packaging of cargo proteins *via* multiple trafficking routes. The trans-Golgi network (TGN) takes a central position in endosomal trafficking [43, 44, 45, 46].

1.3.5 Endocytosis

Signalling from the PM is regulated by endocytosis, a process by which receptors and extracellular material are internalised and sorted by a variety of membrane trafficking pathways [47, 48]. Plant endocytosis remained a highly controversial topic for many years [49, 50, 51]. However, the styryl dyes FM1-43 and FM4-64 have been used to confirm and study plant endocytosis. These dyes insert into the outer lipid bilayer of the PM and are trafficked through the cell until they reach the vacuolar tonoplast [52, 53].

The best characterised receptors in plant endocytosis are the leucine-rich repeat receptor like kinases (LRR-RLK), BRASSINOSTEROID-INSENSITIVE 1 (BRI1), and FLAGELLIN-SENSITIVE 2 (FLS2, also FLAGELLIN SENSING 2). BRI1 is involved in plant development by perceiving brassinosteroids and undergoes constitutive endocytosis [54, 55]. FLS2 is involved in plant defence response and is internalised after binding its ligand, the bacterial flagellin peptide flg22 [56]. Both BRI1 and FLS2 share a common co-receptor, the LRR-RLK, BRI1-ASSOCIATED RECEPTOR KINASE 1 (BAK1). It appears, BAK1 is a positive regulator for signalling of both BRI1 and FLS2. It is required for FLS2 endocytosis [55, 57]. Overexpression of BAK1 leads to increased intracellular accumulation of BRI1 in protoplasts, suggesting a role for BAK1 in BRI1 trafficking [55], however, this finding cannot be reproduced in intact plants [58].

The function of plant receptor like kinases is regulated by autophosphorylation, oligomerisation, and transphosphorylation [59, 60].

1.3.6 Traffic during cytokinesis

Plant cytokinesis starts from the center of a cell to the periphery and is aided by the phragmoplast, a dynamic entity of the cytoskeleton, which delivers membrane vesicles to the division plane [61, 62]. A network of tubular membranes is formed by homotypic vesicle fusion that leads to the formation of a disk-shaped structure, the cell plate, a unique feature of plants [62, 63]. Vesicles are targeted to the margins of the cell plate, which grows to the cell periphery until it fuses eventually with the PM [64]. The accumulation of PM proteins such as PIN1 and KORRIGAN (KOR) suggest that trafficking to the division plane is the default pathway in dividing cells [65, 66].

Cell plate formation presumably arises from vesicle fusion as *Arabidopsis* mutants lacking the

cytokinesis-specific syntaxin KNOLLE or its interactor KEULE accumulate unfused transport vesicles [67, 68, 69].

1.3.7 Polar auxin transport

Plants maintain developmental continuity and adapt their development according to environmental factors by regulating cell polarity, a process involving cell division, differentiation, cellular signalling and intercellular communication. Cell polarity is reflected not only at tissue and organ levels but is also visible in the overall shape of the organism.

A crucial mediator for tissue and organ polarity is the plant hormone auxin (also known as IAA or indole-3-acetic acid). It was discovered in 1926 by Went [70] following experiments carried out by Darwin (1880), Fitting (1907), Boysen-Jensen (1913) and Paal (1919) on plant phototropism.

PIN proteins: regulators of polar auxin transport

PIN proteins are PM localised auxin efflux carriers with mostly polar localisation [71] and are key regulators of auxin-mediated developmental processes. They are involved in the regulation of tropic growth [72, 73, 74, 75, 76], axis formation in embryogenesis [77], postembryonic organogenesis [78, 79], root meristem maintenance [80, 81], and vascular tissue differentiation and regeneration [82, 83].

There are a total of eight members in the PIN family of *Arabidopsis,* most of which display different polarity in the various cell types that reflects the direction of auxin transport [84].

The probably best studied representatives of the PIN proteins are the apically localised PIN1 and basally localised PIN2. After the *de novo* synthesis, both are initially delivered to the PM in a nonpolar fashion before their apical or basal polarity is then established by internalisation from the PM and polar recycling [85].

Brefeldin-A inhibits PIN cycling

PIN trafficking is sensitive to Brefeldin-A (BFA), a fungal toxin that has been widely used to study membrane traffic, more specifically protein cycling dependent on endosomes [37, 65]. Treatment with BFA causes formation of 'BFA bodies' in *Arabidopsis* root cells as early as

30 minutes after treatment with a concentration of 50μM BFA. These BFA bodies consist of an accumulation of early endosomal compartments in its core that are surrounded by Golgi stacks. BFA is known to inhibit cycling of proteins between PM and the TGN *via* endosomes in *Arabidopsis* [86]. However, differential effects between plant species and tissues have been described [87, 88] and are listed in table 1.1.

Table 1.1: BFA effects are plant and tissue specific.

Plant species	**Tissue**	**Effect of BFA on Golgi and TGN**
Tobacco	all tissues	Golgi cisternae are redistributed in the ER, formation of BFA compartments arise from TGN material
Arabidopsis	roots	BFA compartments consist of an aggregation of TGN material in the BFA core, surrounded by Golgi stacks
Arabidopsis	cotyledons	BFA compartments consist of an aggregation of TGN material in the BFA core, surrounded by Golgi stacks
Arabidopsis	true leaves	Golgi cisternae are redistributed in the ER, formation of BFA compartments arise from TGN material

A major target of BFA is the ADP-Ribosylation Factor Guanine nucleotide Exchange Factor (ARF-GEF) GNOM, an exchange factor for ARF GTPases [89]. ARF-GEFs are regulators of vesicle formation and are required for the GDP to GTP exchange step that drives activity of GTPases [86]. GNOM is implicated in a lot of trafficking events, such as polar cycling of PIN1 [89] and PIN2 [90] and thereby involved in polar auxin transport. Additionally, GNOM is required for focal accumulation of PEN1 [91], which is required for innate immune responses in fungal attack. It appears GNOM is a more crucial factor for apical polar targeting. Kleine-Vehn and colleagues showed that the apical PM localisation of PIN proteins and AUX1 is not strongly affected when GNOM function is inhibited [90], indicating that apical cargos may use a different targeting pathway.

PIN1 was shown to localise in these BFA bodies upon BFA treatment, even when *de novo* synthesis was inhibited. This internalisation is completely reversible and indicates constitutive endocytosis and recycling of PIN proteins [37]. Bilou and colleagues (2005) [92] showed that prolonged BFA treatment causes a shift of PIN2 localisation from the basal to the apical membrane, a process called 'transcytosis'. Transcytosis describes a process in which the localisation of a polar protein is shifted *via* recycling endosomes and provides a mechanism for rapid changes in PIN polarity in response to various signals, such as developmental [82, 83] or environmental signals [76, 93]. Transcytosis is also a well known mechanism for polar delivery

of cargos in animal cells [94, 95].

It appears that the trafficking pathways for polar PIN delivery are highly diverse. Interestingly, while polar PIN targeting is dependent on the actin cytoskeleton in interphase cells, in dividing cells, PIN proteins are delivered to the forming cell plate by the microtubule-dependent pathway [37, 96].

1.4 Rab GTPases as membrane traffic regulators and tools to study membrane traffic

As mentioned earlier, one of the key regulatory protein families for membrane traffic is the Rab family of small GTPases, which contribute variously to the specification of membrane identity, the acuracy of vesicle targeting and the recruitment of molecular motors to membranes. Rab GTPases are molecular switches that undergo a regulated cycle between inactive GDP- and active GTP-bound forms (figure 1.4). They cycle on and off particular endomembranes where they provide transient interaction surfaces for recruitment of effector proteins or complexes. Rab effectors are diverse and can include tethering factors, enzymes of phosphatidyl-inositiol metabolism, myosins, kinesins, and regulators of SNARE protein assembly.

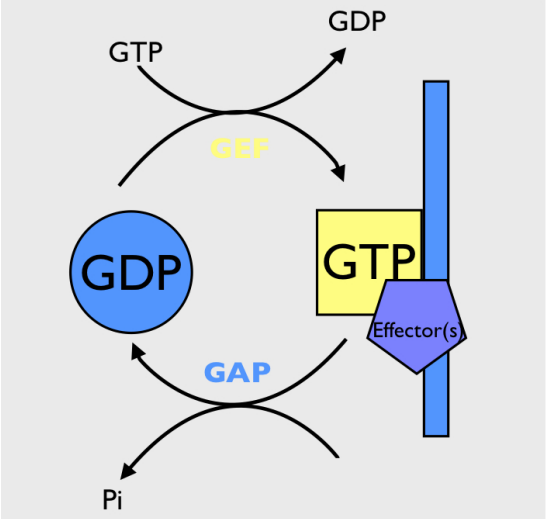

Figure 1.4: Rab activity cycle: Rab proteins cycle between an inactive GDP- and an active GTP-bound state. The GTP to GDP exchange is catalysed by GEF. GTP-bound Rabs are recruited to their target membrane where they recruit effectors to the membrane or interact with effectors already present at the membrane. GTP hydrolysis is achieved by action of the GAP protein.

1.4.1 Structure of Rab GTPases

The topological structure of Rab proteins is highly conserved and consists of β-strands and α-helices with conserved cysteine residues near the carboxy-terminus [97, 98]. Binding of either GDP or GTP induces conformational changes that are localised in the two switch regions. These switch regions are highly exposed on the surface on the protein and act as recognition sites for effectors [97, 99, 100]. Several mutations have been identified that affect the GTPase cycle (see figure 1.5) and lead to constitutively-active or dominant-negative proteins [101]. Targeting of Rab proteins is accomplished through sequence motifs in the hypervariable domain [102].

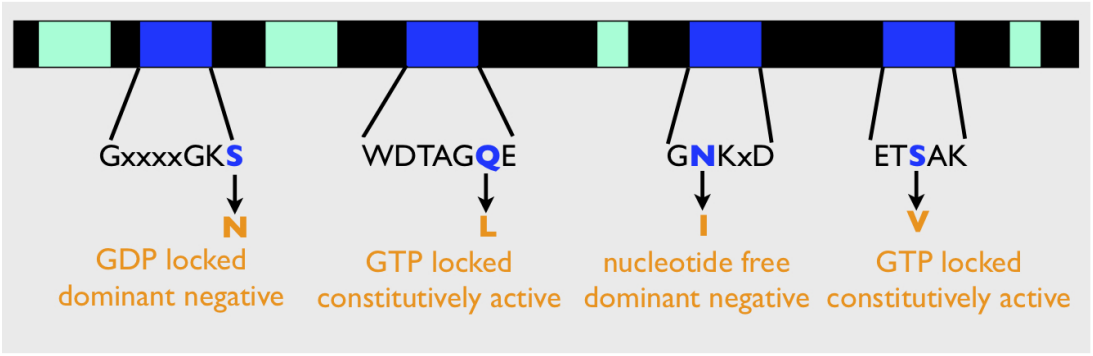

Figure 1.5: Graphical representation of typical Rab sequence. Green boxes represent sequence motifs that are conserved within structural sub-clades of plant Rab proteins, blue boxes are sequence motifs conserved amongst all Rabs. The one-letter amino acid code below these boxes show mutations that keep Rab proteins in a preferentially GTP-bound ('GTP locked'), GDP-bound ('GDP locked') or nucleotide free conformation.

1.4.2 Regulation of Rab GTPases

Membrane localisation of Rab proteins is achieved by their post-translational prenylation with usually two geranylgeranyl moieties on their C-terminal cysteine [103, 104] catalysed by the RabGGTase (Rab geranylgeranyl transferase) [105]. RabGGTase consists of two tightly associated α and β subunits and recognises its substrate only in association with the Rab escort protein (REP). First, a heterodimeric complex of Rab, preferably in the GDP-bound form, and REP is formed in the cytoplasm. The Rab-REP complex then binds to the RabGGTase in a geranylgeranyl pyrophosphate (GGPP) dependent manner which increases the GGTase affinity to the Rab-REP complex. REP is also able to bind to GGPP without the Rab protein to form a pre-activated complex. Mutant Rabs partially or completely lacking prenylation motifs inhibit the activity of the RabGGTase[105].

An *Arabidopsis* REP was identified by performing a Basic Local Alignment Search Tool (BLAST) search in the *Arabidopsis* genome using yeast and mammalian REP protein sequences. GST-*Ath*REP was pulled-down with 6-His-Ypt1 and 6-His-*Nta*RabA1a preloaded with GDP. *Ath*REP-6His also does bind to the AthRabA2a GTP-bound form but still binds preferably to the GDP-bound form. *Ath*REP and the geranylgeranylation activity is localised to the cytoplasm in plant cells. Geranylgeranylation activity was stimulated by addition of *Ath*REP-6His in *Arabidopsis* and BY-2 extracts 2.5- to 5-fold. AthREPs were unable to stimulate RabGGTase activity in vitro when added to the extract prepared from the mrs6-2 yeast strain mutated in a gene coding for yeast REP indicating that the plant REP maybe unable to cooperate with the yeast RabGGTase core complex. The reciprocal experiment revealed that the yeast REP (*Sce*Mrs6) was able to increase GGTase activity two-fold [105]. Sequence analysis revealed a conserved substitution of the *Sce*Mrs6 R198 in angiosperms. When mutating the corresponding amino acid in *Ath*REP [N188R] and transforming it into the mrs6-2 yeast strain, growth was restored. This indicates that the substitution of arginine at this position is an important condition for plant-specific features of the REP molecule [105].

The GDP-bound form of the protein exists predominantly in the cytosol in a complex with Rab GDI (GDP-Displacement Inhibitor), which masks the prenyl-groups. Rabs are recruited to membranes by interaction with Rab GDI-displacement factors; then specific nucleotide exchange factors convert the protein to the GTP-bound form, which is insensitive to removal by GDI and can recruit effectors. GTPase activating proteins (GAPs) stimulate the intrinsic GTPase activity of the Rab protein thus returning it to its inactive GDP-bound form which is removed from the membrane by GDI [103, 106]. GDI orthologues between major eukaryotic lineages were identified by sequence analysis and turned out to be highly conserved throughout their whole length. Phylogenetic analysis separated GDIs clearly from REPs but the similar structure of both suggest a common progenitor of the whole superfamily. It is proposed that a bi-functional REP/GDI protein is the likeliest evolutionary precursor rather than a REP or GDI alone [105].

PRA1 (prenylated rab acceptor 1) proteins have been shown to regulate vesicle trafficking as receptors of Rab GTPases and the v-SNARE vesicle associated membrane protein 2 (VAMP2) in mammalian cells [107, 108]. In plants, little is known about the PRA1 family members [109, 110]. It has been shown that a PRA1 related protein in plants interacts with the Cauliflower Mosaic Virus (CaMV) movement protein [109]. The *Arabidopsis* PRA1 family

consists of 19 members, identified by BLAST and HMMER analysis, comparing six species with complete genome sequences (*Arabidopsis,* poplar, rice, moss and two green algae). The 19 members can be grouped into eight clades (A to H). It was shown by yeast-two-hybrid based interaction analysis that most of the PRA1 proteins were able to form homo- and heterodimers. GUS expression was frequently observed in vascular tissues. Four PRA1 genes (PRA1.B5, PRA1.B6, PRA1.D and PRA1.E) were expressed in leaf veins, with expression of PRA1.B6 being restricted to young leaf veins. PRA1.F3 shared a common distribution with other AtPRA1 gene in regions of lateral root initiation but not in vascular tissues. In roots, GUS staining was frequently observed at the lateral and/or the columella cells of the root cap. PRA1.B5, PRA1.B6, PRA1.D and PRA1.E expression was detected in both regions, while expression of PRA1.B4 and PRA1.E was restricted to the lateral and the columella root cap cells. In aerial tissues, expression of PRA1 genes was detected in trichomes, stomata, shoot apex and the leaf basis. Comparison of gene expression profiles reveald co-expression of PRA1 genes with Rab GTPases. As a general distribution most PRA1 proteins localise to vesicular structures often associated with a light network of ER strands (PRA1.A2, PRA1.A3, PRA1.B1, PRA1.B2, PRA1.B3, PRA1.B4, PRA1.B5, PRA1.D, PRA1.E, PRA1.F1, PRA1.F2, PRA1.F4 and PRA1.G1). Representatives from different clades were selected to investigate these structures. Analysis of PRA1.A2, PRA1.B5, PRA1.D, PRA1.E, PRA1.F1 and PRA1.G1 showed localisation to endosomal compartments using FM4-64. PRA1.A1, PRA1.B6, PRA1.C and PRA1.H showed clear localisation to the ER. Members of clades D and F entirely colocalised with RAB-F2b. B-clade members were more distributed to the Golgi than members of other clades. None of the analysed PRA1 proteins resided entirely in the Golgi [110].

Direct interaction of PRA1 members and Rabs could neither be shown by yeast-two-hybrid nor by tandem affinity purification [110].

1.4.3 Classification of Rab GTPases

The *Arabidopsis* Rab GTPase family contains 57 members, which can be divided into eight clades, designated A to H. Sequence analysis suggests that these eight clades can be further sub-divided into structural subclasses that reflect different functions [111].

Genomic data have shown that yeasts, metazoans, and higher plants have each elaborated distinct sets of Rab proteins. *Arabidopsis* and mammals each have roughly 60 Rab GTPases compared to the six to ten that are found in yeasts, but it is striking that 80% of the predicted

mammalian Rab GTPase subclasses are missing in *Arabidopsis* [111, 112, 113]. The diversity of the Rab GTPase family in mammals relative to that of yeasts appears to reflect the greater complexity and diversity of membrane trafficking events that occur in the diverse cell types of mammals [7, 114]. The situation is less clear in angiosperms where phylogenetic analysis has shown that all 57 *Arabidopsis* Rab sequences fall into just eight clades (Rab-A to Rab-H) that form the basis of a systematic nomenclature for plant Rabs [112]. Each of the eight higher plant clades is clearly related either to one of six Rab subclasses that are common to yeasts, animals, and plants or to mammalian Rab2 or Rab18 [111, 113], both of which are missing from yeasts. Rice and basal lineages also contain at least one homologue of mammalian Rab21 [115]. Homologues of an additional mammalian subclass, Rab23, which is implicated in cilliary or flagellar function have been identified in basal land plant basal lineages, correlating with the presence of flagellated sperm [116]. Analysis of specificity-determining regions of Rab GTPases [112, 117] suggest that several plant Rab clades may have diversified to the extent that they may contain functionally distinct proteins [111, 112]. If so, it would mean that the Rab GTPase family has undergone distinct adaptive radiations in mammalian and angiosperm lineages and that many Rab subclasses in *Arabidopsis* are plant-specific [111].

In the following sections I will describe the current understanding of the *Arabidopsis* Rab GTPases in membrane traffic.

1.4.4 The Rab-A clade

With 26 out of 57 Rab GTPase members, this is the largest of all eight *Arabidopsis* Rab clades. The clade is further subdivided into Rab-A1 (nine proteins), Rab-A2 (four proteins), Rab-A3 (one protein), Rab-A4 (five proteins), Rab-A5 (five proteins), and Rab-A6 (two proteins) [111].

RAB-A1a colocalises with FM4-64 in *Arabidopsis* roots and is thus an endosomal compartment. A *rab-A1a* T-DNA insertion line displays increased primary root elongation and lateral root branching, especially in medium containing low levels of auxin. Plants overexpressing RAB-A1a exhibit decreased root elongation, especially under high auxin concentrations, and almost no lateral root branching at lower auxin concentrations. Further, the expression of RAB-A1a is induced following the presence of auxin but the induction of auxin responsive genes, such as IAA12 or IAA17 is not detectable in *rab-A1a* plants. Thus, RAB-A1a function may be necessary for auxin homeostasis [118].

RAB-A1b (BEX5) localises to the TGN and early endosomes and is involved in TGN to PM trafficking of PM cargos, such as PIN1:GFP, PIN2 and GFP:PIP2a. This link was discovered through a forward genetic screen for *Arabidopsis* mutants that showed increased intracellular accumulation of PIN1 in response to the trafficking inhibitor BFA. *bex5* is hypersensitive to BFA and is defective in PM traffic as shown by absence of recovery of PM traffic after BFA washout. However, even though endosome morphology is reportedly abnormal in *bex5,* the PM labelling of PIN1:GFP and PIN2:GFP appears intact and comparable to wild type [119].

It was recently shown that RAB-A1c localises to an Endosidin 1 (ES1) sensitive population of the TGN, partially overlapping the VHA-a1 domain and is believed to play a role in cytokinesis as it localises to the cell plate in dividing cells [120]. Further, it is speculated that RAB-A1c is indirectly involved in auxin-mediated responses as ES1 is known to block trafficking of PIN2 and AUX1. This is also observed in TRAPPII mutants, a protein complex that acts upstream of RAB-A1c [120].

RAB-A4b accumulates at a putatively novel *trans*-Golgi compartment at the young root tip that is labelled by neither Golgi nor TGN markers. In mature root tip cells, RAB-A4b spread thinly around the edge of the cell or accumulated in compartments in the base of the cell [121]. It was shown to interact with the N-terminal region and a Δ1-421 truncation variant of PI-4Kβ1 (a phosphatidyl-inositol 4-OH kinase) in a yeast-two-hybrid assay, but not with the full length PI-4Kβ1 protein. Both PI-4Kβ1 truncations colocalise to tip-localised membranes of growing root hairs that are distinct from the Golgi. Disruption in either the PI-4Kβ1 or the PI-4Kβ2 gene results in aberrant root hair morphogenesis and results in morphologically altered RAB-A4b labelled TGN compartments. This result indicates that PI-4Kβ1/ PI-4Kβ2 activity is necessary for proper organisation of the TGN and post-Golgi secretion. Further, tip localisation of RAB-A4b is disrupted by collapsing the tip-focused Ca^{2+} gradient in root hair cells which could mean that RAB-A4b and PI-4Kβ1 function is required during polarised root expansion [121]. Distribution of RAB-A4b varies in *rhd4-1* mutant lines, which are defective in root development (short, bulged, branched root hairs). *rhd4-1* root epidermal cells also show altered actin-filament organisation (more actin patches, thinner filament). RHD4 is a Sac1p-like phosphoinositide phosphatase that is suggested to regulate either proper distribution and/or accumulation of tip-localised RAB-A4b compartments during polarised growth in root cells and it may play a role in coordinating delivery of cell wall material to the tips of root hairs. RAB-A4b colocalises with RHD4 in the tips of root hairs in compartments that are

distinct from the Golgi and the ER but colocalise in post-Golgi / TGN [122]. EYFP:RAB-A4b localises to the tips of growing root hairs, a process regulated by intracellular calcium gradients, but disappears in mature root hair cells that have stopped expanding; application of defensins causes rapid dissipation of the EYFP:RABA4b at the apical tip of the root hair and a concomitant cessation of root hair elongation. However, EYFP:RAB-A4b gradient is re-established after antifungal proteins were removed [123].

Involvment in cytokinesis

The Rab-A2/A3 compartment has been placed on the biosynthetic secretory pathway from Golgi to PM by Chow and colleagues [45]. Endogenous and tagged RAB-A2a is present at the PM and a mutant form of RAB-A2a, which is predicted to be GTPase-deficient accumulates exclusively there. Conversely, the S26N and N125I mutants that are predicted to stabilise the interaction with the exchange factor distribute between the Golgi and the Rab-A2/A3 compartment. The Rab-A2/A3 compartment and the overlapping VHA-a1 compartment have been identified as the sites at which newly synthesised KNOLLE protein accumulates during mitosis [45, 124]. Using protein synthesis inhibitors Dettmer and colleagues [124] provided evidence that the VHA-a1 compartment accumulates biosynthetic and endocytosed proteins and thus lies on both pathways [43]. The compartment in mammalian cells that most closely resembles the Rab-A2/A3 compartment is the recycling endosome which also resides on the secretory and endosomal pathways [125].

RAB-A homologues in yeast and mammalian cells

The mammalian subclasses in the Rab-A clade, Rab11 and Rab25, localise to the recycling endosome where they regulate traffic to specific PM domains and to the TGN in various cell types [125]. The recycling endosome receives slowly recycling material from early endosomes but also receives a subset of secreted proteins from the TGN. Thus, it represents an intersection of secretory and recycling pathways. In polarised epithelial cells, Rab11A and Rab25 are spatially segregated from Rab11B [125]. The paralogous *S. cerevisiae* Rab proteins Ypt31 and Ypt32 promote exit of secretory cargo from the late Golgi and are required for traffic from the Post-Golgi Endosome (PGE) to the late Golgi compartment [126, 127, 128]. The PGE acts as an early endosome in yeast [126, 129] and shares several markers such as the V-ATPase subunit Stv1 and the SNARE Tlg2 with late Golgi compartment [130].

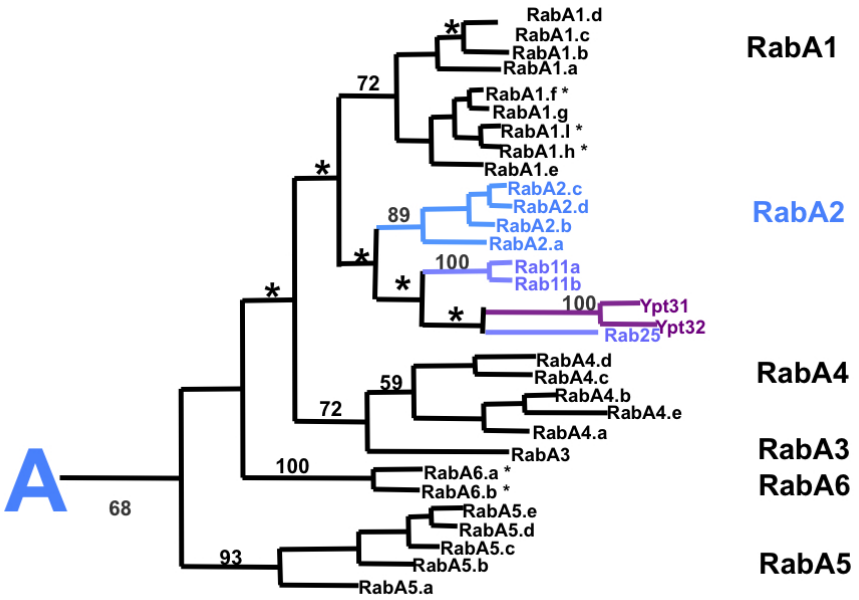

Figure 1.6: The Rab-A clade of *Arabidopsis* and its homologues in mammals and yeast. Numbers indicate bootstrap values, asterisks indicate nodes with bootstrap support of less than 50% (Tree was constructed by Dr Ian Moore).

1.4.5 The Rab-B clade

The Rab-B clade comprises only three members: Rab-B1a, Rab-B1b and Rab-B1c [111].

Moore *et al* (1997) speculate on an involvement of RAB-B in ER to Golgi traffic as the observed GUS expression patterns of RAB-B corresponded to the requirements of certain plant cell types that undergo rapid growth and/or membrane biogenesis where ER to Golgi traffic is particularly important. These cell types were mostly pollen and vascular tissues of vegetative and floral organs, but expression was also found to a lesser extent in root cells [131].

The tobacco homologue RAB2 is implicated in ER to Golgi transport. GFP:RAB2 associates with Golgi bodies in tobacco pollen tubes and the expression of a dominant negative mutant substantially decreased the delivery of GFP labelled Golgi proteins while their ER and cytoplasmic signals were increased, suggesting a role for RAB2 in an early secretory pathway [132].

1.4.6 The Rab-C clade

The Rab-C is another very small clade with the three members Rab-C1, Rab-C2a and Rab-C2b [111].

Rab-C proteins have not yet been well studied in *Arabidopsis.* The only information available is that RAB-C1 transcript is induced two hours earlier in BABA-treated (β-aminobutyric acid, amino acid) plants compared to non-induced control plants [133] and that its transcript is also induced by the application of ABA (aminobutyric acid) [134].

The mammalian homologue of *Arabidopsis* Rab-C proteins, Rab18, is crucial for ER to Golgi traffic [135]. The overexpression of Rab18 wild type protein causes dispersal of the Golgi complex and reduces the secretion of the secretory marker VSVG:GFP in HeLa cells. The same effect was achieved by directing three siRNAs against Rab18. Expression of the CFP:Rab18(S22N) enhances retrograde Golgi-ER transport and also potentiates BFA-induced ER-Golgi fusion [135].

1.4.7 The Rab-D clade

The Rab-D clade comprises four members: Rab-D1, Rab-D2a, Rab-D2b and Rab-D2c [111].

Rab-D2a was shown to participate in ER to Golgi transport as evidenced by tobacco infiltration experiments where the dominant negative mutant of Rab-D2a caused the accumulation of secreted GFP in the ER [32].

1.4.8 The Rab-E clade

The Rab-E clade has five members: Rab-E1a, Rab-E1b, Rab-E1c, Rab-E1d and Rab-E1e [111].

RAB-E1a was shown to interact with agrobacterial VirB2 which is a major component of the Type 4 Secretion System (T4SS) pilus of *Agrobacterium tumefaciens.* However, other components of the T4SS of *A. tumefaciens* do not interact with RAB-E1a. Rab-E1d antisense plants show reduced susceptibility to transformation indicating its importance for agrobacterium-mediated root transformation [136].

secGFP is used to study a possible default route of transport from the ER to the apoplast. Under conditions that inhibit biosynthetic traffic to the apoplast, secGFP protein accumulates

inside the cells and can be visualised in the endomembrane compartments. Coexpression of secGFP with wild type RAB-E1d does not change the localisation of secGFP as it appears unaltered relative to secGFP alone. The presence of dominant negative RAB-E1d (RAB-E1d[NI]) results in increase of GFP fluorescence and intracellular accumulation which suggests secGFP traffic to be inhibited by RAB-E1d[NI]. Presence of RAB-E1d[NI] also increases the number of fluorescent cells and the proportion of cells that accumulate GFP in punctate structures as well as in the ER. In the presence of RAB-E1d[NI], YFP-HDEL (an ER marker) colocalised with secGFP in the ER retrieval pathway but not in the punctate structures. These post-ER secGFP punctate structures colocalise with ST-YFP (a Golgi marker) and RAB-F2b, which is known to localise predominantly to the PVC. RAB-E1d appears not to affect traffic to the vacuole along the ER-Golgi-PVC pathway as distribution of spo:GFP is not altered when co-expressed with RAB-E1d[NI]. It is suggested that RAB-E1d[NI] acts specifically in the late secretory pathway to the apoplast. A portion of secGFP can also be transported to the vacuole but this transport is not inhibited by RAB-E1d[NI] but appears to increase the proportion of secGFP that accumulates in the vacuole relative to the cell wall. Localisation of secRFP to the ER and the apoplast but not to the PVC reveals that the default pathway to the apoplast does not involve the RAB-F2b positive PVC and that secGFP might carry a cryptic vacuolar sorting signal. In comparing these results to data gained through investigation of RAB-D2a (dominant negative RAB-D2a inhibits ER to Golgi traffic) it is suggested that RAB-E1d acts downstream of the Rab-D subclass [137].

An interactor of RAB-E1d, PIP5K2 (phosphatidylinositol-4-phosphate 5-kinase 2) has been described by Camacho *et al.* Rab-E proteins interact with PIP5K2 via its MORN (membrane occupancy and recognition nexus) domain and it is proposed that this interaction may stimulate temporally or spatially localised PtdIns(4,5)P(2) production at the PM [138].

1.4.9 The Rab-F clade

The Rab-F clade has only three members: Rab-F1, Rab-F2a and Rab-F2b [111].

RAB-F1 and RAB-F2b may be functionally equivalent (92% sequence identity) in respect to vacuolar trafficking; S24N mutants of RAB-F1 show inhibition of vacuolar trafficking and localisation experiments show that RAB-F1 compartments reside at the PVC. [26]

Lee *et al* (2004) showed the localisation of RAB-F2a and RAB-F2b to the PVC. S24N, T24A

and [C198S, C199S] mutants give diffuse GFP signals. The Q69L mutant exhibits strong GFP signals at the tonoplast of the central vacuole [139].

RAB-F2a and RAB-F2b colocalise to the same punctate subpopulations labelled by FM4-64. RAB-F1 only partially overlaps with RAB-F2a/F2b; this may reflect partially overlapping but different populations of endosomes. Colocalisation of RAB-F1 can be observed with the SNARE proteins SYP21 and SYP22 both of which label the PVC. Therefore it is suggested that RAB-F1 acts at a later stage of the endocytic pathway because SYPs are reported to function in membrane fusion in late endosomes and/or the vacuole in the vacuolar transport pathway. GFP:AtVAMP727 colocalises with RAB-F2a and RAB-F2b which suggest that they represent an earlier compartment that is important for recycling to the PM [140].

In *gnom* mutants RAB-F2b positive endosomes lose their punctate shape and appear as larger patches or clustering ring-like structures, which suggests that RAB-F2b positive endosomes are the site of GNOM dependent recycling of PM proteins such as PIN1. RAB-F2a and VAMP727 also colocalise on those abnormally deformed endosomes. RAB-F1 was found less frequently on those endosomes. GFP:SYP41, GFP:SYP21 and GFP:SYP22, GFP:SYP31 show same localisation in *gnom* mutant as in wild type which suggests that RAB-F2b, RAB-F2a and VAMP727 are mainly residing in the sole place where GNOM-dependent recycling takes place [140].

VPS9a (important for embryo development) can activate all three Rab5 members to their GTP-bound forms despite their diverged structures. Yeast-two-hybrid experiments showed that VPS9a interacts with the [S24N] and the [N123I] RAB-F2a mutant forms but not with the wild type and the [Q69L] mutant form. Further, it interacts with the [S24N] and the [N123I] mutant form of RAB-F1 but not with the wild type or [Q93L] mutant. In *vps9a-2* plants, which are defective in root elongation, RAB-F2b[Q69L] but not RAB-F1[Q93L] suppresses this defect. GFP:RabF2b and RabF1:GFP show diffuse localisation in mutant embryos (punctate localisation in wild type plants) therefore VPS9a seems to be the activator for RAB-F1 and RAB-F2b [141].

Rab-F proteins have been mainly described in the context of vacuolar or pre-vacuolar traffic but have also been implicated in endocytic transport pathways. The human transferrin receptor (hTfR), for example, is found mainly in RAB-F2b endosomal compartments but also on the PM. Treartment with BFA leads to the accumulation of hTfR and transfer into larger patches inside the cell. Ortiz-Zapater *et al* conclude that hTfR may cycle between the PM and endo-

somes and used this model to investigate receptor mediated endocytosis [142]. Interestingly, the AAA ATPase SKD1, which is required for endosomal sorting of secretory and endocytic cargo, partially colocalises on MVBs with RAB-F1, RAB-F2a, RAB-F2b and FM4-64 [143]. The boron transporter BOR1 is a PM transporter which is endocytosed upon binding boron. It colocalises with RAB-F2b in dot-like structures in high-boron containing medium. BOR1 is transported to and degraded in the vacuole in high-boron conditions [144].

Jaillais *et al* [145] described the colocalisation of RAB-F1 and RAB-F2b with Sorting Nexin 1 (SNX1) which is involved in the auxin pathway. Dhonukshe *et al* [96] observed cytokinesis defects in plants expressing a dominant negative mutant form of RAB-F2b.

RAB-F1 colabels with sterol containing BFA-induced compartments. Cytochalasin D causes co-accumulation of sterols and RAB-F1 in small intracellular compartments and colocalisation of FM4-64 with RAB-F1. Both, BFA and cytochalasin D observations, were reversible after drug washout. Cytochalasin D treatment after BFA-treatment inhibited sterol redistribution from BFA compartments, therefore sterol redistribution requires the actin cytoskeleton [38].

In tobacco, RAB-F2b partially colocalises with the Golgi marker ST-YFP. The S24N mutant labels the cytosol and colabels with ST-YFP in punctate structures. The RAB-F2b[Q69L] mutant colocalises with the tonoplast marker BobTIP26-1 but not with the ER marker *Nt*AQP1. The N123I and [C198, 199S] mutants appear entirely cytosolic. Further, RAB-F2b colocalises with PS1 (a peaBP80 construct) which suggests localisation at the PVC [146].

1.4.10 The Rab-G clade

The Rab-G clade comprises eight members spread across three subclasses: Rab-G1 (one protein), Rab-G2 (one protein), and Rab-G3 (six proteins) [111].

Mazel *et al* (2004) suggest that RAB-G3e is involved in induction of salt and osmotic stress tolerance. Rab-G3e was increased after treatment with high concentrations of superoxide, and induced by infection with avirulent *P. syringae* (bacteria) or *B. cinerea* (mold). No induction was seen after methyl jasmonate, cold or wounding treatment and only minor induction by salt stress. RAB-G3e overexpressing plants appear greener and show higher amount of chlorophyll at seven days after germination, accelerated flowering time, faster growth as well as longer petioles. FM1-43 uptake was faster in RAB-G3e overexpressing plants compared to wild type plants. 200mM NaCl treatment inhibited the growth of wild type and RAB-G3e overexpressing

plants, but transgenic plants were less sensitive and achieved higher fresh weight. RAB-G3e overexpressing plants accumulate sodium in the vacuole. Sorbitol treatment in transgenic plants causes less growth retardation than in the wild type [147].

Nahm *et al* (2003) investigated subcellular localisation of *Os*Rab7, a rice (*Oryza sativa*) homologue of *Arabidopsis* Rab-G. It was shown that GFP-OsRab7 is localised to the vacuolar membrane in Arabidopsis protoplasts which suggests that OsRab7 is involved in transport to the vacuole in plant cells [148]. The yeast homologue Ypt7p is involved in traffic from late endosome to the vacuole [149].

A YFP fusion protein of RAB-G3f was generated that shows localisation to PVC and vacuole [150].

1.4.11 The Rab-H clade

The Rab-H clade consists of five members: Rab-H1a, Rab-H1b, Rab-H1c, Rab-H1d and Rab-H1e [111].

RAB-H1b was shown to complement a yeast YPT6 null mutant [151]. Johansen *et al* (2008) showed that YFP:RAB-H1b and YFP:RAB-H1c localise at the Golgi and the cytosol in both *Nicotiana tabaccum* and in *Arabidopsis.* Additionally, YFP:RAB-H1b locates to another undefined compartment, not labelled by either YFP:RAB-H1c or Golgi markers; only little colocalisation could be observed with the PVC marker BP80:GFP as well as with FM4-64. The function of this GTPase is yet unclear [152]. RAB-H1b and RAB-H1c interact with the C-terminus of GC5, a golgin candidate, in a yeast-two- hybrid assay. This interaction was also confirmed by affinity chromatography and is independent of the nucleotide status of RAB-H1b and RAB-H1c [153], which might suggest a role for RAB-H1b in recruiting matrix proteins to the trans-Golgi cisternae [152].

1.5 The discovery of GFP as a tool in cell biology

The use of fluorescent proteins has revolutionised many areas of research, including membrane traffic. It took, however, a long time from its discovery until its first use in endomembrane traffic research.

In 1955 Davenport and Nicol first described the luminescence properties of the hydromedusa *Aequoria vicotria,* and found that the luminescence properties originated from the umbrella margin, which appeared as glowing points when excited with a light source of 450 - 600nm[154]. It was not until 1962 that the actual substance was isolated and first described as protein [155]. Although a lot of the properties of the now called GFP were described in 1966 [156], it took another five years for researchers to realise that this protein followed a Förster type fluorescence radiationless energy transfer [157]. In 1974 GFP was finally crystallised [158] and its structure resolved in 1979: GFP consists of 238 amino acids, its fluorophore is composed of three post-translationally modified amino acids (Ser65, Tyr66, Gly67) [159, 160].

In 1992 the gfp gene was cloned [161], another two years later it was first demonstrated that the GFP protein fluoresces upon ultra violet or blue light excitation in a heterologous organism system, in the sensory neurons of the nematode *C. elegans* [162]. The first report of its use in plant research was from Baulcombe and colleagues in 1995, where the expression of wild type GFP was achieved using cytoplasmic RNA viruses [163]. In 1996, GFP was first used in plant endomembrane research to visualise the ER and the nuclear envelope [164]. The localisation of GFP markers were validated with immunolocalisation studies and have since been increasingly used to study membrane traffic. The first plant endomembrane component to be illuminated was the ER (1996, [164]), followed by the nuclear envelope (1997, [165]), Golgi bodies (1998, [166]), the apoplast (1999, [167]), the vacuole (2000, [168]), the tonoplast (2002, [169]), and the PM (2002, [170]). The first plant Rab GTPase to be fused to GFP was RabG3e [171].

GFP exhibits remarkable stability to pH, heat, proteases and denaturating agents owing to its compact structure [172, 173]. GFP isolated from *A. victoria* has been used to engineer blue, cyan and yellow mutants, fluorescent proteins from other species have also been identified, resulting in further expansion of available colours to orange, red and far-red spectral regions [174, 175, 176, 177].

Fluorescent protein technology has enabled non-invasive imaging of protein dynamics in live cells; it can be used to monitor gene expression, label proteins, and identify oligomeric states. Photoactivable proteins allow for temporally controlled observation of proteins and thus offer an alternative to Fluorescence Recovery After Photobleaching (FRAP) or Fluorescence Loss In Photobleaching (FLIP) experiments. Further Fluorescence Resonance Energy Transfer (FRET) protocols allow for detection of protein protein interactions, helping to distinguish interactions from co-localisations [178, 179]. Fluorescent proteins can also be used to act as

genetically encoded sensors, which allow monitoring of physiological parameters, such as pH [180]. An overview of fluorescent protein techniques and its uses are given in figure 1.7.

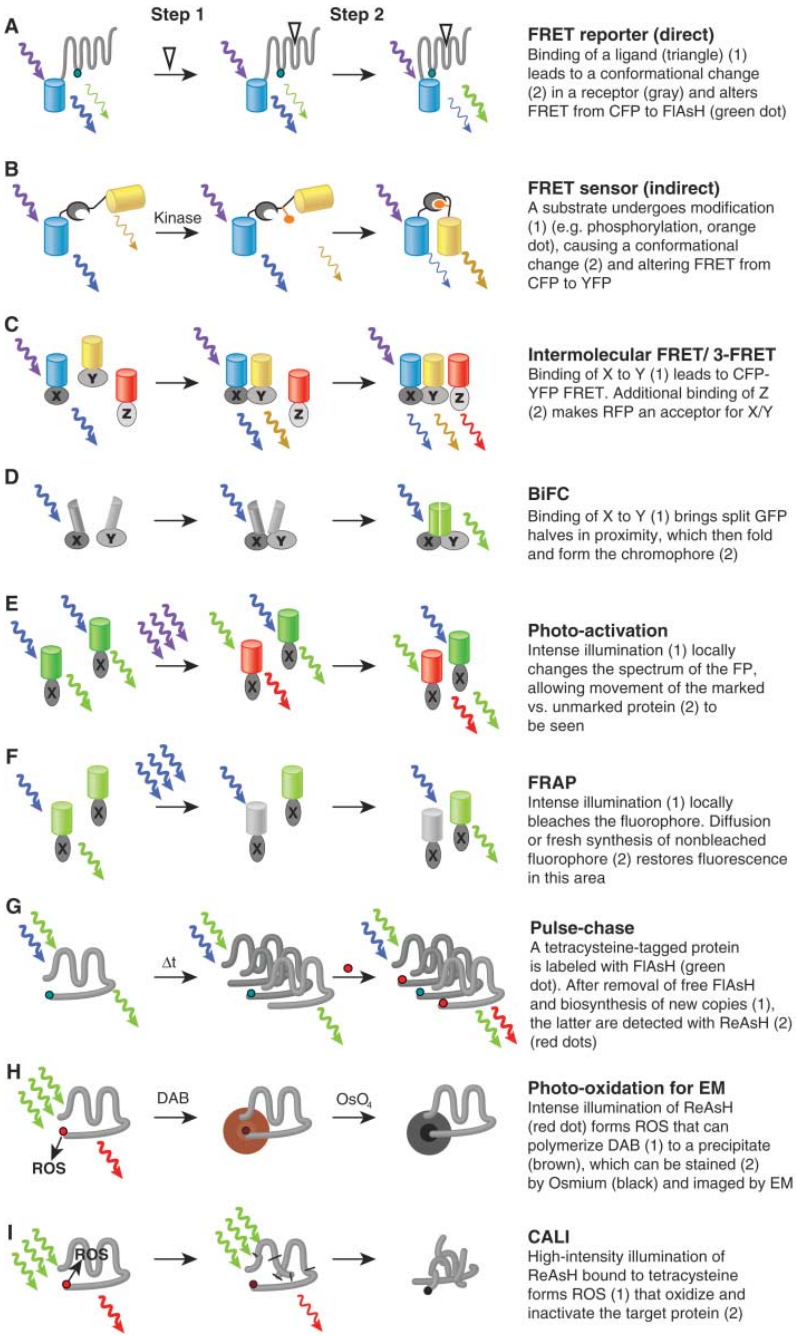

Figure 1.7: Overview of fluorescent protein techniques with genetic tags. Images A to I show principles of advanced techniques. Barrels represent fluorescent proteins. X, Y, and Z represent target proteins. Thickness of waves indicates light intensity. Descriptions are given next to the images [181].

1.6 Thesis objective

Plant membrane traffic is still poorly understood. Although some aspects of the cellular organisation are similar to other eukaryotic cells, there are some unique features, like cell plate formation that can only be studied in plants. Since plants are sessile organisms, alternative strategies are required and the underlying trafficking machinery may be different.

As mentioned earlier, Rab GTPases are key regulatory elements of membrane traffic, clearly defining organelle membranes. Therefore, studying trafficking functions of Rab GTPases will lead to greater understanding of the dynamics and organisation of the plant endomembrane system.

The *Arabidopsis* Rab-A clade consists of 26 members, which are further sub-divided into six functional subclasses, but there are only three homologues in mammals (Rab11a, Rab11b and Rab25) and two in yeast (Ypt31, Ypt32). Thus, the Rab-A clade represents a highly expanded and diversified protein group. An interesting question to address is whether this diversification represents a range of plant specific processes due to their sessile life or whether future research will discover redundancies in trafficking functions that may be attributable to an expansion due to environmental factors, such as pathogen attack.

The aim of this work is to provide an insight into *Arabidopsis* endomembrane trafficking by studying one of the 26 Rab-A family members, RAB-A2a. The early-endosomal Rab-A2/A3 compartment localises to a particularly intriguing place in the endomembrane system, the TGN, which is a central hub for endocytic and secretory traffic. A role for RAB-A2a in cytokinesis has been described [45], but it is unclear which trafficking routes are dependent on RAB-A2a function in non-dividing cells. The following chapters aim to address the following hypotheses:

1. RAB-A2a is required for default traffic to the PM. This hypothesis is supported by the localisation studies of the preferentially GDP- and GTP-bound mutants of RAB-A2a.
2. RAB-A2a is involved in protein recycling, like its mammalian homologue RAB-11.
3. RAB-A2a acts in a completely different pathway, e.g. an endocytic route that leads to the vacuole.

In the following chapters, I will address these hypotheses by utilising the dominant negative approach in conjunction with selected fluorescent protein markers.

Chapter 2

Materials and Methods

2.1 Materials

2.1.1 Plant material and growth medium

Plant material:

Arabidopsis thaliana ecotype Columbia-0 (Col-0) was used for stable transformation.

Murashige Skoog (MS) medium was prepared by dissolving Murashige and Skoog Basal Salts (Duchefa Biochemie) in distilled water (dH_2O) to a concentration of 0.43% (w/v). Sucrose (1%, w/v) was added and the pH was adjusted to 5.7 using 1M potassium hydroxide [182]. For agar plates, 0.8% (w/v) Bacto-agar was added. The medium was autoclaved at 121°C for 20 minutes. For preparation of selection medium, agar was cooled to approximately 50°C before adding antibiotics.

2.1.2 Bacterial strains and growth media

For cloning, the *Escherichia coli (E. coli)* strains DH5α [183] and DB3.1 were used.

For stable *Arabidopsis* transformation, the disarmed *Agrobacterium tumefaciens* strain GV3101::pMP90 [184] was used.

Two bacterial growth media were used, Luria Bertani (LB) medium and X-Broth:

Table 2.1: Antibiotics and their concentrations used in this project

Antibiotic	**Final Concentration**
Kanamycin	25µg/ml for selection of plants
Kanamycin	50µg/ml for selection of bacteria
Ampicillin	100µg/ml
Gentamycin	10-20µg/ml
Hygromycin	15µg/ml
Timentin	2µg/ml
Carbenicillin	200µg/ml
Spectinomycin	75µg/ml

LB medium was used to grow *E. coli* cultures. It contains 1% (w/v) bacto tryptone, 0.5% (w/v) bacto yeast extract, and 1% (w/v) sodium chloride. The pH was adjusted to 7.0 using sodium hydroxide. For selection medium, the agar was cooled to 50°C before adding antibiotics. The autoclaved medium was stored at 4°C.

X-broth is a nutrient-rich variation of LB medium. It was used for the recovery of *E. coli* immediately after heat shock. It contains 2 % (w/v) bacto tryptone, 0.5 % (w/v) bacto yeast extract, 0.4 % (w/v) magnesium sulphate and 10mM potassium chloride. The pH was adjusted to 7.6 with sodium hydroxide. The autoclaved medium was stored at room temperature.

All media were autoclaved for 20 minutes at 121°C.

2.1.3 Antibiotics

All antibiotics were prepared as 1000x stock solutions in water and filter sterilised (0.22µm filters). The stock solutions were stored at -20°C and added to the medium at the appropriate concentrations (see table below). Hygromycin (Calbiochem, Feltham, UK) was available as stock solution and was added directly into the medium.

2.1.4 Chemicals

Chemicals were supplied by Sigma-Aldrich (St. Louis, Missouri, USA) or Duchefa Biochemie (Haarlem, The Netherlands).

2.1.5 Plasmids

The plasmid pOpON2.1 (generated by former DPhil student Luisa Camacho) was used to generate transgenic *Arabidopsis* lines used in this project. The pOpON2.1 vector (figure 2.1)

consists of 20145 base pairs, confers spectinomycine resistance in bacteria (Tn7 SpecR) and kanamycin resistance in plants (NPT II-nos). The LhGR transcription factor (LhGR) is under the control of the 35S promoter (35S). The promoter for the LhGR transcription factor is the pOp6 promoter (pOp6), which in turn drives transcription of the GUS reporter gene (GUS) and the gene of interest (SENSE). Poly-adenlylation sites (pA-OCS) are introduced to stop transcription of SENSE, GUS and LhGR.

Genes of interest are introduced by Gateway cloning (see section 2.3.5).

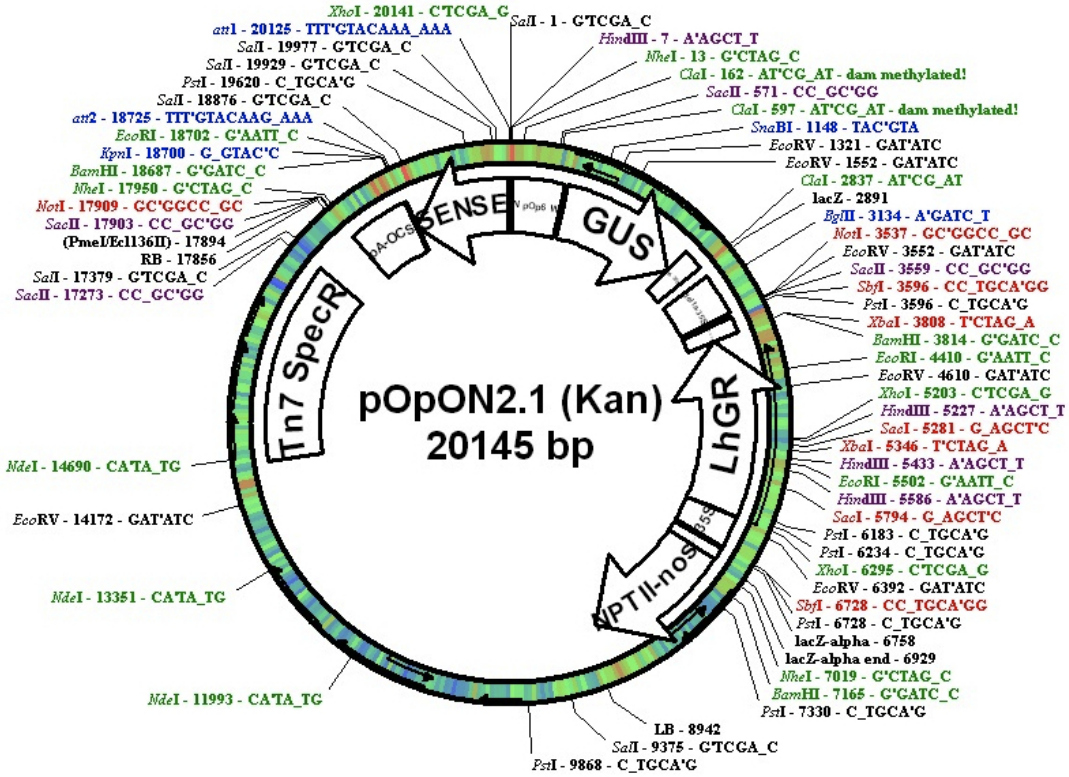

Figure 2.1: Graphical representation of the pOpON2.1 vector generated with pDRAW software. The pOpON2.1 vector consists of 20145 base pairs and includes the following elements: spectinomycine resistance in bacteria (Tn7 SpecR), kanamycin resistance in plants (NPT II-nos), 35S promoter (35S) controlled LhGR transcription factor (LhGR), the pOp6 promoter (pOp6, target promoter of LhGR), GUS reporter gene (GUS), gene of interest (SENSE), poly-adenlylation sites (pA-OCS). Colour coding is as follows: blue: unique sites, red: two sites, purple: three sites, green: four sites, black: restriction site occurs more than four times.

2.1.6 Oligonucleotide primers

Oligonucleotide primers for PCR reactions were obtained from Bioneer, Daejeon, Republic of Korea.

Primer sequences used for Gateway cloning:

Rab-A2a forward primer:
5'-GGGGAGAAGTTTGTACAAAAAAGCAGGCTTCACCATGGGCGAGAAGACCGGACGAA-3'

Rab-A2a reverse primer:
5'-GGGGACCACTTTGTACAAGAAAGCTGGGTCTCAAGACGATGAGCAACAAGG-3'

2.1.7 Enzymes

Restriction endonucleases were obtained from New England Biolabs (NEB, Hitchin, UK) or Fermentas (Loughborough, UK).

2.1.8 Antibodies

Antibodies were either stored at 4°C with 0.05% (w/v) sodium azide or -20°C after addition of 1 volume of glycerol (Sigma-Aldrich, St. Louis, Missouri, USA, 99.5%). Antibodies used in this thesis were Anti-Rabbit IgG alkaline phosphatase conjungate (goat) A-3687 from Sigma-Aldrich, St. Louis, Missouri, USA (a dilution of 1:10000 was used) and an anti-RabA2a (rabbit) antibody, which has been described in Chow, C. (2006) Specialisation of *Arabidopsis* RabA GTPases, D.Phil thesis, University of Oxford, UK (a dilution 1:5000 was used).

2.1.9 Other lab equipment

For centrifugation involving microfuge tubes, the microfuges Biofuge pico, Biofuge fresco (Heraeus Instruments GmbH, Hanau, Germany) and Sigma 1-15K Sigma-Aldrich (St. Louis, Missouri, USA) were used with supplied rotors. For centrifugation of 15mL or 50mL falcon tubes, an Allegra 21R Centrifuge (Beckman-Coulter, High Wycombe, UK Ltd.) was used.

2.2 Methods

2.2.1 Plant growth conditions and transformation

Plant growth conditions

Routine procedures:

Seeds were aliquoted into in 1.5mL Eppendorf tubes and surface sterilised in 1mL of 70% (v/v) ethanol by inverting four to six times. The tubes were left to stand for five minutes. The seeds were the pipetted onto sterile Whatman papers (sterilised with absolute ethanol) in a flow hood and allowed to dry. Sterilised seeds were then transferred to MS media agar using a sterile toothpick.

Procedure for primary transformants:

Carbenicillin and timentin were added to the medium, in addition to the line specific antibiotic (kanamycin or hygromicin). Seeds were washed once with 70% (v/v) ethanol for 10 minutes in 10mL Falcon tubes. Then, the 70% (v/v) ethanol was replaced by the bleach solution (1/10 volume of sodium hypochlorite solution (12%, v/v) and 25% SDS (w/v) and applied for 10 minutes. Tubes were inverted four times. The seeds were washed with sterile dH_2O four times and resuspended in two volumes sterile dH_2O. The 2mL to 4mL mixture was transferred to an agar plate and allowed to dry for two to four hours.

After imbibition at 4°C for two days, plants were grown in the tissue culture growth room (TCR1: 16 hours light, 8 hours dark, 22°C). Ten to 15 days old seedlings were transferred into soil and grown in the growth cabinets under same conditions.

Plant transformation

The *Agrobacterium* mediated floral dip method [185] was used to transform *Arabidopsis.* Plants of approximately three weeks of age, with numerous immature floral buds and few siliques were used for transformation. A 200mL overnight culture of *Agrobacterium tumefaciens* (OD_{600} = 1.8) was centrifuged, the pellet was resuspended in 200mL sucrose solution (5% (w/v) sucrose and 0.05% (v/v) Silwet L-77). Plants were then immersed upside down into the solution and mixed for 30 seconds. The plants were laid down on the wet tray and covered with cling film overnight before returning to the growth cabinet.

2.3 Cloning

2.3.1 Polymerase Chain Reaction

To amplify DNA fragments from plasmid or genomic DNA, a 20µL PCR reaction mixture containing template DNA, Proof I buffer (50mM Tris HCl pH9.1, 14mM $(NH_4)_2SO_4$), 200µM dNTPs (Fermentas, Loughborough, UK), 1 - 2.5mM magnesium chloride, primers each at 0.3µM and Taq DNA polymerase (homemade) was prepared.

Where high sequence accuracy was required, pfu Polymerase (Fermentas, Loughborough, UK) was used with its appropriate buffer. The mixture was then incubated in a thermal cycler (Biometra T1 themocycler or Biometra T-Gradient). The lid was heated to prevent evaporation of the reaction mixture. A typical PCR program included heating step to 94°C for five minutes followed by 20 to 35 cycles of denaturation, annealing and extension at appropriate temperatures.

2.3.2 Restriction enzyme digestion of DNA

Restriction enzyme digestion was carried out according to the product manuals from NEB, Hitchin, UK or Fermentas, Loughborough, UK. Prediction of restriction band patterns was done with Mac Serial Cloner (SerialBasics, France).

Restriction enzyme digest for restriction digestion mapping of a plasmid was performed with a total of 20µL reaction mixture, containing 5µL plasmid (obtained by alkaline lysis protocol or Qiagen (Hilden, Germany) Spin miniprep), 1x buffer, 0.5U restriction enzyme and dH_2O. The mixture was incubated at 37°C for two hours or overnight.

Five to 10µL of the total digestion was used for gel electrophoresis analysis.

2.3.3 Agarose Gel Electrophoresis

0.5x TBE buffer was used as running buffer and was prepared from a 5x stock (55g Tris, 27.5g orthoboric acid and 3.72g EDTA in 1L dH_2O with pH adjusted to 8.0) with dH_2O. The final concentration of agarose was 0.8% (w/v), achieved by dissolving 0.8g agarose (Bioline, London, UK) in 100mL 0.5x TBE by microwaving the mixture. Once the gel reached approximately 50°C, 4µL ethidium bromide (10mg/mL) was added. The gel was shaken gently and poured

into a gel tray with inserted combs (typically 20 slots). The whole gel electrophoresis chamber was flooded with running gel to a level that the agarose gel was well covered by the buffer.

1x loading dye (0.042% (w/v) bromophenol blue, 0.042% (w/v) xylene cyanol FF, 5% (v/v) glycerol) was added to the samples and loaded into the wells of the solidified gel. 5μL 1kb and/or 100bp DNA ladders (Fermentas, Loughborough, UK) were loaded as markers.

The gel was run at a constant voltage (100V) on Horizon 11.14 gel electrophoresis equipment (Life Technologies Ltd., Paisley, UK). DNA was visualised using a UV transilluminator.

2.3.4 DNA gel purification

To isolate DNA fragments from an agarose gel after electrophoresis, the necessary portion of the gel was excised and the DNA extracted by following the Qiagen Gel Purification Kit (Qiagen, Hilden, Germany) protocol according to the manufacturers instructions.

2.3.5 Gateway cloning

Gateway cloning procedures were performed according to the manufacturer's recommendations (Invitrogen, Paisley, UK, 2008).

2.3.6 DNA ligation

Ligation reaction was set by preparing a 10μL mixture containing insert DNA, vector DNA, 1μL T4 DNA ligase (Fermentas, Loughborough, UK) and 1x ligase buffer (Fermentas, Loughborough, UK). Insert and vector were added at an approximate 3:1 molar ratio. The mixture was at room temperature for 2 hours or at 16°C overnight.

2.3.7 Bacterial transformation

E. coli was cultured at 37°C with Luria Bertani (LB) medium, either on 1% (w/v) agar plate or in liquid, with appropriate concentration of antibiotic.

Agrobacterium tumefaciens GV3101::pMP90 was grown at 28°C on LB medium with gentamycin plus suitable antibiotic for selecting the transformed binary vector.

To prepare glycerol stocks of bacterium strains, 88µL of fresh culture was mixed with 122µL sterile glycerol and freezing in liquid nitrogen before storing at -80°C.

E. Coli (heat shock)

To transform *E. coli* cells, 5µL DNA was added to a tube of competent cells (40µL) and left on ice for 20 to 30 minutes. The cells were heat shocked at 42°C for two minutes, 1mL X-broth was added immediately after the heat shock. The cells were gently shaken at 37°C for one hour. Afterwards, the tube was centrifuged (4500 rpm (1500 x g), 5 minutes) and the cells resuspended in 150µL liquid LB medium. This resuspended culture was plated out on LB medium selection plate.

For blue/white screening, 80µL X-gal (Melford Laboratories, Chelsworth, UK, 20mg/ml in DMF) and sterilised 80µL IPTG (1M in dH_2O, Melford Laboratories, Chelsworth, UK) was streaked on the respective plate and left to dry in a flow hood.

Plates were incubated overnight at 37°C for approximately 16 hours.

Agrobacteria (electroporation)

1µL plasmid DNA (QIAGEN kit prep) was added to 20µL electrocompetent *Agrobacterium tumefaciens* cells (cells were thawed on ice beforehand). The mixture was pipetted into an electroporation cuvette which was then pulsed at 2.5kV for approximately 4.5ms using a Biorad Gene Pulser (BioRad, Hemel Hempstead, UK) and Pulse Controller set with 25µF capacitance and 200Ω resistance. 1mL LB medium without antibiotic was added immediately after the electroporation and the solution was transferred to a 1.5mL Eppendorf tube. The cells were incubated for two hours at 28°C without shaking and then plated out onto LB medium selection plates. These plates were then incubated for two days at 28°C.

2.3.8 Competent cells for transformation

Competent *E. coli:*
250mL SOB medium (2% (w/v) bacto-tryptone, 0.5% (w/v) yeast extract, 10mM NaCl, 2.5mM KCl, 10mM $MgCl_2$, 10mM $MgSO_4$, pH = 6.7 - 7.0) was inoculated from an overnight grown LB-culture (ca. 1:50 to OD_{600} = 0.05 to 0.08) and culture was grown 28°C with vigorous

shaking until OD_{600} reached approximately 0.6. Culture was left on ice for 10 minutes before spinning down for 10 minutes at 2500g and 4°C. The pellet was gently resuspended in 80mL ice cold TB (10mM PIPES, 55mM $MnCl_2$, 15mM $CaCl_2$, 250mM KCl, adjust pH = 6.7 with 1N KOH before adding $MnCl_2$ to the solution, filter sterilise) and left on ice for 10 minutes. A further spinning step for 10 minutes at 2500g and 4°C followed. The pellet was then gently resuspended in 20mL ice cold TB and left on ice for 10 minutes. DMSO was slowly added to this mix until a final concentration of 7% (v/v) was reached. Suspension was left on ice for 10 minutes before aliquoting to cold tubes on ice and immediately quick freezed in liquid nitrogen (store at -80°C).

Agrobacterium electrocompetent cells:
5mL of an GV3101 overnight culture was added to 200mL LB medium containing 20µg/mL gentamycin. The mixture was shaken at 28°C until it reached an OD_{600} between 0.5 and 0.6. The culture was left on ice for 30 minutes and centrifuged at 4800 rpm (2200 x g) for 10 minutes at 4°C. The pellet was resuspended in 25mL ice-cold HEPES buffer (1mM HEPES; pH7.5, filter sterilised). After being washed again with 25mL ice-cold HEPES buffer, the cells were then washed once with 20mL of ice-cold HEPES buffer with 10% (v/v) glycerol before being finally resuspended in 20mL of ice-cold HEPES buffer with 10% (v/v) glycerol. Aliquots were frozen in liquid nitrogen and stored at -80°C.

2.3.9 Purification of plasmid DNA from bacteria

E.Coli

Plasmid DNA from *E.coli* cells was extracted by either alkaline lysis miniprep or QIAprep Spin Miniprep Kit (Qiagen, Hilden, Germany) according to the manufacturer instructions. When using QIAprepe Spin Miniprep Kit 20µL elution buffer was added in the elution step.

Alkalyne lysis minipreps of transformed *E.coli* was done as follows: 1.5mL of an overnight grown culture was transferred to an Eppendorf tube and pelleted at 14000rpm, 1 minute. The pellet was resuspended in 150µL buffer P1 (50mM Tris-HCl pH 8.0, 10mM EDTA pH 8.0, 100µg/mL RNase A). When the pellet was well resuspended, 150µL buffer P2 (0.2M NaOH, 1% SDS (w%v)) was added and the mixture incubated for 5 minutes at room temperature. 150µL buffer P3 (3M KAc, pH 5.5) was added, the solution well mixed and left for 20 minutes

on ice. After this, the suspension was centrifuged for 20 minutes at 4°C and 14000rpm (19300 x g). The supernatant was transferred into a fresh tube containing 1mL absolute ethanol. A further 20 minutes centrifugation step at 4°C and 14000rpm (19300 x g) followed, the final pellet was resuspended in 20µL autoclaved H_2O.

Agrobacteria

An alkaline lysis isolation method was used to extract plasmid DNA from *Agrobacteria*. The protocol was adapted from Birnboim and Doly [186].

A 2mL overnight grown culture was centrifuged at 4500 rpm (1500 x g) for 4 minutes. The pellet was washed in 500µL glucose buffer and resuspended in 200µL glucose buffer (50mM glucose, 25mM Tris, 10mM EDTA) containing 10µL lysozyme (10mg/mL). After leaving the mixture on ice for 10 minutes, 400µL freshly prepared lysis solution (0.2M sodium hydroxide, 1% (w/v) SDS) was added by gentle mixing. The tube was left on ice for 10 minutes (solution turns clear) and 300µL neutralisation solution (3M potassium acetate, pH4.8) was added. The solution was gently inverted and left on ice for 5 to 10 minutes. The solution was centrifuged at 13000rpm (16600 x g) for 20 minutes at 4°C. The supernatant was transferred to another microfuge tube and 0.7 volumes of isopropanol (ca. 600µL) was added. After mixing, the solution was centrifuged at 13000rpm (16600 x g) for 30 minutes at 4°C; the pellet was rinsed with 70% (v/v) ethanol and left to dry by air. The dried pellet was resuspended in 10µL water; 5µL were used for *E. coli*transformation.

2.3.10 Sequencing

A 20µL sequencing reaction was prepared as follows: 4µL Big Dye dilution buffer (Invitrogen, Paisley, UK), 4µL 5x Big Dye reaction mix (Invitrogen, Paisley, UK), 250ng template DNA, 0.8µL primer (5µM). The used sequencing PCR programme was as follows: 96°C for 2 minutes followed by 25 cycles of 96°C for 30s, 50°C for 15s and 60°C for 4 minutes. The DNA was precipitated by adding 50µL 95% (v/v) ethanol and 2µL 3M sodium acetate (pH 5.2). The sample was left at -20°C for 30 minutes and centrifuged at 13000rpm (16600 x g) at 16°C for 20 minutes. After an air-drying step, the pellet was resuspended in template suspension reagent. The sequencing reaction products were analysed using the Applied Biosystems 3730xl DNA Analyzer at the Zoology DNA Sequencing Service (Oxford University). Sequence chromatography

files were analysed by Chromas software (Technelysium, South Brisbane, Australia).

2.4 Histochemical GUS staining

GUS staining solution was prepared by freshly adding 1mL 10% (w/v) 5-bromo 4-chloro 3-indolyl-β-D-glucuronide dissolved in DMF to GUS staining buffer, which contained 100mM sodium phosphate (from 1M stock, pH 7.0), 10mM Tris (from 1M stock, pH 8.0), 1mM EDTA (from 0.5M stock), 0.05% (v/v) Triton X-100 and 0.5mM ferro/ferricyanide. Seedlings were immersed in GUS staining solution and kept at 37°C for one hour. Destaining was done by replacing the GUS staining solution with 70% (v/v) ethanol. After overnight incubation at 37°C, the solution was replaced with a 50% (v/v) ethanol / 50% (v/v) glycerol solution. The glucuronidase activity was indicated by the formation of blue coloured 5-bromo-4-chloroindigo and the samples were examined by using a Leica microscope. A coolSNAP dital camera (Photometrics, Tucson, USA) together with the ImagePro software (MediaCybernetics, Rockville, USA) were used to record the images.

2.5 Protein analysis

2.5.1 Protein extraction

A 50 to 150mg fresh sample (*Arabidopsis* seedlings, seven days after germination) was collected in a microfuge tube and immediately frozen in liquid nitrogen. Two volumes of extraction buffer (50mM sodium citrate at pH 5.5, 5% SDS (w/v), 0.01% BSA (w/v) and 150mM NaCl) with 2% (v/v) beta-mercapthoethanol was added to the samples before it was ground using a pre-cooled micropestle. After being vortexed briefly, the mixture was boiled for 10 minutes. It was then centrifuged at 13000rpm (16600 x g) for 30 minutes at 4°C. The supernatant was transferred to a new microfuge tube, frozen by liquid nitrogen and stored at -80°C.

2.5.2 Western Blot

SDS-PAGE was performed on a BioRad Mini 2D gel system (BioRad, Hemel Hempstead, UK), using a 12% polyacrylamide gel. First, the running gel was prepared (9.2mL sterile dH_2O, 4.8mL Tris (1.5M, pH 8.8), 200µL SDS (10% w/v, Biorad), 6mL acrylamide (40% v/v,

Anachem), 6µL TEMED (BioRad, Hemel Hempstead, UK) and 160µL ammonium persulfate (10% w/v, freshly prepared, Biorad, Hemel Hempstead, UK) of which 6ml was transferred into the assembled apparatus and overlaid with water. After the gel was set after about one hour at room temperature, the stacking gel was prepared (8.3mL sterile dH2O, 3.8mL Tris (0.5M, pH 6.8), 150µL SDS (10% w/v, BioRad, Hemel Hempstead, UK), 1.9mL acrylamide (40% v/v, Anachem, Luton, UK), 15µL TEMED (BioRad, Hemel Hempstead, UK) and 225µL ammonium persulfate (10% w/v, freshly prepared, BioRad, Hemel Hempstead, UK). The water overlay was removed from the running gel and the stacking gel mix was added. The approproate comb was inserted into the stacking gel mixture before the gel was left to polymerise for approximately 20 minutes.

In the meantime, the running buffer (14.4g glycine, BioRad, Hemel Hempstead, UK), 3g Tris and 1g SDS (BioRad, Hemel Hempstead, UK), add dH_2O to a final volume of 1L) was prepared and poured in the electrophoresis tank assembly, containing the gels.

The appropriate volume of 5x SDS loading buffer (0.375g Trizma Base, 5mL glycerol, 0.5g SDS, 20mg bromophenol blue in 10mL solution, pH 6.8) was added to each protein sample. The mixture was heated at 95°C for five minutes and then loaded into the wells. As protein marker, 5µL of pre-stained ladder (Fermentas, Loughborough, UK) was used. The gels were run at constant amperage (25mA for the stacking gel and 30mA for the running gel) until the dye reached the bottom.

The set-up was then disassembled and the running gel transferred into a plastic container, which contained transfer buffer (200mL methanol, 3g Tris and 14.4g glycine in 1L solution).

The gel and a hydrophilised PVDF membrane were sandwiched between Whatman 3MM filter papers and sponges in the following order: (cathode side) one sponge, one filter paper, the gel, the membrane, one filter paper, one sponge (anode side). The cassettes were inserted into the electrode module which was then put into the tank filled with transfer buffer with 3mL 10% (w/v) SDS.

Electrophoretic transfer happened at 75mA to 100mA constant amperage for 1.5 hours under constant magnetic stirring. After the transfer was completed and the set up disassembled, the membrane was blocked with blocking buffer (5% w/v non-fat milk powder in 1x TBS buffer containing 0.1% v/v Tween 20) for 1 hour at room temperature. The membrane was then incubated with the primary antibody in blocking solution (overnight at 4°C). On the following

day, the membrane was washed three times (15 minutes each) with 1x TBS buffer containing 0.1% v/v Tween 20. The membrane was incubated with alkaline phosphatase conjugated secondary antibodies in blocking solution (not containing any milk powder) for one hour. The membrane was washed in 1x TBS buffer containing 0.1% v/v Tween 20 for three times at 15 minutes and further washed in dH_2O for two minutes. After this, the membrane was developed in dark with 1 - 1.5mL Westran Blue (Promega, Madison, Wisconsin, USA). The reaction was stopped by adding a 20mM EDTA solution.

Western Blot quantification was done with ImageJ Gel-Analyzer software.

2.6 Confocal Laser Scanning Microscopy

2.6.1 Imaging

Whole *Arabidopsis* seedlings (three to seven days after germination) were mounted on slides with dH_2O, except for FRAP experiments where liquid MS medium was used.

Fluorescence was examined with a Zeiss LSM 510 confocal scanning microscope at high magnification using a C-Apochromat 40x/1.2NA water-immersion lens. The acquired images were analysed and processed with the Zeiss LSM software to construct 3D images or adjust brightness and contrast settings (Carl Zeiss, Jena, Germany).

GFP or YPF were imaged using the excitation wavelength 488nm (typically 5%) with emission filter 505-550nm or LP505nm. FM4-64 was excited by 488nm or 543nm and collected in channel S by selecting a suitable range of spectra.

2.6.2 Drug treatments

Drugs and their concentration used in this project are listed in table 2.2.

Table 2.2: Drugs and their concentrations used in this project

Drug	**Source**	**Concentration used**	**Reference**
Brefeldin-A	Sigma-Aldrich	50µm	[37]
Wortmannin	Sigma-Aldrich	33µm	[187]
Cytochalasin-D	Sigma-Aldrich	50µm	[37]
Tyrphostin A51	Sigma-Aldrich	30µM	[188]
Tyrphostin A23	Sigma-Aldrich	30µM	[188]

2.6.3 Stainings

FM4-64 (Invitrogen, Paisley, UK): Seedlings were mounted in water with 5µM FM4-64 (5mM water stock) for the time specified within the individual experiments to visualise endosomes or to study endocytosis.

2.6.4 FRAP analysis

Arabidopsis seedlings were germinated on MS plates containing DMSO. At the age of three days after germination, seedlings were transferred into liquid MS medium containing either DMSO or 20µm DEX for 20 hours. DEX induced seedlings were then screened and selected according to their phenotype (i.e. strong intracellular accumulation of PIN2:GFP in root cap cells and minor cytokinesis defects in meristematic cells if, visible).

Seedlings were observed under a cover slide with liquid MS as mounting medium. Slides were kept moist throughout the time course and only water was added to the edges of the slide to prevent accumulation of toxic concentrations of salts in the slide environment. Large root areas were bleached over Z-sections. *Arabidopsis* main root cells were bleached by a 488nm Argon laser (80% laser strength, 100% laser output) twice over a Z-section.

Individual PMs were measured, which were at least one bleached cell away from unbleached areas to exclude effects arising from lateral diffusion. Initial experiments concluded that it would be necessary to observe a period of 300 minutes after photo-bleaching until maximum recovery at the PM of PIN2:GFP was observed. Intervals of 60 minutes were chosen to avoid unnecessary bleaching by the imaging routine.

At the end of the experiment, images were analysed by the Zeiss LSM 510 Imaging software (figure 2.2). First, the threshold of the samples was determined by selecting an area of the background where no part of the root had been imaged (figure 2.2 A). Three values of standard deviation were added to the threshold and used as low threshold base (figure 2.2 B). Then, the signal intensity of individual PMs was measured by defining a region of interest around these membranes (figure 2.2 C). Both bleached and unbleached membranes were measured. However, for recovery measurements of bleached areas, only PMs were selected, which were part of a cell that was separated from unbleached areas by at least one bleached cell. This avoids measuring fluorescence recovery from lateral diffusion. The values for the same set of membranes were measured and recorded over time. The obtained values were then normalised

to 100% initial fluorescence (corrected ratio of bleached and unbleached areas) and plotted in a graph.

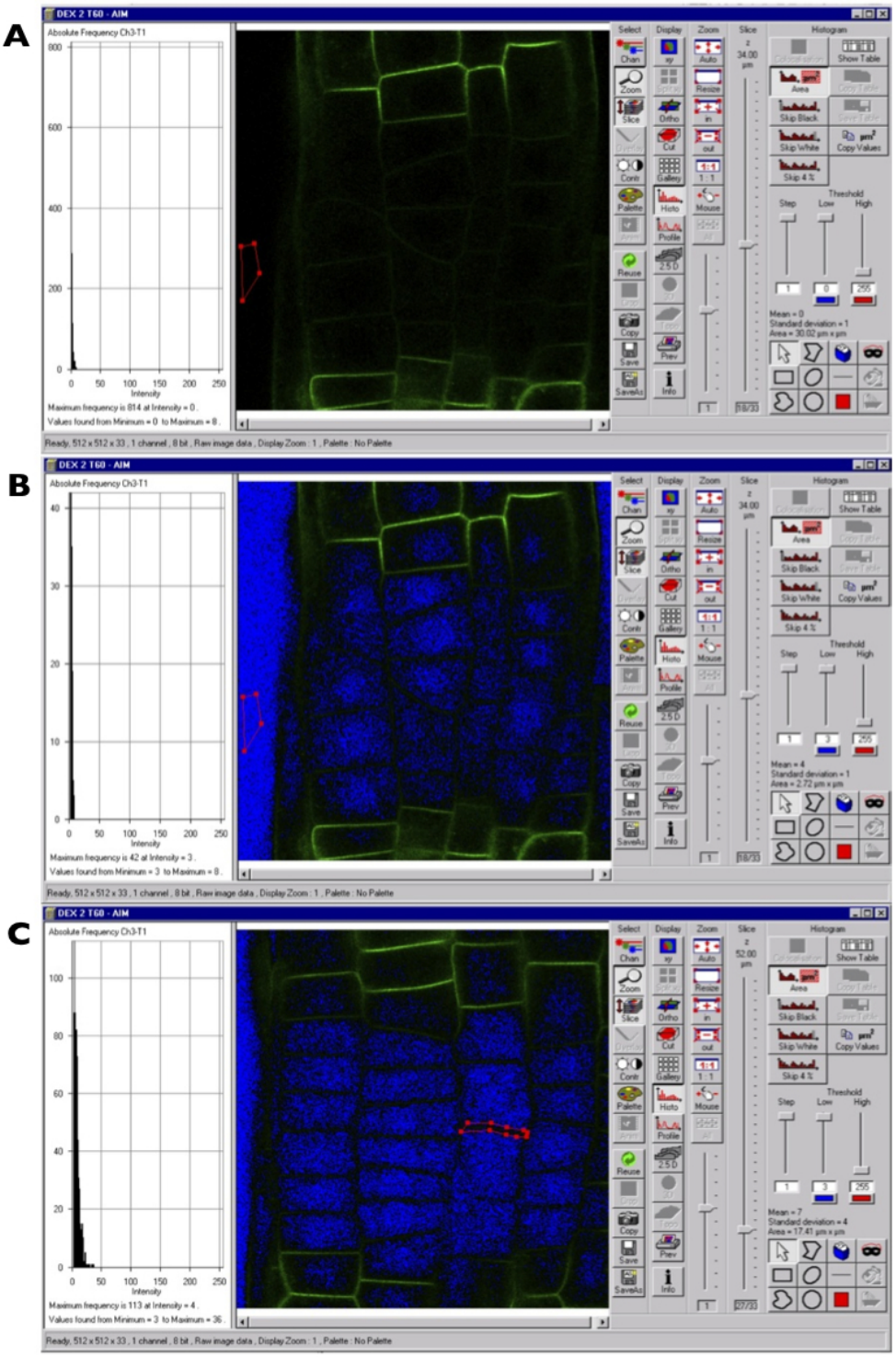

Figure 2.2: Screenshots demonstrating analysis of FRAP experiments using Zeiss LSM Browser. (A) The threshold was determined by selecting an area of the background. (B) Background cut off was set by adding three standard deviations to the threshold. (C) Values of membranes were measured by defining the region of interest giving the mean and area number value.

Chapter 3

Generation and characterisation of dominant negative marker lines

3.1 Introduction

The aim of this project is to provide an insight into RAB-A2a dependent membrane traffic in *Arabidopsis thaliana.* To do this, I chose a set of fluorescent markers that are trafficked through the main routes in the *Arabidopsis* endomembrane system. A dexamethasone inducible genetic trait, the dominant negative RAB-A2a mutant, was introduced into these fluorescent marker plant lines and the effect of the dominant negative mutant on the localisation of these fluorescent markers was studied.

This chapter describes the generation and the rationale for the selection of the transgenic *Arabidopsis* lines for the investigation of RAB-A2a dependent membrane traffic in this project. A detailed description of the trafficking pathways of the selected fluorescent markers is given in Chapter 4.

3.1.1 The dominant negative approach

Previous work by Cherry Chow on the *Arabidopsis* Rab-A clade showed that classic genetic approaches cannot successfully be used to study the function of these proteins, due to functional redundancy [189]. Thus, I chose to make use of the dominant negative approach, which has previously been used to determine Rab GTPase function in transient expression systems [32, 137].

Dominant negative proteins carry mutations that abolish an aspect of the protein's normal function. These mutants compete with the wild type protein for interactors and thus, the function of the wild type protein is effectively inhibited [190].

This is a very powerful alternative approach for studying a protein's function, compared to time-consuming immunolocalisation protocols, or where proteins are expressed and studied in heterologous systems where crucial interactors might be missing, or gene knockout, where the protein of interest may be required for early developmental processes and thus results in embryonic lethality [190]. The limitation of this approach lies in the limited knowledge about interactors of dominant negative Rab GTPase in plants [115, 141]. Thus, in addition to inhibiting normal protein function, dominant negative mutants may cause secondary effects that do not reflect the function of the wild type protein.

As mentioned in 1.4.1, mutants have been identified that will keep Rab proteins in preferentially GDP-bound ('GDP-locked'), GTP-bound ('GTP-locked') or nucleotide free conformation. The dominant negative Rab mutants are believed to interact with the GEF that catalyses the GDP to GTP exchange thus shifting the activity cycle towards the 'off' or 'inactive' state. However, it has been shown that dominant negative Rab mutants can be instable with half lives of 2.5 to 6 hours [191], which is why a high concentration of ten times or more in excess to the wild type protein and a constant supply of dominant negative protein is required to observe trafficking defects [106]. This can be achieved by making use of dexamethasone inducible systems which has been employed successfully in the past to study Rab GTPase function in plants [32, 45, 192, 193].

3.1.2 The dexamethasone inducible system

Chemically inducible systems are especially desirable in conditions when overexpression of gene products are lethal. The advantage over constitutive promoters is that inducible systems are

quiescent in the absence of the respective inducer and therefore do not interfere with plant development. With such systems, gene expression can be regulated by application of the inducing chemical at a particular developmental stage and for a specific duration. Further, by selecting the appropriate promoter to drive expression of the chemically inducible transcription factor, the expression can be restricted to specific organs, tissues or cell types.

The dexamethasone inducible system was first described by Schena and colleagues in 1991 [194]. Schena and colleagues constructed a two plasmid system, one of them being the effector and the other one the reporter construct. In one of their effector systems, the rat glucocorticoid receptor (GR) is fused to the CaMV 35S promoter, a promoter widely used to achieve constitutive expressionin plants. In their reporter construct, a glucocorticoid receptor element (GRE) was cloned in front of the gene of interest (see figure 3.1). This system lead to a 270-fold increase in expression in tobacco protoplasts [194].

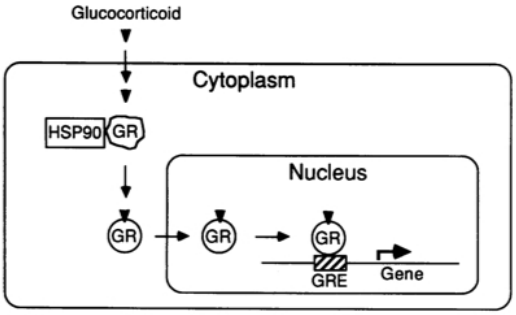

Figure 3.1: The dexamethasone inducible system: The GR resides in the cytoplasm bound to the 90kDa heat shock protein HSP90. When dexamethasone is taken up by the cell, dexamethasone binds to GR, thereby releasing it from HSP90. GR is released into the cytoplasm and transported into the nucleus where it binds GRE and initiates transcription of the gene of interest [194].

This system has been further developed into the GVG system: The GVG transcription factor is a chimera of the DNA-binding domain of the yeast GAL4 transcription factor, the trans-activating sequence of the herpes virus protein VP16, and the regulatory region of GR. The reporter construct consists of six tandem repeats of the GAL4 activating sequence upstream of a luciferase gene. At concentrations greater than 6µM, a more than 100-fold increase of expression in transgenic *Arabidopsis* plants is observed [195]. It was later shown that these systems can cause growth defects in transgenic *Arabidopsis* plants, similar to plants exhibiting ethylene signalling defects, and induces the expression of defence-related genes. However, this is apparently not a direct cause of dexamethasone but results from the expression of GVG [196].

The pOp/LhG4 system developed by Moore and colleagues offered a solution to the physiological problems caused by GVG. The pOp promoter consists of two repeats of a lac operator cloned upstream of a minimal promoter. LhG4 consists of the *Saccharomyces cerevisiae* Gal4 transcription activation domain-II and the high affinity DNA-binding mutant of the lac repressor of *E. coli,* which binds its operator with increased affinity [197]. However, the disadvantages of this system were the minimal capability of temporal control of expression and reduced expression levels compared to the GR-systems. Thus, the LhG4 system was further improved by Craft and colleagues (2005) by adding the ligand-binding domain of GR to the N-terminus of LhG4 to facilitate glucocorticoid-inducible transgene expression from the pOp promoter in *Arabidopsis.* This system is superior to the previous GR-systems as it does not affect plant growth [198].

The dexamethasone inducible system used in this project is based on the pOp6/LhGR system from Samalova and colleagues (2005) [199]. This system makes use of the characteristics of the before mentioned constructs by Craft *et al* and introduced an improved operator array: pOp6, a six tandem repeat of the pOp operator that increases binding efficiency of the pOp promoter. The pOp6/LhGR variant is a high efficiency dexamethasone inducible system with a reported 10000-fold increase of transgene expression upon induction [199].

3.1.3 The fluorescent marker line set

The marker set allowed me to investigate whether RAB-A2a was involved in (1) default traffic to the PM, (2) in protein recycling or (3) in a different pathway, e.g. an endocytic or vacuolar route.

To address objective (1) of this project, markers for default secretion (35S::nlsRm-2A-secGFP [200]) and PM traffic (UBI10::YFP:PIP1;4 [150], UBI10::YFP:NPSN12 [150]) were selected. The markers BRI1::BRI1:EGFP [58] and PIN2::PIN2:EGFP [201] were used to address objective (2) of the project. Objective (3) is addressed by the investigation of PVC and vacuolar trafficking markers (UBI10::YFP:VAMP711 [150], UBI10::YFP:RAB-G3f [150], 35S::BP80:GFP [202], 35S::RAB-F2b:GFP [203]) and the internalisation of the endocytic tracer dye FM4-64. These marker lines are described in Chapter 4.

The markers YFP:RAB-A1e [150], mCherry:RAB-A2a (Monika Kalde, unpublished) and mCherry:RAB-A5c (Monika Kalde, unpublished) were used to determine the specificity of

the dominant negative approach. As mentioned in Chapter 1, the Rab-A clade represents the largest of the eight *Arabidopsis* Rab GTPase clades, comprising 26 members across six Rab-A families. Out of these, the Rab-A1 and Rab-A5 families have been implicated in TGN-associated traffic [118, 119, 120, 204]. There may be at least two possible implications related to this for this project. Firstly, the TGN is taking a central place in endomembrane traffic. It might be that the localisation of several Rab-A GTPase members reflects the diversity of trafficking routes going through this compartment. However, there is also a possibility that the Rab-A proteins have common trafficking functions and thus share common interactors. Such interactors could be interacting with the dominant negative mutants of one or more Rab GTPase and thus lead to wrong conclusions when interpreting data. Thus, it was necessary to study the effect of the dominant negative RAB-A2a on other members of the Rab-A family as a control for the specificity of the dominant negative approach.

3.2 Results

3.2.1 The dexamethasone inducible system: pOpON2.1

Although there were already published inducible dominant negative RAB-A2a lines available [45], I decided to generate a new set of inducible lines by making use of the new vector pOpON2.1. While the previously used pH-TOP system [45] required separate driver and reporter constructs, this vector contains both the driver and the reporter on one plasmid (see figure 3.2). This simplifies selection of plant lines and allows more rapid generation of lines. The gene of interest is introduced by Gateway cloning.

Figure 3.2: Graphical representation of the pOpON2.1 dexamethasone inducible construct: The expression of the LhGR transcription factor ('LhGR') is under the control of the 35S promoter ('35S'). When the inducing agent dexamethasone is added, LhGR binds to the pOp6 promoter ('pOp6'), driving the expression of the GUS reporter ('GUS') and the gene of interest, in this case RabA2a ('RabA2a'). Purple boxes represent poly-adenylation sites, the yellow box represents non-coding pOpON2.1 sequence, light blue arrows represent the respective genes and point into the direction of transcription, dark blue boxes show promoters.

The full length genomic DNA of wild type Rab-A2a and its dominant negative mutant (nucleotide free 'NI') were amplified by PCR, with the respective Gateway cloning sites on the 5' and 3' ends. This fragment was then introduced into pDONR207 by a BP reaction and

then inserted into pOpON2.1 by the LR reaction. The RabA2a sequences were checked by sequencing in pDONR207, the insertion of the fragment and the general integrity of pOpON2.1 were tested by four different restriction enzyme digests (PvuII, XbaI, AflII, BglII). The plasmids were introduced into the *Agrobacterium* strain GV3101, plasmid DNA was isolated and re-introduced into *E. coli* , and checked by restriction digests (PvuII, XbaI, AflII, BglII) before using the strains for plant transformation (as described in Chapter 2).

3.2.2 Dominant negative RAB-A2a pOpON2.1 transgenic *Arabidopsis* plants show stronger root growth inhibition than pH-TOP lines

Dominant negative RAB-A2a induced pOpON2.1 lines show complete root growth inhibition at three days after germination

It was crucial to establish that the newly generated dominant negative lines used for confocal microscopy analysis in this project exhibit similar characteristics as published by Chow and colleagues [45], e.g. they should exhibit a gradual inhibition of growth of the main root. In order to select the best candidate lines for further analysis, T2 lines were germinated on MS plates containing either 20µM dexamethasone or the respective amount of DMSO as control. Seedling growth was monitored over a period of up to seven to eight days after germination and scored each day. As figure 3.3 shows, the induced lines were already affected in their root growth at day three after germination.

Shoot growth of these lines was severely affected (data not shown). Cotyledons remained very small with dark green colouring, the ability to grow true leaves was lost.

Dominant negative RAB-A2a induced pH-TOP lines show complete root growth inhibition from five days after germination

Root growth of two formerly published [45] inducible dominant negative lines of the pH-TOP system were monitored. These were previously categorised as lines showing strongest root growth defects in comparison to other available lines of this system. The two graphs (figures 3.4 and 3.5) show inhibition of root growth when treated with dexamethasone. However, the degree of root growth inhibition varies between these two lines and are less severe than

compared to root growth inhibition of the strongest pOpON2.1 lines (figure 3.3).

Shoot growth of dominant negative induced pH-TOP lines only exhibited a minor shoot growth defect (data not shown). Cotyledons were marginally smaller, true leaves are developed.

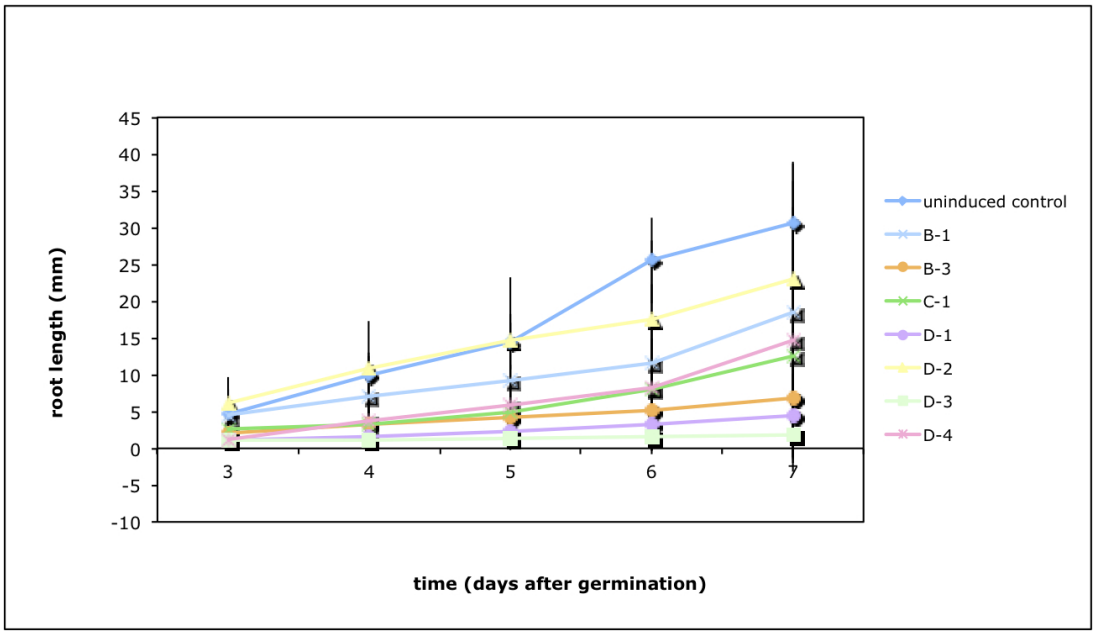

Figure 3.3: Root growth of selected *Arabidopsis* Col-0 pOpON2.1 dominant negative RAB-A2a lines (B-1 to D-4). 15 to 20 seedlings per line and treatment were scored for their root growth from three to seven days after germination. The data points represent the mean average root length per line and day, standard deviations are given. The lines B-1, B-3, D-1 and D-3 represent the strongest lines and were used for further analysis.

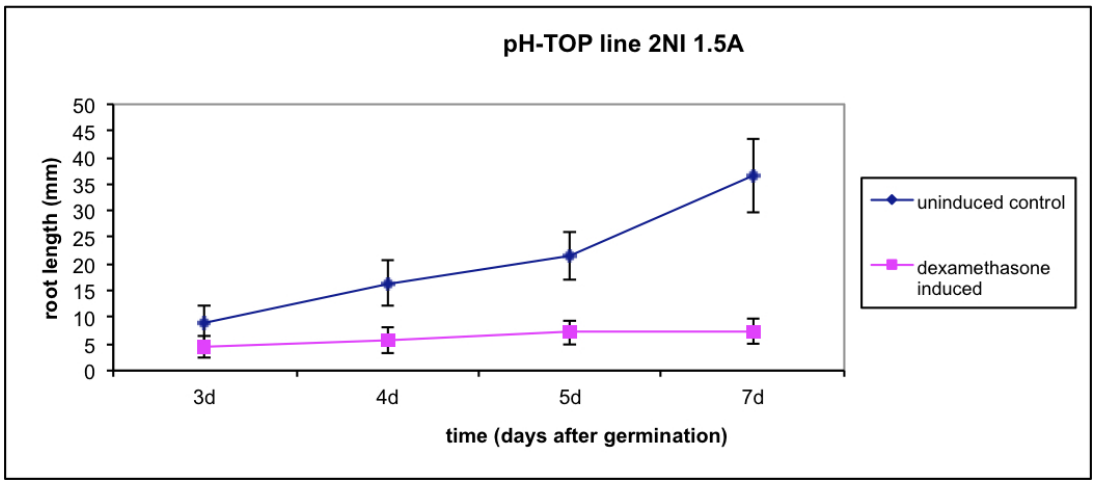

Figure 3.4: Root growth analysis of the dexamethasone inducible, dominant negative pH-TOP line 2NI 1.5A (*Arabidopsis* Col-0). Plants were germinated on 20µM dexamethasone or the corresponding amount of DMSO as control. Root growth was monitored over seven days. Data points represent mean average root growth, error bars show standard deviation.

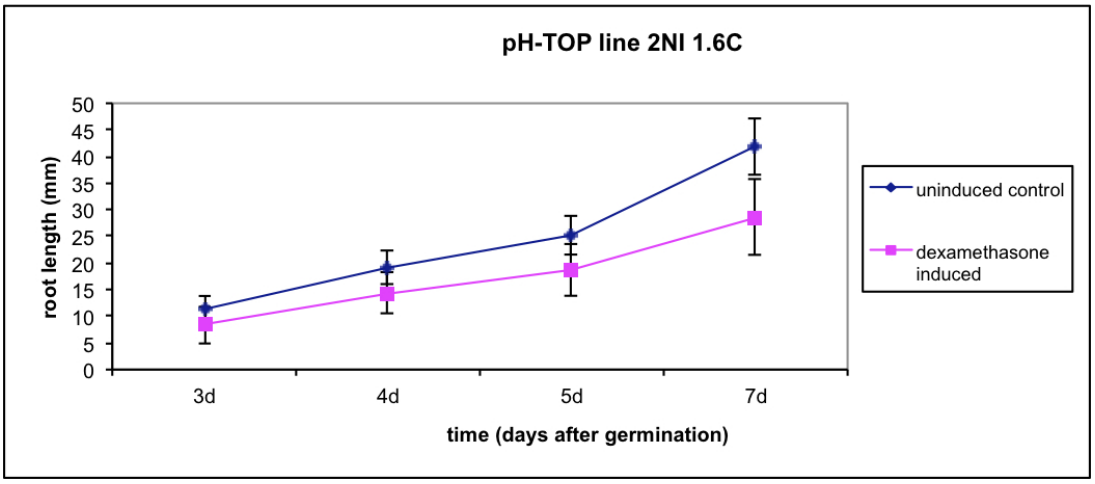

Figure 3.5: Root growth analysis of the dexamethasone inducible, dominant negative pH-TOP line 2NI 1.6C (*Arabidopsis* Col-0). Plants were germinated on 20µM dexamethasone or the corresponding amount of DMSO as control. Root growth was monitored over seven days. Data points represent mean average root growth, error bars show standard deviation.

3.2.3 pOpON2.1 transgenic plant lines are more rapidly induced than pH-TOP lines.

Knowing the rate of the dominant negative RAB-A2a protein induction upon dexamethasone treatment is crucial in trying to understand data that comes from correlation of inducible protein expression and its effect on localisation of fluorescent markers. In order to analyse the expression pattern of the dexamethasone-inducible lines, GUS stainings were carried out with individual plant lines. As mentioned earlier, not only the gene of interest is expressed after induction with dexamethasone, but also the reporter gene GUS. GUS activity is visible through the formation of blue coloured 5-bromo-4-chloroindigo upon adding the substrate solution. The following time points were chosen: 0 hours, 2 hours, 4 hours, 8 hours, 16 hours, and 24 hours after induction with dexamethasone.

GUS reporter gene expression is visible after two hours upon induction with dexamethasone in dominant negative pOpON2.1 lines.

In pOpON2.1 inducible lines, GUS expression is visible in the vascular tissue at two hours after induction with dexamethasone (figure 3.6). At four hours after induction, GUS expression is visible in the epidermal cell layer with a steady increase in staining along the main root. It appears that the induced protein reaches its maximum in a period of 16 to 24 hours after

induction with dexamethasone.

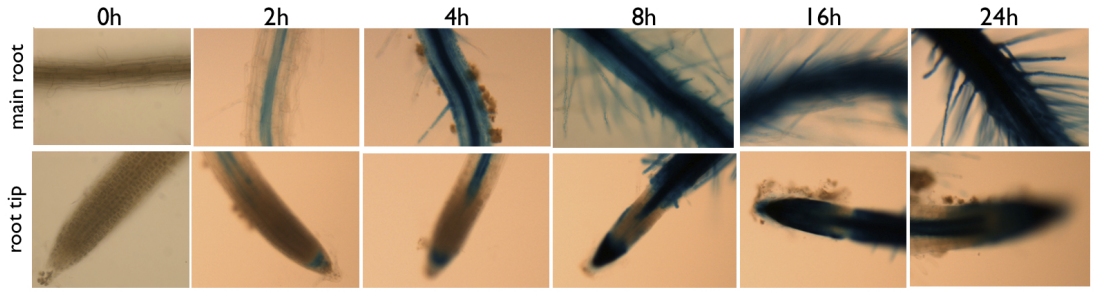

Figure 3.6: GUS stainings of pOpON2.1 inducible dominant negative lines (*Arabidopsis* Col-0). The top lane of images shows a representative image of the main root, the lower lane of images shows representative images of the root tip. GUS stainings were carried out before induction (0h) as well as two to 24 hours after induction with dexamethasone. GUS expression is detected by GUS staining from two hours after induction with dexamethasone. Maximum staining of roots is already achieved 16 hours after induction with dexamethasone.

GUS reporter gene expression is visible after four hours upon induction with dexamethasone in dominant negative pOpON2.1 lines.

In pH-TOP inducible lines, GUS expression in the vascular root tissue is visible at four hours after induction with dexamethasone (figure 3.7). The epidermal cell layer shows GUS expression at eight hours after induction. The intensity of GUS staining increases over time but it appears that a stable staining level has not yet been reached by 24 hours after induction, indicating that the maximum expression of GUS reporter has not yet been achieved.

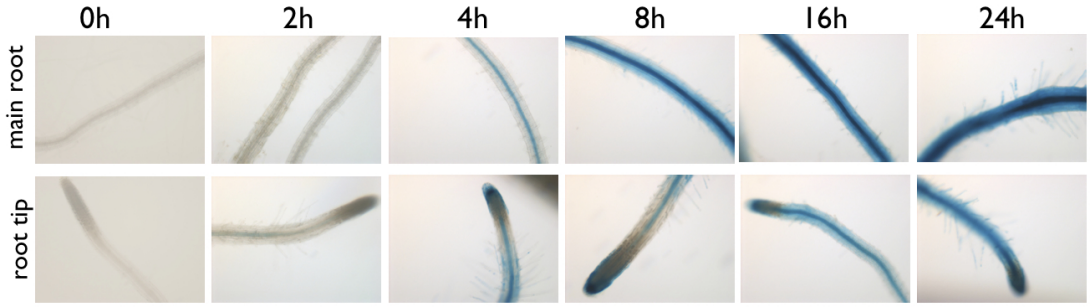

Figure 3.7: GUS stainings of pH-TOP inducible dominant negative lines (*Arabidopsis* Col-0). The top lane of images shows a representative image of the main root, the lower lane of images shows representative images of the root tip. GUS stainings were carried out before induction (0h) as well as two to 24 hours after induction with dexamethasone. GUS expression is detected by GUS staining from four hours after induction with dexamethasone. The maximum staining of reporter gene expression is apparently not yet reached at 16 to 24 hours after induction with dexamethasone.

3.2.4 pOpON2.1 transgenic plants accumulate more dominant negative RAB-A2a than pH-TOP lines

pOpON2.1 lines reach maximum protein levels at 16 to 24 hours following dexamethasone induction

Next, I wanted to address the question whether the observed root defects and GUS expression patterns correlate to an increase of protein over time. Thus, western blot experiments with a time course from 0 to 48 hours after induction were carried out. Indeed, the results confirm the findings of the GUS stainings that the amount of protein reaches its maximum between 16 to 24 hours after induction with dexamethasone (figure 3.8).

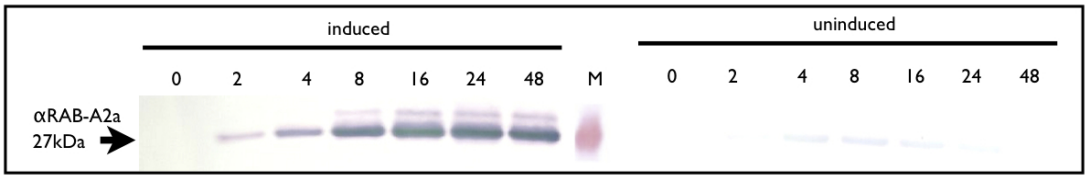

Figure 3.8: Western blot of a pOpON2.1 line with inducible dominant negative RAB-A2a (*Arabidopsis* Col-0 2NI). The left side of the blot shows the amount of RAB-A2a before induction (0 hours) and after induction (2 to 48 hours). The lanes to the right of the 27kDa marker ('M') are controls of uninduced, DMSO treated samples taken at the same time points. A steady increase in protein concentration is observed. The maximum is reached at about 16 hours after induction with dexamethasone. In uninduced samples, light bands of endogenous RAB-A2a protein are visible.

pH-TOP lines do not reach maximum protein expression before 24 hours after induction with dexamethasone

The strongest of the two pH-TOP lines, 2NI 1.5A, was compared to the pOpON2.1 system. RAB-A2a protein starts to accumulate at 2 hours after induction with a steady increase of protein concentration up to 24 hours (figure 3.9). It appears that the maximum amount of protein is reached between 16 and 24 hours after induction with dexamethasone.

Quantitative comparison of pOpON2.1 and pH-TOP western blots confirm qualitative findings

The next question I addressed was whether the stronger root growth inhibition was due to more dominant negative RAB-A2a present in pOpON2.1 *versus* pH-TOP lines as the kinetics of induction appear the same in the western blot. Hence, I quantified the western blots by

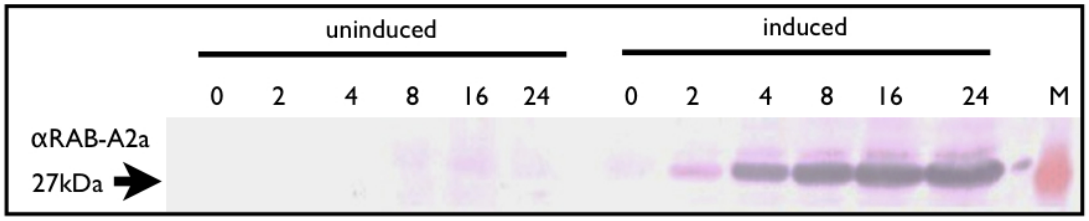

Figure 3.9: Western blot of a pH-TOP line (*Arabidopsis* Col-0 2NI 1.5A) with inducible dominant negative RAB-A2a. The first six lanes show uninduced, DMSO treated control samples taken at 0h to 24h. The second set of six lanes shows dexamethasone induced samples at 0 to 24 hours after induction. The last lane shows the 27kDa marker ('M'). There is a steady amount of protein expression that reaches a maximum level between 16 and 24 hours after induction. In uninduced samples, light bands of endogenous RAB-A2a protein is visible.

the ImageJ Gel-Analyzer software. To quantify the western blots shown in figure 3.8 and 3.9, images were converted into grayscale by Adobe Photoshop CS4. Lanes from two to 24 hours (pOpON2.1) or two to 48 hours (pH-TOP) after induction were defined by rectangular boxes. ImageJ generated a profile plot, which was used to quantify relative protein content. The area under the curve was measured by ImageJ, and relative amounts to lane one or the background were calculated. The results show that both pOpON2.1 and pH-TOP reach maximum protein levels between 16 to 24 hours after induction with dexamethasone. However, induction of pOpON2.1 lines results in 10-fold increase of protein content, while pH-TOP only reach a maximum of 7-fold compared to the 2 hour time point. This reflects a 15000-fold increase in protein concentration in pOpON2.1 lines *versus* a 10000-fold increase in pH-TOP lines, compared to non-induced samples. Thus, the pOpON2.1 systems accumulates protein faster and at a higher concentration than pH-TOP lines.

3.2.5 Selection of marker lines and transformants

The fluroescent marker lines used for this project (see section 3.1.3) were pre-screened by confocal microscopy to check that the fluorescent markers localise to the cellular areas as has been published (as referenced in section 3.1.3), before they were transformed with the pOpON2.1 dexamethasone inducible system. Further, to ensure only homozygous plants were used, 30 seedlings were germinated on MS agar plates and checked for fluorescence by epifluorescence microscopy. Only lines where fluorescence was evident in all seedlings, were used for transformation.

In addition to the previously mentioned root growth phenotype, lines were checked that non-induced seedlings would not show GUS staining to avoid studying 'leaky' lines (i.e. that

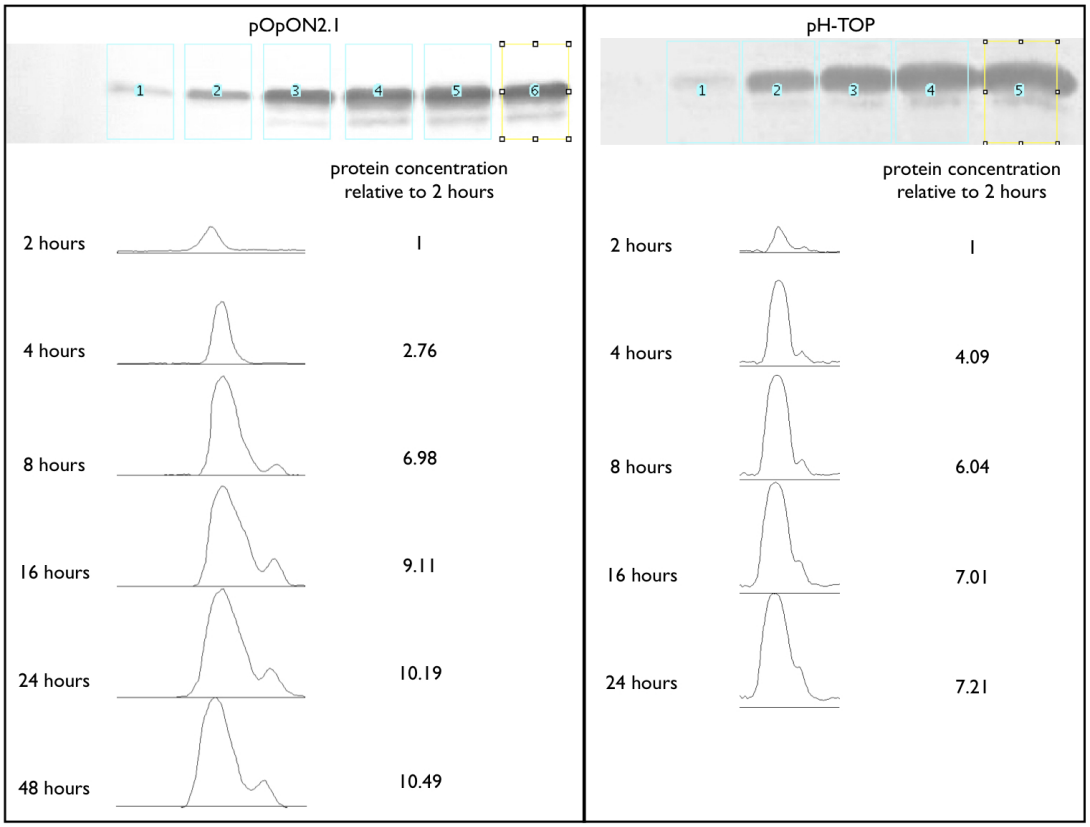

Figure 3.10: Quantification of western blot results. Western blot images were converted into grayscale by Adobe Photoshop CS4 and then analysed by the ImageJ Gel-Analyzer package. Rectangular boxes defined blot lanes and were used to generate a profile plot. From this profile plot, relative content measurements were calculated. pOpON2.1 accumulates about 10-fold of protein at 16 and 24 hours after induction compared to two hours after dexamethasone induction. pH-TOP accumulates about 7-fold protein in the same time frame.

expression of dominant negative RAB-A2a was already present without induction with dexamethasone). Further, several unsuccessful crossing experiments with pH-TOP lines suggested these particular lines were wound inducible, possibly due to the location of insertion of the T-DNA in the *Arabidopsis* genome. Both, a dominant negative (lab name 2NI 1.5A) and a wild type (lab name 2WT 1.45G) RAB-A2a *Arabidopsis* line were cut at their base with scissors at the age of three weeks after germination. Two weeks later shoot growth was examined. All seedlings from the dominant negative line showed strongly inhibited shoot growth, whereas the wounded wild type line exhibited normal growth (figure 3.11). Thus, pOpON2.1 lines were screened for non-wound inducibility before carrying out confocal analysis (GUS staining was carried out 24 hours after wounding the plant leaf with scissors). Table 3.1 shows a sample table of these screenings. For example, the *Arabidopsis* Col-0 line 2NI 11 C-1 does not show GUS staining without dexamethasone treatment and no GUS staining 24 hours after wounding and was used for further experiments. In contrast, line 2NI 11 B-1 showed wound inducibility

and was excluded from further experiments.

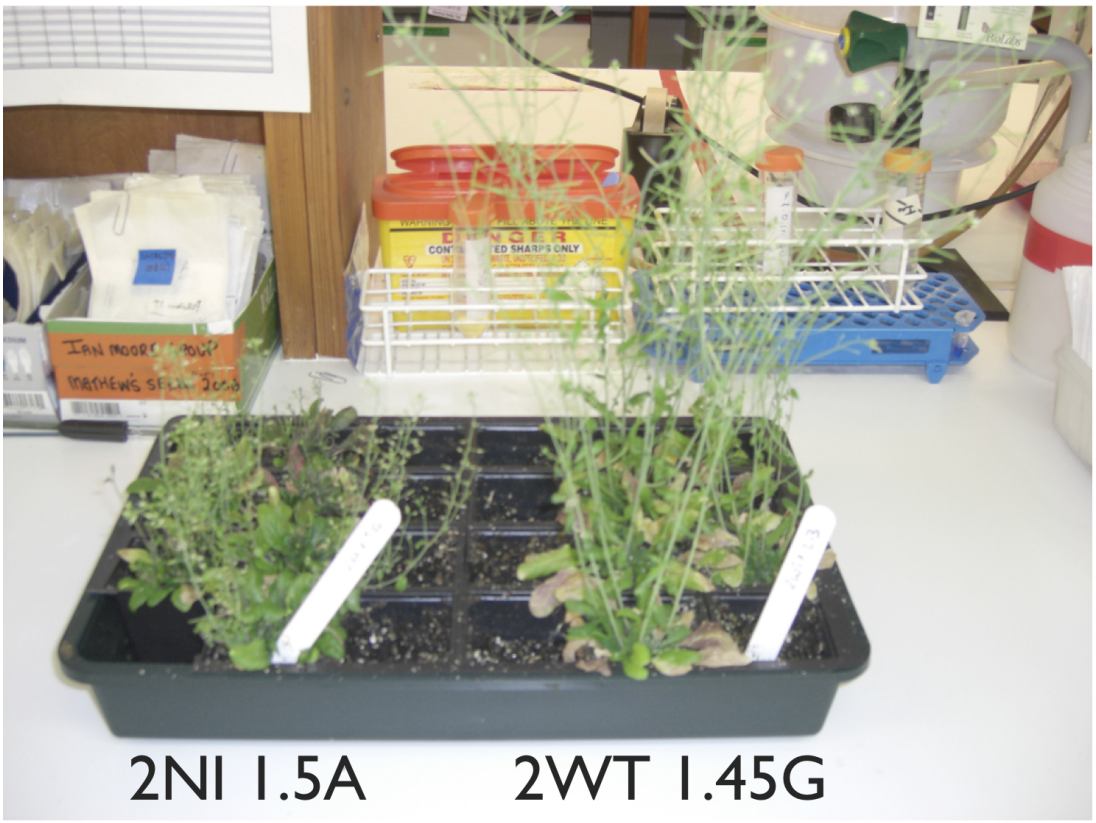

Figure 3.11: Possible wound inducibility of pH-TOP lines. Both, a dominant negative and a wild type RAB-A2a *Arabidopsis* line were cut at their base with scissors at the age of 3 weeks. Two weeks later, the dominant negative line (left) showed strongly inhibited shoot growth, whereas the wounded wild type line (right) exhibited comparably normal shoot growth.

Table 3.1: Further screening of pOpON2.1 lines. Typically, five to eight seedlings per line were investigated. '-' means absence of GUS staining, '+' to '++++' describes the degree of GUS staining observed. Samples labeled '+/-' could not be determined with certainty.

Plant line	2NI11 C-1	2NI11 C-1	2NI11 C-1	2NI11 C-1	2NI11 C-1	2NI11 C-1
Plant no.	1	2	3	4	5	6
DEX treatment	+++	++	-	+++	++	+
DMSO control	-	-	-	-	-	-
Leaf wounding	-	-	-	-	-	-

Plant line	2NI11 A-1	2NI11 A-1	2NI11 A-1	2NI11 A-1	2NI11 A-1	2NI11 B-1
Plant no.	1	2	3	4	5	1
DEX treatment	++++	++	++ +/-	+++	+++	++
DMSO control	-	-	-	-	-	-
Leaf wounding	+	-	-	-	-	+

Plant line	2NI11 B-1	2NI11 B-1	2NI11 B-1	2NI11 B-1	2NI11 B-1	2NI11 B-1
Plant no.	2	3	4	5	6	7
DEX treatment	++++	-	++	++ +/-	+++	+++
DMSO control	-	-	-	-	-	-
Leaf wounding	+	-	+++	+++	-	+

Plant line	2NI21 B-3	2NI21 B-3	2NI21 B-3	2NI21 B-3	2NI21 B-3	2NI21 B-2
Plant no.	1	2	3	4	5	1
DEX treatment	+/-	-	+/-	-	-	-
DMSO control	-	-	-	-	-	-
Leaf wounding	+	-	-	-	-	-

3.2.6 Specificity of dominant negative RAB-A2a

As described in 3.1.1, it is believed that the dominant negative mutant of a Rab GTPase will interfere with the activity cycle of the wild type protein and thus inhibit trafficking that relies on the functionality of this particular Rab GTPase. Hence, if a fluorescent marker is not able to reach its normal steady state localisation in presence of a particular dominant negative Rab GTPase, its trafficking requires a pathway that is dependent on intact wild type Rab GTPase function. Equally, markers that reach their usual localisation in the presence of the dominant negative protein are trafficked through a pathway independent of the studied Rab GTPase.

Seedlings of two independent lines were germinated on MS plates containing 20µM dexamethasone or the respective amount of DMSO as control. Triplicate sets of experiments were conducted for each of the lines, observing three to six individuals per experiment and treatment.

mCherry:RAB-A2a localises to Golgi-like bodies in the presence of dominant negative RAB-A2a

First, I addressed the question whether dominant negative RAB-A2a would indeed interfere with the localisation of RAB-A2a itself. If the working model is correct that the dominant negative mutant keeps the wild type protein in an inactive state and therefor cannot perform its function as interactors of the activity cycle are titrated out, one would expect RAB-A2a to appear more cytosolic and its localisation shift towards the Golgi apparatus. Localisation studies of different mutants have shown that a RAB-A2a mutant that preferentially binds GDP colocalises with Golgi markers, whereas a RAB-A2a mutant, which preferentially binds GTP, is found at the cell periphery [45].

The data showed that the dominant negative RAB-A2a affected the localisation of mCherry:RAB-A2a (figure 3.12). In the control, mCherry:RAB-A2a localised in punctate structures and at the cell periphery (figure 3.12, A1). However, in the presence of dominant negative RAB-A2a, mCherry:RAB-A2a was localised to structures that closely resemble Golgi (figure 3.12, A2). Golgi bodies have a very characteristic 'doughnut' shape that appears slim when observed from the side. The mCherry:RAB-A2a signal at the cell periphery appeared reduced in the dexamethasone induced sample compared to the control. Please see Appendix A for further image examples.

YFP:RAB-A1e localises to Golgi-like bodies in the presence of dominant negative RAB-A2a

YFP:RAB-A1e was chosen as a representative for the Rab-A1 class. Members of the Rab-A1 family reportedly traffic between the Golgi apparatus and the TGN where they play a role in endosomal recycling (see section 1.4.4). This fluorescent marker was transformed with the inducible dominant negative RAB-A2a and analysed to test whether the dominant negative RAB-A2a specifically interferes with RAB-A2a activity or if it interacts with the activity of other Rab GTPases.

The localisation of YFP:RAB-A1e was affected in the presence of dominant negative RAB-A2a (figure 3.12, B1 compared to B2). While RAB-A1e localised in small punctate structures and at the cell periphery in the control (figure 3.12, B1), YFP:RAB-A1e was found in doughnut shaped compartments and exhibited strong cytosolic localisation in the presence of dominant negative RAB-A2a (figure 3.12, B2). The appearance of these doughnut-like structures strongly resemble Golgi bodies. Please see Appendix A for further image examples.

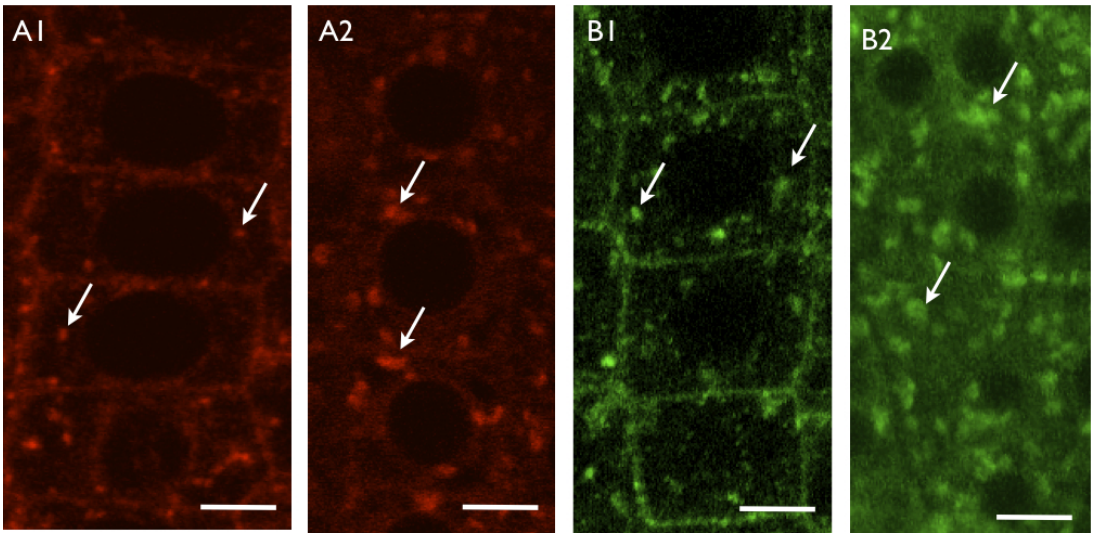

Figure 3.12: Dominant negative RAB-A2a causes localisation of mCherry:RAB-A2a and YFP:RAB-A1e to Golgi-like bodies. Localisation of mCherry:RAB-A2a (A1 and A2) and YFP:RAB-A1e (B1 and B2) in meristematic, epidermal root cells of two independent transgenic *Arabidopsis* Col-0 lines were analysed three days after germination on DMSO or dexamethasone containing MS agar plates (triplicate experiments per line, utilising four to six seedlings per line and treatment). A1: In the control samples (DMSO), the mCherry:RAB-A2a appears in intracellular structures and at the PM (white arrows). A2: In dexamethasone induced samples, the PM localisation is lost and mCherry:RAB-A2a appears in intracellular, enlarged compartments, resembling Golgi bodies (white arrows). B1: YFP:RAB-A1e localises in intracellular punctate structures and at the PM (white arrows) in DMSO control samples. B2: In dexamethasone induced samples, the PM localisation is lost, YFP:RAB-A1e is localised to intracellular, enlarged compartments, resembling Golgi bodies (white arrows). Scale bar = 5µm.

The localisation of mCherry:RAB-A5c is not affected by the dominant negative RAB-A2a mutant

mCherry:RAB-A5c was chosen as a representative of the Rab-A5 family to determine whether the dominant negative RAB-A2a would interfere with trafficking and thus with the function of a more distantly related Rab-A protein (figure 1.6). In *Arabidopsis* roots, RAB-A5c is normally found along the cell edges in lateral roots, however, this localisation is less prominent in the main root (Cherry Chow, DPhil thesis).

Three dominant negative RAB-A2a inducible mCherry:RAB-A5c lines were examined. Two different mCherry:RAB-A5c localisation patterns were observed in the main root of *Arabidopsis.* One line exhibited cell edge localised RAB-A5c with intracellular, punctate structures (figure 3.13, A1 and A2). The other two lines showed only intracellularly localised RAB-A5c in punctate structures (figure 3.13, B1 and B2). In both cases, the localisation of mCherry:RAB-A5c was not affected by the presence of the dominant negative RAB-A2a in comparison to control samples.

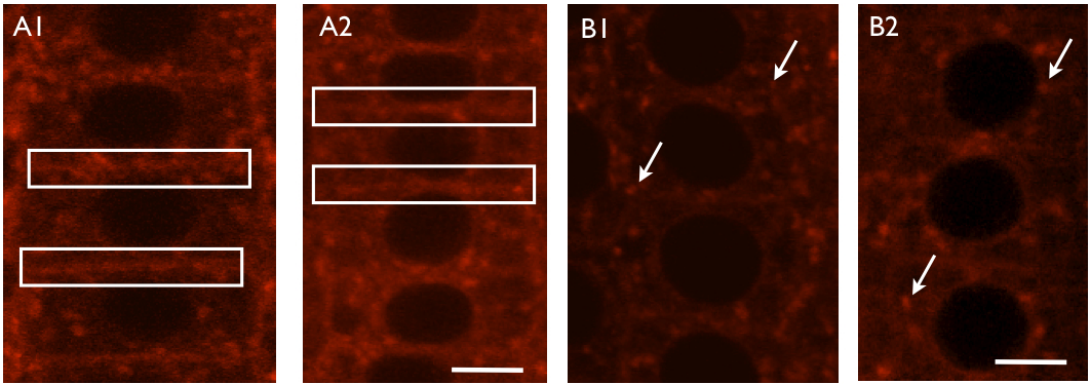

Figure 3.13: Localisation of mCherry:RAB-A5c. A1 and A2 (mCherry:RAB-A5c lines with edge localisation): In both the DMSO control samples (A1) and in the presence of dominant negative RAB-A2a (A2), mCherry:RAB-A5c localises at the cell edges (white arrows) and in intracellular puntuate compartments. B1 and B2 (mCherry:RAB-A5c lines with mostly intracellular localisation): mCherry:RAB-A5c localises to intracellular punctate structures (white arrows) in DMSO control samples (B1) and in the presence of dominant negative RAB-A2a (B2). Meristematic, epidermal root cells of three independent transgenic *Arabidopsis* Col-0 lines were analysed at three days after germination on DMSO or dexamethasone containing MS agar plates (triplicate experiments per line, utilising four to six seedlings per line and treatment). Scale bar = 5 μm.

3.3 Conclusions

In this chapter, the generation of the transgenic lines required for this project and the rationale for the selection of marker lines were described. Either wild type Rab-A2a or the dominant negative mutant form were introduced into the pOpON2.1 vector, a one vector dexamethasone inducible system. The resulting plasmids were transformed into *Arabidopsis* Col-0, which were either marker free or expressed a fluorescent marker.

Root growth of dexamethasone induced pOpON2.1 and pH-TOP lines were observed until seven to eight days after germination. The shoot phenotype was examined on the last day of analysis. The induction of the dominant negative RAB-A2a by the pOpON2.1 system caused faster and stronger inhibition of root growth. The effect on shoot growth is more evident with pOpON2.1 lines, where cotyledons remained very small with dark green colouring, the ability to grow true leaves was lost. pH-TOP lines only exhibited a minor shoot growth defect.

The pattern of GUS expression of the two different inducible systems was examined by GUS stainings. Stainings with induced seedlings were carried out at 0 hours, two hours, four hours, eight hours, 16 hours, 24 hours after induction with dexamethasone. In pOpON2.1 lines, the root tip of the main *Arabidopsis* root, which is the region of interest for this project, started to stain at eight hours after dexamethasone induction. Maximum staining of the root was achieved at 16 hours after induction. In pH-TOP lines, GUS staining appears much weaker with a well stained root tip at 16 to 24 hours after induction. The vasculature of the main root showed staining at four hours but did not reach a similar staining intensity as the pOpON2.1 lines, which already exhibited staining 2 hours after induction with dexamethasone.

The GUS staining results correlated well with western blot experiments. The treatment with dexamethasone resulted in a steady increase of dominant negative RAB-A2a concentration and reached a maximum at around 16 hours to 24 hours after induction with dexamethasone in both pOpON2.1 and pH-TOP lines. However, it appeared that pH-TOP lines only reached a 7-fold increase of protein while pOpON2.1 lines showed a 10-fold increase of protein, corresponding to an absolute level of 10000-fold and 15000-fold increase respectively.

In conclusion, the pOpON2.1 lines are induced more rapidly and give rise to a stronger dominant negative RAB-A2a phenotype than the pH-TOP lines. As a result, I decided to proceed with the pOpON2.1 system for this project.

Transgenic plant lines exhibiting the strongest inhibition of root growth were selected for

further studies. Weak lines may be more difficult to interpret as the insufficient concentration of dominant negative RAB-A2a protein, which is required to act inhibitory, may lead to incorrect conclusions concerning the dependence of a fluorescent marker on an intact RabA2a pathway. However, this problem was solved by selecting for lines with strong root growth inhibition, as this is an effect caused by expression of dominant negative RAB-A2a [45]. When using lines showing strong root growth inhibition, and where the presence of dominant negative RAB-A2a does not have an effect on the localisation or appearance of a marker, one can safely assume that this particular protein is not trafficked *via* a RAB-A2a dependent pathway. Nevertheless, if the localisation of a marker is affected, more experiments are required to decide whether RAB-A2a is in fact required for its trafficking or if the observation reflects a secondary effect.

To test the specificity of the dominant negative approach, I tested the effect of the dominant negative RAB-A2a on fluorescent fusion proteins of selected Rab-A family members: mCherry:RAB-A2a, YFP:RAB-A1e and mCherry:RAB-A5c. If the dominant negative RAB-A2a mutant interferes with wild type RAB-A2a activity, I would expect to see more cytosolic and a predominantly Golgi localised RAB-A2a signal. This is a localisation pattern that has been described for the preferentially GDP-bound RAB-A2a mutant, which putatively mimics the localisation of inactive RAB-A2a [45]. Indeed, mCherry:RAB-A2a localised to doughnut-shaped, Golgi-like bodies and showed increased cytosolic labelling. Surprisingly though, YFP:RAB-A1e also localised to these Golgi-like bodies in the presence of dominant negative RAB-A2a. A possible explanation could be that the dominant negative RAB-A2a interferes with a trafficking pathway that is common to both Rab-A1 and Rab-A2 subclasses. Both subclasses are implicated in TGN-associated traffic [45, 118, 119, 120], are closely related [111] and thus could potentially share a common trafficking pathway. It could also be that RAB-A2a and RAB-A1e are partners of a 'Rab cascade'. Such Rab cascades are known in mammals and yeast where the insertion of one Rab GTPase into its target membrane leads to recruitment of a GAP that will then in turn activate a second Rab GTPase to be recruited to its target membrane [205]. This sequential action of GAPs and GEFs is essential to accurately determine the identities of membrane compartments.

However, it is currently unclear how exactly dominant negative Rab GTPases act as inhibitors. It has been suggested that the dominant negative mutant will interact with the exchange factor of the wild type Rab GTPase, thereby titrating it out of the Rab activity cycle [190]. Thus, the wild type Rab GTPase is no longer able to exchange its GDP for a GTP and is not activated.

The dominant negative protein could potentially interact with factors shared between different Rab-GTPases, thereby affecting several routes, or with a factor completely independent of membrane trafficking functions.

Nevertheless, it appears that dominant negative RAB-A2a only affects a subset of Rab-A proteins. Both mCherry:RAB-A2a and YFP:RAB-A1e are visible in Golgi-like compartments but the localisation of mCherry:RAB-A5c, a representative of the more distantly related Rab-A5 family, is unaffected. mCherry:RAB-A5c is normally found along the cell edges in lateral roots (Cherry Chow, DPhil thesis). I observed two different localisation patterns of RAB-A5c in the main root of *Arabidopsis.* One pattern resembles the edge localisation seen in lateral roots, the second pattern is an intracellular, punctate pattern. In both cases the localisation of mCherry:RAB-A5c is not altered in the presence of dominant negative RAB-A2a. This result suggests that the dominant negative RAB-A2a mutant does not generically inhibit all members of the Rab-A clade.

In summary, this chapter validated pOpON2.1 as a potent dexamethasone inducible system that can be used to address the objectives of this work, which is to study RAB-A2a dependent membrane traffic in *Arabidopsis thaliana* and to propose a trafficking function for RAB-A2a. However, the analysis of data generated with the dominant negative RAB-A2a mutant needs precaution as it is affecting YFP:RAB-A1e localisation and thus potentially normal RAB-A1e function.

In the following chapter, I will use this system to investigate the effect of the expression of the dominant negative RAB-A2a mutant on a range of selected trafficking markers. This will enable me to address the question which trafficking pathways are dependent on RAB-A2a function.

Chapter 4

Investigating the effect of the dominant negative RAB-A2a mutant on membrane traffic in *Arabidopsis thaliana.*

4.1 Introduction

The aim of this study was to investigate RAB-A2a dependent membrane traffic in *Arabidopsis thaliana* and to propose a role for the RAB-A2a compartment as part of the TGN. As mentioned in Chapter 1, the Rab-A2 subclass targets YFP to a BFA-sensitive compartment in *Arabidopsis* root tips, where also endogenous RAB-A2a resides. It was suggested that the YFP:RAB-A2a compartment is an early endosomal compartment as it is labelled by internalised FM4-64 before the PVC. Furthermore, it was shown to overlap the TGN, defined by the marker VHA-a1, close to the Golgi [45].

4.1.1 RAB-A2a and the TGN as a central trafficking hub

A possible role of the RAB-A2/A3 compartment in cytokinesis has been proposed [45]. However, its function in non-dividing cells is unclear. The compartment in mammalian cells that most closely resembles the Rab-A2/A3 compartment is the recycling endosome which also resides on the secretory and endosomal pathways [125]. Previous localisation studies with the preferentially GDP or GTP binding mutants suggest a role of the RAB-A2a compartment in traffic to the PM [45]. Recently, Botanelli and colleagues [206] observed increased secretion of amy:SPO in the presence of the dominant negative RAB-A2a mutant. Chow and colleagues (2008) showed that the predicted GTP bound mutant of RAB-A2a is localised to the cell plate which also reflects the involvement of RAB-A2a in cytokinetic processes as the dominant negative RAB-A2a mutant disrupts these processes [45]. Nevertheless, it cannot be excluded that other trafficking pathways might be dependent on the RAB-A2/A3 compartment as the TGN takes a putatively central position in the plant endomembrane system as a multi-domain complex that is involved in many trafficking pathways [207].

Studies on the sorting nexin (SNX) group of proteins have contributed a significant controversy to the plant endomembrane field. Early observations described the sorting nexins, which together with VPS35, VPS29 and VPS26 form the plant retromer, as part of the TGN and the MVBs [145]. It was argued that especially the latter aspect contributed to defects in vacuolar sorting in *snx1 snx2* double mutants [208]. However, more recent studies using electron microscopy rather than confocal laser scanning microscopy revealed that SNX proteins localise to the TGN and that localisation to PVCs could not be identified with certainty [209]. This shows the higher complexity of the TGN and suggests that the TGN is not just 'a' compartment but rather a multi-domain complex with different functions. Again, this is highlighted by using the SNX example and their differential involvement in PIN recycling. While both PIN1 and PIN2 are believed to cycle *via* the TGN, it is only PIN2 that has been shown to use a SNX1 dependent route [145, 210].

BFA is a fungal toxin that has been widely used to study membrane traffic, more specifically protein cycling dependent on endosomes. Treatment with BFA causes formation of 'BFA bodies' in *Arabidopsis* root cells as early as 30 minutes after treatment with a concentration of 50µM BFA. These BFA bodies consist of an accumulation of early endosomal compartments in its core that are surrounded by Golgi stacks. BFA is known to inhibit cycling of proteins between PM and the TGN *via* endosomes in *Arabidopsis* [86]. However, differential effects

between plant species and tissues have been described [87, 88] (see Chapter 1).

A major target of BFA is the ADP-Ribosylation Factor Guanine nucleotide Exchange Factor (ARF-GEF) GNOM, an exchange factor for ARF GTPases [89]. ARF-GEFs are regulators of vesicle trafficking and are required for the GDP to GTP exchange step that drives activity of GTPases [86]. GNOM is implicated in a lot of trafficking events, such as polar cycling of PIN1 [89] and PIN2 [90] and thereby involved in polar auxin transport. Additionally, GNOM is required for focal accumulation of PEN1 [91], which is required for innate immune responses in fungal attack. Furthermore, the function of *Arabidopsis* Rab GTPases RAB-F2a and RAB-F2b (but not RAB-F1) were shown to be dependent on GNOM [89]. An example for a BFA-resistant ARF-GEF is GNOM LIKE 1 (GNL1) that functions in endocytosis but not in protein recycling [211].

4.1.2 Selected fluorescent markers help to elucidate trafficking pathways dependent on RAB-A2a

To investigate the role of RAB-A2a in interphase cells, I decided to investigate the effect of its dominant negative mutant on a range of fluorescent protein markers in *Arabidopsis.* Trafficking markers were selected to cover a range of major trafficking pathways in *Arabidopsis:* traffic to the PM, endocytic and PVC traffic, traffic to the vacuole and recycling pathways.

The selected fluorescent markers traffic to known steady state locations within the plant cell through the endomembrane system (figure 4.1 and table 4.1). Dominant negative proteins compete with wild type proteins for interactors and thus inhibit the function of wild type proteins [190]. In the case of Rab GTPases, dominant negative mutants are believed to interact with the GEF that catalyses the GDP to GTP exchange thus shifting the activity cycle towards the 'off' or 'inactive' state [106]. By introducing the dominant negative RAB-A2a GTPase mutant into the plant, the trafficking pathways of selected fluorescent markers (table 4.1) are tested for dependency on an intact RAB-A2a trafficking route. In cases where trafficking of a particular marker requires RAB-A2a mediated trafficking, an altered fluorescence distribution pattern is expected in the presence of dominant negative RAB-A2a.

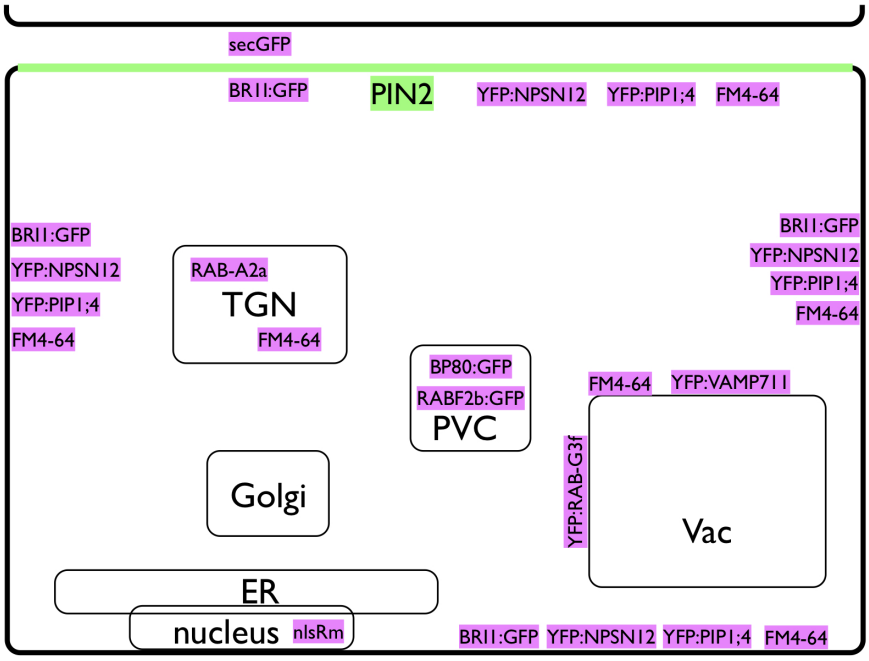

Figure 4.1: Steady state localisations of fluorescent marker lines used in this work. TGN = trans-Golgi network, PVC = pre-vacuolar compartment, Vac = vacuole, ER = Endoplasmic reticulum. Details and references are provided in table 4.1 and in the text.

Table 4.1: Fluorescent proteins are used as markers to study different trafficking pathways. This table gives an overview of the selected fluorescent markers, their steady state localisations and the probed trafficking pathway.

Marker	Localisation	Trafficking pathway	Reference
nlsRm-2A-secGFP	Nuclear RFP and secreted GFP	Default secretion, nuclear morphology	[200]
YFP:NPSN12	PM	Traffic to PM	[212]
YFP:PIP1;4	PM	Traffic to PM	[150]
YFP:VAMP711	PVC and vacuole	PVC to vacuole	[150]
YFP:RAB-G3f	PVC and vacuole	PVC to vacuole	[150]
BP80:GFP	PVC	Traffic to PVC	[40, 213, 214, 215]
RAB-F2b:GFP	PVC	Traffic to PVC	[26, 139]
PIN2:GFP	Endosomes and apical PM	Polarised secretion, protein recycling	[73, 92, 211, 216]
BRI1:GFP	Endosomes and PM	Traffic to PM and protein recycling	[58, 217, 218]
FM4-64	PM, endosomes, PVC, tonoplast	Endocytosis	[219]

Markers used to probe PM traffic

To test the hypothesis that RAB-A2a is involved in traffic to the PM, I chose to analyse nlsRm-2A-secGFP to probe for default secretion of a secreted soluble marker and the membrane bound markers YFP:NPSN12 and YFP:PIP1;4 to analyse effects on traffic to the PM of insoluble cargo. In addition, the effect of the dominant negative RAB-A2a in combination with the drug BFA was studied in the latter two markers to test for a role in protein cycling.

nlsRm-2A-secGFP is a ratiometric marker that was used to determine changes in default secretion. The 2A-peptide is cleaved within the cell, the RFP is fused to a nuclear localisation signal that will allow transport of RFP to the nucleus; the GFP is default secreted to the plant apoplast where it remains largely invisible when trafficking is intact [220]. Changes in secretory traffic can be determined by comparing the intensities of RFP versus GFP in the samples where secGFP is accumulated and visible due to trafficking defects [200].

NPSN12 (Novel Plant Snare protein 12) is one of three members of a novel class of SNARE proteins. YFP:NPSN12 localises to the PM and occasionally to punctate structures within the plant cell that are believed, but have not been shown, to be Golgi. However, not much is known about the exact trafficking pathway or function of this protein and thus requires further study [212].

PIP1;4 (Plasma membrane Intrinsic Protein 1;4) is an aquaporin. YFP:PIP1;4 was previously shown to localise exclusively to the PM; the exact trafficking route or function of this protein is unknown [150].

Selected vacuolar markers to study RAB-A2a dependent membrane traffic

The following selection of vacuolar markers was used to study a possible involvement of RAB-A2a in a variety of vacuolar trafficking pathways.

YFP:VAMP711 (Vesicle Associated Membrane Protein 711) is a SNARE fusion protein that is believed to traffic between the PVC and the vacuole [150].

YFP:RAB-G3f is another member of the *Arabidopsis* Rab GTPase family. This marker was used to study the effect of the dominant negative RAB-A2a on PVC and vacuole morphology [150] and further served to probe specificity of the dominant negative RAB-A2a mutant.

RAB-F2b:GFP is a marker for PVC morphology and in addition, was used to investigate

specificity of the RAB-A2a dominant negative mutant. A possible role in endocytosis and cycling have been described [26, 139], which are discussed in section 1.6.

BP80:GFP is a well known and studied vacuolar sorting receptor. BP80:GFP is enriched in clathrin-coated vesicle fractions [213] and has been located in the *trans*-Golgi and the PVC [40, 214, 215].

Markers for endocytic and recycling pathways

PIN-FORMED 2 (PIN2) is an auxin transporter which directs root gravitropsim [73] and received wide attention due to its polar localisation at the basal PM in meristematic, epidermal root cells. It has been shown that PIN2 initially localises to both apical and basal PM of *Arabidopsis* root cells after cytokinesis but will subsequently disappear from one, owing to sterol-dependent endocytosis [216]. PIN2 is transported to the PM via the Golgi/TGN from where PIN2 is endocytosed *via* a GNL1 dependent pathway [211]. It cycles back to the TGN *via* GNOM-independent endosomes and is then re-delivered to the PM by recycling endosomes. As all members of the PIN family, it is believed that this protein cycles rapidly between PM and internal compartments to be able to respond to environmental factors influencing auxin metabolism quickly [221]. Kleine-Vehn and colleagues (2008) showed that prolonged BFA treatment causes a shift of PIN2 localisation from the apical to the basal membrane, a process called 'transcytosis'. Transcytosis describes a process in which the localisation of a polar protein is shifted *via* recycling endosomes. This was shown to be dependent on intact microtubules but independent of the ARF-GEF GNL1 in the case of PIN2 across 30 different *Arabidopsis* ecotypes [92].

However, to distinguish possible effects on either polarity control or protein cycling and recycling, it was also necessary to study a non-polar, recycling protein. For this purpose, I chose to study BRI1:GFP, which is a steroid receptor that localises to the PM and endosomal compartments [58]. Similarly to PIN2:GFP, it is a recycling protein and uses a pathway that involves the VHA-a1 compartment [217], but mostly *via* a GNOM dependent pathway [218].

FM4-64 is a synthetic styryl dye commonly used to probe the endocytic pathway in plant cells. The described pathway begins at the PM where FM4-64 is internalised in endocytic vesicles, is gradually transported to the TGN, and subsequently to the PVC until it reaches the vacuole [219].

4.2 Results

If not otherwise stated, seedlings were germinated and grown on plates containing 20µM dexamethasone or the respective amount of its solvent DMSO as control. Seedling roots were analysed by confocal microscopy at three days after germination. Induced seedlings are clearly distinguishable from non-induced seedlings by short roots and small, dark green cotyledons.

Images represent the findings of triplicate experiments per two independent lines with at least three seedlings per treatment. The analysed cell types from the *Arabidopsis* main root are mainly meristematic. In rare occasions mature, elongated root cells were imaged (indicated in the respective images).

In cases were BFA treatments were applied to marker lines, both dexamethasone induced seedlings as well as their DMSO treated controls were treated with 50µM BFA. Times vary depending on experimental purpose and are indicated in the individual experiments.

4.2.1 Dominant negative RAB-A2a affects PIN2:GFP trafficking

PIN2:GFP localisation is affected in the presence of dominant negative RAB-A2a

Chow and colleagues showed that expression of the dominant negative RAB-A2a mutant causes severe root growth defects [45], which leads to the hypothesis that RAB-A2a may be involved in trafficking of crucial factors of root development, such as PINs. Therefore PIN2:GFP trafficking was investigated as representative of the PIN protein family. As mentioned before, PIN2:GFP is a polar localised, recycling protein that localises to the basal PM in meristematic, epidermal *Arabidopsis* root cells.

24 different inducible dominant negative RAB-A2a (A2aNI) *Arabidopsis* lines in the PIN2:GFP background were screened for root growth inhibition upon induction with dexamethasone. Out of these lines, two lines exhibiting the strongest root growth inhibition were selected for confocal analysis (figure 4.2).

In the presence of dominant negative RAB-A2a, the localisation of PIN2:GFP was dramatically changed (figure 4.3). PIN2:GFP exhibited a strong intracellular pattern in addition to a weak PM labeling. Polairty of PIN2:GFP was not clearly visible in both the control and in the presence of dominant negative RAB-A2a, possibly due to overexpression of the PIN2:GFP

marker. Please see Appendix A for a wider range of PIN2:GFP examples of these experiments.

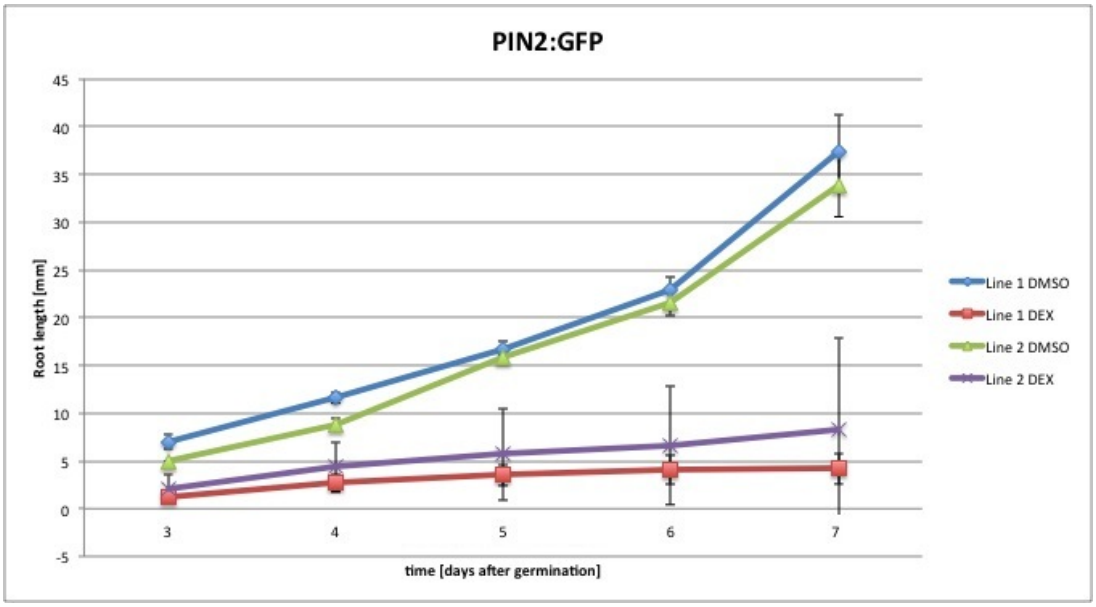

Figure 4.2: Root growth assay of selected PIN2:GFP A2aNI lines (lab names: Line 1: PIN2 2NI11 B-3, Line 2: PIN2 2NI11 B-4). Root growth was monitored for three to seven days after germination on 20µM dexamethasone or DMSO containing plates. Dexamethasone induced seedlings exhibit root growth inhibition compared to control seedlings. Data points represent mean average root growth from 15 to 20 seedlings per line and treatment. Error bars represent standard deviation.

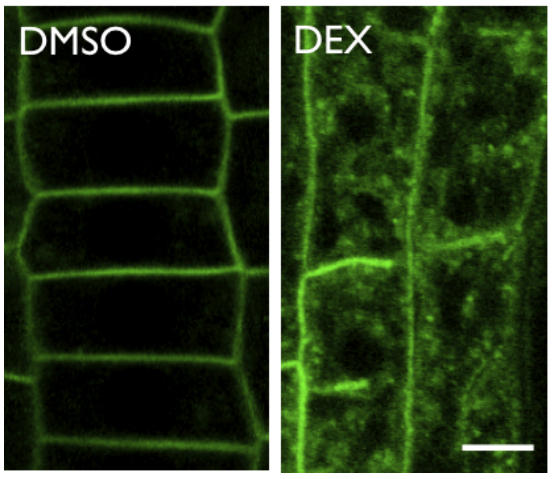

Figure 4.3: Trafficking of PIN2:GFP is affected by the dominant negative RAB-A2a. DMSO: PIN2:GFP labels the PM in control samples. DEX: Cytokinesis defects (cell wall stubs) are present. In the presence of dominant negative RAB-A2a, PIN2:GFP exhibits a strong intracellular localisation. Meristematic, epidermal root cells of two independent transgenic *Arabidopsis* Col-0 lines were analysed at three days after germination on DMSO or dexamethasone containing MS agar plates (triplicate experiments per line, utilising four to six seedlings per line and treatment). Scale bar = 5µm.

PIN2:GFP localisation is not affected by RAB-A2a overexpression or dexamethasone treatment

Following the results obtained on PIN2:GFP localisation with dominant negative RAB-A2a, it was necessary to test whether this change in localisation was due to either the dexamethasone treatment itself or a protein overexpression effect. Thus, *Arabidopsis* PIN2:GFP lines, where the expression of wild type RAB-A2a (A2aWT) is dexamethasone inducible through the pOpON2.1 system were screened (figure 4.4) and analysed (figure 4.6).

A western blot probed with anti-RAB-A2a antibodies (figure 4.5) ensured that the inducible expression of RAB-A2a wild type protein was at least as strong or stronger than that of the studied inducible dominant negative RAB-A2a lines. In both control and wild type RAB-A2a overexpressing samples, PIN2:GFP localised to the PM. The analysis of the inducible wild type RAB-A2a lines revealed no effect on the localisation pattern of PIN2:GFP (figure 4.6), suggesting that the effect observed in figure 4.3 iwas due to the presence of dominant negative RAB-A2a and was not an effect of the dexamethasone treatment or the overexpression of RAB-A2a.

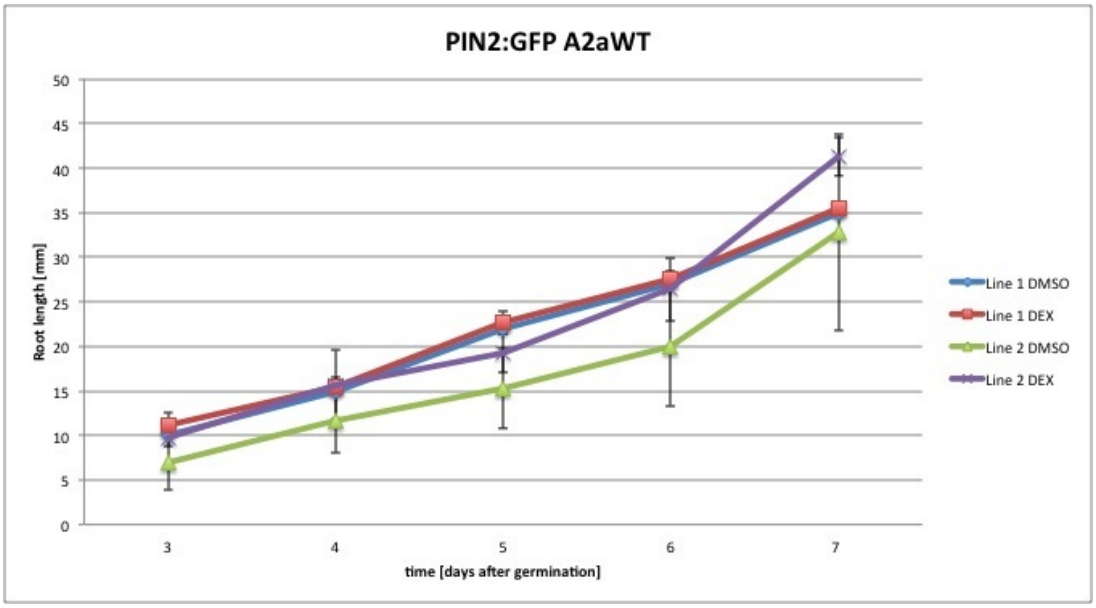

Figure 4.4: Root growth assay of selected PIN2:GFP A2aWT lines (lab names: Line 1: PIN2 WT1, Line 2: PIN2 WT3). Root growth was monitored for three to seven days after germination on 20µM dexamethasone or DMSO containing plates. Dexamethasone induced seedlings showed slightly increased root growth compared to control seedlings. Data points represent average root growth from 15 to 20 seedlings per line and treatment. Error bars represent standard deviation.

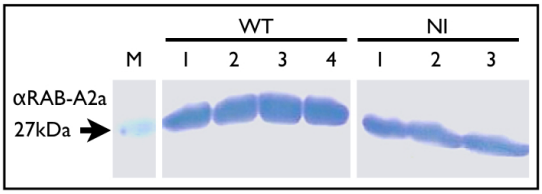

Figure 4.5: Western blot of PIN2:GFP A2aWT and A2aNI. Four inducible A2aWT PIN2:GFP lines (WT 1 - 4) were compared to three of the strongest A2aNI PIN2:GFP lines (NI 1 - 3). Equal amounts of sample, standardised to seedling fresh weight, were loaded on a gel and visualised by western blotting probed with an anti-RAB-A2a antibody. The inducible wild type RAB-A2a lines ('WT') express more protein than the inducible dominant negative RAB-A2a lines ('NI'). 'M' is a 27kDa marker.

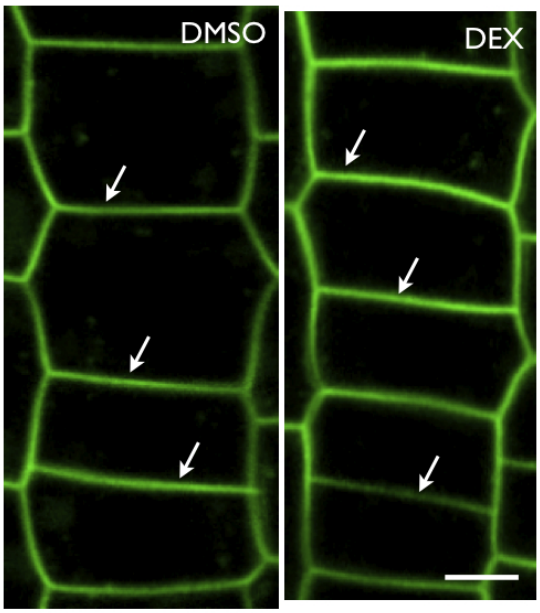

Figure 4.6: Localisation of PIN2:GFP is not altered in the presence of excess wild type RAB-A2a. DMSO: PIN2:GFP localises to the PM (white arrows) in control samples. DEX: In dexamethasone induced wild type RAB-A2a overexpressing seedlings, PIN2:GFP localises to the PM (white arrows). Meristematic, epidermal root cells of two independent transgenic *Arabidopsis* Col-0 lines were analysed at three days after germination on DMSO or dexamethasone containing MS agar plates (triplicate experiments per line, utilising four to six seedlings per line and treatment). Scale bar = 5µm.

BFA treatment enhances intracellular accumulation of PIN2:GFP

PIN2:GFP A2aNI lines were treated with BFA to address the question whether RAB-A2a is involved in cycling of PIN2:GFP. Induced dominant negative RAB-A2a PIN2:GFP seedlings and uninduced control seedlings were treated with 50µM BFA for 90 minutes and then analysed by confocal microscopy. In BFA treated control samples, PIN2:GFP was localised at the PM and in BFA bodies (figure 4.7). In dominant negative RAB-A2a induced BFA treated samples, PIN2:GFP was found in BFA bodies and exhibited a weak PM signal. It appeared

the intracellular signal of PIN2:GFP observed in the presence of dominant negative RAB-A2a was now accumulated in the BFA bodies, indicating a possible role for RAB-A2a in PIN2:GFP cycling.

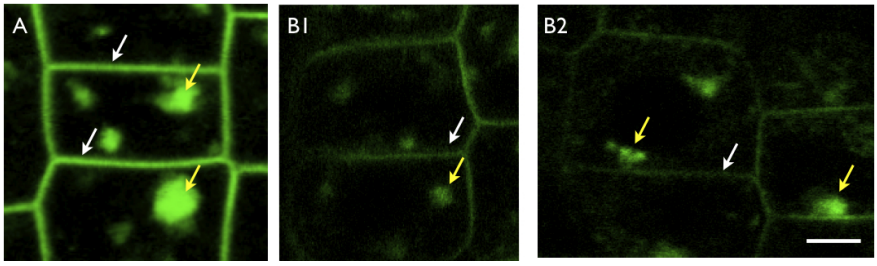

Figure 4.7: BFA treatment reveals a possible role for RAB-A2a in PIN2:GFP cycling. A: After BFA treatment PIN2:GFP labels the PM (white arrows) and localises in BFA bodies (yellow arrows) in DMSO control samples. B1 and B2: After BFA treatment and in the presence of dominant negative RAB-A2a, PIN2:GFP localises in BFA bodies (yellow arrows) and exhibits a weak PM signal (white arrows). Meristematic, epidermal root cells of two independent transgenic *Arabidopsis* Col-0 lines were analysed at three days after germination on DMSO or dexamethasone containing MS agar plates (triplicate experiments per line, utilising four to six seedlings per line and treatment). Scale bar = 5µm.

PIN2:GFP traffic is not affected by dominant negative RAB-A5c

As a next step, I wanted to address the question whether trafficking of PIN2:GFP was specifically affected by the dominant negative RAB-A2a mutant or if the localisation of this marker is in general more sensitive to trafficking defects. For this purpose, I analysed the effect of dominant negative RAB-A5c on PIN2:GFP traffic. The dexamethasone inducible dominant negative RAB-A5c pOpON2.1 lines in PIN2:GFP background were previously generated by Camille Foucart (unpublished data). Two lines were selected and analysed.

First, root growth assays were carried out to analyse the severity of root growth inhibition of dominant negative RAB-A5c on the main root of *Arabidopsis.* As the graph in figure 4.8 shows, expression of dominant negative RAB-A5c inhibited root growth, albeit to a lesser extent than dominant negative RAB-A2a.

Seedlings were then analysed by confocal microscopy. In the control samples, PIN2:GFP exhibited the expected PM labeling (figure 4.9). In the presence of dominant negative RAB-A5c, the localisation and thus trafficking of PIN2:GFP was not affected in meristematic cells. However, PIN2:GFP exhibited strong intracellular accumulation in lateral root cap cells (data not shown) which may indicate a role for RAB-A5c in a different trafficking aspect of PIN2:GFP. This result implies that trafficking of PIN2:GFP is specifically affected by dominant negative

RAB-A2a, at least in meristematic, epidermal root cells.

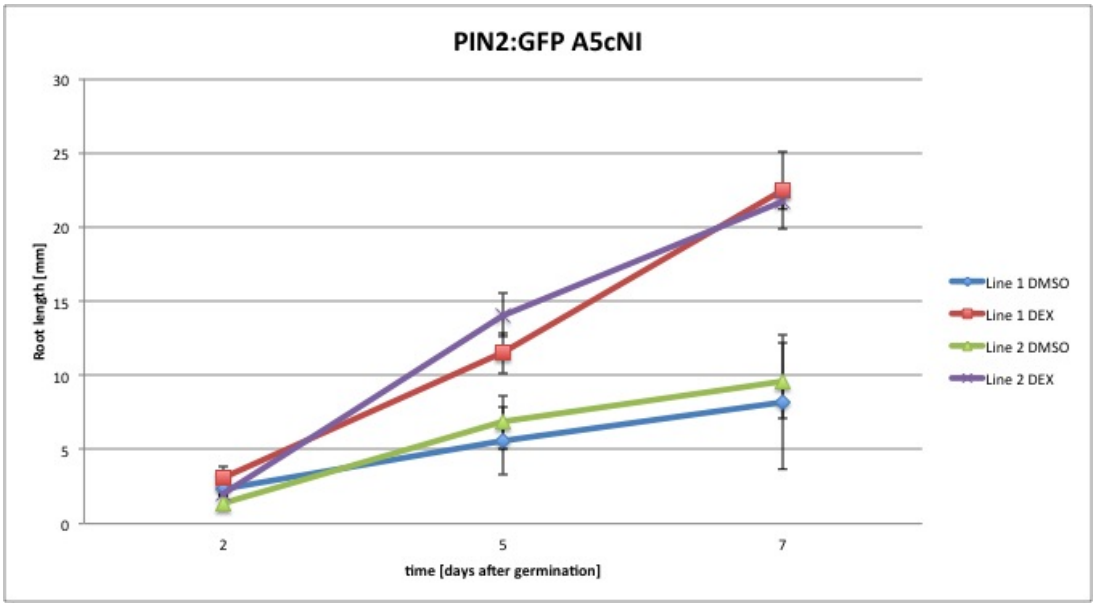

Figure 4.8: Root growth assay of selected PIN2:GFP A5cNI lines (lab names: Line 1: 2366-2c, Line 2: 131a8b). Root growth was monitored for three to seven days after germination on 20µM dexamethasone or DMSO containing plates. Dexamethasone induced seedlings exhibited root growth inhibition compared to control seedlings. Data points represent average root growth from 15 to 20 seedlings per line and treatment. Error bars represent standard deviation.

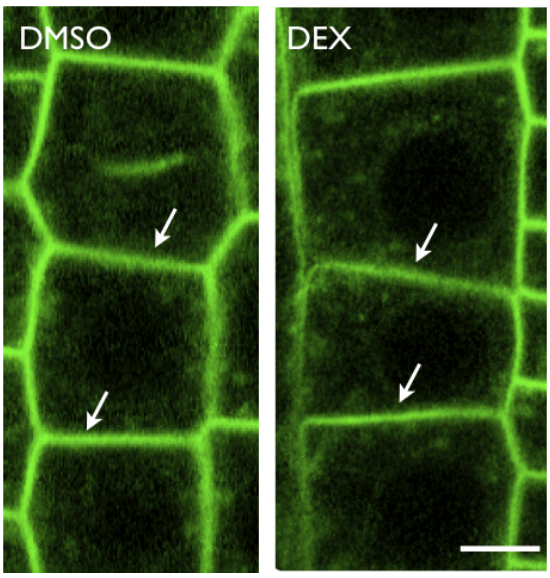

Figure 4.9: Trafficking of PIN2:GFP in meristematic, epidermal root cells is not affected by dominant negative A5c. (DMSO) PIN2:GFP labels the PM (white arrows) in control samples. (DEX) PIN2:GFP labels the PM (white arrows) in dexamethasone induced samples. Meristematic, epidermal root cells of two independent transgenic *Arabidopsis* Col-0 lines were analysed at three days after germination on DMSO or dexamethasone containing MS agar plates (triplicate experiments per line, utilising four to six seedlings per line and treatment). Scale bar = 5µm

The localisation of BRI1:GFP is not affected in the presence of dominant negative RAB-A2a

12 different inducible A2aNI *Arabidopsis* lines in the BRI1:GFP background were screened for root growth inhibition upon induction with dexamethasone. Out of these lines, two lines exhibiting the strongest root growth inhibition were selected for confocal analysis (figure 4.10).

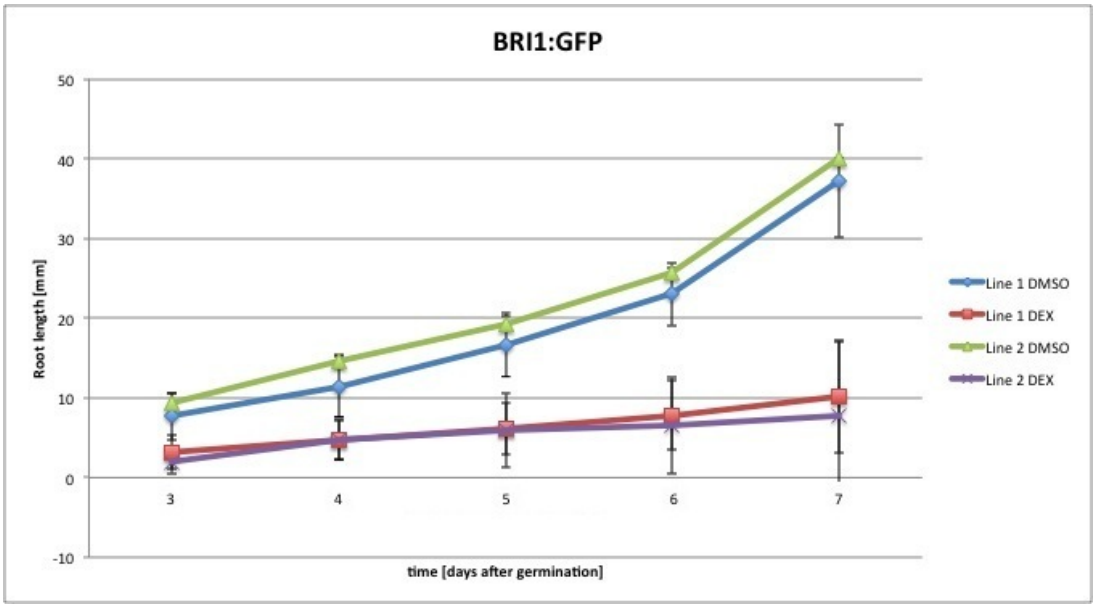

Figure 4.10: Root growth assay of selected BRI1:GFP A2aNI lines (lab names: Line 1: BRI1 2NI11 D-7, Line 2: BRI1 2NI11 D-9). Root growth was monitored for three to seven days after germination on 20µM dexamethasone or DMSO containing plates. Dexamethasone induced seedlings exhibit root growth inhibition compared to control seedlings. Data points represent average root growth from 15 to 20 seedlings per line and treatment. Error bars represent standard deviation.

BRI1:GFP labeled the PM and the cell plate in control samples (figure 4.11). This localisation was not affected in presence of dominant negative RAB-A2a, BRI1:GFP localised to the PM and was present on cell wall stubs. The results suggest that RAB-A2a does not play a role in PM trafficking of BRI1:GFP.

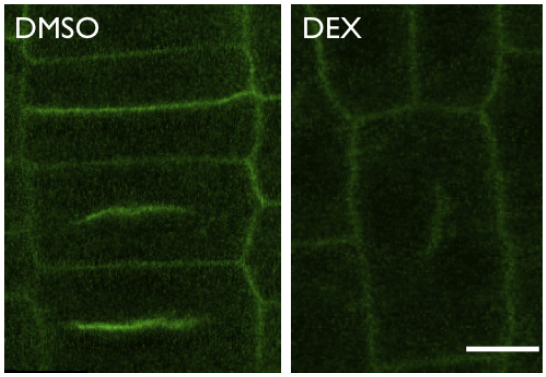

Figure 4.11: Localisation of BRI1:GFP is not affected in the presence of dominant negative RAB-A2a. DMSO: BRI1:GFP labels the PM and localises to the cell plate in control samples. DEX: In the presence of dominant negative RAB-A2a, BRI1:GFP localises to the PM and to cell plate aberrations. Meristematic, epidermal root cells of two independent transgenic *Arabidopsis* Col-0 lines were analysed at three days after germination on DMSO or dexamethasone containing MS agar plates (triplicate experiments per line, utilising four to six seedlings per line and treatment). Scale bar = 5µm.

BRI1:GFP cycling is not affected in the presence of dominant negative RAB-A2a

To test whether RAB-A2a was involved in cycling of BRI1:GFP, BFA treatments were carried out. Induced dominant negative RAB-A2a BRI1:GFP seedlings and uninduced control seedlings were treated with 50µM BFA for 90 minutes and then analysed by confocal microscopy. In BFA treated control samples, BRI:GFP was localised at the PM and in BFA bodies (figure 4.12). In dominant negative RAB-A2a induced BFA treated samples, BRI1:GFP was found in BFA bodies and also labeled the PM. It appears that BRI1:GFP cycling is not affected by dominant negative RAB-A2a.

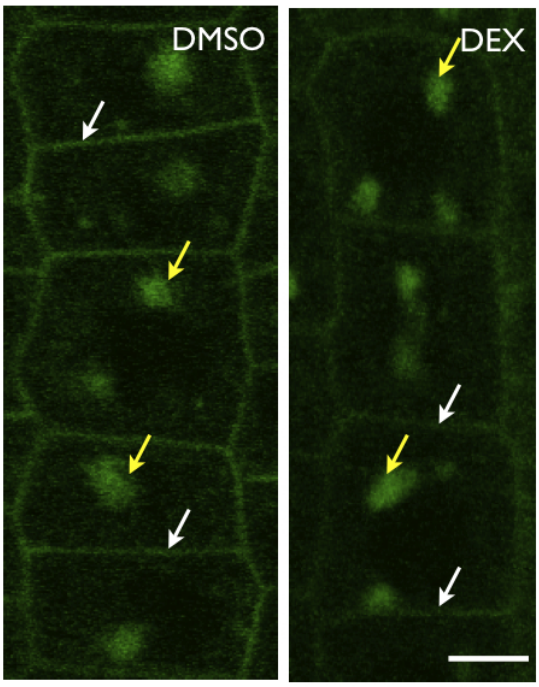

Figure 4.12: BRI1:GFP cycling is not affected by the dominant negative RAB-A2a. DMSO: After BFA treatment BRI1:GFP labels the PM (white arrows) and localises in BFA bodies (yellow arrows) in control samples. DEX: After BFA treatment and in the presence of dominant negative RAB-A2a, BRI1:GFP labels the PM (white arrows) and localises in BFA bodies (yellow arrows). Meristematic, epidermal root cells of two independent transgenic *Arabidopsis* Col-0 lines were analysed at three days after germination on DMSO or dexamethasone containing MS agar plates (triplicate experiments per line, utilising four to six seedlings per line and treatment). Scale bar = 5µm.

4.2.2 Default traffic to the PM is not affected by dominant negative RabA2a

Previous mutant localisation studies revealed that the preferentially GDP binding mutant of RAB-A2a localises to Golgi stacks while the GTP binding mutant is found mostly at the cell periphery [45]. These findings suggest that the RAB-A2a compartment might play a role in a trafficking route from the Golgi / TGN to the PM. Therefore, it appeared likely that default secretory or PM pathways could be affected by the expression of dominant negative RAB-A2a.

Default secretion is not affected by presence of dominant negative RAB-A2a

24 different inducible A2aNI *Arabidopsis* lines in the nlsRm-2A-secGFP background were screened for root growth inhibition upon induction with dexamethasone. Out of these lines, two lines exhibiting the strongest root growth inhibition were selected for confocal analysis (figure 4.13).

Due to a high degree of silencing of the 35S promoter and thus expression of both the fluorescent marker and the inducible construct, data was collected from various cell types across the seedling root that showed marker expression. The nuclear RFP signal was clearly visible but no intracellular accumulation of secGFP was observed (figure 4.14). It appears that the dominant negative RAB-A2a mutant does not affect default secretion of this marker.

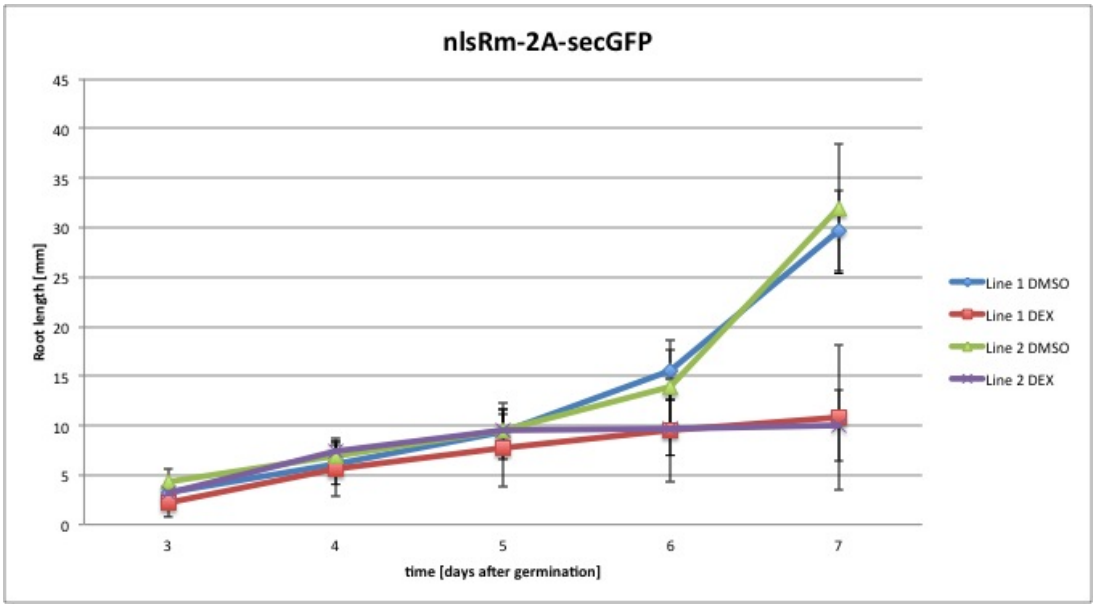

Figure 4.13: Root growth assay of selected nlsRm-2A-secGFP A2aNI lines (lab names: Line 1: 74-6E 2NI11 B-2. Line 2: 74-6E 2NI11 B-3). Root growth was monitored for three to seven days after germination on 20µM dexamethasone or DMSO containing plates. Dexamethasone induced seedlings exhibit root growth inhibition compared to control seedlings. Data points represent mean average root growth from 15 to 20 seedlings per line and treatment. Error bars represent standard deviation.

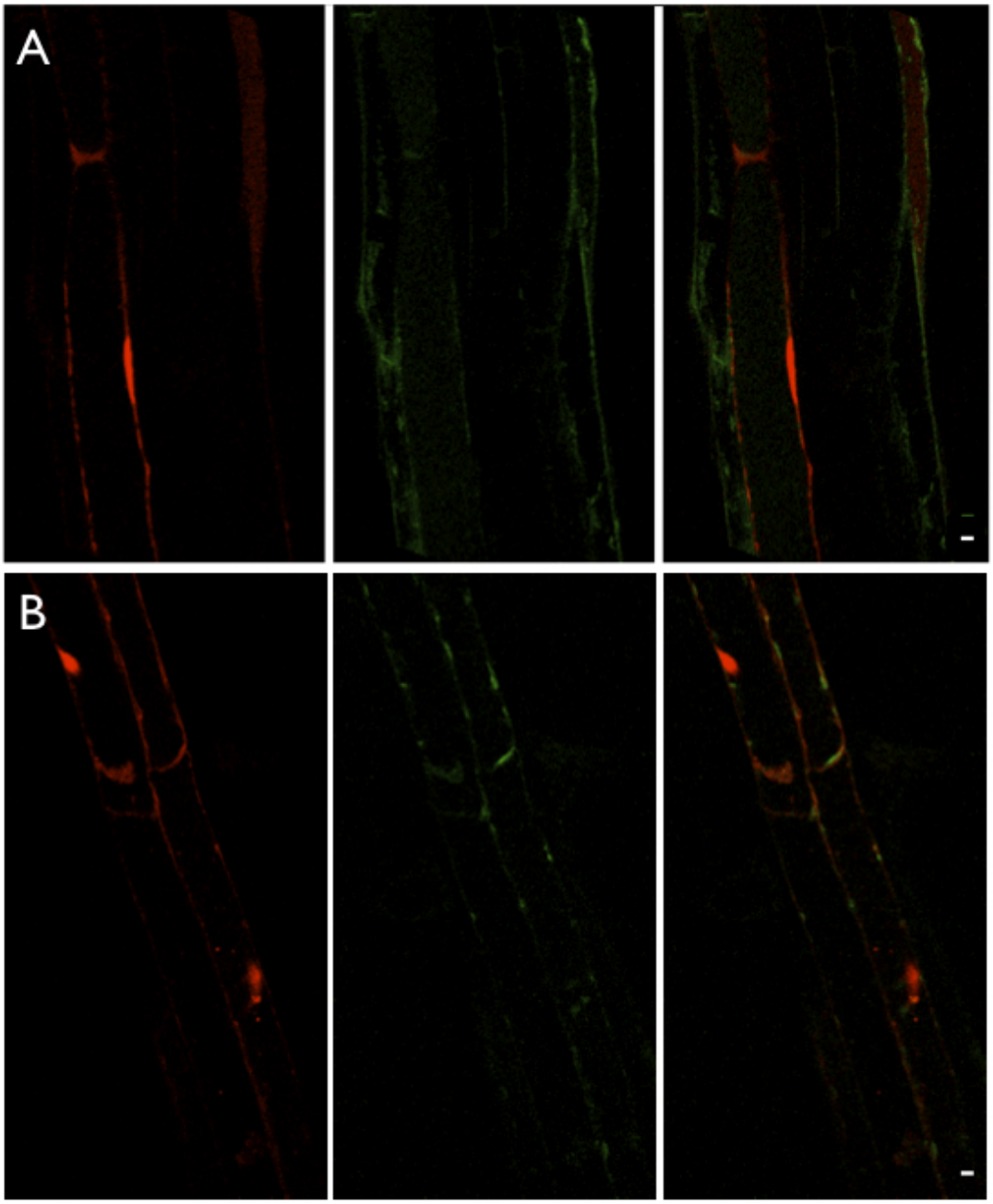

Figure 4.14: Dominant negative RAB-A2a does not affect default secretion. The images show nlsRm (red channel), secGFP (green channel), and the merged image. In both DMSO treated (A) and dexamethasone induced (B) samples, the red nulcear signal is clearly visible in the nucleus; the nucleus has normal appearance. In both cases, a trafficking defect of secGFP signal is not visible. Mature, elongated root cells of two independent *Arabidopsis* Col-0 lines were analysed at three days after germination on DMSO or dexamethasone containing MS agar plates (triplicate experiments per line, utilising four to six seedlings per line and treatment). Scale bar = 5µm

Trafficking of YFP:NPSN12 to the PM is not affected by dominant negative RAB-A2a

12 different inducible A2aNI *Arabidopsis* lines in the YFP:NPSN12 background were screened for root growth inhibition upon induction with dexamethasone. Out of these lines, two lines exhibiting the strongest root growth inhibition (figure 4.15) were selected for confocal analysis.

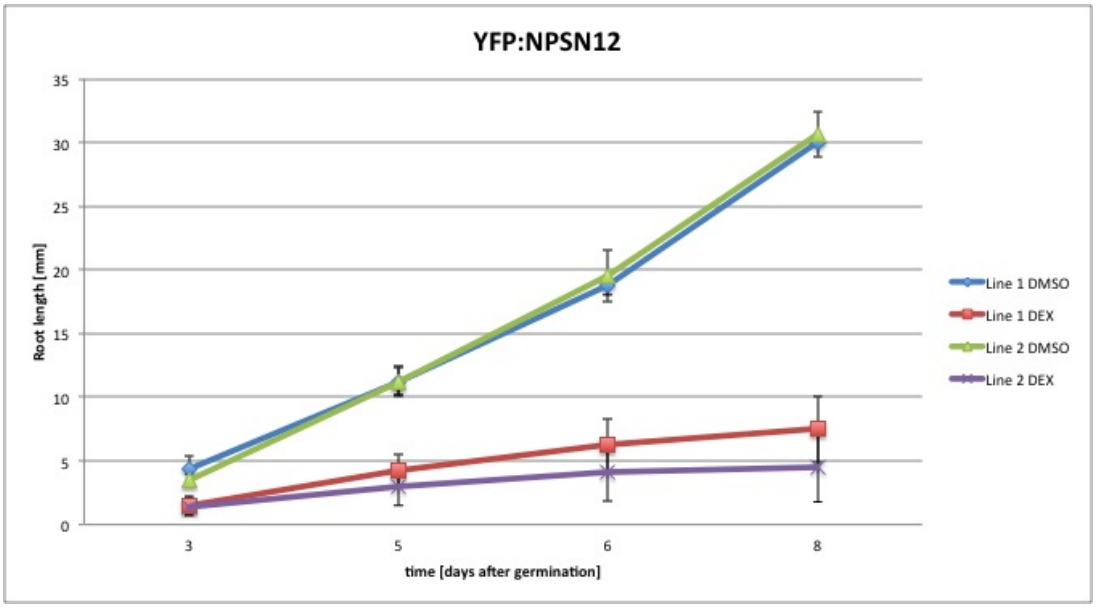

Figure 4.15: Root growth assay of selected YFP:NPSN12 A2aNI lines (lab names: Line 1: NPSN12 2NI11 C-1 Line 2: NPSN12 2NI21 A-3). Root growth was monitored for three to eight days after germination on 20µM dexamethasone or DMSO containing plates. Dexamethasone induced seedlings exhibit root growth inhibition compared to control seedlings. Data points represent mean average root growth from 15 to 20 seedlings per line and treatment. Error bars represent standard deviation.

YFP:NPSN12 was localised at the PM in DMSO control seedlings (figure 4.17, A and B). In the presence of dominant negative RAB-A2a, YFP:NPSN12 was localised at the PM with no visible intracellular accumulations. It appears that the trafficking of YFP:NPSN12 is not affected by the dominant negative RAB-A2a mutant.

Cycling of YFP:NPSN12 is not affected by dominant negative RAB-A2a.

Seedlings were treated with 50µM BFA for two hours and then imaged by confocal microscopy. In both the control and dexamethasone induced samples, BFA bodies were clearly visible with no effect on the PM localisation of YFP:NPSN12 (figure 4.17, C and D). This suggests that RAB-A2a is not invovled in cycling or PM trafficking of YFP:NPSN12.

Trafficking of YFP:PIP1;4 to the PM is not affected by dominant negative RAB-A2a.

14 different inducible A2aNI *Arabidopsis* lines in the YFP:PIP1;4 background were screened for root growth inhibition upon induction with dexamethasone. Out of these lines, two lines exhibiting the strongest root growth inhibition were selected for confocal analysis (figure 4.16).

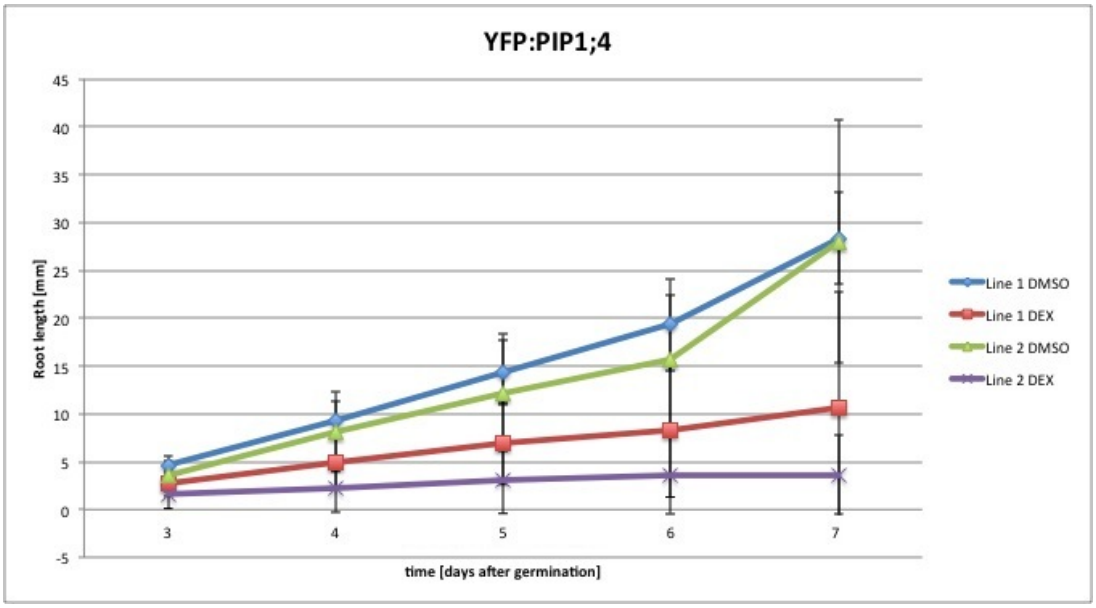

Figure 4.16: Root growth assay of selected YFP:PIP1;4 A2aNI lines (lab names: Line 1: PIP1;4 2NI21 A-1 Line 2: PIP1;4 2NI21 B-10). Root growth was monitored for three to seven days after germination on 20µM dexamethasone or DMSO containing plates. Dexamethasone induced seedlings exhibit root growth inhibition compared to control seedlings. Data points represent mean average root growth from 15 to 20 seedlings per line and treatment. Error bars represent standard deviation.

YFP:PIP1;4 is localised at the PM in *Arabidopsis* roots (figure 4.17, E and F). YFP:PIP1;4 was able to reach the PM in the presence of dominant negative RAB-A2a. It appears that YFP:PIP1;4 is not prevented from reaching the PM in the presence of dominant negative RAB-A2a.

BFA treatment does not reveal an effect on YFP:PIP1;4 cycling in presence of dominant negative RAB-A2a

Experiments with BFA treatments were carried out with YFP:PIP1;4 to test the possibility that RAB-A2a might be required for cycling of this marker (figure 4.17, G and H). In both, control and induced samples, YFP:PIP1;4 was localised at the PM and in BFA bodies. This suggests that RAB-A2a dependent traffic is not required for YFP:PIP1;4 cycling.

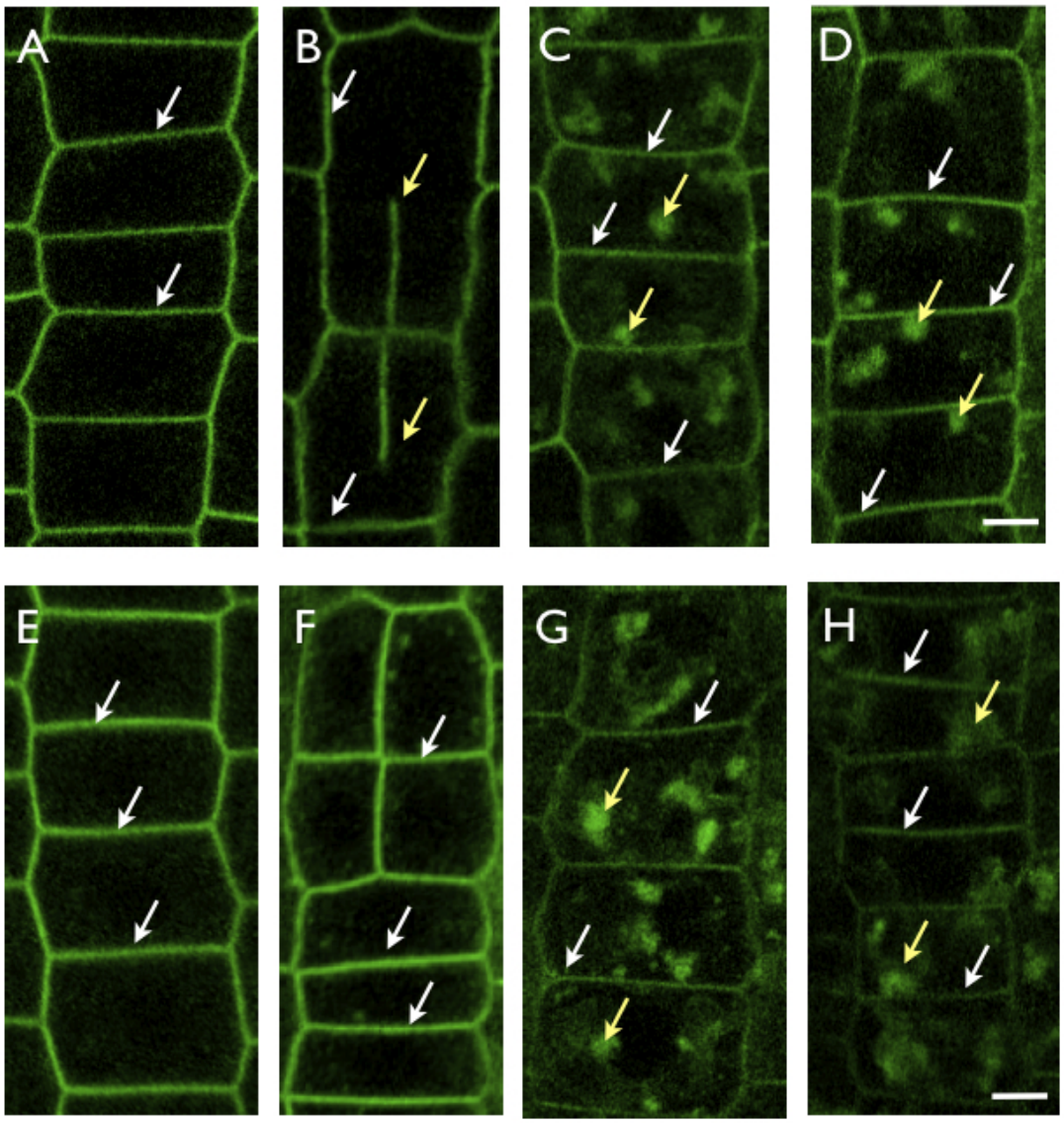

Figure 4.17: Trafficking of the PM markers YFP:NPSN12 and YFP:PIP1;4 is not affected by dominant negative RAB-A2a. A: YFP:NPSN12 localises to the PM in DMSO control samples (white arrows). B: Cytokinesis defects are visible in the dexamethasone induced sample (yellow arrows). YFP:NPSN12 localises to the PM (white arrows) in the presence of dominant negative RAB-A2a. C: After BFA treatment, YFP:NPSN12 is observed in BFA bodies (yellow arrows) and at the PM (white arrows) in DMSO control seedlings. D: In the presence of dominant negative RAB-A2a, YFP:NPSN12 localises to the PM (white arrows) and in BFA bodies (yellow arrows) after BFA treatment. E: In DMSO control seedlings, YFP:PIP1;4 signal is observed at the PM (white arrows), no intracellular signals are visible. F: In the presence of dominant negative RAB-A2a, YFP:PIP1;4 is localised at the PM (white arrows). G: After BFA treatment, YFP:PIP1;4 localises in BFA bodies (yellow arrows) and at the PM (white arrows) in control seedlings. H: In the presence of dominant negative RAB-A2a, YFP:PIP1;4 localises to the PM (white arrows) and in BFA bodies (yellow arrows) after treatment with BFA. Meristematic, epidermal root cells of two independent transgenic *Arabidopsis* Col-0 lines were analysed at three days after germination on DMSO or dexamethasone containing MS agar plates (triplicate experiments per line, utilising four to six seedlings per line and treatment). Scale bar = 5μm.

4.2.3 Traffic to the vacuole is not affected by dominant negative RAB-A2a

As a next step, the effect of the dominant negative RAB-A2a mutant on selected vacuolar markers was investigated.

Trafficking of YFP:VAMP711 is not affected by dominant negative RAB-A2a.

Only two lines of inducible A2aNI *Arabidopsis* lines in the YFP:VAMP711 background were obtained. These were screened for root growth inhibition upon induction with dexamethasone. Both lines exhibit strong root growth inhibition and were selected for confocal analysis (figure 4.18).

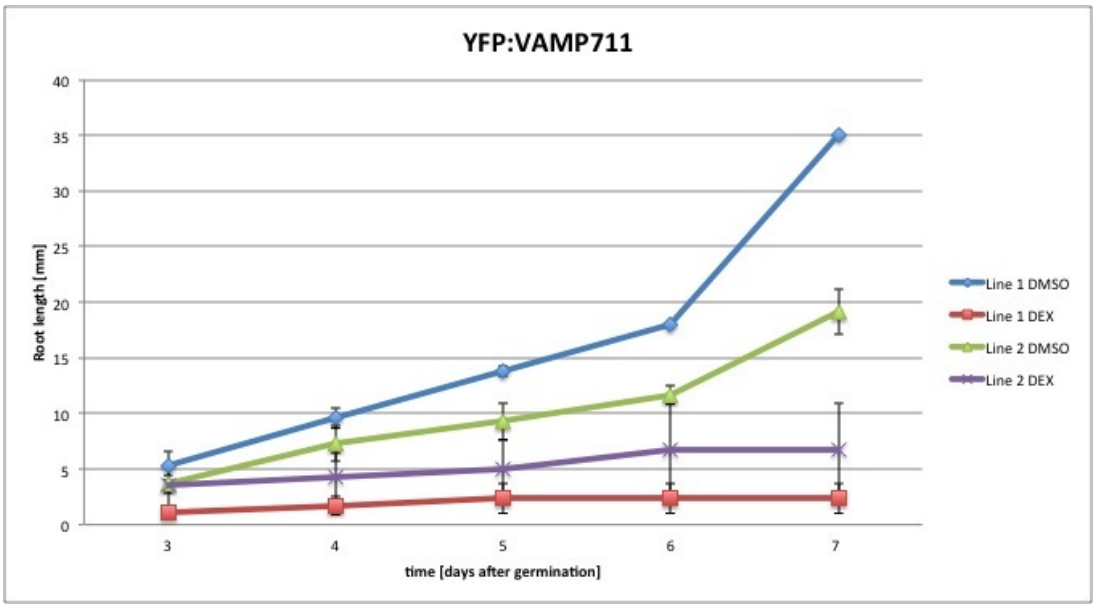

Figure 4.18: Root growth assay of selected YFP:VAMP711 A2aNI lines (lab names: Line 1: VAMP711 2NI11 A-1 Line 2: VAMP711 2NI11 A-2). Root growth was monitored for three to seven days after germination on 20µM dexamethasone or DMSO containing plates. Dexamethasone induced seedlings exhibit root growth inhibition compared to control seedlings. Data points represent mean average root growth from 15 to 20 seedlings per line and treatment. Error bars represent standard deviation; where no error bar is visible standard deviation is (close to) zero.

YFP:VAMP711 is a marker for vacuolar traffic that is localised at the tonoplast (figure 4.20). The analysis of the vacuolar marker YFP:VAMP711 shows that there was a subtle effect on vacuolar morphology resulting from the expression of the dominant negative RAB-A2a; the vacuolar tonoplast appeared more tubular. However, there was no trafficking defect of the marker as such as it was possible for the YFP:VAMP711 to reach the tonoplast. The

appearance of PVCs appeared unaffected.

Trafficking of YFP:RAB-G3f is not affected by dominant negative RAB-A2a.

15 different inducible A2aNI *Arabidopsis* lines in the YFP:RAB-G3f background were screened for root growth inhibition upon induction with dexamethasone. Out of these lines, two lines exhibiting the strongest root growth inhibition were selected for confocal analysis (figure 4.19).

YFP:RAB-G3f is a marker for vacuolar traffic that is localised in PVCs and at the tonoplast, but also serves as specificity control of the dominant negative approach. Appearance of PVCs appeared unaffected, the vacuoles showed subtle morphological difference (figure 4.19). However, since RAB-G3f reached the tonoplast, it appears that trafficking of this marker was not perturbed by dominant negative RAB-A2a.

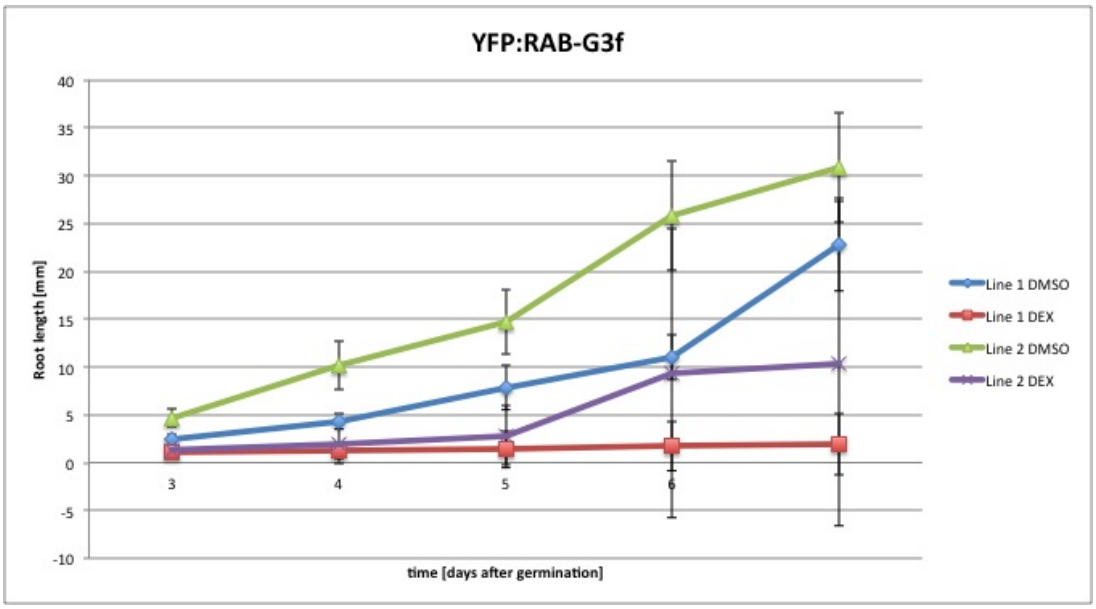

Figure 4.19: Root growth assay of selected YFP:RAB-G3f A2aNI lines (lab names: Line 1: RAB-G3f 2NI11 A-6, Line 2: RAB-G3f 2NI21 A-12). Root growth was monitored for three to seven days after germination on 20µM dexamethasone or DMSO containing plates. Dexamethasone induced seedlings exhibit root growth inhibition compared to control seedlings. Data points represent mean average root growth from 15 to 20 seedlings per line and treatment. Error bars represent standard deviation.

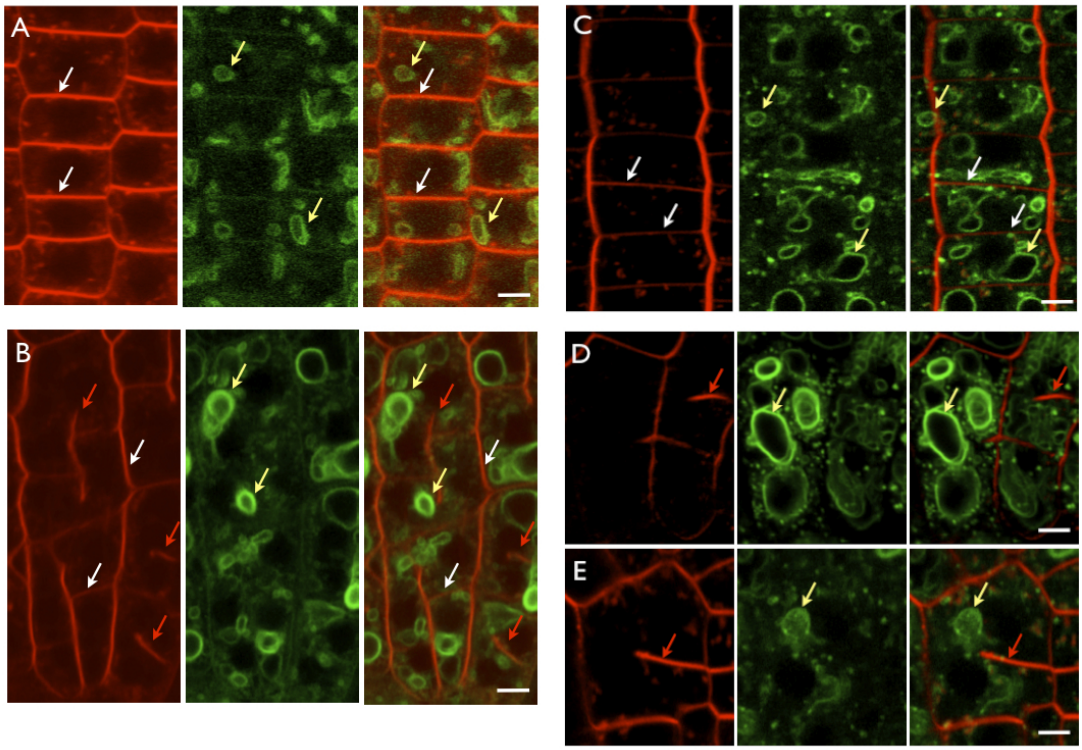

Figure 4.20: Trafficking of YFP:VAMP711 and YFP:RAB-G3f is not affected by dominant negative RAB-A2a. The images show FM4-64 stain (15 minutes prior to imaging, red channel), YFP:VAMP711 or YFP:RAB-G3f (green channel), and the merged image. A: YFP:VAMP711 localises to the tonoplast in control cells (yellow arrows), the endocytic tracer dye FM4-64 localises to the PM (white arrows) and endosomal compartments. B: Cytokinesis defects are visible by FM4-64 staining (red arrows). YFP:VAMP711 localises to the tonoplast in dexamethasone induced samples (yellow arrows). C: YFP:RAB-G3f localises to the tonoplast (yellow arrows) and PVCs in control cells. D and E: Cytokinesis defects are visible by FM4-64 staining (red arrows). YFP:RAB-G3f localises to the tonoplast in dexamethasone induced samples (white arrows) and PVCs. Meristematic, epidermal root cells of two independent transgenic *Arabidopsis* Col-0 lines were analysed at three days after germination on DMSO or dexamethasone containing MS agar plates (triplicate experiments per line, utilising four to six seedlings per line and treatment). Scale bar = 5μm.

Trafficking of BP80:GFP is not affected by dominant negative RAB-A2a

38 different inducible A2aNI *Arabidopsis* lines in the BP80:GFP background were screened for root growth inhibition upon induction with dexamethasone. Out of these lines, two lines exhibiting the strongest root growth inhibition were selected for confocal analysis (figure 4.21).

BP80:GFP is a marker for prevacuolar trafficking and localises to PVC. In presence of dominant negative RAB-A2a, BP80:GFP localised to punctate intracellular compartments that exhibited FM4-64 staining characteristics to PVCs (figure 4.23). It appears that neither trafficking of BP80:GFP to the PVC nor its morphology was altered in any visible way in the presence of dominant negative RAB-A2a.

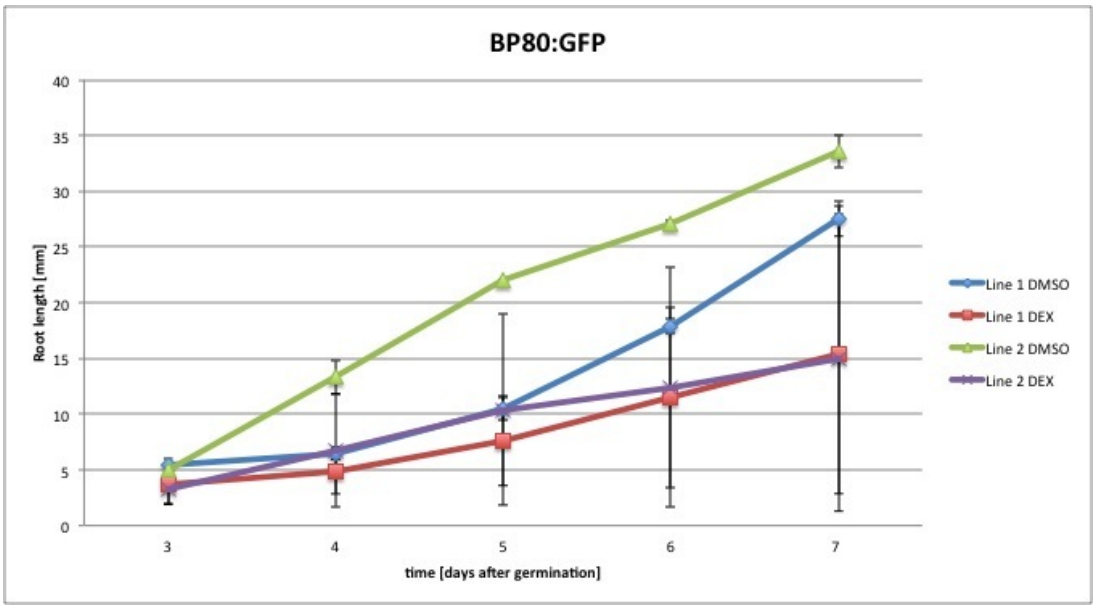

Figure 4.21: Root growth assay of selected BP80:GFP A2aNI lines (lab names: Line 1: BP80 2NI11 B-2.2 D-14, Line 2: BP80 2NI11 B-2.2 D-11). Root growth was monitored for three to seven days after germination on 20µM dexamethasone or DMSO containing plates. Dexamethasone induced seedlings exhibit root growth inhibition compared to control seedlings. Data points represent mean average root growth from 15 to 20 seedlings per line and treatment. Error bars represent standard deviation; where no error bar is visible standard deviation is (close to) zero.

Trafficking of RAB-F2b:GFP is not affected by dominant negative RAB-A2a.

24 different inducible A2aNI *Arabidopsis* lines in the RAB-F2b:GFP background were screened for root growth inhibition upon induction with dexamethasone. Out of these lines, two lines exhibiting the strongest root growth inhibition were selected for confocal analysis (figure 4.22).

RAB-F2b:GFP is a marker for prevacuolar trafficking, is localised at the PVC and serves as a specificity control for the dominant negative approach. In presence of dominant negative RAB-A2a, RAB-F2b:GFP localised to punctate intracellular compartments that showed similar FM4-64 staining characteristics as PVCs (figure 4.23). It appears that trafficking of RAB-F2b:GFP to the PVC was not affected in the presence of dominant negative RAB-A2a. Further, the appearance of PVC was also not affected. Thus, the analysis shows that RAB-F2b trafficking was not affected by dominant negative RAB-A2a.

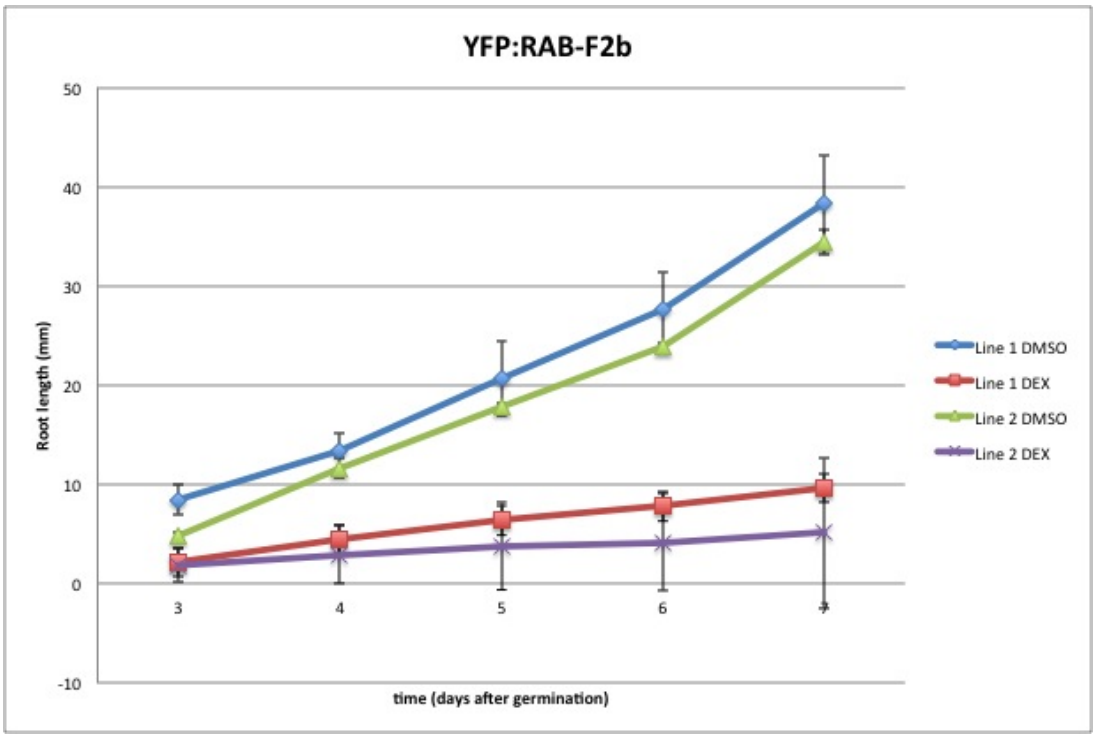

Figure 4.22: Root growth assay of selected RAB-F2b:GFP A2aNI lines (lab names: Line 1: RAB-F2b 2NI11 A-9, Line 2: RAB-F2b 2NI21 A-9). Root growth was monitored for three to seven days after germination on 20µM dexamethasone or DMSO containing plates. Dexamethasone induced seedlings exhibit root growth inhibition compared to control seedlings. Data points represent mean average root growth from 15 to 20 seedlings per line and treatment. Error bars represent standard deviation; where no error bar is visible standard deviation is (close to) zero.

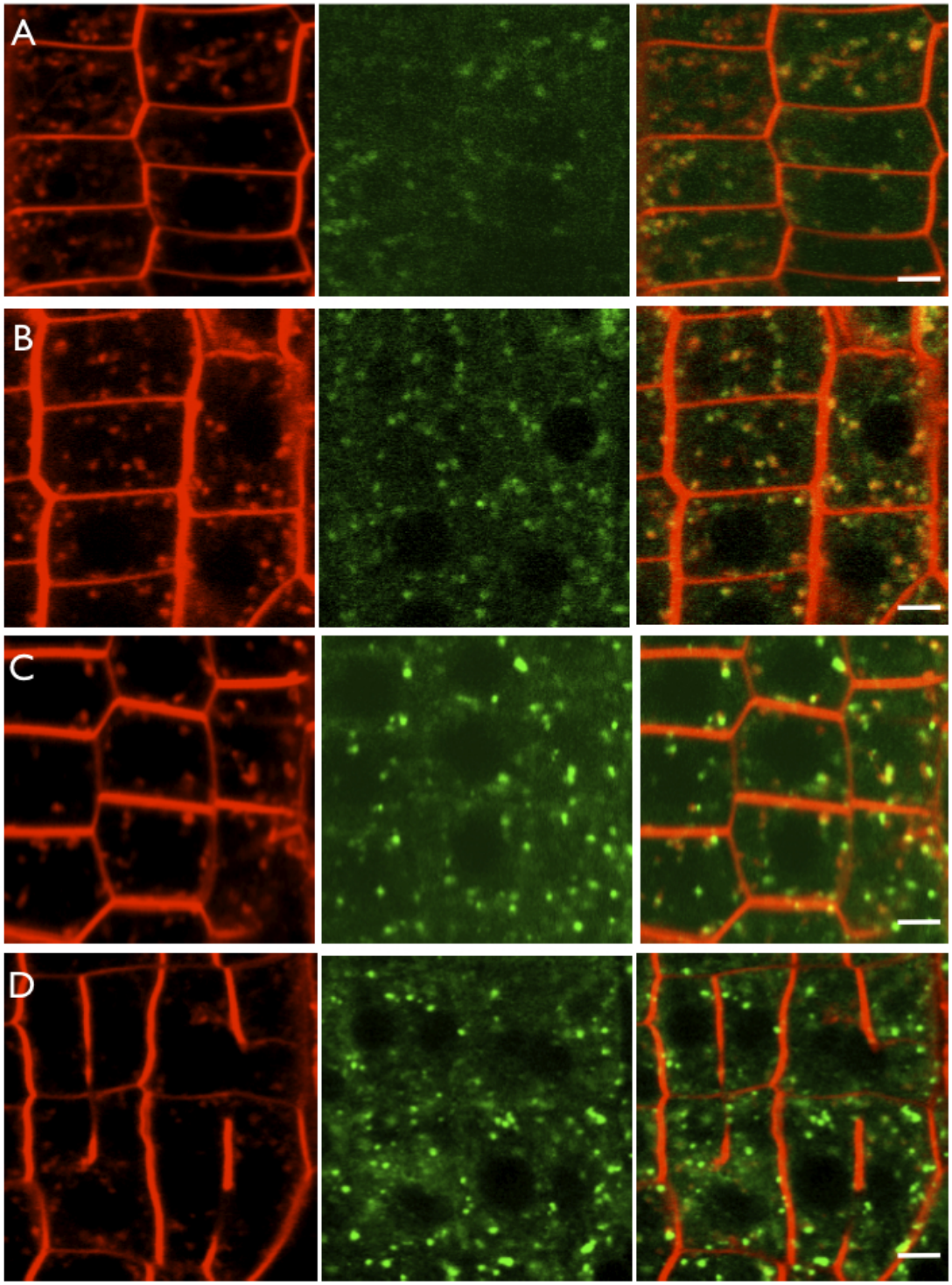

Figure 4.23: Trafficking of BP80:GFP and RAB-F2b:GFP is not affected by dominant negative RAB-A2a. The images show the FM4-64 channel (15 minutes staining prior to imaging, red), BP80:GFP or RAB-F2b:GFP (green) and the merged channel. A: BP80:GFP localises to PVC, of which some colocalise with the styryl dye FM4-64. B: In the presence of dominant negative RAB-A2a, BP80:GFP is localised to punctate PVC structures. C: RAB-F2b:GFP localises to PVCs. D: Cytokinesis defects are visible by FM4-64 staining. In the presence of dominant negative RAB-A2a, RAB-F2b:GFP is localises to punctate PVC structures. Meristematic, epidermal root cells of two independent transgenic *Arabidopsis* Col-0 lines were analysed at 3 days after germination on DMSO or dexamethasone containing MS agar plates (triplicate experiments per line, utilising four to six seedlings per line and treatment). Scale bar = 5µm.

4.2.4 Endocytosis of FM4-64 and transport to the tonoplast is not affected by dominant negative RAB-A2a

To test whether RAB-A2a was involved in endocytosis and subsequent transport to the vacuole, I used the styryl dye FM4-64 and observed its endocytosis at different time points after dye application. When FM4-64 is applied to *Arabidopsis* seedlings, it immediately labels the PM and was then endocytosed by the plant cell. After 10 to 15 minutes of dye application, FM4-64 was visible in endosomes (intracellular punctate structures) and was transported to the vacuole after two to three hours, where it initially labeled the tonoplast. Examples of early FM4-64 endocytosis are shown in figure 4.23. In both control and induced dominant negative RAB-A2a samples, FM4-64 was endocytosed and visible in endosomes. Figure 4.24 shows endocytosis of FM4-64 in the previously mentioned PIN2:GFP A2aNI lines (see section 4.2.1) after 2.5 hours of dye application. It appeared that FM4-64 reached the tonoplast in both the control and induced dominant negative RAB-A2a samples. However, it appears that the morphology of vacuoles was slightly altered, i.e. vacuoles exhibit more protrusions. The data suggests that the endocytic route used by FM4-64 was not affected by the expression of the dominant negative RAB-A2a.

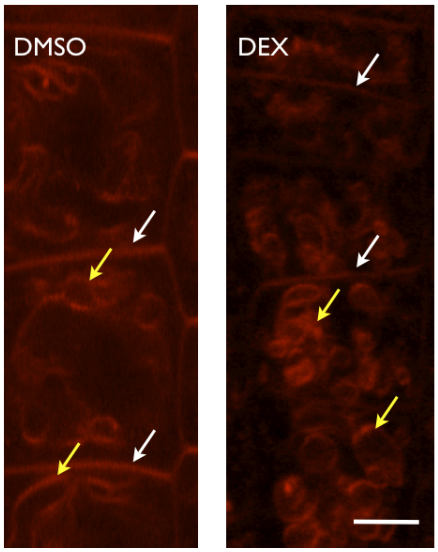

Figure 4.24: FM4-64 endocytosis and transport to the tonoplast are not affected by dominant negative RAB-A2a. (DMSO) FM4-64 labels the PM (white arrows) and the tonoplast (yellow arrows) after 2.5 hours of dye application. (DEX) FM4-64 is also visible at the PM (white arrows) and the tonoplast (yellow arrows) in presence of dominant negative RAB-A2a. Meristematic, epidermal root cells of two independent transgenic *Arabidopsis* Col-0 lines were analysed at three days after germination on DMSO or dexamethasone containing MS agar plates (triplicate experiments per line, utilising four to six seedlings per line and treatment). Scale bar = 5µm

4.3 Conclusions

In this chapter, the influence of the expression of the dominant negative RAB-A2a mutant on several trafficking pathways, including default secretion, PM trafficking, traffic to the PVC and vacuolar compartments as well as endocytosis, was studied in the main root of *Arabidopsis.*

The two PM markers YFP:NPSN12 and YFP:PIP1;4 are not prevented from reaching the PM by the dominant negative RAB-A2a mutant in any visible way. Secretory traffic was probed with the ratiometric marker nlsRm-2A-secGFP. No intracellular accumulation of secGFP is observed in the presence of dominant negative RAB-A2a. This result is surprising as RAB-A2a has been implicated in biosynthetic traffic to the PM [45] and it suggests that the RAB-A2a pathway lies on a different route to the PM. Furthermore, neither the formation of BFA bodies nor the recruitment of these markers to these bodies was affected.

The expression of the dominant negative RAB-A2a mutant caused morphological changes in vacuoles. Since vacuolar markers, such as YFP:VAMP711 or YFP:RAB-G3f, were still able to reach the tonoplast, the results suggested that the trafficking route as such was not inhibited, However, it may be that either an interactor of RAB-A2a is involved in sustaining vacuolar morphology or that an important vacuolar factor is held at the TGN and thus is unable to reach its interaction interface, causing secondary effects.

The trafficking of the tested PVC markers was not affected in the presence of dominant negative RAB-A2a. RAB-F2b:GFP as well as BP80:GFP are detected on PVCs. The morphology of PVCs appeared the same with or without dominant negative RAB-A2a present.

The two markers RAB-F2b:GFP and YFP:RAB-G3f were also used to probe for specificity of the dominant negative approach. Trafficking and membrane recruitment of both markers are not affected by dominant negative RAB-A2a, substantiating that this mutant protein only interferes with activity of a subset of Rab-A proteins (see Chapter 3).

Time course experiments with FM4-64 do not show a difference in uptake of this styryl dye in induced dominant negative RAB-A2a samples compared to the controls. In both cases, FM4-64 reached the tonoplast after 2.5 hours of dye application. This demonstrates that the endocytic-vacuolar route was not affected. All vacuolar routes tested in this chapter do not indicate any vacuolar trafficking defects or increase in trafficking. However, the vacuolar route that leads to degradation of proteins has not been tested here and is an obvious next line of enquiry.

The localisation of the polar localised auxin efflux carrier PIN2:GFP was the only affected marker. In the presence of dominant negative RAB-A2a, the majority of PIN2:GFP was localised intracellularly; only a small portion of the protein was detected at the PM. BFA treatment of induced seedlings caused intracellular localised PIN2:GFP to aggregate in BFA bodies while the PM signal appeared weaker compared to control samples. This result revealed a possible role for RAB-A2a in PIN2:GFP cycling.

Specificity experiments in the PIN2:GFP background with the inducible wild type RAB-A2a (acting as overexpressor lines) as well as with the dominant negative mutant of RAB-A5c confirmed that the observed effects on PIN2:GFP traffic are specific to dominant negative RAB-A2a action. The overexpression of wild type RAB-A2a did not affect the localisation of PIN2:GFP despite higher levels of protein present. The dominant negative RAB-A5c mutant only exhibits an abnormal pattern in lateral root cap cells but not mersitematic cells. It may be that RAB-A5c is controlling a different aspect of PIN2:GFP trafficking and that dominant negative RAB-A5cNI does not interfere with this RAB-A2a pathway.

BRI1:GFP trafficking was not affected by the dominant negative RAB-A2a, neither traffic to the PM nor its cycling. While both PIN2:GFP and BRI-1:GFP are cycling markers and it seems that RAB-A2a plays a role in PIN2:GFP cycling, only PIN2:GFP shows polar localisation [201], while BRI-1:GFP localises to all faces of the PM [58]. These differential effects could either lie in the difference of polarity or the presence of multiple recycling pathways [222], of which only PIN2:GFP is trafficked through a RAB-A2a dependent route.

With these results, it is possible to imagine the following scenarios for PIN2:GFP traffic, which will be addressed in the following chapter:

1. The RAB-A2a compartment is required for initial delivery of *de novo* synthesised PIN2:GFP to the apical and basal PM.
2. The RAB-A2a compartment is required for the internalisation of PIN2:GFP.
3. The RAB-A2a compartment is required for PIN2:GFP (re)cycling between TGN and the PM.
4. The RAB-A2a compartment is not involved at all in trafficking of PIN2:GFP. The observed effects are unspecific.

Chapter 5

Investigation of the PIN2:GFP trafficking defect

5.1 Introduction

I showed in the previous chapter that a variety of trafficking pathways are not perturbed by the expression of the dominant negative RAB-A2a mutant in *Arabidopsis* roots. However, the localisation of PIN2:GFP was specifically altered in response to the expression of dominant negative RAB-A2a: PIN2:GFP accumulates intracellularly. Moreover, BFA treatments revealed a synergistic effect of this drug together with dominant negative RAB-A2a. The intracellular PIN2:GFP now agglomerates in BFA bodies, the PM signal appears weaker compared to controls. This may suggest a possible role of RAB-A2a in cycling or recycling of PIN2:GFP.

In this chapter I will address the question which of the different trafficking aspects of PIN2:GFP are dependent on RAB-A2a mediated traffic:

1. Does a defect in PIN2:GFP vacuolar trafficking contribute to the intracellular accumulation, which is seen in the presence of dominant negative RAB-A2a?
2. Is RAB-A2a dependent PIN2:GFP traffic dependent on the actin cytoskeleton?
3. Is RAB-A2a dependent PIN2:GFP traffic dependent on endocytosis?
4. Is the RAB-A2a compartment required for initial delivery of newly synthesised PIN2:GFP to the PM?

5. Is the RAB-A2a compartment required for polarised re-delivery process to the apical membrane?

6. Is the RAB-A2a compartment required for PIN2:GFP recycling between TGN and the PM?

5.1.1 Vacuolar targeting and degradation of PIN2

The accurate targeting of PIN2 to the vacuole involves proteasome activity, which requires ubiquitination of PIN2. This ubiquitination functions as a signal that controls how much PIN2 is recycled back to the PM, and how much PIN2 is internalised and targeted for proteolytic degradation [223]. The function of AMSH3, a de-ubiquitinating enzyme, is required in efficient targeting of PIN2 to the lytic vacuole, as *amsh3* plants do not accumulate GFP in the vacuolar structures. However, polar PIN2:GFP targeting is not affected in *amsh3* plants, which suggests that AMSH3 is not involved in the transport of PIN2 to the PM or its recycling [224].

Experiments involving dark treatments of GFP fusion proteins allow investigation of protein degradation and trafficking to the lytic vacuoles [225]. It has been shown previously that GFP and related proteins exhibit increased stability in lytic vacuoles due to conformational changes [43, 226]. Indeed, dark treatments of PIN2:GFP seedlings for two to four hours showed that GFP can be observed in the lumen of the tonoplast indicating PIN2 degradation in lytic vacuoles [227], a process dependent on a BFA sensitive ARF-GEF, which is not GNOM [228].

The retromer components SNX1 and VPS29 are implicated in vacuolar targeting of PINs and are sensitive to Wortmannin [228, 229]. Wortmannin is a fungal metabolite that inhibits plant endocytosis [27] and also acts on the vacuolar pathway of plants by causing pre-vacuolar bodies to form small vacuoles by homotypic fusion of PVCs [187]. A small portion of PVC and SCAMP (Secretory Carrier Membrane Proteins)-positive TGN fusion has also been observed in Wortmannin-treated tobacco BY-2 cells [230]. Known targets of Wortmannin are PI3K and PI4K [231], the recycling of the plant vacuolar sorting receptor BP80 between PVC and TGN is also inhibited [202].

5.1.2 PIN2 trafficking and the actin cytoskeleton

Trafficking of the auxin efflux carriers PIN1 and PIN3 is dependent on the actin cytoskeleton [37, 76]. However, the situation for PIN2 is less clear as neither latrunculin B nor cytochalasin D treatments visibly cause disruption of PIN2 localisation in meristematic root cells [232]. It appears that the trafficking pathways for polar PIN delivery are highly diverse. Interestingly, while polar PIN targeting is dependent on the actin cytoskeleton in interphase cells, in dividing cells, PIN proteins are delivered to the forming cell plate by the microtubule-dependent pathway [37, 96].

The drug cytochalasin D is used to study actin-dependent processes. It blocks the polymerisation and elongation of actin and causes sterol accumulation in endosomal compartments [38, 214]. Increased instability of actin triggers exocytic trafficking used in plant growth [233].

5.1.3 PIN2 polarity and endocytosis

Polar distribution of PIN2 is maintained by connections between polar domains at the PM and the cell wall. PM localised Celluose Synthase A3 (CESA3) is a component of the cellulose synthase complex, which synthesises β-1,4-glucans that associate to form cellulose microfibrils. *repp3* is a weak allele of the CESA3 gene, has defects in cell wall composition and is defective in PIN polarity. Treating seedlings with the cellulose biosynthesis inhibitors isoxaben or dichlobenil results in defects of the basal localisation of PIN1-HA. Further, cell wall removal by protoplasting causes polarity loss of both PIN1:GFP and PIN2:GFP [234].

PIN2 polarity is also highly dependent on its phosphorylation status. The Protein Phosphatase 2A (PP2A) [235] and PINOID kinase [236] have been identified as important regulators of apical-basal targeting. In both *pp2aa1 pp2aa2* and *pp2aa1 pp2aa3* polar localisation of PIN2 is affected. PIN2 normally exhibits apical localisation in young cortical cells. In both *pp2aa1* double mutants PIN2 changed its polarity to basal in young cortical cells. However, the basal localisation in epidermal cells remains unaffected [235]. Mutations in the phosphorylation site of the central hydrophilic loop of PIN proteins revealed the importance of phosphorylation and de-phosphorylation in apical and basal polarity of PIN proteins. For example, a particular non-phosphorylatable mutant of PIN1-HA, PIN1-HA(Asp), is able to rescue the agravitropic phenotype of the *pin2* mutant and thus acquired PIN2-like function [237]. Overexpression of the PINOID protein kinase induces a shift from basal to apical PIN localisation [238].

After the *de novo* synthesis, PIN2 is initially delivered to the PM in a nonpolar fashion before its polarity is then established by internalisation from the PM, and polar recycling [85]. Endocytosis of PINs is regulated by the auxin levels in the cell [239]. Increased auxin levels inhibit the internalisation of PIN and thus constitutive cycling. As a consequence, concentration of PIN proteins at the PM increase and thereby promote the efflux of auxin out of the cell [240]. Auxin-mediated inhibition of PIN2 endocytosis is impaired by reduction of membrane sterols [216, 239].

Cycling of PIN2 is sensitive to BFA, a potent inhibitor of protein cycling [241]. Prolonged BFA treatment causes a shift of PIN2 localisation from the basal to the apical membrane, a process called 'transcytosis' [92]. Transcytosis describes a process in which the localisation of a polar protein is shifted *via* recycling endosomes and provides a mechanism for rapid changes in PIN polarity in response to various signals, such as developmental [82, 83] or environmental signals [76, 93]. Transcytosis is also a well known mechanism for polar delivery of cargos in animal cells [94, 95].

Recently, Drdova and colleagues (2012) showed that PIN2:GFP recycling is dependent on the exocyst complex, which is implicated in the fusion of exocytic vesicles. A mutant of one of the exocyst complex units, exo70A1, exhibits perturbed PIN1:GFP and PIN2:GFP recycling and impaired trafficking of BRI1:GFP. PIN2:GFP accumulates in abnormally expanded, RAB-A5d labeled endomembrane compartments [204]. RAB-A5d is a marker for recycling endosomes but which are distinct from VHA-a1:GFP labeled TGN [150, 204].

Previous experiments with PIN2:GFP showed that Tyrphostin A23 prevents PIN2:GFP from reaching the BFA body in *Arabidopsis* while FM4-64 internalisation is detected [188]. Tyrphostins are used to study endocytosis in *Arabidopsis,* in particular clathrin mediated endocytosis [142, 242]. Tyrphostin A23 inhibits the interaction between the YXXaφ (aφ is a bulky hydrophobic amino acid) endocytosis signal and the mu2-subunit of the AP2 complex [243]. AP2 is a clathrin adaptor involved in endocytosis (see section 1.2.1). Tyrphostin A51 is a biologically inactive analogue of Tyrphostin A23 and does not inhibit clathrin dependent endocytosis. It is thus routinely used as negative control treatment to study this particular trafficking aspect [243].

5.2 Results

'*Arabidopsis* seedlings' or 'seedlings' in this chapter refer to a transgenic PIN2:GFP line with the additional trait of dexamethasone inducible expression of the dominant negative RAB-A2a mutant. For all experiments, two independent lines were used. Experiments were carried out in triplicates per line with four to six seedlings per experiment and treatment.

5.2.1 Expression of dominant negative RAB-A2a enhances vacuolar traffic of PIN2:GFP

As mentioned before, experiments involving dark treatments of PIN:GFP can be used to study its trafficking to the lytic vacuoles and to address the question whether a defect in PIN2:GFP vacuolar trafficking contributes to the intracellular accumulation that is visible in the presence of dominant negative RAB-A2a.

Arabidopsis seedlings were germinated on MS agar plates containing 20µM dexamethasone or the respective amount of DMSO as control. At three days after germination, the seedlings were subjected to six hours of dark treatment (plates were covered in aluminium foil and kept in the tissue culture room) and then analysed by confocal microscopy. The observed GFP signal in vacuoles appeared stronger in seedlings expressing dominant negative RAB-A2a (figure 5.1).

5.2.2 PIN2:GFP labelled PVCs are insensitive to Wortmannin in presence of dominant negative RAB-A2a

Wortmannin causes homotypic fusion of PVCs and results in generation of small vacuoles. Wortmannin treatments were used to study pre-vacuolar trafficking of PIN2:GFP.

Arabidopsis seedlings were germinated on MS plates containing DMSO; the seedlings were then treated with 20µm dexamethasone or the respective amount of DMSO for 20 hours before being subjected to treatment with 33µM Wortmannin for 1.5 hours. Wortmannin treated PIN2:GFP DMSO controls showed enlarged intracellular compartments as compared to Wortmannin untreated samples (figure 5.2). These enlarged compartments, which might reflect enlarged PVCs, were not visible in the Wortmannin treated samples of dexamethasone induced seedlings.

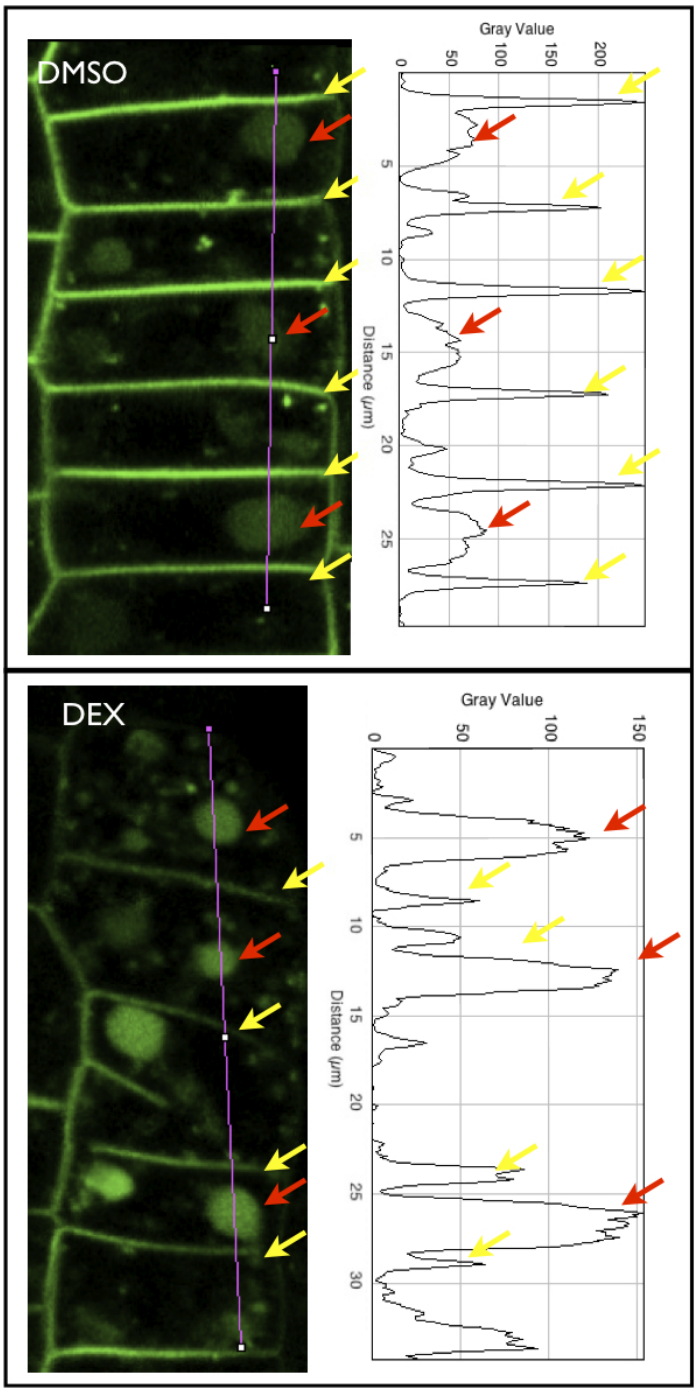

Figure 5.1: Dominant negative RAB-A2a causes enhanced PIN2:GFP signal in lytic vacuoles after dark treatment. The purple line shows where fluorescence intensity measurements (grey value) were taken through the root, over a distance in µm. These values were plotted on a graph (right side of the image). In the presence of the dominant negative RAB-A2a mutant (DEX), stronger vacuolar GFP signals relative to PM signals were observed, compared to uninduced control samples (DMSO). Stronger vacuolar signals correlate with lower PM signals. Red arrows point to vacuoles, yellow arrows to PMs. Meristematic, epidermal root cells of two independent transgenic *Arabidopsis* Col-0 lines were analysed at four days after germination (triplicate experiments per line, utilising four to six seedlings per line and treatment).

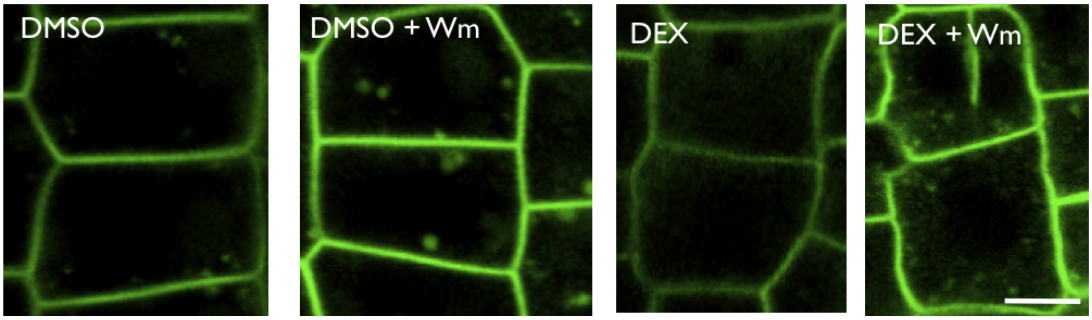

Figure 5.2: PIN2:GFP labelled PVCs are insensitive to Wortmannin in the presence of dominant negative RAB-A2a. Control Seedlings (DMSO + Wm) show larger punctate structures after Wortmannin treatment in comparison to the untreated control (DMSO). These larger structures are not visible in the presence of dominant negative RAB-A2a (DEX, DEX + Wm). Meristematic, epidermal root cells of two independent transgenic *Arabidopsis* Col-0 lines were analysed at four days after germination (triplicate experiments per line, utilising four to six seedlings per line and treatment). Scale bar = 5µm

5.2.3 RAB-A2a dependent traffic of PIN2:GFP is independent of the actin cytoskeleton

Trafficking of PIN1 and PIN3 in interphase cells is dependent on the actin cytoskeleton. Cytochalasin D treatment was used to study possible involvement of actin-dependent processes in RAB-A2a dependent PIN2:GFP trafficking.

Arabidopsis seedlings were germinated on MS plates containing DMSO; then seedlings were treated with 20µm dexamethasone or the respective amount of DMSO for 20 hours before being subjected to treatment with 50µm cytochalasin D treatment for 2.5 hours. The results showed that the PIN2:GFP trafficking defect induced in the presence of dominant negative RAB-A2a was neither enhanced nor inhibited after cytochalasin D treatment, no additional patterns were observed, apart from expected unusual PM formations (figure 5.3). This result suggests that the RAB-A2a dependent PIN2:GFP trafficking is not dependent on the actin cytoskeleton.

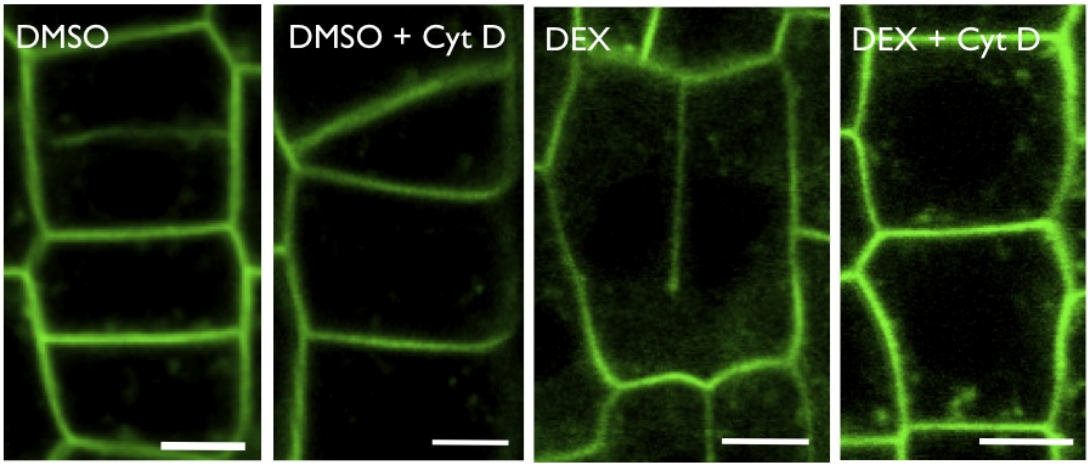

Figure 5.3: The actin cytoskeleton is not involved in RAB-A2a dependent PIN2:GFP trafficking. DMSO: PIN2:GFP localises to the PM in DMSO treated control samples. DMSO + Cyt D: PIN2:GFP localises to the PM in cytochalasin D treated control samples. DEX: PIN2:GFP localises to the PM and to cytokinesis defects. DEX + Cyt D: PIN2:GFP localises to the PM in the presence of dominant negative RAB-A2a and after treatment with cytochalasin D. Meristematic, epidermal root cells of two independent *Arabidopsis* Col-0 lines were analysed at four days after germination (triplicate experiments per line, utilising four to six seedlings per line and treatment). Scale bar = 5µm.

5.2.4 PIN2:GFP recycling is affected by expression of dominant negative RAB-A2a

Recycling of PM proteins can be studied with BFA washout experiments. In these experiments, seedlings are treated with the fungal toxin BFA, which causes the formation of BFA bodies. BFA-sensitive proteins aggregate in these bodies, a process that is reversible. Removal of BFA restores cycling of proteins. This allows observation of PIN2:GFP recycling as it is recycled from BFA bodies to the PM after BFA removal.

BFA washout experiments were carried out to determine if PIN2:GFP recycling was defective in absence of functional RAB-A2a dependent trafficking. Seedlings were germinated on MS agar plates containing DMSO and then transferred into liquid MS medium containing DMSO or 20µM dexamethasone for 20 hours. Seedlings were then treated with 50µM BFA for one hour, imaged, and re-imaged two hours after BFA removal.

In DMSO controls, PIN2:GFP labeled BFA bodies had dispersed two hours after removal of BFA (figure 5.4 A). In contrast, BFA bodies formed in the presence of dominant negative RAB-A2a had not dispersed at two hours after BFA removal. As an additional control, these experiments were also done with BRI1:GFP (figure 5.4 B). As shown in the previous chapter this marker was not affected by the presence of dominant negative RAB-A2a. In contrast

to findings with PIN2:GFP above, the BFA bodies formed in dominant negative RAB-A2a induced BRI1:GFP seedlings dispersed after removal of BFA (figure 5.4 B)

Preliminary results obtained with RAB-A5cNI suggest that PIN2:GFP recycling is specific to RAB-A2a dependent traffic, as BFA bodies resolve upon removal of BFA in RAB-A5c induced PIN2:GFP samples (figure 5.5).

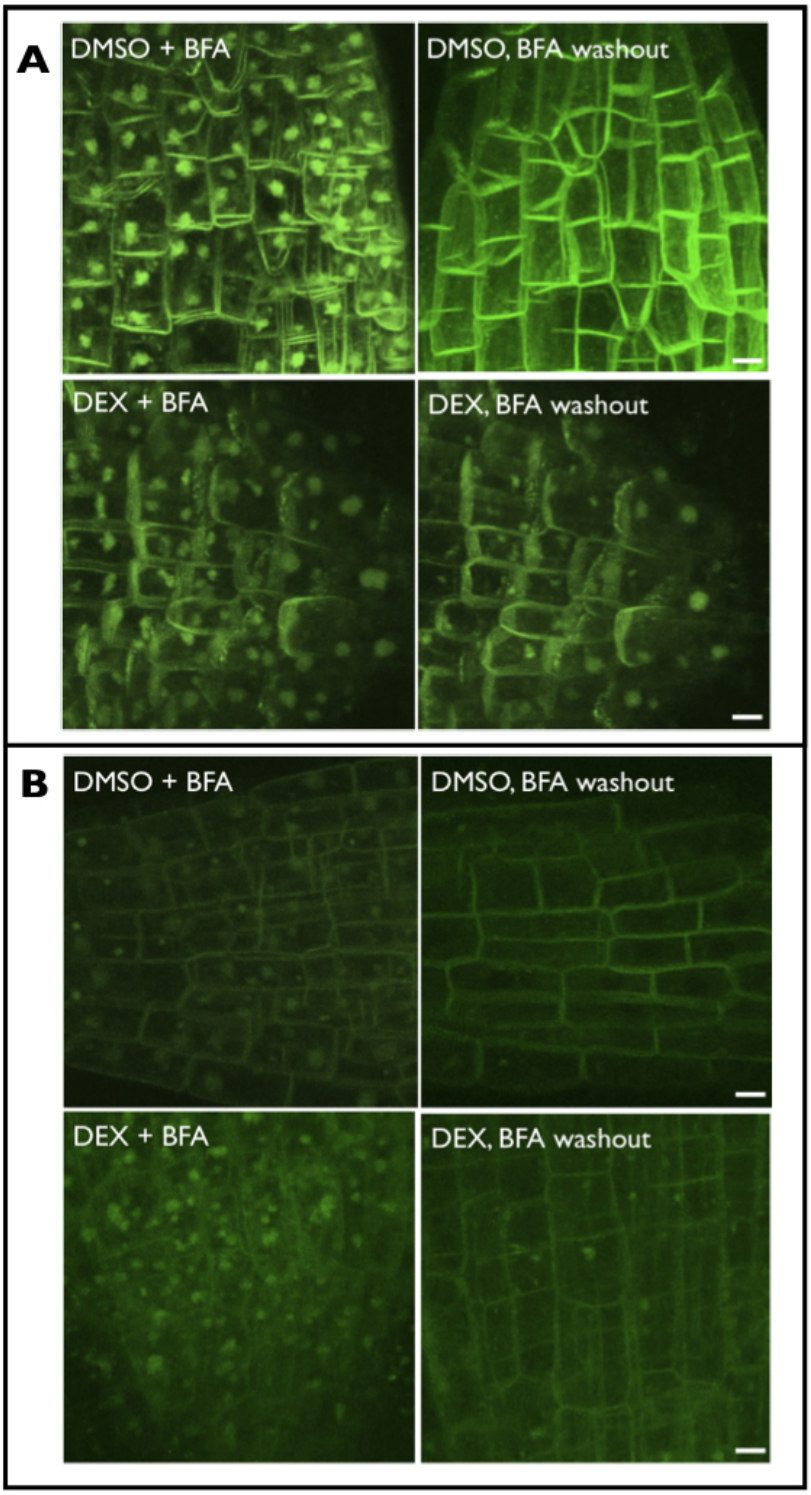

Figure 5.4: RAB-A2a function is involved in PIN2:GFP recycling. Seedlings of PIN2:GFP (A) and BRI1:GFP (B) dominant negative RAB-A2a inducible lines were imaged after treatment with 50µM BFA for one hour (DMSO + BFA, DEX + BFA), and two hours after removal of BFA (BFA washout). (A) While PIN2:GFP control samples resume recycling after removal of BFA, samples expressing the dominant negative RAB-A2a fail to disperse BFA bodies. (B) In both control and induced samples, BRI1:GFP recycling is restored after removal of BFA. Meristematic, epidermal root cells of two independent transgenic *Arabidopsis* Col-0 lines were analysed at four days after germination (triplicate experiments per line, utilising four to six seedlings per line and treatment). Scale bar = 5µm.

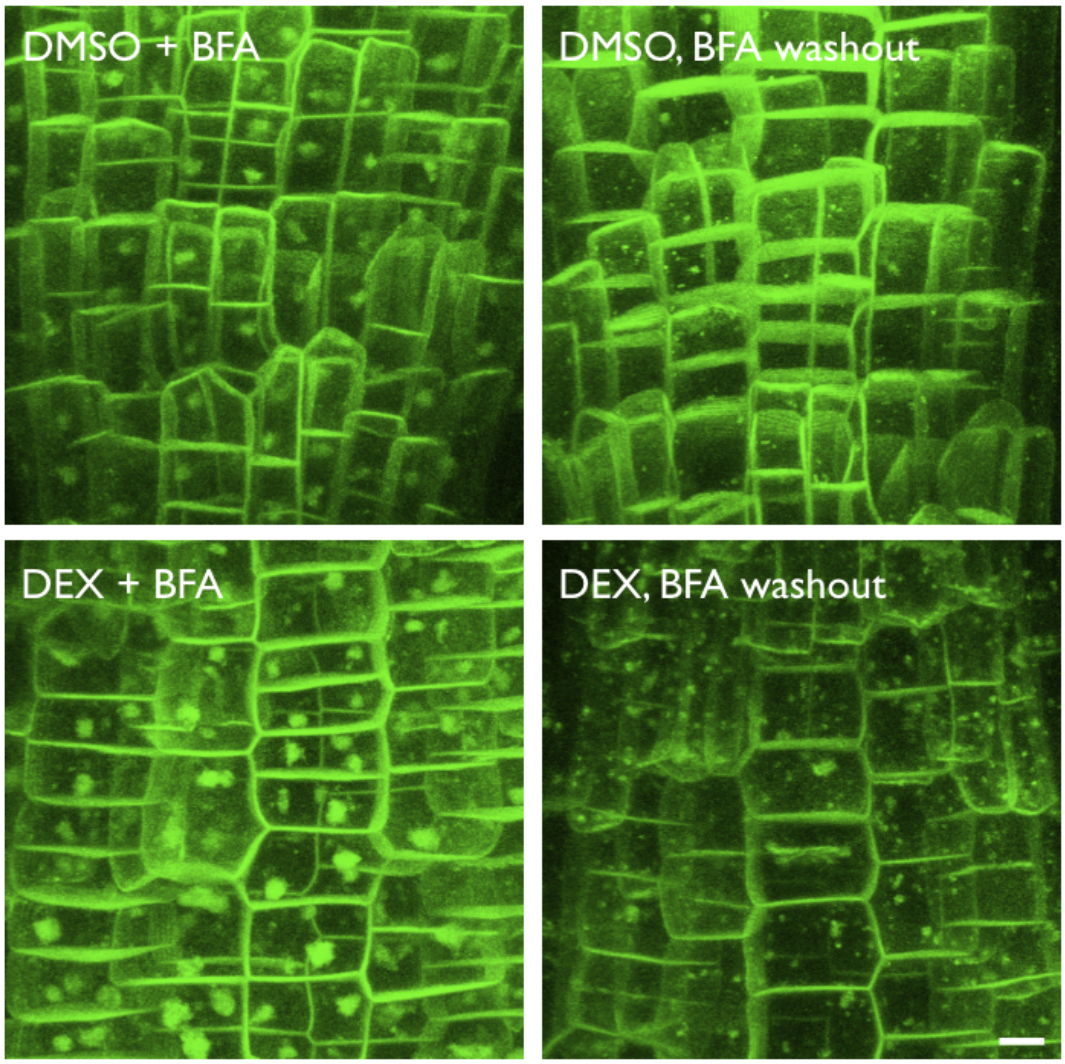

Figure 5.5: RAB-A5c function is not involved in PIN2:GFP recycling. Seedlings of PIN2:GFP dominant negative RAB-A5c inducible lines were imaged after treatment with 50μM BFA for one hour (DMSO + BFA, DEX + BFA), and two hours after removal of BFA (BFA washout). In both control and induced samples, PIN2:GFP recycling is restored after removal of BFA. Meristematic, epidermal root cells of two independent transgenic *Arabidopsis* Col-0 lines were analysed at four days after germination (triplicate experiments per line, utilising four to six seedlings per line and treatment). Scale bar = 5μm.

5.2.5 PIN2:GFP endocytosis is not affected by dominant negative RAB-A2a

As a next step, I wanted to address the question whether the observed intracellular accumulation of PIN2:GFP is derived from endocytosed material. This can be tested by using the endocytosis inhibiting drug Tyrphostin A23 in conjunction with BFA treatment. Dhonukshe and colleagues (2007) reported that PIN2:GFP is prevented from reaching the BFA body after Tyrphostin A23 treatment, showing that endocytosis is required for this trafficking step [96].

Arabidopsis seedlings (three days after germination on DMSO containing MS agar plates, then 20 hours in MS liquid media containing DMSO or 20µM dexamethasone) were pre-treated for 30 minutes with 30µM Tyrphostin followed by a 30µM Tyrphostin/ 50µM BFA double treatment for 60 minutes. In uninduced control samples, a reduction of PIN2:GFP labelling in BFA bodies of DMSO/TyrA23/BFA and DEX/TyrA23/BFA treated samples was observed (figure 5.6). In both cases, a reduction or lack of PIN2:GFP labeling in BFA bodies of DMSO/TyrA23/BFA and DEX/TyrA23/BFA treated samples was observed (figure 5.6).

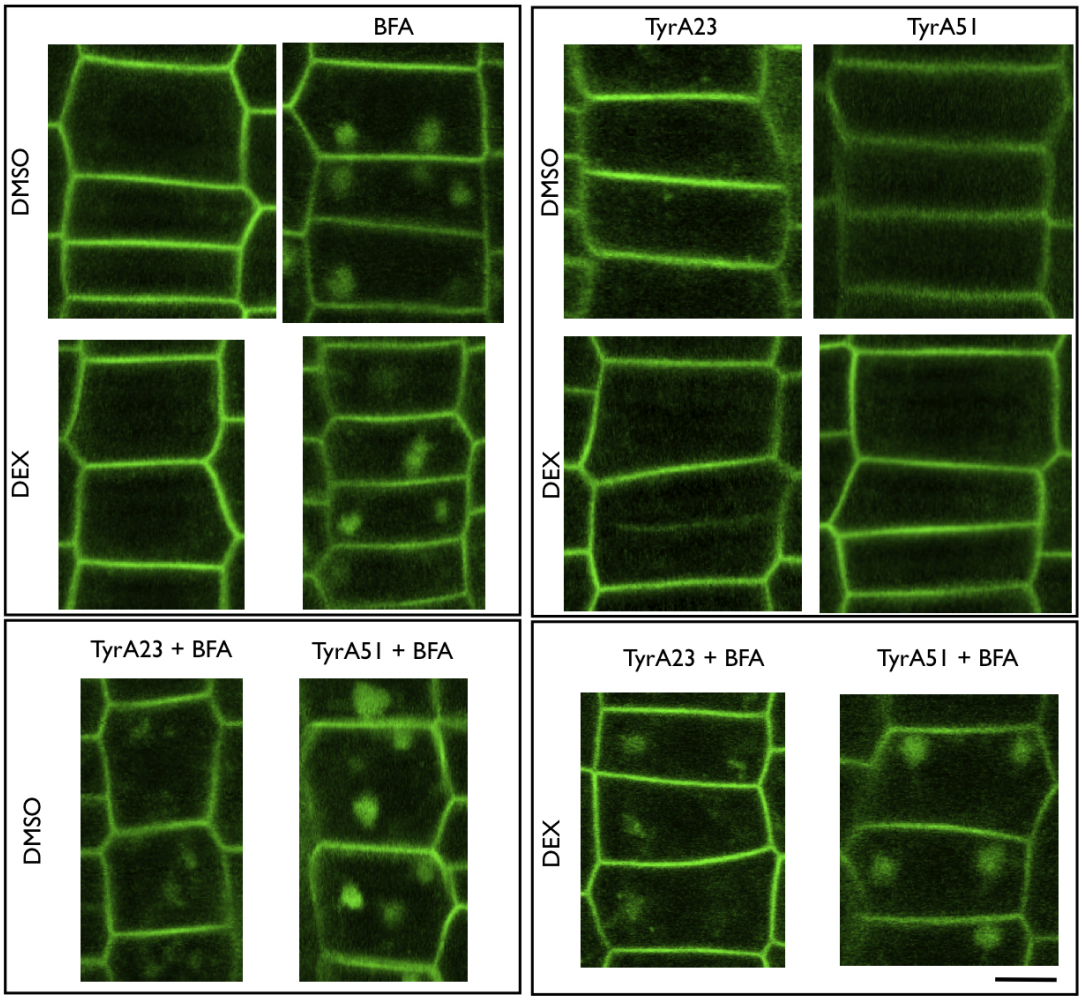

Figure 5.6: PIN2:GFP endocytosis is not affected by dominant negative RAB-A2a. (BFA) PIN2:GFP labels the PM and aggregates in BFA bodies. (TyrA23) PIN2:GFP labels the PM after Tyrphostin A23 treatment. (TyrA51) PIN2:GFP labels the PM after Tyrphostin A23 treatment. (TyrA23 + BFA) FM4-64 stain is visible in BFA bodies, only a minor portion of PIN2:GFP localises to BFA bodies. (TyrA51 + BFA) More PIN2:GFP reaches the BFA body relative to the TyrA23 + BFA treatment. Meristematic, epidermal root cells of two independent transgenic *Arabidopsis* Col-0 lines were analysed at four days after germination (triplicate experiments per line, utilising four to six seedlings per line and treatment). Scale bar = 5µm.

5.2.6 Delivery of *de novo* synthesised PIN2:GFP to the PM is not affected by dominant negative RAB-A2a

FRAP experiments were conducted (as described in Chapter 2) to test whether RAB-A2a was required for delivery of *de novo* synthesised PIN2:GFP to the PM. The relative recovery values are shown in table 5.1 and plotted on a graph in 5.7.

The results showed that there was no difference in the recovery rate of PIN2:GFP at the PM in the presence of dominant negative RAB-A2a compared to control samples. This result suggests that RAB-A2a function is not required for delivery of *de novo* synthesised PIN2:GFP to the PM.

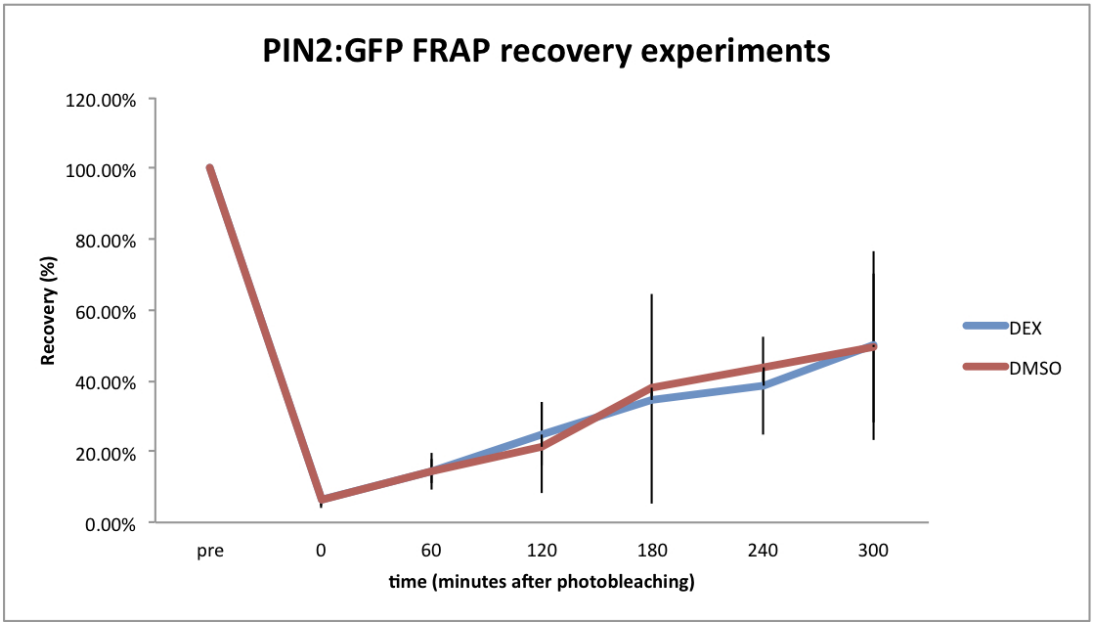

Figure 5.7: PIN2:GFP delivery to the PM is not affected by dominant negative RAB-A2a. The graph shows the recovery of PIN2:GFP fluorescence over a time of 300 minutes after photobleaching. Data points are mean averages of fluorescence intensities, error bars represent standard deviation.

Table 5.1: FRAP measurements. The table shows relative fluroescence intensities compared to initial 100% fluorescence intensity. Numbers were obtained by taking the average of four membranes per time point and seedling, either DMSO treated (DMSO) or induced with dexamethasone (DEX). The final mean averages and standard deviations (STD DEV) were calculated from the values of all seedlings, either induced (DEX) or uninduced (DMSO). 'n.a' means that values for the particular seedling at the given time could not be obtained.

Time [min]	DEX1	DEX2	DEX3	DEX4	DEX5	DEX6	DEX7
pre	100%	100%	100%	100%	100%	100%	100%
0	5.13%	8.02%	10.98%	3.86%	4.36%	5.59%	2.95%
60	16.72%	13.32%	11.73%	12.19%	18.82%	15.01%	7.88%
120	21.11%	24.40%	20.87%	23.24%	30.10%	21.08%	19.10%
180	25.63%	39.04%	13.78%	28.46%	34.10%	28.15%	30.67%
240	42.87%	36.35%	n.a.	35.70%	n.a.	29.24%	28.63%
300	46.31%	43.05%	27.48%	39.49%	81.26%	33.06%	39.61%

Time [min]	DMSO1	DMSO2	DMSO3	DMSO4	DMSO5	DMSO6	DMSO7
pre	100%	100%	100%	100%	100%	100%	100%
0	3.49%	5.46%	10.39%	8.21%	4.50%	8.17%	4.51%
60	12.49%	15.69%	8.32%	18.23%	20.64%	16.15%	9.43%
120	12.84%	24.38%	12.10%	37.72%	23.26%	22.18%	15.41%
180	26.63%	n.a.	n.a.	72.63%	n.a.	29.46%	24.51%
240	42.23%	n.a.	n.a.	55.82%	54.71%	33.33%	33.23%
300	42.19%	71.04%	39.32%	79.58%	42.95%	32.24%	37.69%

Time [min]	Average DEX	STDEV DEX	Average DMSO	STDEV DMSO
pre	100%	0%	100%	0%
0	6.46%	1.66%	6.39%	2.47%
60	14.53%	3.39%	14.42%	5.15%
120	24.91%	8.89%	21.13%	12.81%
180	34.86%	29.52%	38.31%	0.23%
240	38.58%	13.77%	43.86%	0.11%
300	50.05%	26.74%	49.29%	21.21%

5.3 Conclusions

In this chapter, different aspects of PIN2:GFP trafficking were explored and their dependence on RAB-A2a tested.

Vacuolar GFP signals after dark treatment of PIN2:GFP seedlings were higher in the presence of dominant negative RAB-A2a seedlings compared to the DMSO controls. This indicates enhanced trafficking to the vacuole. Interestingly, Botanelli and colleagues observed increased secretion of amy:SPO in presence of dominant negative RAB-A2a [206]. This potential paradox will be discussed in Chapter 6.

PIN2:GFP labelled PVCs are insensitive to Wortmannin treatment in the presence of dominant negative RAB-A2a seedlings. While uninduced PIN2:GFP controls show enlarged spherical structures [228, 229], this effect was not observed in the presence of dominant negative RAB-A2a. Since there is no reason to believe that traffic to the vacuole *via* PVCs is perturbed or inhibited (see Chapter 4 and [206]), this insensitivity could mean that PIN2:GFP is trafficking too fast through PVCs to make these compartments visible. It may also be that the dominant negative RAB-A2a is interacting with a factor that is required for Wortmannin induced PVC fusion, thus preventing swelling. Changes in vacuolar identity have been described in *Arabidopsis* adaptin mutants [244]. Although PVCs appear normal in the presence of dominant negative RAB-A2a (see Chapter 4), it would be interesting to conduct further Wortmannin experiments with PVC markers, such as BP80:GFP or RAB-F2b:GFP, to see what will happen to PVC morphology in the presence of dominant negative RAB-A2a there. Further, PIN2:GFP trafficking to the vacuole following dark treatments in presence of Wortmannin could be useful [228].

Previous studies on the dependence of PIN2:GFP trafficking on the actin cytoskeleton were unclear. While PIN2:GFP trafficking does not appear to be influenced by cytochalasin D treatment, latrunculin B causes formation of round bodies in lateral root cap cells [232]. Both drugs are used to study actin-dependent trafficking processes [38, 214, 232]. It appears than the observed PIN2:GFP trafficking defects in presence of RAB-A2a are not dependent on the actin cytoskeleton as demonstrated by cytochalasin D experiments. Although the drug was effective and aberrant PM formations were visible, no effects of this drug on the PIN2:GFP pattern were observed, neither in uninduced nor induced samples.

BFA washout experiments addressed the question whether the dominant negative RAB-A2a

mutant interfered with PIN2:GFP recycling. These experiments clearly showed the dependence of PIN2:GFP, but not of BRI-1:GFP, recycling on RAB-A2a mediated trafficking. While the formation of BFA bodies was clearly reversible in control samples and in dominant negative RAB-A2a induced BRI-1:GFP seedlings, BFA bodies remained visible in PIN2:GFP samples in presence of dominant negative RAB-A2a. Furthermore, the recruitment of PIN2:GFP material to BFA bodies (and thus into intracellular bodies) is dependent on intact endocytosis. This was shown by double treatment experiments of either Tyrphostin A23 or A51, and BFA. Having observed an effect on endocytosis of PIN2:GFP in both induced and uninduced samples, this further substantiates that RAB-A2a dependent traffic is more likely to be from TGN to PM rather than the reverse direction. In addition, it was interesting to learn that this defect could not be achieved with the dominant negative version of another RAB-A family member, RAB-A5c. These findings highlight the diversity in trafficking routes [207], even in more specialised pathways such as protein recycling.

The mammalian subclasses in the Rab-A clade, Rab11 and Rab25, localise to the recycling endosome where they orchestrate traffic to specific PM domains and to the TGN in various cell types [125]. The recycling endosome receives slowly recycling material from early endosomes but also receives a subset of secreted proteins from the TGN so it represents an intersection of secretory and recycling pathways. In polarised epithelial cells, Rab11A and Rab25 are spatially segregated from Rab11B [125]. The paralogous *S. cerevisiae* Rab proteins Ypt31 and Ypt32 promote exit of secretory membrane from the late Golgi and are required for traffic from the PGE to the late Golgi compartment [126, 127, 128]. The PGE acts as an early endosome in yeast [126, 129] and shares several markers such as the V-ATPase subunit Stv1 and the SNARE Tlg2 with late Golgi compartment [130].

The next question I addressed, was whether the observed PIN2:GFP trafficking defect is exclusively a defect in PIN2:GFP recycling of endocytosed material or if a defect in *de novo* synthesised PIN2:GFP delivery contributed to this phenotype. To investigate this, FRAP experiments were carried out. Large root areas of PIN2:GFP lines were bleached, the recovery of fluorescence measured in the presence of dominant negative RAB-A2a and in uninduced control samples. The results of these FRAP experiments suggest that the dominant negative RAB-A2a GTPase is not interfering with PIN2:GFP delivery to the PM of newly synthesised PIN2:GFP. The rate of fluorescence recovery at the PM is the same with or without dominant negative RAB-A2a protein present. Furthermore, it appears that polarity of PIN2:GFP is not

affected by dominant negative RAB-A2a.

I believe 20 hours of dexamethasone induction is the appropriate measure for the FRAP experiments. Firstly, a clear phenotype was already present in lateral root cap cells, indicating that the dominant negative RAB-A2a mutant was expressed. This is the most rapid effect and can be observed as early as 16 hours after inducing with dexamethasone. Furthermore, in BFA washout experiments a defect in PIN2:GFP recycling was clearly visible at the same time point, i.e. 20 hours after induction with dexamethasone. Hence, I believe that the FRAP experiments were designed appropriately and that RAB-A2a is not mediating initial delivery to the PM of *de novo* synthesised PIN2:GFP.

In summary, this chapter concludes with the discovery that PIN2:GFP recycling is dependent on RAB-A2a function. Thus it appears that RAB-A2a performs a very similar role as its mammalian homologue Rab11.

Chapter 6

General Discussion

This work provides the first systematic analysis of RAB-A2a dependent membrane traffic in *Arabidopsis thaliana.* Fluorescent protein technology and the dominant negative approach were used to probe various trafficking pathways in *Arabidopsis,* including default PM and vacuolar trafficking and more specialised routes such as recycling.

The two PM markers YFP:NPSN12 and YFP:PIP1;4 reach the PM despite the presence of dominant negative RAB-A2a, and are recruited into BFA bodies after BFA treatment. This showed that neither trafficking to the PM nor their cycling was affected by dominant negative RAB-A2a. Secretory traffic was investigated with the ratiometric marker nlsRm-2A-secGFP but no intracellular accumulation of secGFP was observed in the presence of dominant negative RAB-A2a. Further, the expression of the dominant negative RAB-A2a mutant causes subtle morphological changes in vacuoles. Nevertheless, the vacuolar markers YFP:VAMP711 or YFP:RAB-G3f still reach the tonoplast in the presence of dominant negative RAB-A2a. The trafficking of the pre-vacuolar markers RAB-F2b:GFP and BP80:GFP are not affected by the dominant negative RAB-A2a. Both markers are detected on PVCs, the morphology of these PVCs appears the same with or without dominant negative RAB-A2a present. The two markers RAB-F2b:GFP and YFP:RAB-G3f served as further controls of the dominant negative approach. Trafficking and membrane recruitment of these two RAB GTPases were not affected by dominant negative RAB-A2a. Time course experiments with FM4-64 suggest that RAB-A2a is not involved in an endocytic-vacuolar route.

Further, the effect of the dominant negative RAB-A2a mutant on selected Rab-A GTPase

members was tested, of which YFP:RAB-A1e and mCherry:RAB-A2a, but not mCherry:RAB-A5c, appear to re-localise to Golgi-like compartments.

The polar localised auxin efflux carrier PIN2:GFP was the most strikingly affected marker in the presence of dominant negative RAB-A2a. In this chapter I will consolidate the results obtained, discuss them in light of published literature and propose a model explaining how PIN2:GFP recycling may be affected by the dominant negative RAB-A2a.

6.1 A review of PIN2:GFP trafficking

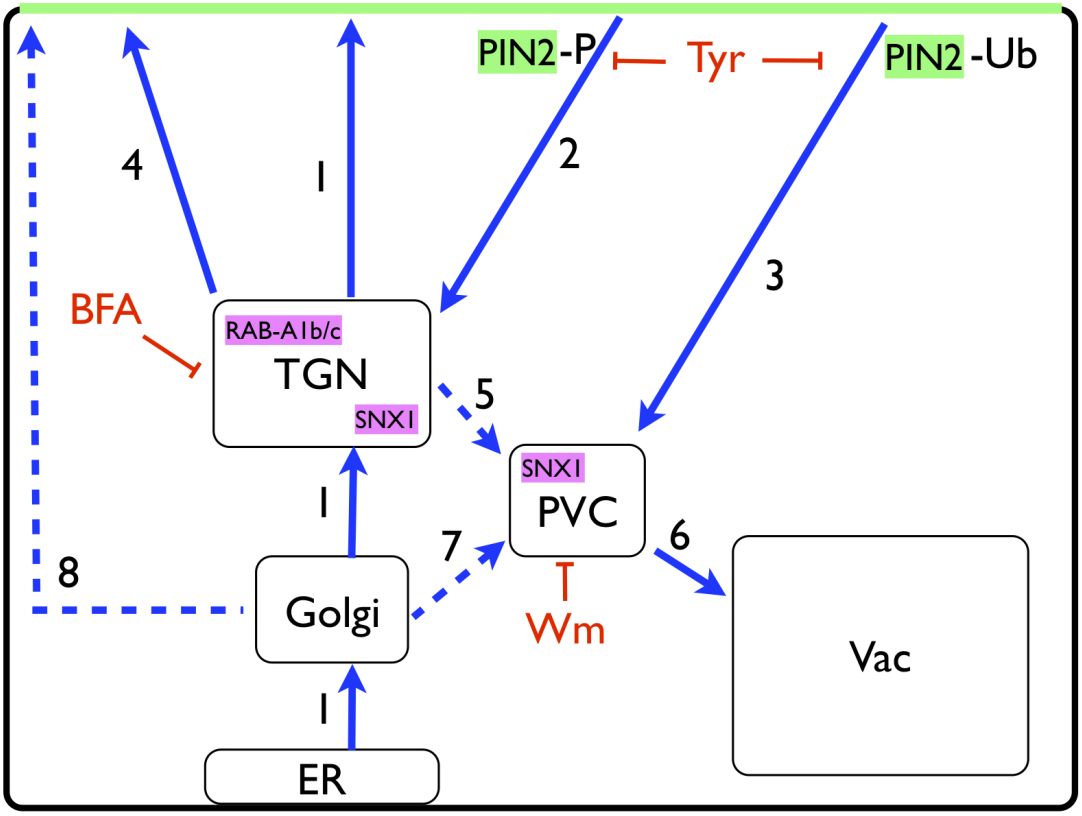

Figure 6.1: Overview of PIN2 trafficking. This simplified model of an *Arabidopsis* epidermal meristematic root cell shows organelles and trafficking pathways (blue arrows) involved in PIN2 trafficking. Dashed arrows indicate alternative routes that have not (yet) been shown to be involved in PIN2 trafficking. Inhibitor treatments are indicated in red, showing their relevant site of action. The PM is indicated as black border, the PIN2 polar domain is marked in green. PIN2-P = phosphorylated PIN2, PIN2-Ub = ubiquitinated PIN2, ER = Endoplasmic Reticulum, TGN = Trans-Golgi Network, PVC = pre-vacuolar compartment, Vac = Vacuole, BFA = Brefeldin-A, Wm = Wortmannin. Details and references are provided in the text.

PIN2 belongs to the family of PIN proteins, which are PM localised auxin efflux carriers with mostly polar localisation [71]. PINs are key regulators of auxin-mediated developmental

processes and are involved in the regulation of tropic growth [72, 73, 74, 75, 76], axis formation in embryogenesis [77], postembryonic organogenesis [78, 79], root meristem maintenance [80, 81], and vascular tissue differentiation and regeneration [82, 83]. There are a total of eight members in the PIN family of *Arabidopsis,* most of which display particular polarities that reflect the direction of auxin transport in various cell types [84].

In *Arabidopsis* root cells, PIN2 localises to the basal membrane in epidermal and root cap cells but exhibits apical localisation in cortical cells of the meristem [232], indicating the direction of auxin flow [221]. After cytokinesis PIN2 initially localises to both apical and basal PM but will subsequently disappear from one, owing to sterol-dependent endocytosis [216]. A similar symmetrical localisation pattern has been demonstrated for PIN1 after *de novo* synthesis but it is not clear whether this is also true for *de novo* synthesised PIN2 [85]. Figure 6.1 shows a simplified model of PIN2 trafficking in a meristematic, epidermal root cell. PIN2 is transported to the PM (figure 6.1, pathway '1') from where it is endocytosed *via* a GNL1 dependent pathway (figure 6.1, pathway '2') [211]. PIN2 cycles *via* GNOM-independent endosomes (figure 6.1, pathway '2') and is then re-delivered to the PM through endosomal compartments (figure 6.1, pathway '4'); this cycling is likely to involve the TGN as my work shows. PIN2 polarity is highly dependent on its phosphorylation status. The PP2A phosphatase [235] and PINOID kinase [236] have been identified as important regulators of apical-basal targeting. In both *pp2aa1 pp2aa2* and *pp2aa1 pp2aa3* mutants, polar localisation of PIN2 is affected [235]: PIN2 normally exhibits apical localisation in young cortical cells, in both *pp2aa1* double mutants PIN2 changed its polarity to basal in young cortical cells. However, the basal localisation in epidermal cells remains unaffected [235]. Mutations in the phosphorylation site of the central hydrophilic loop of PIN1 revealed the importance of phosphorylation and de-phosphorylation in apical and basal polarity of PIN proteins. For example, a particular non-phosphorylatable mutant of PIN1-HA, PIN1-HA(Asp), is able to rescue the agravitropic phenotype of the *pin2* mutant and thus acquired PIN2-like function [237]. Overexpression of the PINOID protein kinase induces a shift from basal to apical PIN localisation [238].

PIN2 trafficking is sensitive to BFA, a fungal toxin that has been widely used to study membrane traffic, more specifically protein cycling dependent on endosomes [37, 65]. Treatment with BFA causes formation of 'BFA bodies' in *Arabidopsis* root cells as early as 30 minutes after treatment with a concentration of 50µM BFA. These BFA bodies consist of an accumulation of early endosomal compartments in its core that are surrounded by Golgi stacks. BFA is known

to inhibit cycling of proteins between PM and the TGN *via* other endosomal compartments in *Arabidopsis* [86] but FRAP experiments of BFA treated *Arabidopsis* roots revealed that this drug does not inhibit delivery of *de novo* synthesised EGFP:LTI6a to the PM, indicating that default PM targeting is intact in BFA treated *Arabidopsis* roots [38].

PIN1 was shown to localise in these BFA bodies upon BFA treatment, even when *de novo* synthesis was inhibited. This internalisation is completely reversible and indicates constitutive endocytosis and recycling of PIN proteins [37]. Kleine-Vehn and colleagues (2008) showed that prolonged BFA treatment causes a shift of PIN2 localisation from the basal to the apical membrane in epidermal root cells, a process called 'transcytosis'. This was shown to be dependent on intact microtubules but independent of the ARF-GEF GNL1 in the case of PIN2 across 30 different *Arabidopsis* ecotypes [90, 92]. Transcytosis describes a process in which the localisation of a polar protein is shifted *via* 'recycling endosomes' and provides a mechanism for rapid changes in PIN polarity in response to various signals, such as developmental or environmental signals [92]. Transcytosis is also a well known mechanism for polar delivery of cargos in animal cells [94, 95].

Recently, Drdova and colleagues (2012) showed that PIN2:GFP recycling is dependent on the exocyst complex (figure 6.1, pathway '4'), which is implicated in the fusion of exocytic vesicles. A mutant of one of the exocyst complex units, exo70A1, exhibits perturbed PIN1:GFP and PIN2:GFP recycling and impaired trafficking of BRI1:GFP. PIN2:GFP accumulates in abnormally expanded, RAB-A5d labeled endomembrane compartments [204]. RAB-A5d is a marker for recycling endosomes that are distinct from VHA-a1:GFP labeled TGN [150, 204].

Previous experiments with PIN2:GFP showed that Tyrphostin A23 prevents PIN2:GFP from reaching the BFA body in *Arabidopsis* while FM4-64 internalisation is detected [188]. In mammalian cells, Tyrphostins act as inhibitors of tyrosine kinases. They are structural analogues of tyrosine and function by binding to the active sites of the enzymes [245]. Tyrphostins are used to study endocytosis in *Arabidopsis,* in particular receptor mediated endocytosis [142, 242]. Tyrphostin A23 inhibits the interaction between the YXXaφ (aφ is a bulky hydrophobic amino acid) endocytosis signal and the mu2-subunit of the AP2 complex [243]. AP2 is a clathrin adaptor involved in endocytosis (see section 1.2.1). In plants, tyrphostin A51 is considered a biologically inactive analogue of Tyrphostin A23 as it does not inhibit this aspect of plant endocytosis. It is thus routinely used as negative control treatment [243].

The accurate targeting of PIN2 to the vacuole involves proteasome activity, which requires

ubiquitination of PIN2 [223] (figure 6.1, pathway '3' and '6'). This ubiquitination functions as a signal that controls how much PIN2 is recycled back to the PM, and how much PIN2 is internalised and targeted for proteolytic degradation [223]. The function of AMSH3, a de-ubiquitinating enzyme, is required in efficient targeting of PIN2 to the lytic vacuole, as *amsh3* plants do not accumulate GFP in the vacuolar structures. However, polar PIN2:GFP targeting is not affected in *amsh3* plants, which suggests that AMSH3 is not involved in the transport of PIN2 to the PM or its recycling [224]. The retromer is a cytosolic protein complex consisting of VPS35, VPS29 and VPS26 and the SNX group of proteins that associates with post-Golgi compartments and is involved in protein targeting to the lytic vacuole, including PINs [246]. SNX1 colocalises with both RAB-F1:GFP and GFP:RAB-F2b and is sensitive to Wortmannin (figure 6.1, pathway '6') [228, 229], a fungal metabolite that inhibits plant endocytosis [27] and also acts on the vacuolar pathway of plants by causing pre-vacuolar bodies to form small vacuoles by homotypic fusion of PVCs [187]. Known targets of Wortmannin are PI3K and PI4K [231], the recycling of the plant vacuolar sorting receptor BP80 between PVC and TGN is also inhibited [202]. Early observations described SNX1 as part of the TGN [247] and the PVCs [145], and described a possible involvement of PVCs in protein recycling to the PM [145]. However, more recent studies using electron microscopy rather than confocal laser scanning microscopy revealed that SNX proteins localise to the TGN and that localisation to PVCs could not be identified with certainty [209]. This may suggest the TGN rather than PVCs are the primary compartment involved protein recycling to the PM.

Experiments involving dark treatments of GFP fusion proteins allow investigation of protein degradation and trafficking to the lytic vacuoles [225]. It has been shown previously that GFP and related proteins exhibit increased stability in lytic vacuoles due to conformational changes [43, 226]. Indeed, dark treatments of PIN2:GFP seedlings for two to four hours showed that GFP can be observed in the lumen of the vacuole indicating PIN2 degradation in lytic vacuoles [227]; its transport to the vacuole is dependent on a BFA sensitive ARF-GEF, which is not GNOM [228].

Two members of the RAB-A family, RAB-A1b and RAB-A1c have been implicated in PIN2 recycling. RAB-A1b (BEX5) localises to the TGN and early endosomes and is involved in TGN to PM trafficking of PM cargos, such as PIN1:GFP, PIN2 and GFP:PIP2a [119]. This link was discovered through a forward genetic screen for *Arabidopsis* mutants that showed increased intracellular accumulation of PIN1 in response to the trafficking inhibitor BFA. *bex5*,

a dominant negative mutant, is hypersensitive to BFA and is defective in PM traffic as shown by absence of recovery of PM traffic after BFA washout. However, even though endosome morphology is reportedly abnormal in *bex5,* the PM labelling of PIN1:GFP and PIN2:GFP appears intact and comparable to wild type; recyling of PIN2:GFP is reportedly defective as BFA bodies do not disperse in *bex5* [119]. Further, it was recently shown that RAB-A1c localises to an endosidin 1 (ES1) sensitive population of the TGN, partially overlapping the VHA-a1 domain and is believed to play a role in cytokinesis as it localises to the cell plate in dividing cells [120]. It is speculated that Rab-A1 is indirectly involved in auxin-mediated responses as ES1 is known to inhibit trafficking of PIN2 and AUX1. This is also observed in TRAPPII mutants, a protein complex that acts upstream of RAB-A1c [120].

6.2 Examination of PIN2:GFP trafficking in the presence of dominant negative RAB-A2a

In the following sections, I will examine how the results of my work relate to the above mentioned literature, propose a model for RAB-A2a PIN2:GFP trafficking and discuss the wider implications of this work.

6.2.1 The default route of PIN2:GFP to the PM is not inhibited by dominant negative RAB-A2a

Two PM markers YFP:NPSN12 and YFP:PIP1;4 reach the PM despite the presence of dominant negative RAB-A2a, and are recruited into BFA bodies after BFA treatment. This showed that neither trafficking to the PM nor their cycling was affected by dominant negative RAB-A2a. Secretory traffic was investigated with the ratiometric marker nlsRm-2A-secGFP but no accumulation of secGFP was observed in presence of dominant negative RAB-A2a. These results indicated that RAB-A2a may be involved in specialised trafficking to the PM. It was speculated earlier that it could be involved in biosynthetic traffic to the PM, a hypothesis based on the localisation of the preferentially GDP- or GTP-bound mutants [45].

The localisation of the polar localised auxin efflux carrier PIN2:GFP was the most strikingly affected marker. In the presence of dominant negative RAB-A2a, PIN2:GFP is strongly localised intracellularly; only a small portion of the PIN2:GFP is detected at the PM. BFA treatment of

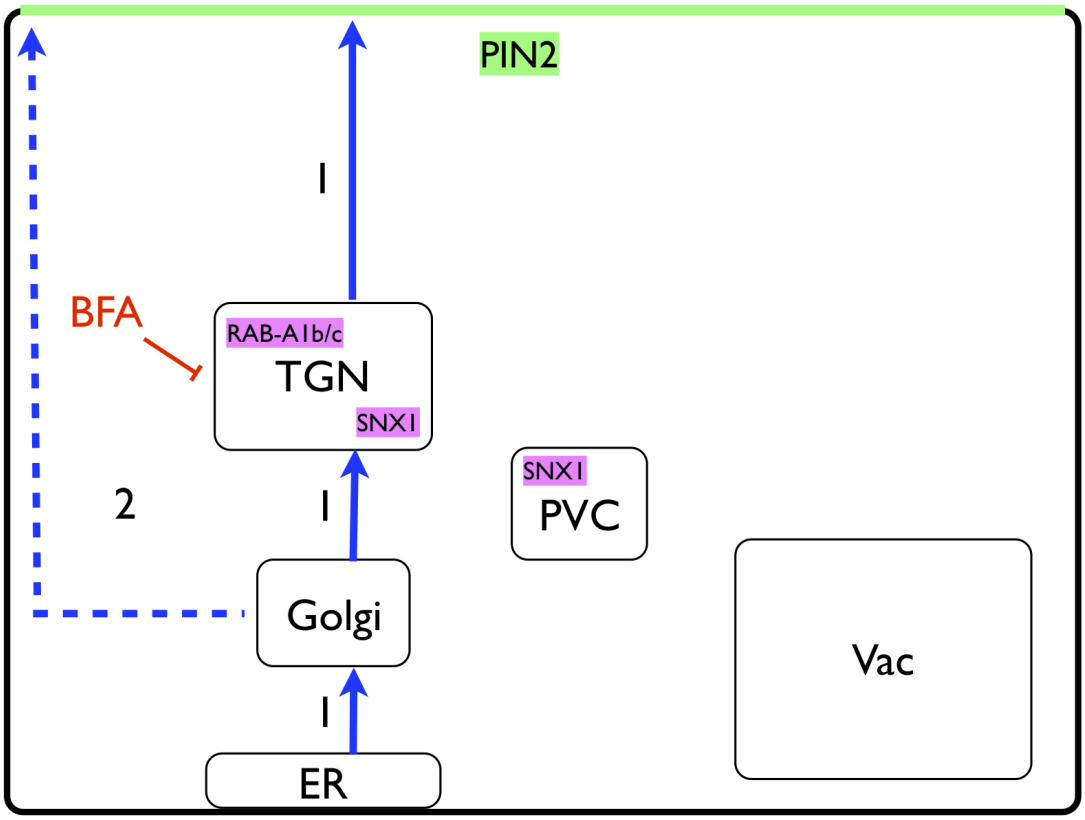

Figure 6.2: Different scenarios for the default route of PIN2:GFP to the PM. Organelles and trafficking pathways (blue arrows) involved in PIN2 trafficking are shown. Dashed arrows indicate alternative routes that have not (yet) been shown to be involved in PIN2 trafficking. Inhibitor treatments are indicated in red, showing their relevant site of action. The PM is indicated as black border, the PIN2 polar domain is marked in green. ER = Endoplasmic Reticulum, TGN = Trans-Golgi Network, PVC = pre-vacuolar compartment, Vac = Vacuole, BFA = Brefeldin-A. Details and references are provided in the text.

seedlings expressing dominant negative RAB-A2a caused aggregation of intracellular localised PIN2:GFP in BFA bodies while the PM signal appeared weaker compared to control samples. This result indicates a possible role for RAB-A2a in PIN2:GFP cycling .

BFA treatments suggest that the nature of PIN2:GFP intracellular accumulation is TGN rather than Golgi, a conclusion that is substantiated by merely comparing the appearance of these accumulations to the characteristic doughnut shape of Golgi bodies in *Arabidopsis*. However, as previously described, treatment with BFA causes the formation of BFA bodies, whereas in *Arabidopsis* root cells TGN material is localised in the core of the BFA body and Golgi bodies are surrounding it [87, 88]. My experiments show that intracellular PIN2:GFP accumulates in the BFA body core in the presence of dominant negative RAB-A2a. The TGN-nature of PIN2:GFP accumulations may also be substantiated by Wortmannin treatments that suggest either decreased sensitivity of PVC to this drug, or a proportional shift of more TGN compart-

ments, where PVCs become less apparent. This would mean that pathway (2) of figure 6.2 is unlikely to be affected by dominant negative RAB-A2a. As the rate of fluorescence recovery after photobleaching at the PM is essentially the same in the presence or absence of dominant negative RAB-A2a, it appears that pathway (1) of figure 6.2 is not inhibited. Thus, the overall conclusion is that default traffic of PIN2:GFP to the PM is not affected in the presence of dominant negative RAB-A2a.

6.2.2 PIN2:GFP recycling is inhibited in the presence of dominant negative RAB-A2a

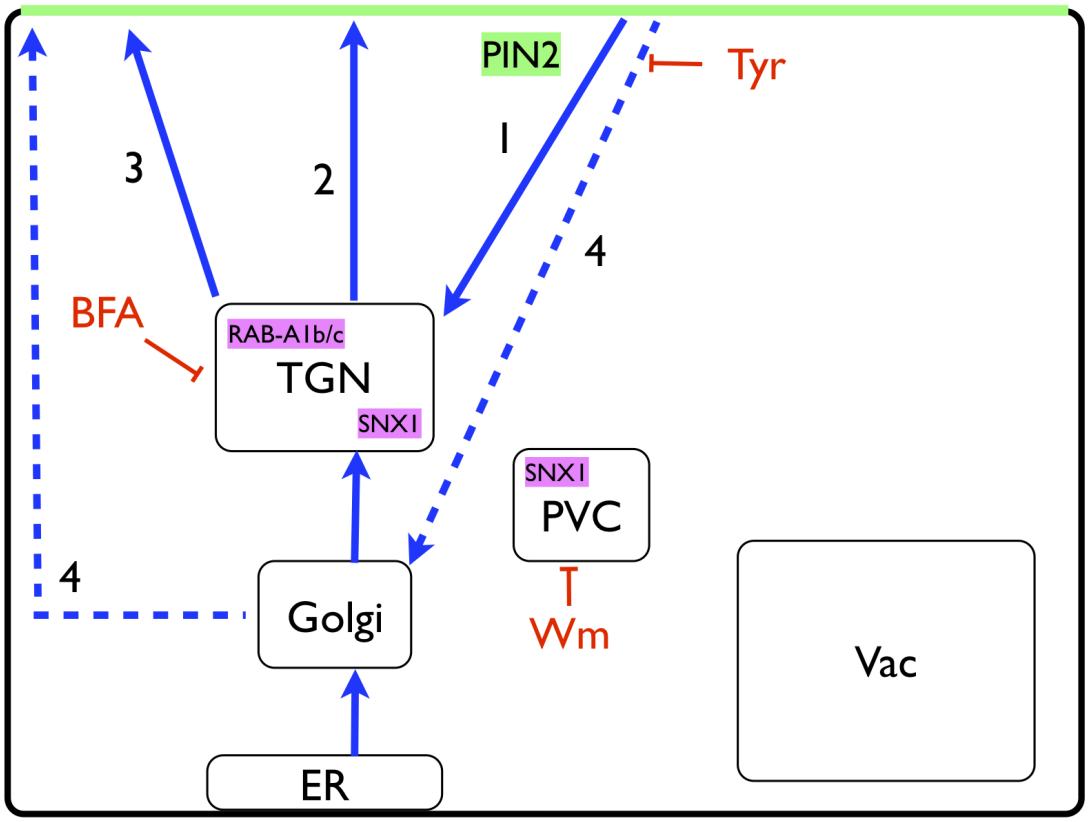

Figure 6.3: Possible trafficking scenarios of PIN2:GFP to the vacuole. Organelles and trafficking pathways (blue arrows) involved in PIN2 trafficking are shown. Dashed arrows indicate alternative routes that have not (yet) been shown to be involved in PIN2 trafficking. Inhibitor treatments are indicated in red, showing their relevant site of action. The PM is indicated as black border, the PIN2 polar domain is marked in green. ER = Endoplasmic Reticulum, TGN = Trans-Golgi Network, PVC = pre-vacuolar compartment, Vac = Vacuole, BFA = Brefeldin-A, Wm = Wortmannin, Tyr = Tyrphostin A23. Details and references are provided in the text.

The literature on PIN2:GFP recycling allows several possible scenarios in epidermal root cells, which are are shown in figure 6.3. Once PIN2:GFP reaches the PM and is phosphoylated by

the respective kinase [248], it is endocytosed *via* a Tyrphostin A23 sensitive pathway to the TGN (1) or perhaps Golgi (4). From the TGN, it could either follow a recycling step through the default secretory route (2) or a specialised recycling route (3), or, PIN2:GFP is trafficked from Golgi directly to the PM (4) or from Golgi through the TGN *via* the default secretory route (2).

BFA treatments cause the formation of BFA bodies, a process that is completely reversible [37]. BFA washout experiments addressed the question whether RAB-A2a is involved in PIN2:GFP recycling. These experiments showed that PIN2:GFP recycling is dependent on RAB-A2a mediated trafficking. The formation of BFA bodies was clearly reversible in control samples but BFA bodies remained visible in PIN2:GFP samples in the presence of dominant negative RAB-A2a, at least two hours after removal of BFA.

It has been previously shown that the recruitment of PIN2:GFP to BFA bodies is dependent on endocytosis [188]. Utilising the double drug treatment approach of Tyrphostin A23 and BFA as described by Dhonukshe and colleagues[188], my results show that endocytosis and recruitment of PIN2:GFP to BFA bodies is not inhibited by dominant negative RAB-A2a. Thus, the question is which of the pathways (2), (3) or (4) is perturbed in presence of dominant negative RAB-A2a. Section 1.2.1 established that the nature of intracellular PIN2:GFP accumulations is rather TGN than Golgi, so it appears unlikely that pathway (4) is utilised by PIN2:GFP for recycling, although such a recycling pathway may exist for other proteins [48]. FRAP experiments indicate that default traffic of PIN2:GFP to the PM is intact in presence of dominant negative RAB-A2a, therefore pathway (2) can be ruled out. Therefore, the data suggests that dominant negative RAB-A2a interferes with a recycling pathway from the TGN to PM, here shown as pathway (3).

6.2.3 Trafficking of PIN2:GFP to the vacuole is enhanced in the presence of dominant negative RAB-A2a

There are several possibilities of how PIN2:GFP could be trafficked to the vacuole that conform with reports from the literature (figure 6.4). PIN2 is ubiquitinated at the PM which directs the protein into the proteolytic route to the vacuole [223]. Along this trafficking pathway, PIN2 is passed through SNX1 and RAB-F labeled compartments [228, 229]. In the case of SNX1, it is not entirely clear whether it is localised to TGN only or additionally localises to PVC

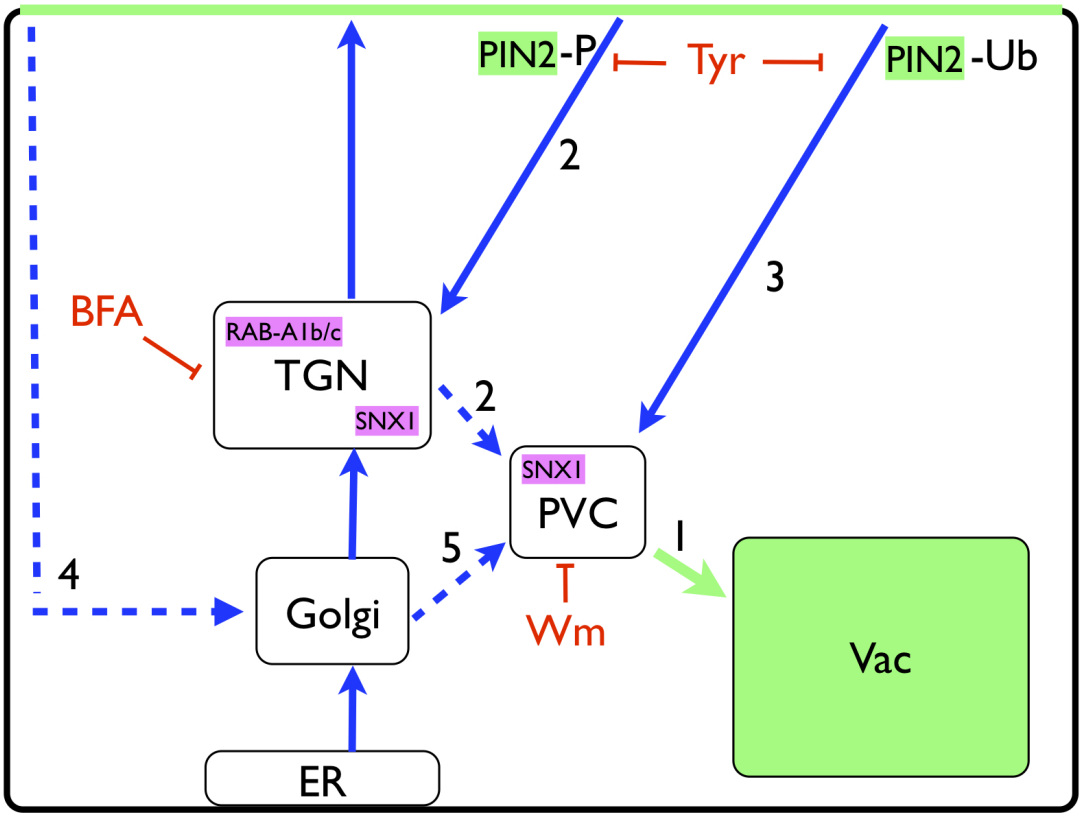

Figure 6.4: Different scenarios for PIN2:GFP recycling pathways. Organelles and trafficking pathways (blue arrows) involved in PIN2 trafficking are shown. Dashed arrows indicate alternative routes that have not (yet) been shown to be involved in PIN2 trafficking. Inhibitor treatments are indicated in red, showing their relevant site of action. The PM is indicated as black border, the PIN2 polar domain is marked in green. PIN2-P = phosphorylated PIN2, PIN2-Ub - ubiquitinated PIN2, ER = Endoplasmic Reticulum, TGN = Trans-Golgi Network, PVC = pre-vacuolar compartment, Vac = Vacuole, BFA = Brefeldin-A, Wm = Wortmannin, Tyr = Tyrphostin A23. Details and references are provided in the text.

[209]. Therefore, it might be that PIN2:GFP is either directly transported to PVC (pathway 3) and then to the vacuole (pathway 1), or it might well be that PIN2:GFP is trafficked to a domain of the TGN (pathway 2) that sorts the protein into a vacuolar pathway (pathways 2 and 1) [228]. Another possibility could be the targeting of PIN2:GFP to the Golgi (pathway 4) where it is subsequently sorted to PVC (pathway 5) and then transported to the vacuole (pathway 1). The involvement of dominant negative RAB-A2a can be ruled out in the latter case (pathway 4 and 5 leading to 1), for reasons discussed in the preceding sections.

As shown in Chapter 5, vacuolar GFP signals were higher in the presence of dominant negative RAB-A2a seedlings compared to the control samples following dark treatment, indicating enhanced vacuolar trafficking. However, Botanelli and colleagues showed increased secretion of amy:SPO in presence of dominant negative RAB-A2a [206]. This is seemingly a paradox

that can be resolved with the following scenario: One could assume that if PIN2:GFP follows a pathway from the PM to TGN and one pathway to PVC, and if one trafficking pathway is blocked, that the other is enhanced.

PIN2:GFP labelled intracellular compartments are insensitive to Wortmannin treatment in presence of dominant negative RAB-A2a seedlings. While uninduced PIN2:GFP controls show enlarged spherical structures [228, 229], this effect was not observed in the presence of dominant negative RAB-A2a. Since there is no reason to believe that traffic to the vacuole *via* PVCs is perturbed, as RAB-F2b:GFP and BP80:GFP labeled PVC morphology appears unaffected in the presence of dominant negative RAB-A2a, it could mean that pre-vacuolar membrane identity is altered. Changes in vacuolar identity have been described in *Arabidopsis* adaptin mutants [244]. It might also be that there is a higher ratio of TGN-like compartments visible, making PVC compartments less apparent. It would therefore be interesting to investigate how RAB-F2b:GFP and BP80:GFP labeled PVC respond to Wortmannin treatment. Also, PIN2:GFP trafficking to the vacuole following dark treatments in the presence of Wortmannin could be useful [228].

Taken together, the pathway (2) leading to (1) and pathway (3) leading to (1) may all be possible considering the available literature and the analysis of results in this project.

6.2.4 A model for RAB-A2a dependent PIN2:GFP trafficking in *Arabidopsis thaliana*

In Chapter 3, I tested the specificity of the dominant negative approach by studying the effect of dominant negative RAB-A2a on the localisation of selected the Rab-A family members. The selected markers were mCherry:RAB-A2a, the closely related YFP:RAB-A1e and more distantly related mCherry:RAB-A5c [111]. mCherry:RAB-A2a localises to doughnut shaped bodies, which may be Golgi bodies, and shows increased cytosolic labelling. This was an expected result as Chow and colleagues (2008) showed that a preferentially GDP-binding mutant of RAB-A2a localises to the Golgi in *Arabidopsis* roots [45]. Such preferentially GDP binding mutants reflect the inactive state of a Rab GTPase [106, 190]. Interestingly, YFP:RAB-A1e also localises to these Golgi-like bodies in the presence of dominant negative RAB-A2a. It may be that RAB-A2a and RAB-A1e share a basic trafficking pathway or are part of a Rab cascade, in which the recruitment of one Rab GTPase to the membrane is crucial for activation and

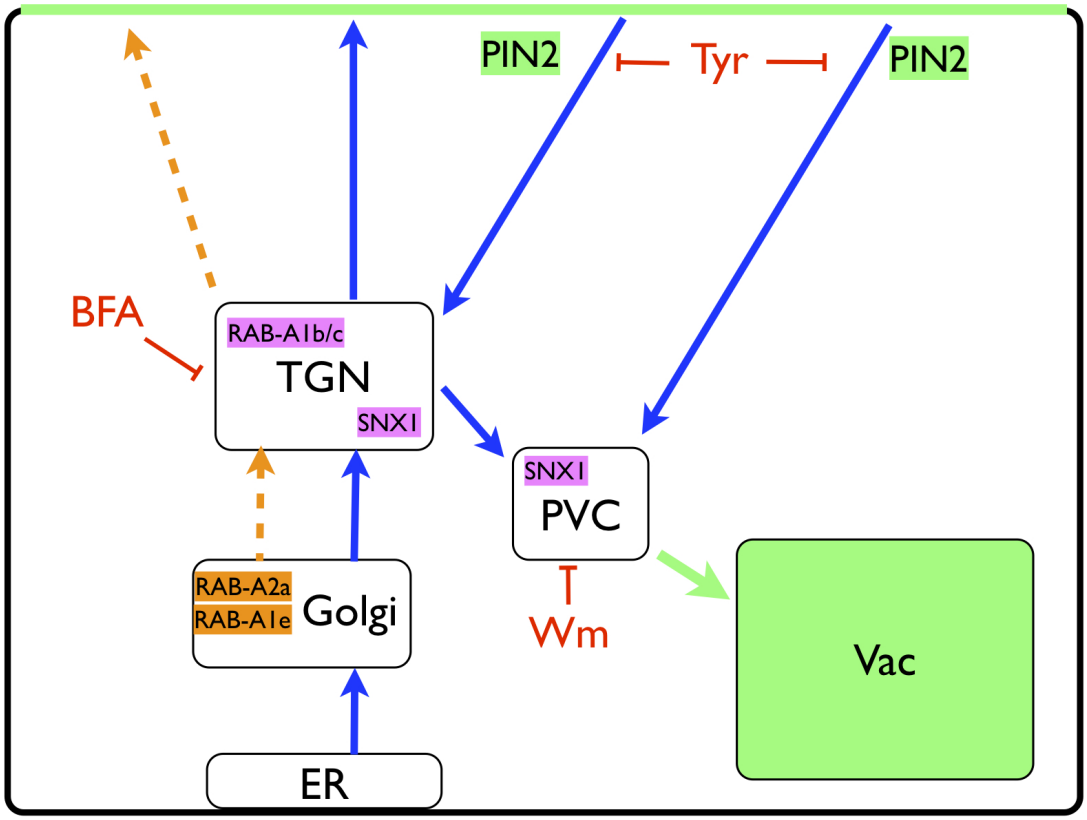

Figure 6.5: A model for RAB-A2a dependent PIN2:GFP trafficking in *Arabidopsis thaliana* epidermal meristematic root cells. Organelles and trafficking pathways (blue arrows) involved in PIN2 trafficking are shown. Blue arrows indicate intact trafficking routes, orange dashed arrows indicate perturbed trafficking route in the presence of dominant negative RAB-A2a. Inhibitor treatments are indicated in red, showing their relevant site of action. The PM is indicated as a black border, the PIN2 polar domain is marked in green. ER = Endoplasmic Reticulum, TGN = Trans-Golgi Network, PVC = pre-vacuolar compartment, Vac = Vacuole, BFA = Brefeldin-A, Wm = Wortmannin, Tyr = Tyrphostin A23. Details and references are provided in the text.

membrane recruitment of another Rab GTPase [205]. Both Rab-A1 and Rab-A2 subclasses are implicated in TGN-associated traffic to the PM [45, 118, 119, 120] and Rab cascades are known in mammals and yeast [205]. Nevertheless, it appears that dominant negative RAB-A2a only affects a subset of Rab-A proteins. The localisation of mCherry:RAB-A5c, a representative of the more distantly related Rab-A5 family, is unaffected. This may mean that PIN2:GFP cannot be sorted from TGN into the recycling route as neither RAB-A2a nor RAB-A1e reach their site of action in presence of dominant negative RAB-A2a.

According to these results and the preceding discussion, I propose a PIN2:GFP trafficking model that is depicted in figure 6.5. My data have shown that default PM and endocytic traffic are intact in the presence of dominant negative RAB-A2a. Additionally, vacuolar trafficking of PIN2:GFP is enhanced. It appears that only the recycling step from TGN to the

PM is inhibited by expression of dominant negative RAB-A2a. Expression of dominant negative RAB-A2a causes localisation of mCherry:RAB-A2a and YFP:RAB-A1e to compartments closely resembling Golgi bodies. Thus, mCherry:RAB-A2a and YFP:RAB-A1e are no longer able to reach their site of action, the TGN, in the presence of dominant negative RAB-A2a, where they would normally engage in recycling functions. I propose that PIN2:GFP is held at a TGN/ early endosomal compartment (possibly RAB-A5d positive?) from which its recycling to the PM is inhibited, due to the lack of functional RAB-A2a (and RAB-A1e) at the TGN.

As mentioned in section 1.1, two other members of the Rab-A family, RAB-A1b and RAB-A1c have been implicated in PIN2:GFP recycling from TGN to PM [119, 120]. Interestingly, the localisation of YFP:RAB-A1e is affected in the presence of dominant negative RAB-A2a. However, neither of the first two Rab-A members cause a comparably strong intracellular accumulation of PIN2:GFP as was observed in this work in the presence of dominant negative RAB-A2a. Thus, it might be that Rab-A1 members aide in 'cleaning up' polarity of PIN2:GFP, i.e. to recycle PIN2:GFP that is localised in excess at the extremities of the polar domain, whereas RAB-A2a is the major regulator of constitutive recycling, which proportionally may take place more frequently thus explaining the more dramatic phenotype. This assumes that experiments were conducted under similar conditions and proteins were expressed at similar levels. However, RAB-A2a mediated recycling appears different from polar delivery processes as polarity is not visibly affected in the presence of dominant negative RAB-A2a. As suggested by Kleine-Vehn and colleagues, polarity control of PIN2 may involve spatial regulation of PIN2 endocytosis and immobilisation in the PM rather than recycling [249].

However, one issue that needs to be addressed in the future concerns the definition of the TGN. As mentioned in Chapter 1, the TGN is believed to be a multi-domain complex, a central hub for secretory and endocytic traffic. Considering the results of my work, I am not convinced this single compartment view is correct. It is surprising that while the default pathway of PIN2:GFP to the PM is intact, PIN2:GFP that enters the recycling route is not just re-delivered to the PM *via* the default pathway. As my results suggest, PIN2:GFP is held at a TGN-like state, caused by a trafficking inhibition through the expression of the dominant negative RAB-A2a. This could mean that there is not just a TGN but many different TGNs that employ different targeting mechanisms and are thus required for different trafficking steps, as has been suggested previously [44, 250]. It could be that the TGN is made up of individual endosomal compartments, of which some are required for either default PM delivery, recylcing

or vacuolar targeting. The TGN in *Arabidopsis* was first defined by Staehelin and Moore as clathrin-coated tubular network [251]. Dettmer and colleagues showed that VHA-a1 localised to tubulovesicular membranes close to the *trans* site of Golgi bodies and based the definition of the TGN in *Arabidopsis* upon this marker [43]. But what is the evidence for a single multi-domain compartment? The marker VHA-a1 is currently used to spot the TGN in EM images but it does not appear as a distinctive organelle, such as ER and Golgi [43]. The TGN appears rather as an agglomeration of vesicular structures that lie in close proximity to each other [43, 45]. I thus challenge the current view of a single TGN compartment and rather suggest that the TGN is a 'network' of associated but distinct endosomal compartments with distinct functions. In this way, it appears plausible why PIN2:GFP is held intracellularly but is not transported to the PM through the default TGN mechanism, and may provide an explanation why BRI1:GFP recycling is intact in the presence of dominant negative RAB-A2a (as it is trafficked through other TGN compartments and therefore does not merge with PIN2:GFP into the same recycling pathway).

Taken together, this work contributes to a better understanding of PIN2:GFP traffic, highlighting that there may be more than one TGN compartment, and reveals that researchers may have to reconsider past experiments involving dominant negative mutants of trafficking regulators, as dominant negative RAB-A2a not only alters the localisation of mCherry:RAB-A2a but also of another RAB, YFP:RAB-A1e.

6.3 Future directions

Cytokinesis and PIN proteins have polar traffic in common. It will be interesting to see whether RAB-A2a is specifically involved in the recycling of polar proteins, as recycling of non-polar markers is not dependent on RAB-A2a function. FRAP experiments with a controlled gravity vector could help to address this question. Also, the effect of dominant negative RAB-A2a on other polar markers such as PIN1, AUX1 or NIP5;1 could be investigated.

This work revealed and analysed PIN2:GFP trafficking defects in the presence of a dominant negative RAB-A2a. It would be of great interest to see whether endogenous PIN2 trafficking is affected too; this can be achieved by immunolocalisation experiments.

Identification of Rab interactors would help in understanding cellular functions of these proteins and shed light on the exact mechanism of membrane traffic interference by dominant negative

mutants. Yeast-two-hybrid assays did not prove very useful in identifying interactors, however, immunoprecipitation may be a possibility. Further, it would be interesting to determine the cargo of Rab vesicles. By making use of fluorescent protein technology, FACS (fluorescence assisted cell sorting) could be used to separate different vesicles and other techniques such as mass spectrometry could be used to determine cargo.

Finally, RAB-A2a acts on traffic between TGN and the PM. This makes RAB-A2a an interesting candidate for protein trafficking to the plant apoplast and root secretion. At present, there is no information on how plants regulate the composition of the apoplast or how root secretion is achieved. In both cases, membrane trafficking could be involved and could be studied by investigating the effect of dominant negative Rab GTPases on leaf apoplast composition or root secretion, which may also lead to important results in other fields such as plant pathology.

Appendix A

Additional images

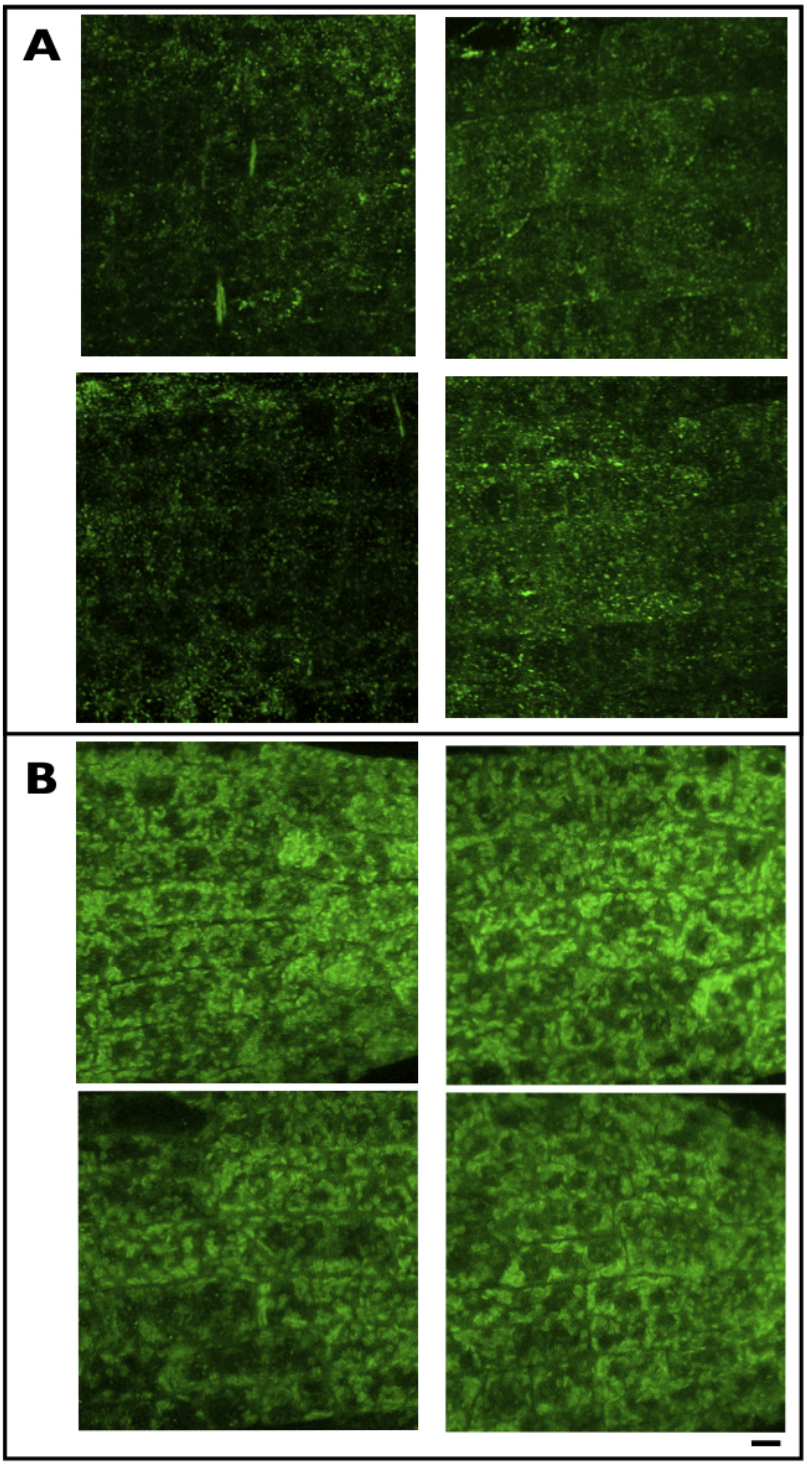

Figure A.1: Dominant negative RAB-A2a causes localisation of YFP:RAB-A1e to Golgi-like bodies. Localisation of YFP:RAB-A1e in roots of two independent transgenic *Arabidopsis* Col-0 lines were analysed three days after germination on DMSO or dexamethasone containing MS agar plates (triplicate experiments per line, utilising four to six seedlings per line and treatment). A: YFP:RAB-A1e localises in intracellular punctate structures and at the PM in DMSO control samples. B: In dexamethasone induced samples, the PM localisation is lost, YFP:RAB-A1e is localised to intracellular, enlarged compartments, resembling Golgi bodies. Images are 3D projections. Scale bar = 5µm.

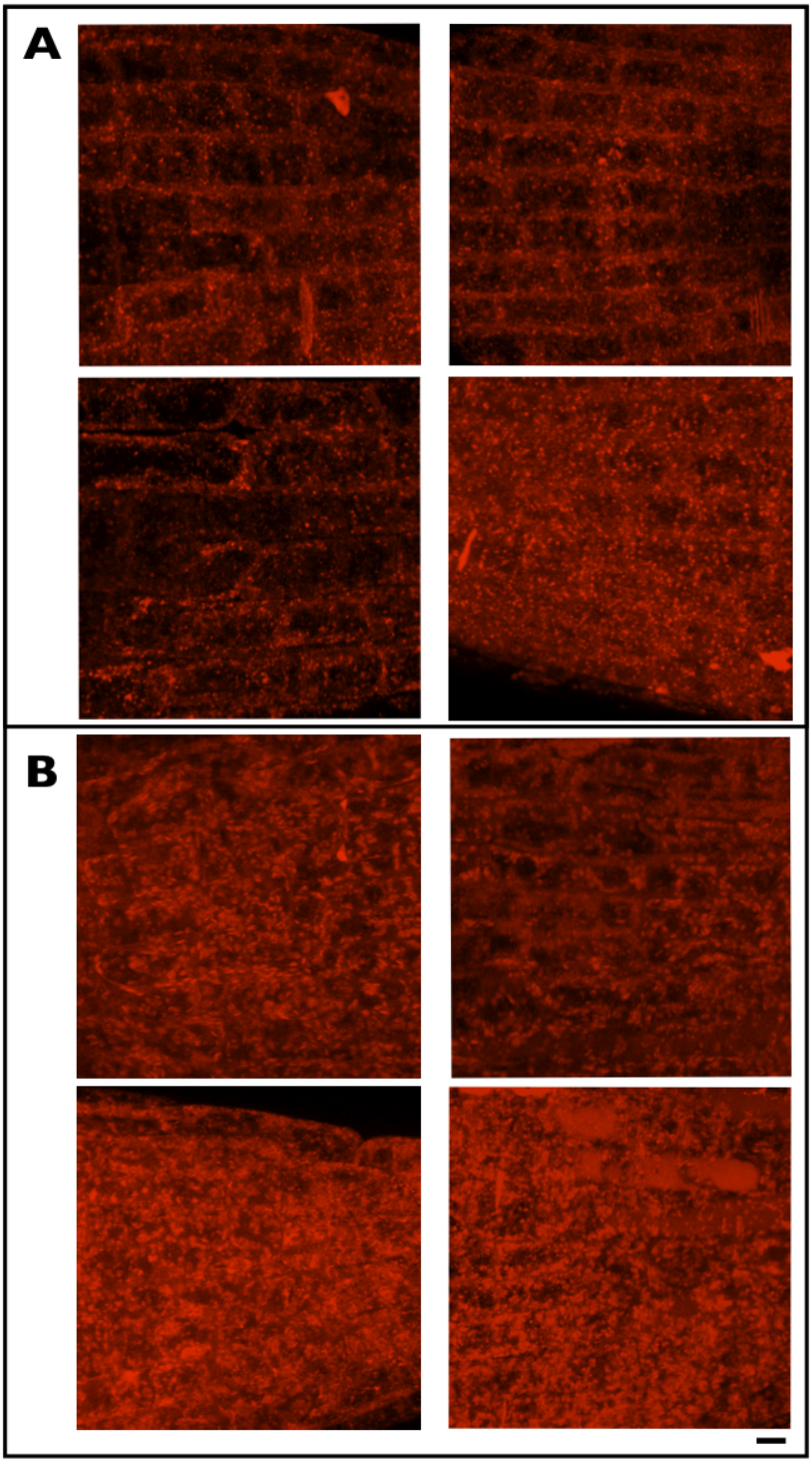

Figure A.2: Dominant negative RAB-A2a causes localisation of mCherry:RAB-A2a to Golgi-like bodies. Localisation of mCherry:RAB-A2a in roots of two independent transgenic *Arabidopsis* Col-0 lines were analysed three days after germination on DMSO or dexamethasone containing MS agar plates (triplicate experiments per line, utilising four to six seedlings per line and treatment). A: In DMSO control samples, the mCherry:RAB-A2a appears in intracellular structures and at the PM. B: In dexamethasone induced samples, the PM localisation is lost and mCherry:RAB-A2a appears in intracellular, enlarged compartments, resembling Golgi bodies. Images are 3D projections. Scale bar = 5µm.

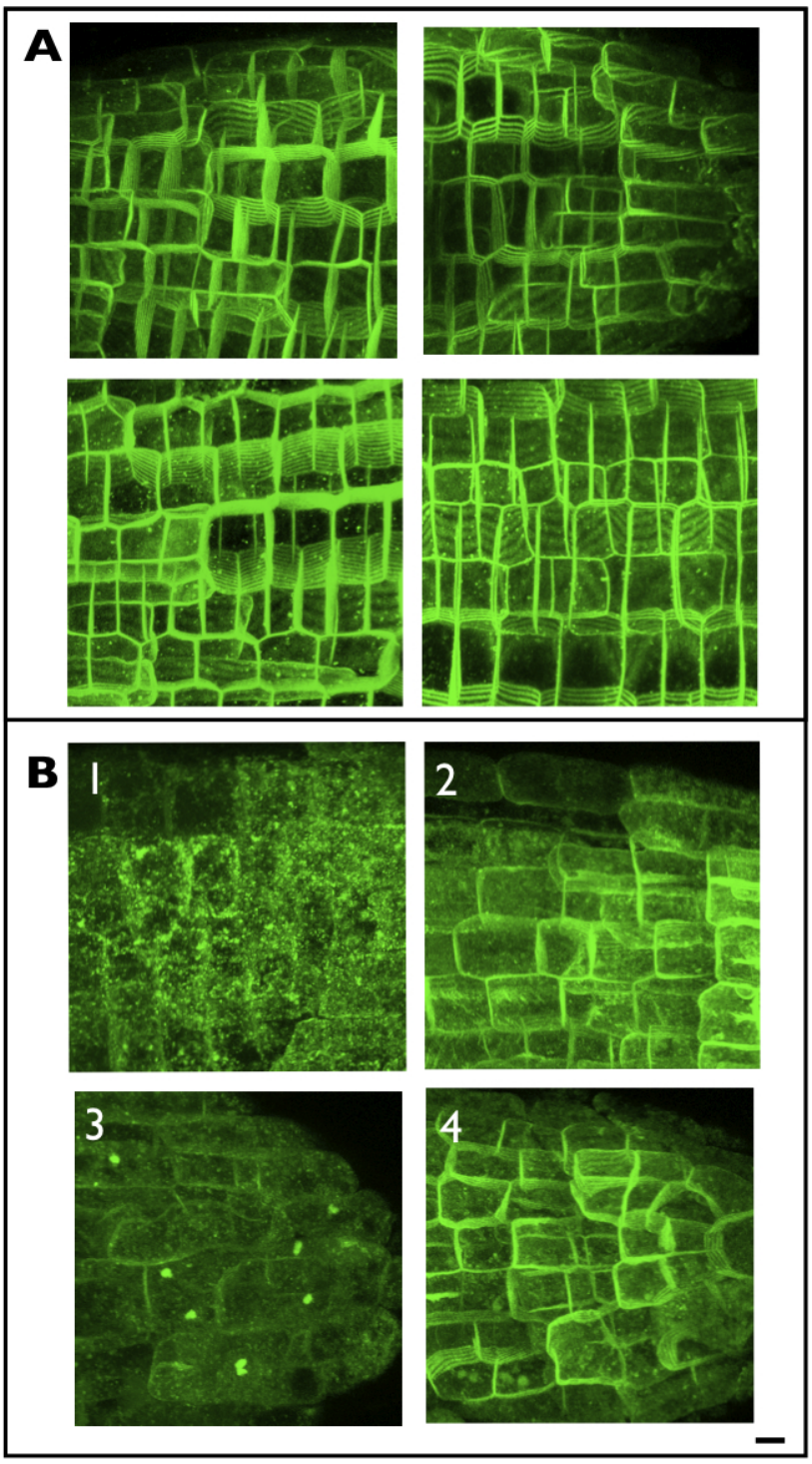

Figure A.3: Dominant negative RAB-A2a causes prominent intracellular localisation of PIN2:GFP. Localisation of PIN2:GFP in roots of two independent transgenic *Arabidopsis* Col-0 lines were analysed three days after germination on DMSO or dexamethasone containing MS agar plates (triplicate experiments per line, utilising four to six seedlings per line and treatment). A: PIN2:GFP localises to the PM and few endosomes in DMSO control samples. B: In the presence of dominant negative RAB-A2a, PIN2:GFP exhibits prominent intracellular localisation, that ranges from clustered aggregates (1) to comparably even distribution (2). In 10% of analysed seedlings either BFA body like structures (3) or vacuolar like accumulations (4) were visible. Images are 3D projections. Scale bar = 5µm.

Bibliography

[1] Alberts, B., Bray, D., Johnson, A., Lewis, J., Raff, M., Roberts, K., and Walter, P. *Molecular Biology of the Cell.* Garland Science, (2002).

[2] Gupta, R. S. and Golding, G. B. The origin of the eukaryotic cell. *Trends Biochem. Sci.* **21**, 166–171 (1996).

[3] Martin, W. and Muller, M. The hydrogen hypothesis for the first eukaryote. *Nature* **392**, 37 – 41 (1998).

[4] Moreira, D. and Lopez-Garcia, P. Symbiosis between methanogenic archaea and delta-proteobacteria as the origin of eukaryotes: the syntrophic hypothesis. *J. Mol. Evol.* **47**, 517–530 (1998).

[5] Cavalier-Smith, T. The origin of nuclei and of eukaryotic cells. *Nature* **256**, 463 – 468 (1975).

[6] Cavalier-Smith, T. The origin of eukaryote and archaebacterial cells. *Ann. N. Y. Acad. Sci.* **503**, 17 – 54 (1987).

[7] Dacks, J., Peden, A., and Field, M. Evolution of specificity in the eukaryotic endomembrane system. *Int J Biochem Cell Biol.* **41**, 330 – 340 (2009).

[8] Cavalier-Smith, T. Eukaryotes with no mitochondria. *Nature* **326**, 332 – 333 (1987).

[9] Herskovits, A., Shimoni, E., Minsky, A., and Bibi, E. Accumulation of endoplasmic membranes and novel membrane-bound ribosome-signal recognition particle receptor complexes in *Escherichia coli*. *J. Cell Biol.* **159**, 403 – 410 (2002).

[10] Fuerst, J. Intracellular compartmentation in *planctomycetes*. *Annu. Rev. Microbiol.* **59**, 299 – 328 (2005).

[11] Bonifacino, J. and Lippincott-Schwartz, J. Coat proteins: shaping membrane transport. *Nat. Rev. Mol. Cell Biol.* **4**, 409 – 414 (2003).

[12] Barlowe, C. Molecular recognition of cargo by the COPII complex: a most accommodating coat. *Cell* **114**, 395 – 397 (2003).

[13] Sanderfoot, A. and Raikhel, N. The secretory system of Arabidopsis. In The *Arabidopsis* Book, eds. CR Somerville, EM Meyerowitz. *Am. Soc. Plant Biologists.* **1**, 24pp (2003).

[14] Boehm, M. and Bonifacino, J. Adaptins: the final recount. *Mol. Biol. Cell.* **12**, 2907 2920 (2001).

[15] Hadlington, J. and Denecke, J. Sorting of soluble proteins in the secretory pathway of plants. *Curr. Opin. Plant Biol.* **3**, 461 – 468 (2000).

[16] Matsuoka, K. and Neuhaus, J. Cis-elements of protein transport to the plant vacuoles. *J. Exp. Bot.* **50**, 165 – 174 (1999).

[17] Ahmed, S., Rojo, E., Kovaleva, V., Venkataraman, S., Dombrowski, J., Matsuoka, K., and Raikhel, N. V. The plant vacuolar sorting receptor AtELP is involved in transport of Nh_2-terminal propeptide-containing vacuolar proteins in *Arabidopsis thaliana. J. Cell Biol.* **149**, 1335 – 344 (2000).

[18] Shimada, T., Fuji, K., Tamura, K., Kondo, M., Nishimura, M., and Hara-Nishimura, I. Vacuolar sorting receptor for seed storage proteins in *Arabidopsis thaliana* . *Proc Natl Acad Sci U S A* **100**, 16095 – 16100 (2003).

[19] Sato, K., Ueda, T., and Nakano, A. The *Arabidopsis thaliana* RER1 gene family: its potential role in the endoplasmic reticulum localization of membrane proteins. *Plant Mol. Biol.* **41**, 815 – 824 (1999).

[20] Saint-Jore-Dupas, C., Gomord, V., and Paris, N. Protein localization in the plant Golgi apparatus and the trans-Golgi network. *Cell. Mol. Life Sci.* **61**, 159 – 171 (2004).

[21] Whyte, J. and Munro, S. Vesicle tethering complexes in membrane traffic. *J. Cell Sci.* **115**, 2627 – 2637 (2002).

[22] Jürgens, G. and Geldner, N. Protein secretion in plants: from the trans-Golgi network to the outer space. *Traffic* **3**, 605 – 613 (2002).

[23] Elias, M., Drdova, E., Ziak, D., Bavlnka, B., Hala, M., Cvrckova, F., Soukupova, H., and Zarsky, V. The exocyst complex in plants. *Cell Biol. Int.* **27**, 199 – 120 (2003.).

[24] Murshid, A. and Presley, J. ER-to-Golgi transport and cytoskeletal interactions in animal cells. *Cell. Mol. Life Sci.* **61**, 133 – 145 (2004).

[25] Takeuchi, M., Ueda, T., Yahara, N., and Nakano, A. Arf1 GTPase plays roles in the protein traffic between the endoplasmic reticulum and the Golgi apparatus in tobacco and *Arabidopsis* cultured cells. *Plant J.* **31**, 499 – 515 (2002).

[26] Sohn, E., Kim, E., Zhao, M., Kim, S., Kim, H., Lee, Y., Hillmer, S., Sohn, U., Jiang, L., and Hwang, I. Rha1, an *Arabidopsis* Rab5 homolog, plays a critical role in the vacuolar trafficking of soluble cargo proteins. *Plant Cell* **15**, 1057 – 1070 (2003).

[27] Park, M., Kim, S., Vitale, A., and Hwang, I. Identification of the protein storage vacuole and protein targeting to the vacuole in leaf cells of three plant species. *Plant Physiol.* **134**, 625 – 639 (2004).

[28] Saint-Jore, C., Evins, J., Batoko, H., Brandizzi, F., Moore, I., and Hawes, C. Redistribution of membrane proteins between the Golgi apparatus and endoplasmic reticulum in plants is reversible and not dependent on cytoskeletal networks. *Plant J.* **29**, 661 – 678 (2002).

[29] Pimpl, P., Movafeghi, A., Coughlan, S., Denecke, J., Hillmer, S., and Robinson, D. *In situ* localization and in vitro induction of plant COPI-coated vesicles. *Plant Cell* **12**, 2219 – 2236 (2000).

[30] Ritzenthaler, C., Nebenfuhr, A., Movafeghi, A., Stussi-Garaud, C., and Behnia, L. Reevaluation of the effects of brefeldin A on plant cells using tobacco Bright Yellow 2 cells expressing Golgi-targeted green fluorescent protein and COPI antisera. *Plant Cell* **14**, 237 – 261 (2002).

[31] Lee, M., Min, M., Lee, Y., Jin, J., Shin, D., Kim, D., Lee, K., and Hwang, I. ADP-ribosylation factor 1 of *Arabidopsis* plays a critical role in intracellular trafficking and maintenance of endoplasmic reticulum morphology in *Arabidopsis*. *Plant Physiol.* **129**, 1507 – 1520 (2002).

[32] Batoko, H., Zheng, H., Hawes, C., and Moore, I. A Rab1 GTPase is required for transport between the endoplasmic reticulum and Golgi apparatus and for normal Golgi movement

in plants. *Plant Cell* **12**, 2201 – 2218 (2000).

[33] Collins, N., Thordal-Christensen, H., Lipka, V., Bau, S., Kombrink, E., Qiu, J., Hueckelhoven, R., Stein, M., Freialdenhoven, A., Somerville, S., and Schulze-Lefert, P. SNARE-protein-mediated disease resistance at the plant cell wall. *Nature* **425**, 973 – 977 (2003).

[34] Leyman, B., Geelen, D., and Blatt, M. Localization and control of expression of Nt-Syr1, a tobacco SNARE protein. *Plant J.* **24**, 369 – 381 (2000).

[35] Nühse, T., Boller, T., and Peck, C. A plasma membrane syntaxin is phosphorylated in response to the bacterial elicitor flagellin. *J. Biol. Chem.* **278**, 45258 – 45254 (2003).

[36] Swarup, R., Friml, J., Marchant, A., Ljung, K., Sandberg, G., Palme, K., and Bennett, M. Localization of the auxin permease AUX1 suggests two functionally distinct hormone transport pathways operate in the *Arabidopsis* root apex. *Genes Dev.* **15**, 2648 – 2653 (2001).

[37] Geldner, N., Friml, J., Stierhof, Y., Jürgens, G., and Palme, K. Auxin transport inhibitors block PIN1 cycling and vesicle trafficking. *Nature* **413**, 425 – 428 (2001).

[38] Grebe, M., Xu, J., Mobius, W., Ueda, T., Nakano, A., Geuze, H., Rook, M., and Scheres, B. *Arabidopsis* sterol endocytosis involves actin-mediated trafficking via ARA6-positive early endosomes. *Curr. Biol.* **13**, 1378 – 13787 (2003).

[39] Matsuoka, K., Bassham, D., Raikhel, N., and Nakamura, K. Different sensitivity to wortmannin of two vacuolar sorting signals indicates the presence of distinct sorting machineries in tobacco cells. *J. Cell Biol.* **130**, 1307 – 1318 (1995).

[40] Sanderfoot, A., Ahmed, S., Marty-Mazars, D., Rapoport, I., and Kirchhausen, T. A putative vacuolar cargo receptor partially colocalizes with AtPEP12p on a prevacuolar compartment in *Arabidopsis* roots. *Proc Natl Acad Sci U S A* **95**, 9920 – 9925 (1998).

[41] Hohl, I., Robinson, D., Chrispeels, M., and Hinz, G. Transport of storage proteins to the vacuole is mediated by vesicles without a clathrin coat. *J. Cell Sci.* **109**, 2539 – 2550 (1996).

[42] Sanderfoot, A., Kovaleva, V., Bassham, D., and Raikhel, N. Interactions between syntaxins identify at least five SNARE complexes within the Golgi/prevacuolar system of the *Arabidopsis* cell. *Mol. Biol. Cell* **12**, 3733 – 3743 (2001).

[43] Dettmer, J., Hong-Hermesdorf, A., Stierhof, Y., and Schumacher, K. Vacuolar H+-ATPase activity is required for endocytic and secretory trafficking in *Arabidopsis* . *Plant Cell* **18**, 715 – 730 (2006).

[44] Viotti, C., Bubeck, J., Stierhof, Y., Krebs, M., Langhans, M., van den Berg, W., van Dongen, W., Richter, S., Geldner, N., Takano, J., Jürgens, G., de Vries, S., Robinson, D., and Schumacher, K. Endocytic and secretory traffic in *Arabidopsis* merge in the trans-Golgi network/early endosome, an independent and highly dynamic organelle. *Plant Cell.* **22**, 1344 – 1357 (2010).

[45] Chow, C.-M., Neto, H., Foucart, C., and Moore, I. Rab-A2 and Rab-A3 GTPases define a trans-golgi endosomal membrane domain in *Arabidopsis* that contributes substantially to the cell plate. *Plant Cell* **20**, 101–1–23 (2008).

[46] Otegui, M., Herder, R., Schulze, J., Jung, R., and Staehelin, L. The proteolytic processing of seed storage proteins in *Arabidopsis* embryo cells starts in the multivesicular bodies. *Plant Cell* **18**, 2567 – 2581 (2006).

[47] Richter, S., Voß, U., and Jürgens, G. Post-Golgi traffic in plants. *Traffic* **10**, 819 – 828 (2009).

[48] Robinson, D. G., Jiang, L., and Schumacher, K. The Endosomal System of Plants: Charting New and Familiar Territories. *Plant Physiol* **147**, 1482 – 1492 (2008).

[49] Cram, W. Pinocytosis in plants. *New Phytol* **84**, 1 – 17 (1980).

[50] Hillmer, S., Depta, H., and Robinson, D. Confirmation of endocytosis in higher-plant protoplasts using lectin-gold conjugates. *Eur J Cell Biol* **41**, 142 – 149 (1986).

[51] Baluska, F., Samaj, J., Hlavacka, A., Kendrick-Jones, J., and Volkmann, D. Actin-dependent fluid-phase endocytosis in inner cortex cells of maize root apices. *J Exp Bot* **55**, 463 – 473 (2004).

[52] Emans, N., Zimmermann, S., and Fischer, R. Uptake of a fluorescent marker in plant cells is sensitive to brefeldin A and wortmannin. *Plant Cell* **14**, 71 – 86 (2002).

[53] Tse, Y., Mo, B., Hillmer, S., Zhao, M., Lo, S., Robinson, D., and Jiang, L. Identification of multivesicular bodies as prevacuolar compartments in *Nicotiana tabacum* BY-2 cells. *Plant Cell* **16**, 672 – 693 (2004).

[54] Kinoshita, T., Cao-Delgado, A., Seto, H., Hiranuma, S., Fujioka, S., Yoshida, S., and Chory, J. Binding of brassinosteroids to the extracellular domain of plant receptor kinase BRI1. *Nature* **433**, 167 – 171 (2005).

[55] Russinova, E., Borst, J., Kwaaitaal, M., Cao-Delgado, A., Yin, Y., Chory, J., and de Vries, S. Heterodimerization and endocytosis of *Arabidopsis* brassinosteroid receptors BRI1 and AtSERK3 (BAK1). *Plant Cell* **16**, 3216 – 3229 (2004).

[56] Chinchilla, D., Bauer, Z., Regenass, M., Boller, T., and Felix, G. The *Arabidopsis* receptor kinase FLS2 binds flg22 and determines the specificity of flagellin perception. *Plant Cell* **18**, 465 – 476 (2006).

[57] Chinchilla, D., Zipfel, C., Robatzek, S., Kemmerling, B., Nurnberger, T., Jones, J., Felix, G., and Boller, T. A flagellin-induced complex of the receptor FLS2 and BAK1 initiates plant defence. *Nature* **448**, 487 – 500 (2007).

[58] Geldner, N., Hyman, D. L., Wang, X., Schumacher, K., and Chory, J. Endosomal signaling of plant steroid receptor kinase BRI1. *Genes & Dev.* **21**, 1598 – 1602 (2007).

[59] Robatzek, S., Chinchilla, D., and Boller, T. Ligand-induced endocytosis of the pattern recognition receptor FLS2 in *Arabidopsis*. *Genes and Development* **20**, 537 – 542 (2006).

[60] Wang, X., Kota, U., He, K., Blackburn, K., Li, J., Goshe, M., Huber, S., and Clouse, S. Sequential transphosphorylation of the BRI1/BAK1 receptor kinase complex impacts early events in brassinosteroid signaling. *Dev Cell* **15**, 220 – 235 (2008).

[61] Staehelin, L. and Hepler, P. Cytokinesis in higher plants. *Cell* **84**, 821 – 824 (1996).

[62] Otegui, M., Mastronarde, D., Kang, B., Bednarek, S., and Staehelin, L. Three-dimensional analysis of syncytial-type cell plates during endosperm cellularization visualized by high resolution electron tomography. *Plant Cell* **13**, 2033 – 2051 (2001).

[63] Samuels, A., Giddings, T., and Staehelin, L. Cytokinesis in tobacco BY-2 and root tip cells: a new model of cell plate formation in higher plants. *J. Cell Biol.* **130**, 1345 – 1357 (1995).

[64] Cutler, S. and Ehrhardt, D. Polarized cytokinesis in vacuolate cells of *Arabidopsis*. *Proc Natl Acad Sci U S A* **99**, 2812 – 2817 (2002).

[65] Steinmann, T., Geldner, N., Grebe, M., Mangold, S., Jackson, C., Paris, S., Gälweiler, L., Palme, K., and Jürgens, G. Coordinated polar localization of auxin efflux carrier PIN1 by GNOM ARF GEF. *Science* **286**, 316 – 318 (1999).

[66] Zuo, J., Niu, Q., Nishizawa, N., Wu, Y., Kost, B., and Chua, N. KORRIGAN, an *Arabidopsis* endo-1,4-beta-glucanase, localizes to the cell plate by polarized targeting and is essential for cytokinesis. *Plant Cell* **12**, 1137 – 1152 (2000).

[67] Lauber, M., Waizenegger, I., Steinmann, T., Schwarz, H., Mayer, U., and et al. The *Arabidopsis* KNOLLE protein is a cytokinesis-specific syntaxin. *J. Cell Biol.* **139**, 1485 – 1493 (1997).

[68] Waizenegger, I., Lukowitz, W., Assaad, F., Schwarz, H., Jürgens, G., and Mayer, U. The *Arabidopsis* KNOLLE and KEULE genes interact to promote vesicle fusion during cytokinesis. *Curr. Biol.* **10**, 1371 – 1374 (2000).

[69] Assaad, F., Huet, Y., Mayer, U., and Jürgens, G. The cytokinesis gene KEULE encodes a Sec1 protein that binds the syntaxin KNOLLE. *J. Cell Biol.* **152**, 531 – 543 (2001).

[70] Went, F. On growth accelerating substances in the coleoptile of *Avena sativa*. *Proc K Akad Wet Amsterdam* **30**, 10 – 19 (1926).

[71] Petrasek, J., Mravec, J., Bouchard, R., Blakeslee, J. J., Abas, M., Seifertova, D., Wisniewska, J., Tadele, Z., Kubes, M., Covanova, M., Dhonukshe, P., Skup, P., Benkova, E., Perry, L., Krecek, P., Lee, O. R., Fink, G. R., Geisler, M., Murphy, A. S., Luschnig, C., Zazimalova, E., and Friml, J. PIN Proteins Perform a Rate-Limiting Function in Cellular Auxin Efflux. *Science* **312**, 914 – 918 (2006).

[72] Chen, R., Hilson, P., Sedbrook, J., Rosen, E., Caspar, T., and Masson, P. The *Arabidopsis thaliana* AGRAVITROPIC1 gene encodes a component of the polar-auxin-transport efflux carrier. *Proc Natl Acad Sci U S A* **95**, 15112 – 15117 (1998).

[73] Luschnig, C., Gaxiola, R. A., Grisafi, P., and Fink, G. R. EIR1, a root-specific protein involved in auxin transport, is required for gravitropism in *Arabidopsis thaliana* . *Genes and Development* **12**, 2175–2187 (1998).

[74] Müller, A., Guan, C., Gälweiler, L., Tänzler, P., Huijser, P., Marchant, A., Parry, G., Bennett, M., Wisman, E., and Palme, K. AtPIN2 defines a locus of *Arabidopsis* for root gravitropism control. *EMBO Journal* **17**, 6903 – 6911 (1998).

[75] Utsuno, K., Shikanai, T., Yamada, Y., and Hashimoto, T. AGR, an Agravitropic locus of *Arabidopsis thaliana,* encodes a novel membrane-protein family member. *Plant Cell Physiol* **39**, 1111 – 1118 (1998).

[76] Friml, J., Wisniewska, J., Benkova, E., Mendgen, K., and Palme, K. Lateral relocation of auxin efflux regulator PIN3 mediates tropism in *Arabidopsis*. *Nature* **415**, 806 – 809 (2002).

[77] Friml, J., Vieten, A., Sauer, M., Weijers, D., Schwarz, H., andR Offringa, T. H., and Jürgens, G. Efflux-dependent auxin gradients establish the apical- basal axis of *Arabidopsis*. *Nature* **426**, 147 – 153 (2003).

[78] Benkova, E., Michniewicz, M., Sauer, M., Teichmann, T., Seifertova, D., Jürgens, G., and Friml, J. Local, efflux-dependent auxin gradients as a common module for plant organ formation. *Cell* **115**, 591 – 602 (2003).

[79] Reinhardt, D., Pesce, E., Stieger, P., Mandel, T., Baltensperger, K., Bennett, M., Traas, J., Friml, J., and Kuhlemeier, C. Regulation of phyllotaxis by polar auxin transport. *Nature* **426**, 255 – 260 (2003).

[80] Friml, J., , E. B., Blilou, I., Wisniewska, J., Hamann, T., Ljung, K., Woody, S., Sandberg, G., Scheres, B., Jürgens, G., and Palme, K. AtPIN4 mediates sink driven auxin gradients and root patterning in *Arabidopsis*. *Cell* **108**, 661 – 673 (2002).

[81] Blilou, I., Xu, J., Wildwater, M., Willemsen, V., Paponov, I., Friml, J., Heidstra, R., Aida, M., Palme, K., and Scheres, B. The PIN auxin efflux facilitator network controls growth and patterning in *Arabidopsis* roots. *Nature* **433**, 39 – 44 (2005).

[82] Sauer, M., Balla, J., Luschnig, C., Wisniewska, J., Reinohl, V., Friml, J., and Benkova, E. Canalization of auxin flow by Aux/IAA-ARF-dependent feed- back regulation of PIN polarity. *Genes Dev* **20**, 2902 – 2911 (2006).

[83] Scarpella, E., Marcos, D., Friml, J., and Berleth, T. Control of leaf vascular patterning by polar auxin transport. *Genes Dev* **20**, 1015 – 1027 (2006).

[84] Vieten, A., Sauer, M., Brewer, P., and Friml, J. Molecular and cellular aspects of auxin-transport-mediated development. *Trends Plant Sci* **12**, 150 – 168 (2007).

[85] Dhonukshe, P., Tanaka, H., Goh, T., Ebine, K., Mähönen, A. P., Prasad, K., Blilou, I., Geldner, N., Xu, J., Uemura, T., Chory, J., Ueda, T., Nakano, A., Scheres, B., and

Friml, J. Generation of cell polarity in plants links endocytosis, auxin distribution and cell fate decisions. *Nature* **456**, 962–966 (2008).

[86] Anders, N. and Jürgens, G. Large ARF guanine nucleotide exchange factors in membrane trafficking. *Cell. Mol. Life Sci.* **65**, 3433 – 3445 (2008).

[87] Robinson, D. G., Langhans, M., Saint-Jore-Dupas, C., and Hawes, C. BFA effects are tissue and not just plant specific. *Trends Plant Sci* **13**, 405 – 408 (2008).

[88] Langhans, M., Foerster, S., Helmchen, G., and Robinson, D. G. Differential effects of the brefeldin A analogue (6R)-hydroxy-BFA in tobacco and *Arabidopsis* . *J Exp Bot* **62**, 2949 – 2957 (2011).

[89] Geldner, N., Anders, N., Wolters, H., Keicher, J., Kornberger, W., Muller, P., Delbarre, A., Ueda, T., and Jürgens, G. The *Arabidopsis* GNOM ARF-GEF Mediates Endosomal Recycling, Auxin Transport, and Auxin-Dependent Plant Growth. *Cell* **112**, 219 – 230 (2003).

[90] Kleine-Vehn, J., Dhonukshe, P., Sauer, M., Brewer, P. B., Wiśniewska, J., Paciorek, T., Benkova, E., and Friml, J. ARF GEF-Dependent Transcytosis and Polar Delivery of PIN Auxin Carriers in *Arabidopsis*. *Current Biology* **16**, 526 – 531 (2008).

[91] Nielsen, M. E., Freechan, A., Boehlenius, H., Ueda, T., and Thordal-Christensen, H. *Arabidopsis* ARF-GEF exchange factor, GNOM, mediates transport required for innate immunity and focal accumulation of syntaxin PEN1. *Proc Natl Acad Sci U S A* **109**, 11443 – 11448 (2012).

[92] Kleine-Vehn, J., Łangowski, Ł., Wiśniewska, J., Dhonukshe, P., Brewer, P. B., and Friml, J. Cellular and Molecular Requirements for Polar PIN Targeting and Transcytosis in Plants. *Molecular Plant* **1**, 1056–1066 (2008).

[93] Harrison, B. and Masson, P. ARL2, ARG1 and PIN3 define a gravity signal transduction pathway in root statocytes. *Plant J* **53**, 380 – 392 (2008).

[94] Rodriguez-Boulan, E., Kreitzer, G., and Müsch, A. Organization of vesicular trafficking in epithelia. *Nat Rev Mol Cell Biol* **6**, 233 – 247 (2005).

[95] Leibfried, A. and Bellache, Y. Functions of endosomal trafficking in Drosophila epithelial cells. *Curr Opin Cell Biol* **19**, 446 – 452 (2007).

[96] Dhonukshe, P., Baluska, F., Schlicht, M., Hlavacka, A., Samaj, J., Friml, J., and Gadella, T. Endocytosis of cell surface material mediates cell plate formation during plant cytokinesis. *Dev Cell* **10**, 137 – 150 (2006).

[97] Milburn, M., Tong, L., DeVos, M., Brunger, A., Yamaizumi, Z., Nishimura, S., and Kim, S.-H. Molecular switch for signal transduction: structural differences between active and inactive forms of protooncogenic ras proteins. *Science* **247**, 939 – 945 (1990).

[98] Chattopadhyay, D., Langsley, G., Carson, M., Recacha, R., DeLucas, L., and Smith, C. Structure of the nucleotide-binding domain of *Plasmodium falciparum* Rab6 in the GDP-bound form. *Acta Crystallogr* **D56**, 937 – 944 (2000).

[99] Schlichting, I., Almo, S., Rapp, G., Wilson, K., Petratos, K., Lentfer, A., Wittinghofer, A., Kabsch, W., Pai, E., Petsko, G., and Goody, R. Time-resolved X-ray crystallographic study of the conformational change in Ha-Ras p21 protein on GTP hydrolysis. *Nature* **345**, 309 – 315 (1990).

[100] Esters, H., Alexandrov, K., Constantinescu, A.-T., Goody, R., and Scheidig, A. High-resolution crystal structure of *S. cerevisiae* Ypt51(DC15)-GppNHp, a small GTP-binding protein involved in the regulation of endocytosis. *J Mol Biol* **298**, 111 – 121 (2000).

[101] Bourne, H., Sanders, D., and McCormick, F. The GTPase superfamily: conserved structure and molecular mechanism. *Nature* **349**, 117 – 127 (1991).

[102] Chavrier, P., Gorbel, J., Stelzer, E., Simons, K., Gruenberg, J., and Zerial, M. Hypervariable C-termmal domain of rab proteins acts as a targeting signal. *Nature* **353**, 769 – 772 (1991).

[103] Magee, M. and Seabra, M. Are prenyl groups on proteins sticky fingers or greasy handles? *Biochem J* **376**, e3 – e4 (2003).

[104] Dumas, J., Zhu, Z., Connolly, J., and Lambright, D. Structural basis of activation and GTP hydrolysis in Rab proteins. *Structure* **7**, 413 – 423 (1998).

[105] Hala, M., Elias, M., and Zarsky, V. A specific feature of the Angiosperm Rab Escort Protein (REP) and Evolution of the REP/GDI Superfamily. *J. Mol. Biol.* **348**, 1299 – 1313 (2005).

[106] Olkkonen, V. and Stenmark, H. Role of Rab GTPases in membrane traffic. *Int Rev Cytol* **176**, 1 – 85 (1997).

[107] Figueroa, C., Taylor, J., and Vojtek, A. Prenylated Rab acceptor protein is a receptor for prenylated small GTPases. *J Biol Chem.* **276**, 28219 – 28225 (2001).

[108] Hutt, D., Da-Silva, L., Chang, L., Prosser, D., and Ngsee, J. PRA1 inhibits the extraction of membrane-bound rab GTPase by GDI1. *J Biol Chem.* **275**, 18511– 18519 (2000).

[109] Huang, Z., Andrianov, V., Han, Y., and Howell, S. Identification of *Arabidopsis* proteins that interact with the cauliflower mosaic virus (CaMV) movement protein. *Plant Mol Biol.* **47**, 663 – 675 (2001).

[110] Kamei, C., Boruc, J., Vandepoele, K., den Daele, H. V., Maes, S., Russinova, E., Inze, D., and Veylder, L. D. The PRA1 gene family in *Arabidopsis*. *Plant Physiol.* **1**, 1 (2008).

[111] Rutherford, S. and Moore, I. The *Arabidopsis* Rab GTPase family: another enigma variation. *Curr Opin Plant Biol* **5**, 518 – 528 (2002).

[112] Pereira-Leal, J. and Seabra, M. Evolution of the Rab family of small GTP-binding proteins. *J Mol Biol* **213**, 889 – 901 (2001).

[113] Vernoud, V., Horton, A., Yang, Z., and Nielsen, E. Analysis of the small GTPase gene superfamily of *Arabidopsis*. *Plant Physiol* **131**, 1191 –1208 (2003).

[114] Bock, J., Matern, H., Peden, A., and Scheller, R. A genomic perspective on membrane compartment organization. *Nature* **409**, 839 – 841 (2001).

[115] Woollard, A. A. D. and Moore, I. The functions of Rab GTPases in plant membrane traffic. *Current Opinion in Plant Biology* **11**, 610 – 619 (2008).

[116] Wang, Y., Ng, E., and Tang, B. Rab23: what exactly does it traffic? *Traffic* **7**, 746 – 750 (2006).

[117] Moore, I., Schell, J., and Palme, K. Subclass-specific sequence motifs identified in Rab GTPases. *Trends Biochem Sci* **20**, 10 – 12 (1995).

[118] Koh, E., Kwon, Y., Kim, K., Hong, S., and Lee, H. Altered ARA2 (RABA1a) expression in *Arabidopsis* reveals the involvement of a Rab/YPT family member in auxin-mediated responses. *Plant Mol Biol.* **70**, 113 – 122 (2009).

[119] Feraru, E., Feraru, M. I., Asaoka, R., Paciorek, T., Rycke, R. D., Tanaka, H., Nakano, A., and Friml, J. BEX5/RabA1b Regulates trans-Golgi Network-to-Plasma Membrane Protein Trafficking in *Arabidopsis*. *The Plant Cell* **24**, 3072 – 3086 (2012).

[120] Qi, X. and Zheng, H. *Arabidopsis* TRAPPII is functionally linked to Rab-A, but not Rab-D in polar protein trafficking in trans-Golgi network. *Plant Signal Behav.* **6**, 1679 –1683 (2011).

[121] Preuss, M., Schmitz, A., Thole, J., Bonner, H., Otegui, M., and Nielsen, E. A role for the RabA4b effector protein PI-4Kβ1 in polarized expansion of root hair cells in *Arabidopsis thaliana*. *J Cell Biol* **172**, 991 – 998 (2006).

[122] Thole, J., Vermeer, J., Zhang, Y., Gadella, T., and Nielsen, E. ROOT HAIR DEFECTIVE4 Encodes a Phosphatidylinositol-4-Phosphate Phosphatase Required for Proper Root Hair Development in *Arabidopsis thaliana*. *The Plant Cell* **20**, 381 – 395 (2008).

[123] Allen, A., Snyder, A., Preuss, M., Nielsen, E., Shah, D., and Smith, T. Plant defensins and virally encoded fungal toxin KP4 inhibit plant root growth. *Planta* **227**, 331– 339 (2008).

[124] Reichardt, I., Stierhof, Y.-D., Mayer, U., Richter, S., Schwarz, H., Schumacher, K., and Jürgens, G. Plant Cytokinesis Requires De Novo Secretory Trafficking but Not Endocytosis. *Current Biology* **17**, 2047 – 2053 (2007).

[125] van Ijzendoorn, S. Recycling endosomes. *J Cell Sci* **119**, 1679 – 1681 (2006).

[126] Pelham, H. Insights from yeast endosomes. *Curr Opin Cell Biol* **14**, 454 – 462 (2002).

[127] Chen, S., Chen, S., Tokarev, A., Liu, F., Jedd, G., and Segev, N. Ypt31/32 GTPases and their novel F-box effector protein Rcy1 regulate protein recycling. *Mol Biol Cell* **16**, 178 – 192 (2005).

[128] Ortiz, D. and Novick, P. Ypt32p regulates the translocation of Chs3p from an internal pool to the plasma membrane. *Eur J Cell Biol* **85**, 107 –116 (2006).

[129] Prescianotto-Baschong, C. and Riezman, H. Ordering of compartments in the yeast endocytic pathway. *Traffic* **3**, 37 – 49 (2002).

[130] Kane, P. The where, when, and how of organelle acidification by yeast vacuolar H+-ATPase. *Microbiol Mol Biol Rev* **70**, 177 – 191 (2006).

[131] Moore, I., Diefenthal, T., Zarsky, V., Schell, J., and Palme, K. A homolog of the mammalian GTPase Rab2 is present in *Arabidopsis* and is expressed predominantly in pollen grains and seedlings. *Proc Natl Acad Sci U S A* **94**, 762 – 767 (1997).

[132] Cheung, A., Chen, C., Glaven, R., de Graaf, B., Vidali, L., Hepler, P., and Wu, H. Rab2 GTPase regulates vesicle trafficking between the endoplasmic reticulum and the Golgi bodies and is important to pollen tube growth. *Plant Cell* **14**, 945 – 962 (2002).

[133] Jakab, G., Ton, J., Flors, V., Zimmerli, L., Metraux, J., and Mauch-Mani, B. Enhancing *Arabidopsis* salt and drought stress tolerance by chemical priming for its abscisic acid responses. *Plant Physiol.* **139**, epub (2005).

[134] Reyes, D., Rodrguez, D., Gonzlez-Garca, M., Lorenzo, O., Nicols, G., Garca-Martnez, J., and Nicols, C. Overexpression of a protein phosphatase 2C from beech seeds in *Arabidopsis* shows phenotypes related to abscisic acid responses and gibberellin biosynthesis. *Plant Physiol.* **141**, 1414 – 1424 (2006).

[135] Dejgaard, S., Murshid, A., Erman, A., Kizilay, O., Verbich, D., Lodge, R., Dejgaard, K., Ly-Hartig, T., Pepperkok, R., Simpson, J., and Presley, J. Rab18 and Rab43 have key roles in ER-Golgi trafficking. *J Cell Sci.* **121**, 2768 – 2781 (2008).

[136] Hwang, H. and Gelvin, S. Plant proteins that interact with VirB2, the *Agrobacterium tumefaciens* pilin protein, mediate plant transformation. *Plant Cell.* **16**, 3148 – 3167 (2004).

[137] Zheng, H., Camacho, L., Wee, E., Batoko, H., Legen, J., Leaver, C., Malh, R., Hussey, P., and Moore, I. A Rab-E GTPase mutant acts downstream of the Rab-D subclass in biosynthetic membrane traffic to the plasma membrane in tobacco leaf epidermis. *Plant Cell* **17**, 2020 – 2036 (2005).

[138] Camacho, L., Smertenko, A., Prez-Gmez, J., Hussey, P., and Moore, I. *Arabidopsis* Rab-E GTPases exhibit a novel interaction with a plasma-membrane phosphatidylinositol-4-phosphate 5-kinase. *J Cell Sci* **122**, 4383 – 4392 (2009).

[139] Lee, G., Sohn, E., Lee, M., and Hwang, I. The *Arabidopsis* rab5 homologs rha1 and ara7 localize to the prevacuolar compartment. *Plant Cell Physiol* **45**, 1211 – 1220 (2004).

[140] Ueda, T., Uemura, T., Sato, M., and Nakano, A. Functional differentiation of endosomes in *Arabidopsis* cells. *Plant J* **40**, 783 – 789 (2004).

[141] Goh, T., Uchida, W., Arakawa, S., Ito, E., Dainobu, T., Ebine, K., Takeuchi, M., Sato, K., Ueda, T., and Nakano, A. VPS9a, the common activator for two distinct types of

Rab5 GTPases, is essential for the development of *Arabidopsis thaliana*. *Plant Cell* **19**, 3504– 3515 (2007).

[142] Ortiz-Zapater, E., Soriano-Ortega, E., Marcote, M., Ortiz-Masi, D., and Aniento, F. Trafficking of the human transferrin receptor in plant cells: effects of tyrphostin A23 and brefeldin A. *Plant J.* **48**, 757 – 770 (2006).

[143] Haas, T., Sliwinski, M., Martinez, D., Preuss, M., Ebine, K., Ueda, T., Nielsen, E., Odorizzi, G., and Otegui, M. The *Arabidopsis* AAA ATPase SKD1 is involved in multivesicular endosome function and interacts with its positive regulator LYST-INTERACTING PROTEIN5. *Plant Cell* **19**, 1295 – 1312 (2007).

[144] Takano, J., Miwa, K., Yuan, L., von Wiren, N., and Fujiwara, T. Endocytosis and degradation of BOR1, a boron transporter of *Arabidopsis thaliana*,regulated by boron availability. *Proc Natl Acad Sci U S A* **102**, 12276 – 12281 (2005).

[145] Jallais, Y., Fobis-Loisy, I., Miege, C., Rollin, C., and Gaude, T. AtSNX1 defines an endosome for auxin-carrier trafficking in *Arabidopsis*. *Nature* **443**, 106–109 (2006).

[146] Kotzer, A., Brandizzi, F., Neumann, U., Paris, N., Moore, I., and Hawes, C. AtRabF2b (Ara7) acts on the vacuolar trafficking pathway in tobacco leaf epidermal cells. *J Cell Sci* **117**, 6377 –6389 (2004).

[147] Mazel, A., Leshem, Y., Tiwari, B., and Levine, A. Induction of salt and osmotic stress tolerance by overexpression of an intracellular vesicle trafficking protein AtRab7 (AtRabG3e). *Plant Physiol* **134**, 118 – 128 (2004).

[148] Nahm, M., Kim, S., Yun, D., Lee, S., Cho, M., and Bahk, J. Molecular and biochemical analyses of OsRab7, a rice Rab7 homolog. *Plant Cell Physiol* **44**, 1341 – 1349 (2003).

[149] Schimmller, F. and Riezman, H. Involvement of Ypt7p, a small GTPase, in traffic from late endosome to the vacuole in yeast. *J Cell Sci* **106**, 823 – 830 (1993).

[150] Geldner, N., Dnervaud-Tendon, V., Hyman, D., Mayer, U., Stierhof, Y., and Chory, J. Rapid, combinatorial analysis of membrane compartments in intact plants with a multicolor marker set. *Plant J.* **59**, 169 – 178 (2009).

[151] Bednarek, S., Reynolds, T., Schroeder, M., Grabowski, R., Hengst, L., Gallwitz, D., and Raikhel, N. A small GTP-binding protein from *Arabidopsis thaliana* functionally complements the yeast YPT6 null mutant. *Plant Physiol* **104**, 591 – 596 (1994).

[152] Johansen, J., Chow, C., Moore, I., and Hawes, C. AtRAB-H1b and AtRAB-H1c GTPases, homologues of the yeast Ypt6, target reporter proteins to the Golgi when expressed in *Nicotiana tabacum* and *Arabidopsis thaliana*. *J Exp Bot* **60**, 3179 – 3193 (2009).

[153] Latijnhouwers, M., Gillespie, T., Boevink, P., Kriechbaumer, V., Hawes, C., and Carvalho, C. Localization and domain characterization of *Arabidopsis* golgin candidates. *J Exp Bot.* **58**, 4373 – 4386 (2007).

[154] Davenport, D. and Nicol, J. Luminescence in Hydromedusae. *Proc. R. Soc. Lond. B* **144**, 399 – 411 (1955).

[155] Shimomura, O., Johnson, F., and Saiga, Y. Extraction, purification and properties of aequorin, a bioluminescent protein from the luminous hydromedusae, *Aequorea*. *J Cell Comp Physiol.* **59**, 223 – 239 (1962).

[156] Kishi, Y., Goto, T., Hirata, Y., Shimomura, O., and Johnson, F. Cypridina bioluminescence I: structure of Cypridina luciferin. *Tetrahedron Lett* **1**, 3427 – 3436 (1966).

[157] Morin, J. and Hastings, J. Energy transfer in a bioluminescent system. *J Cell Physiol* **77**, 313–318 (1971).

[158] Morise, H., Shimomura, O., Johnson, F., and Winant, J. Intermolecular energy transfer in the bioluminecent system of *Aequorea*. *Biochemistry* **13**, 2656 – 2562 (1974).

[159] Shimomura, O. Structure of the chromophore of *Aequorea* green fluorescent protein. *FEBS Letters* **104**, 220 – 222 (1979).

[160] Cody, C., Prasher, D., Westler, W., Prendergast, F., and Ward, W. Chemical structure of the hexapeptide chromophore of the *Aequorea* green fluorescent protein. *Biochemistry* **32**, 1212 – 1218 (1993).

[161] Prasher, D., Eckenrode, V., Ward, W., Prendergast, F., and Cormier, M. Primary structure of the *Aequorea victoria* green-fluorescent protein. *Gene* **111**, 229 – 233 (1992).

[162] Chalfie, M., Tu, Y., Euskirchen, G., Ward, W., and Prasher, D. Green fluorescent protein as a marker for gene expression. *Science* **263**, 802 – 805 (1994).

[163] Baulcombe, D., Chapman, S., and Cruz, S. S. Jellyfish green fluorescent protein as a reporter for virus infections. *Plant J* **7**, 1045 –1053 (1995).

[164] Boevink, P., Cruz, S. S., Hawes, C., Harris, N., and Oparka, K. Virus-mediated delivery of the green fluorescent protein to the endoplasmic reticulum of plant cells. *Plant J* **10**, 935 – 941 (1996).

[165] Haseloff, J., Siemering, K. R., Prasherand, D. C., and Hodge, S. Removal of a cryptic intron and subcellular localization of green fluorescent protein are required to mark transgenic *Arabidopsis* plants brightly. *Proc Natl Acad Sci U S A* **94**, 2122 – 2127 (1997).

[166] Boevink, P., Oparka, K., Cruz, S. S., Martin, B., Betteridge, A., and Hawes, C. Stacks on tracks: the plant Golgi apparatus traffics on an actin/ER network. *Plant J* **15**, 441–447 (1998).

[167] Boevink, P., Martin, B., Oparka, K., Cruz, S., and Hawes, C. Transport of virally expressed green flourescent protein through the secretory pathway in tobacco leaves is inhibited by cold shock and brefeldin A. *Planta* **208**, 392 – 400 (1999).

[168] Cutler, S., Ehrhardt, D., Griffitts, J., and Somerville, C. Random GFP: cDNA fusions enable visualization of subcellular structures in cells of *Arabidopsis* at a high frequency. *Proc Natl Acad Sci U S A* **28**, 3718 – 3723 (2000).

[169] Saito, C., Ueda, T., Abe, H., Wadaand, Y., Kuroiwa, T., Hisada, A., Furuya, M., and Nakano, A. A complex and mobile structure forms a distinct subregion within the continuous vacuolar membrane in young cotyle- dons of *Arabidopsis*. *Plant J.* **29**, 245 – 255 (2002).

[170] Brandizzi, F., Frangne, N., Marc-Martin, S., Hawes, C., Neuhaus, J., and Paris, N. The destination for single-pass membrane proteins is influenced markedly by the length of the hydrophobic domain. *Plant Cell* **14**, 1077 – 1092 (2002).

[171] Saito, K., Murai, J., Kajiho, H., Kontani, K., Kurosu, H., and Katada, T. A novel binding protein composed of homophilic tetramer exhibits unique properties for the small GTPase Rab5. *J Biol Chem* **277**, 3412– 3418 (2002).

[172] Nagy, A., Malnasi-Csizmadia, A., Somogyi, B., and Lorinczy, D. Thermal stability of chemically denatured green fluorescent protein (GFP) - A preliminary study. *Thermochimica Acta* **410**, 161 – 163 (2004).

[173] Penna, T., Ishii, M., Junior, A., and Cholewa, O. Thermal stability of recombinant green fluorescent protein (GFPuv) at various pH values. *Appl Biochem Biotechnol. 2004*

Spring;113-116:469-83. **113 - 116**, 469 – 483 (2004).

[174] Matz, M., Fradkov, A., Labas, Y., Savitsky, A., Zaraisky, A., Markelov, M., and Lukyanov, S. Fluorescent proteins from nonbioluminescent anthozoa species. *Nat Biotechnol.* **17**, 969 – 973 (1999).

[175] Shaner, N., Campbell, R., Steinbach, P., Giepmans, B., Palmer, A., and Tsien, R. Improved monomeric red, orange and yellow fluorescent proteins derived from Discosoma sp. red fluorescent protein. *Nat Biotechnol.* **22**, 1567 – 1572 (2004).

[176] Shaner, N., Lin, M., McKeown, M., Steinbach, P., Hazelwood, K., Davidson, M., and Tsien, R. Improving the photostability of bright monomeric orange and red fluorescent proteins. *Nat Methods* **5**, 545 – 551 (2008).

[177] Shcherbo, D., Murphy, C., Ermakova, G., Solovieva, E., Chepurnykh, T., Shcheglov, A., Verkhusha, V., Pletnev, V., Hazelwood, K., Roche, P., Lukyanov, S., Zaraisky, A., Davidson, M., and Chudakov, D. Far-red fluorescent tags for protein imaging in living tissues. *Biochem J.* **418**, 567 – 574 (2009).

[178] Magliery, T., Wilsonand, C., Pan, W., Mishler, D., Ghosh, I., Hamilton, A., and Regan, L. Detecting protein-protein interactions with a green fluorescent protein fragment reassembly trap: scope and mechanism. *J Am Chem Soc.* **127**, 146 – 157 (2005).

[179] Bracha-Drori, K., Shichrur, K., Katz, A., Oliva, M., Angelovici, R., Yalovsky, S., and Ohad, N. Detection of protein-protein interactions in plants using bimolecular fluorescence complementation. *Plant J* **40**, 419 – 427 (2004).

[180] Kneen, M., Farinas, J., Li, Y., and Verkman, A. Green fluorescent protein as a noninvasive intracellular pH indicator. *Biophys J.* **74**, 1591 –1599 (1998).

[181] Ben, N., Giepmans, R., Adams, M., Ellisman, R., and Tsien. The fluorescent toolbox for assessing protein location and function. *Science* **312**, 217 – 224 (2006).

[182] Murashige, T. and Skoog, F. A revised medium for rapid growth and bioassays with tobacco tissue cultures. *Physiol Plant* **15**, 473 – 497 (1962).

[183] Hanahan, D. Studies on transformation of *Escherichia coli* with plasmids. *J Mol Biol* **166**, 557 – 580 (1983).

[184] Koncz, C. and Schell, J. The promoter of TL-DNA gene 5 controls the tissue-specific expression of chimeric genes carried by a novel type of *Agrobacterium* binary vector. *Mol Gen Genet* **204**, 383 – 395 (1986).

[185] Clough, S. and Bent, A. Floral dip: a simplified method for *Agrobacterium*-mediated transformation of *Arabidopsis thaliana*. *Plant J* **16**, 735 – 743 (1998).

[186] Birnboim, H. and Doly, J. A rapid alkaline extraction procedure for screening recombinant plasmid DNA. *Nucleid Acid Res.* **7**, 1513 – 1523 (1979).

[187] Jallais, Y. and Gaude, T. Sorting out the sorting functions of endosomes in *Arabidopsis*. *Plant Signal Behav.* **2**, 556–558 (2007).

[188] Dhonukshe, P., Aniento, F., Hwang, I., Robinson, D. G., Mravec, J., Stierhof, Y.-D., and Friml, J. Clathrin-Mediated Constitutive Endocytosis of PIN Auxin Efflux Carriers in *Arabidopsis*. *Current Biology* **17**, 520–527 (2007).

[189] Chow, C. *Specialisation of Arabidopsis* RabA GTPases. PhD thesis, University of Oxford, (2006).

[190] Sheppard, D. Dominant Negative Mutants: Tools for the Study of Protein Function In Vitro and In Vivo. *Am. J. Respir. Cell Mol. BioI.* **11**, 1 – 6 (1994).

[191] Ramalho, J. S., Anders, R., Jaissle, G. B., Seeliger, M. W., Huxley, C., and Seabra, M. C. Rapid degradation of dominant-negative Rab27 proteins in vivo precludes their use in transgenic mouse models. *BMC Cell Biology* **3**, 26 (2002).

[192] Pinheiro, H., Samalova, M., Geldner, N., Chory, J., Martinez, A., and Moore, I. Genetic evidence that the higher plant Rab-D1 and Rab-D2 GTPases exhibit distinct but overlapping interactions in the early secretory pathway. *J Cell Sci* **122**, 3749 – 3758 (2009).

[193] Osterrieder, A., Hummel, E., Carvalho, C. M., and Hawes, C. Golgi membrane dynamics after induction of a dominant-negative mutant Sar1 GTPase in tobacco. *J Exp Bot* **61**, 405 – 422 (2010).

[194] Schena, M., Lloyd, A., and Davis, R. A steroid-inducible gene expression system for plant cells. *Proc Natl Acad Sci U S A* **88**, 10421 – 10425 (1991).

[195] Aoyama, T. and Chua, N. A glucocorticoid-mediated transcriptional induction system in transgenic plants. *Plant J* **11**, 605 – 612 (1997).

[196] Kang, H., Fang, Y., and Singh, K. A glucocorticoid-inducible transcription system causes severe growth defects in *Arabidopsis* and induces defense-related genes. *Plant J* **20**, 127 – 133 (1999).

[197] Moore, I., Galweiler, L., Grosskopf, D., Schell, J., and Palme, K. A transcription activation system for regulated gene expression in transgenic plants. *Proc Natl Acad Sci U S A* **95**, 376 – 381 (1998).

[198] Craft, J., Samalova, M., Baroux, C., Townley, H., Martinez, A., Jepson, I., Tsiantis, M., and Moore, I. New pOp/LhG4 vectors for stringent glucocorticoid-dependent transgene expression in *Arabidopsis*. *Plant J* **41**, 899 918 (2005).

[199] Samalova, M., Brzobohaty, B., and Moore, I. pOp6/LhGR: a stringently regulated and highly responsive dexamethasone-inducible gene expression system for tobacco. *Plant J* **41**, 919 – 935 (2005).

[200] Samalova, M., Fricker, M., and Moore, I. Ratiometric fluorescence-imaging assays of plant membrane traffic using polyproteins. *Traffic* **7**, 1701 – 1723 (2006).

[201] Xu, J. and Scheres, B. Dissection of *Arabidopsis* ADP-RIBOSYLATION FACTOR 1 function in epidermal cell polarity. *Plant Cell* **17**, 525 – 536 (2005).

[202] daSilva, L., Taylor, J., Hadlington, J., Hanton, S., Snowden, C., Fox, S., Foresti, O., Brandizzi, F., and Denecke, J. Receptor salvage from the prevacuolar compartment is essential for efficient vacuolar protein targeting. *Plant Cell* **17**, 132 – 148 (2005).

[203] Ueda, T., Yamaguchi, M., Uchimiya, H., and Nakano, A. Ara6, a plant-unique novel type Rab GTPase, functions in the endocytic pathway of *Arabidopsis thaliana*. *EMBO J* **20**, 4730 – 4741 (2001).

[204] Drdova, E., Synek, L., Pecenkova, T., Hala, M., Kulich, I., Fowler, J. E., Murphy, A. S., and Zarsky, V. The exocyst complex contributes to PIN auxin efflux carrier recycling and polar auxin transport in *Arabidopsis*. *Plant J* **1**, 1 (2012).

[205] Hutagalung, A. H. and Novick, P. J. Role of Rab GTPases in Membrane Traffic and Cell Physiology. *Physiol Rev* **91**, 119 – 149 (2011).

[206] Botanelli, F., Foresti, O., Hanton, S., and Denecke, J. Vacuolar transport in tobacco leaf epidermis cells involves a single route for soluble cargo and multiple routes for membrane cargo. *Plant Cell* **23**, 3007–3025 (2011).

[207] Reyes, F., Buono, R., and Otegui, M. Plant endosomal trafficking pathways. *Curr Opin Plant Biol.* **14**, 666 – 673 (2011).

[208] Pourcher, M., Santambrogio, M., Thazar, N., Thierry, A., Fobis-Loisy, I., Miege, C., Jallais, Y., and Gaude, T. Analyses of sorting nexins reveal distinct retromer-subcomplex functions in development and protein sorting in *Arabidopsis thaliana*. *Plant Cell* **22**, 3980–3991 (2010).

[209] Stierhof, Y., Viotti, C., Scheuring, D., Sturm, S., and Robinson, D. Sorting nexins 1 and 2a locate mainly to the TGN. *Protoplasma* **1**, 1 (2012).

[210] Kleine-Vehn, J., Leitner, J., Zwiewka, M., Sauer, M., Abas, L., Luschnig, C., and Friml, J. Differential degradation of PIN2 auxin efflux carrier by retromer-dependent vacuolar targeting. *Proc Natl Acad Sci U S A* **105**, 17812–17817 (2008).

[211] Teh, O. and Moore, I. An ARF-GEF acting at the Golgi and in selective endocytosis in polarized plant cells. *Nature* **448**, 493–496 (2007).

[212] Zheng, H., Bednarek, S., Sanderfoot, A., Alonso, J., Ecker, J., and Raikhel, N. NPSN11 is a cell plate-associated SNARE protein that interacts with the syntaxin KNOLLE. *Plant Physiol* **129**, 530 – 539 (2002).

[213] Kirsch, T., Paris, N., Butler, J., Beevers, L., and Rogers, J. Purification and initial characterization of a potential plant vacuolar targeting receptor. *Proc Natl Acad Sci U S A* **91**, 3403 – 3407 (1994).

[214] Miller, D., Ruijter, N. D., Bisseling, T., and Emons, A. The role of actin in root hair morphogenesis: Studies with lipochito-oligosaccharide as a growth stimulator and cytochalasin as an actin perturbing drug. *Plant J* **17**, 141 – 154 (1999).

[215] Li, Y., Rogers, S., Tse, Y., Lo, S., Sun, S., Jauh, G., and Jiang, L. BP-80 and homologs are concentrated on post-Golgi probable lytic prevacuolar compartments. *Plant Cell Physiol* **43**, 726 – 742 (2002).

[216] Men, S., Boutté, Y., Ikeda, Y., Li, X., Palme, K., Stierhof, Y.-D., Hartmann, M.-A., Moritz, T., and Grebe, M. Sterol-dependent endocytosis mediates post-cytokinetic acquisition of PIN2 auxin efflux carrier polarity. *Nature Cell Biology* **10**, 237–244 (2008).

[217] Robert, S., Chary, S. N., Drakakaki, G., Li, S., Yang, Z., Raikhel, N. V., and Hicks, G. R. Endosidin1 defines a compartment involved in endocytosis of the brassinosteroid

receptor BRI1 and the auxin transporters PIN2 and AUX1. *Proc Natl Acad Sci U S A* **105**, 8464–8469 (2008).

[218] Irani, N., DiRubbo, S., Mylle, E., den Begin, J. V., Schneider-Pizon, J., Hnilikova, J., Sisa, M., Buyst, D., Vilarrasa-Blasi, J., Szatmari, A., Damme, D. V., Mishev, K., Codreanu, M., Kohout, L., Strnad, M., Cano-Delgado, A., Friml, J., Madder, A., and Russinova, E. Fluorescent castasterone reveals BRI1 signaling from the plasma membrane. *Nat Chem Biol* **8**, 583 – 589 (2012).

[219] Bolte, S., Talbot, C., Boutte, Y., Catrice, O., Read, N., and Satiat-Jeunemaitre, B. FM-dyes as experimental probes for dissecting vesicle trafficking in living plant cells. *Journal of Microscopy* **214**, 159 – 173 (2004).

[220] Zheng, H., Kunst, L., Hawes, C., and Moore, I. A GFP-based assay reveals a role for RHD3 in transport between the endoplasmic reticulum and Golgi apparatus. *Plant J* **37**, 398 – 414 (2004).

[221] Grunewald, W. and Friml, J. The march of the PINs: developmental plasticity by dynamic polar targeting in plant cells. *EMBO Journal* **29**, 2700–2714 (2010).

[222] Jürgens, G. and Geldner, N. The High Road and the Low Road: Trafficking Choices in Plants. *Cell* **130**, 977–979 (2007).

[223] Abas, L., Benjamins, R., Malenica, N., Paciorek, T., Wiśniewska, J., MoulinierAnzola, J. C., Sieberer, T., Friml, J., and Luschnig, C. Intracellular trafficking and proteolysis of the *Arabidopsis* auxin-efflux facilitator PIN2 are involved in root gravitropism. *Nature Cell Biology* **8**, 249–256 (2006).

[224] Isono, E., Katsiarimpa, A., Mueller, I. K., Anzenberger, F., Stierhof, Y.-D., Geldner, N., Chory, J., and Schwechheimer, C. The Deubiquitinating Enzyme AMSH3 Is Required for Intracellular Trafficking and Vacuole Biogenesis in *Arabidopsis thaliana*. *The Plant Cell* **22**, 1826 – 1837 (2010).

[225] Flückiger, R., Caroli, M. D., Piro, G., Dalessandro, G., Neuhaus, J.-M., and Sansebastiano, G.-P. D. Vacuolar system distribution in *Arabidopsis* tissues, visualized using GFP fusion proteins. *J Exp Bot* **54**, 1577 – 1584 (2003).

[226] Tamura, K., Shimada, T., Ono, E., Tanaka, Y., Nagatani, A., Higashi, S., Watanabe, M., Nishimura, M., and Hara-Nishimura, I. Why green fluorescent fusion proteins have

not been observed in the vacuoles of higher plants. *Plant J* **35**, 545 – 555 (2003).

[227] Laxmi, A., Pan, J., Morsy, M., and Chen, R. Light Plays an Essential Role in Intracellular Distribution of Auxin Efflux Carrier PIN2 in *Arabidopsis thaliana* . *PLoS ONE* **1**, e1510 (2008).

[228] Kleine-Vehn, J., Leitner, J., Zwiewka, M., Sauer, M., Abas, L., Luschnig, C., and Friml, J. Differential degradation of PIN2 auxin efflux carrier by retromer-dependent vacuolar targeting. *Proc Natl Acad Sci U S A* **105**, 17812–17817 (2008).

[229] Jaillais, Y., Santambrogio, M., Rozier, F., Fobis-Loisy, I., Miege, C., and Gaude, T. The Retromer Protein VPS29 Links Cell Polarity and Organ Initiation in Plants. *Cell* **130**, 1057 1070 (2007).

[230] Wang, Y., Lin, W.-H., Chen, X., and Xue, H.-W. The role of *Arabidopsis* 5PTase13 in root gravitropism through modulation of vesicle trafficking. *Cell Research* **19**, 1191–1204 (2009).

[231] Krinke, O., Ruelland, E., Valentov, O., Vergnolle, C., Renou, J.-P., Taconnat, L., Flemr, M., Burketov, L., and Zachowski, A. Phosphatidylinositol 4-Kinase Activation Is an Early Response to Salicylic Acid in *Arabidopsis* Suspension Cells. *Plant Physiol* **144**, 1347 – 1359 (2007).

[232] Rahman, A., Bannigan, A., Sulaman, W., Pechter, P., Blancaflor, E. B., and Baskin, T. I. Auxin, actin and growth of the *Arabidopsis thaliana* primary roots. *Plant J* **50**, 514 – 528 (2007).

[233] Ketelaar, T., de Ruijter, N., and Emons, A. Unstable F-Actin Specifies the Area and Microtubule Direction of Cell Expansion in *Arabidopsis* Root Hairs. *The Plant Cell* **15**, 285 – 292 (2002).

[234] Feraru, E., Feraru, M. I., Kleine-Vehn, J., Martiniere, A., Mouille, G., Vanneste, S., Vernhettes, S., Runions, J., and Friml, J. PIN Polarity Maintenance by the Cell Wall in *Arabidopsis*. *Current Biology* **21**, 338 – 343 (2011).

[235] Michniewicz, M., Zago, M. K., Abas, L., Weijers, D., Schweighofer, A., Meskiene, I., Heisler, M. G., Ohno, C., Zhang, J., Huang, F., Schwab, R., Weigel, D., Meyerowitz, E. M., Luschnig, C., Offringa, R., and Friml, J. Antagonistic Regulation of PIN Phosphorylation by PP2A and PINOID Directs Auxin Flux. *Cell* **130**, 1044 – 1056 (2007).

[236] Sukumar, P., Edwards, K. S., Rahman, A., DeLong, A., and Muday, G. K. PINOID Kinase Regulates Root Gravitropism through Modulation of PIN2-Dependent Basipetal Auxin Transport in *Arabidopsis*. *Plant Physiology* **150**, 722–735 (2009).

[237] Zhang, J., Nodzyńskia, T., Pěnčíkb, A., Rolčíkb, J., and Friml, J. PIN phosphorylation is sufficient to mediate PIN polarity and direct auxin transport. *Proc Natl Acad Sci U S A* **107**, 918–922 (2010).

[238] Friml, J., Yang, X., Michniewicz, M., Weijers, D., Quint, A., Tietz, O., Benjamins, R., Ouwerkerk, P. B. F., Ljung, K., Sandberg, G., Hooykaas, P. J. J., Palme, K., and Offringa, R. A PINOID-Dependent Binary Switch in Apical-Basal PIN Polar Targeting Directs Auxin Efflux. *Science* **306**, 862 – 865 (2004).

[239] Pan, J., Fujioka, S., Peng, J., Chen, J., Li, G., and Chen, R. The E3 Ubiquitin Ligase SCFTIR1/AFB and Membrane Sterols Play Key Roles in Auxin Regulation of Endocytosis, Recycling, and Plasma Membrane Accumulation of the Auxin Efflux Transporter PIN2 in *Arabidopsis thaliana*. *The Plant Cell* **21**, 568–580 (2009).

[240] Paciorek, T., Zaáímalová, E., Ruthardt, N., Petrek, J., Stierhof, Y.-D., Kleine-Vehn, J., Morris, D. A., Emans, N., Jürgens, G., Geldner, N., and Friml, J. Auxin inhibits endocytosis and promotes its own efflux from cells. *Nature* **435**, 1251–1256 (2005).

[241] Shin, H., Shin, H.-S., Guo, Z., Blancaflor, E. B., Masson, P. H., and Chen, R. Complex regulation of *Arabidopsis* AGR1/PIN2-mediated root gravitropic response and basipetal auxin transport by cantharidin-sensitive protein phosphatases. *Plant J* **42**, 188–200 (2005).

[242] Beck, M., Zhou, J., Faulkner, C., MacLean, D., and Robatzek, S. Spatio-Temporal Cellular Dynamics of the *Arabidopsis* Flagellin Receptor Reveal Activation Status-Dependent Endosomal Sorting. *The Plant Cell* **112**, 1 – 15 (2012).

[243] Banbury, D., Oakley, J., Sessions, R., and Banting, G. Tyrphostin A23 inhibits internalization of the transferring receptor by perturbing the interaction between tyrosine motifs and the medium chain subunit of the AP-2 adaptor complex. *J Biol Chem* **278**, 12022 – 12028 (2003).

[244] Feraru, E., Paciorek, T., Feraru, M., Zwiewka, M., Groodt, R. D., Ryckeb, R. D., Kleine-Vehn, J., and Friml, J. The AP-3 β Adaptin Mediates the Biogenesis and Function of

Lytic Vacuoles in *Arabidopsis*. *Plant Cell* **22**, 2812 – 2824 (2010).

[245] Levitzki, A. and Mishani, E. Tyrphostins and other tyrosine kinase inhibitors. *Annu Rev Biochem* **75**, 93 – 109 (2006).

[246] Robinson, D., Pimpl, P., Scheuring, D., Stierhof, Y., Sturm, S., and Viotti, C. Trying to make sense of retromer. *Trends Plant Sci* **7**, 431–439 (2012).

[247] Niemes, S., Langhans, M., Viotti, C., Scheuring, D., Yan, M. S. W., Jiang, L., Hillmer, S., Robinson, D., and Pimpl, P. Retromer recycles vacuolar sorting receptors from the trans-Golgi network. *Plant J* **61**, 107–121 (2010).

[248] Dhonukshe, P., Huang, F., Galvan-Ampudia, C., Mahonen, A., Kleine-Vehn, J., Xu, J., Quint, A., Prasad, K., Friml, J., Scheres, B., and Offringa, R. Plasma membrane-bound AGC3 kinases phosphorylate PIN auxin carriers at TPRXS(N/S) motifs to direct apical PIN recycling. *Development* **137**, 3245 – 3255 (2010).

[249] Kleine-Vehn, J., Wabnik, K., Martiniere, A., Langowski, L., Willig, K., Naramoto, S., Leitner, J., Tanaka, H., Jakobs, S., Robert, S., Luschnig, C., Govaerts, W., Hell, S., Runions, J., and Friml, J. Recycling, clustering, and endocytosis jointly maintain PIN auxin carrier polarity at the plasma membrane. *Molecular Systems Biology* **7**, 540 (2011).

[250] Staehelin, L. and Kang, B. Nanoscale architecture of endoplasmic reticulum export sites and of Golgi membranes as determined by electron tomography. *Plant Physiol.* **147**, 1454 1468 (2008).

[251] Staehelin, L. and Moore, I. The plant Golgi apparatus. *Annu. Rev. Plant Biol.* **46**, 261288 (1995).